



The
University
Of
Sheffield.

Continuous extrusion of commercially pure titanium powder

Author: Ben M. Thomas

A thesis submitted in partial fulfillment of the requirements for the degree of Doctor of
Philosophy

University of Sheffield
Faculty of Engineering
Department of Materials Science and Engineering

Supervisor: Dr. Martin Jackson

Submitted: September 2015

Abstract

The automotive industry is constantly looking for improvements in materials and processes in order to try and reduce the weight of their vehicles to improve fuel efficiency. While improvements in aluminium alloys and ultra high strength steels can assist in light-weighting improvements have been relatively incremental in recent years. Titanium on the other hand has a superior strength-to-weight and corrosion resistance to both steels and aluminium alloys. There have been small scale demonstrations of titanium in road vehicles but major barrier for titanium's introduction into the mass production automotive market is its cost. The introduction of cost effective solid state extraction routes for titanium from its ores or oxides (Metalysis FFC, Cristal Metals, CSIRO TiROTM and others) has renewed research interest in the cost reduction of titanium. These processes in particular produce powders directly from the extraction cells, which requires a low cost powder consolidation method for a true step change in the economics of the resultant titanium products. Standard solid state consolidation methods tend to rely on batch processes and require multiple steps to produce a fully dense product. The severe plastic deformation that occurs within the Conform process has the potential to solve these problems and provide a truly cost effective thermomechanical processing for titanium particulates. Even though Conform has been around since the 1970s and primarily used to extrude aluminium and copper based alloys significant development has been slowed by a lack of understanding of the thermomechanical behaviour material within the process. Work presented in this thesis demonstrates the successful extrusion of grade 2 hydride-dehydride (HDH) titanium powder through the Conform process to obtain a fully dense rod product with a fine grain size. A finite element model has also been produced in order to demonstrate the evolution of certain microstructural features in the extruded titanium wire. The models are extended to help predict a general titanium powder processing window for continuous extrusion machines.

Contents

| | | |
|----------|---|-----------|
| 1 | Introduction | 2 |
| 1.1 | Automotive Weight Reduction and fuel efficiency | 3 |
| 1.1.1 | Challenges for automotive titanium | 6 |
| 1.2 | Cost effective production of titanium | 8 |
| 1.2.1 | Extraction processes | 8 |
| 1.2.2 | Low cost titanium powder metallurgy | 9 |
| 1.3 | The Conform process | 11 |
| 1.4 | Thesis overview | 12 |
| 2 | Literature review | 14 |
| 2.1 | Titanium metallurgy | 14 |
| 2.2 | Severe plastic deformation processing | 18 |
| 2.2.1 | Discontinuous SPD processing | 18 |
| 2.2.2 | Continuous SPD processing | 22 |
| 2.3 | Conform process | 25 |
| 2.3.1 | Conform of particulate feedstock | 27 |
| 2.4 | Modelling the Conform Process | 31 |
| 2.4.1 | Analytical models | 31 |
| 2.4.2 | Finite element models | 34 |
| 2.4.3 | Grip length in continuous extrusion processing | 36 |
| 2.4.4 | Importance of extrusion ratio in Conform | 37 |
| 3 | Experimental Trials | 39 |
| 3.1 | Equipment | 39 |
| 3.2 | Trial Methodology | 39 |
| 3.2.1 | Feedstock powders | 43 |
| 3.2.2 | Abutment stress metric | 44 |

| | | |
|----------|--|------------|
| 3.2.3 | Process Control | 46 |
| 3.2.4 | Rod analysis methodology | 48 |
| 3.2.5 | Powder flow in to the Conform machine | 48 |
| 3.2.6 | Powder flow from a hopper | 49 |
| 3.2.7 | Hopper design and mass flow rates within the Conform machine | 49 |
| 3.2.8 | Wheel coating process | 52 |
| 3.3 | Machine data from trials | 58 |
| 3.3.1 | Trial 1 | 59 |
| 3.3.2 | Trial 2 | 64 |
| 3.3.3 | Trial 3 | 67 |
| 3.3.4 | Trial 4 | 70 |
| 3.3.5 | Trial 5 | 73 |
| 3.4 | Analysis of extruded titanium wire and strip | 76 |
| 3.4.1 | Round 5mm Die | 80 |
| 3.4.2 | Grain growth for diffusion bonding | 83 |
| 3.4.3 | Rectangular Die | 87 |
| 4 | Analytical model of the Conform process | 89 |
| 4.1 | Analytical model for extrusion pressure and fill height | 89 |
| 4.1.1 | Drive Pressure | 91 |
| 4.1.2 | Upset Length | 92 |
| 4.1.3 | Extrusion Pressure | 93 |
| 5 | Finite element modelling - 2D | 97 |
| 5.1 | Methods | 97 |
| 5.1.1 | Simulation setup in DEFORM TM -2D | 97 |
| 5.2 | Results | 103 |
| 5.2.1 | Effect of changing port height | 105 |
| 5.2.2 | Effect of changing port depth | 106 |
| 5.2.3 | Effect of changing die size | 107 |
| 5.2.4 | Effect of changing die height | 108 |
| 5.2.5 | Conclusions - 2D FEM | 110 |
| 6 | Finite element modelling - 3D | 112 |
| 6.1 | Methods | 112 |
| 6.1.1 | Simulation Setup in DEFORM TM -3D | 112 |

| | | |
|-----------|---|------------|
| 6.1.2 | Truncated Workpiece Simulations | 118 |
| 6.2 | 3D FEM Results | 121 |
| 6.2.1 | Full 3D simulation results | 121 |
| 6.2.2 | Material flow in the Conform process | 124 |
| 6.2.3 | State variables in the workpiece | 127 |
| 6.2.4 | Truncated workpiece simulations | 136 |
| 7 | Comparison of Conform modelling techniques | 139 |
| 7.1 | Comparison with experimental results | 139 |
| 8 | Discussion | 143 |
| 9 | Conclusions | 150 |
| 10 | Future work | 152 |

List of Figures

| | | |
|------|--|----|
| 1.1 | Current manufacturing stages required to produce spring wire from rutile via the common Kroll/VAR and rod rolling route. | 3 |
| 1.2 | Cost break down of the production of 1” titanium alloy plate. Modified from [1] | 4 |
| 1.3 | Possible applications for titanium in a family car. Identified by [2–4] | 5 |
| 1.4 | Processing route of low cost titanium particulates to generate a true step change in the cost of titanium parts for automotive spring applications | 12 |
| 1.5 | Pyramid showing the potential applications of Conform extruded titanium wire. Applications at the top of the pyramid are those that require the best mechanical properties in terms of strength and fatigue and hence are deemed the highest risk, highest reward. | 13 |
| 2.1 | Unit cells of a) HCP α and b) BCC β phases in titanium with their respect lattice parameters and main deformation planes indicated. Reproduced from [5]. | 15 |
| 2.2 | Slip planes and directions in the titanium HCP α phase | 15 |
| 2.3 | Pseudo phase diagram for the addition of alpha and beta stabilising elements in titanium alloys | 16 |
| 2.4 | Schematic representation of the ECAP Process and deformation of a unit volume. | 19 |
| 2.5 | Representation of the four main multiple pass ECAP processing routes. | 19 |
| 2.6 | Schematic of Direct Friction Extrusion Process. Often referred to as Friction Stir Extrusion in the literature. Reproduced from [6] | 22 |
| 2.7 | Schematic representation of the CSIRO Direct Particle Rolling (DPR) process using TiRO TM powders (Also known as Hot Roll Densification (HRD)) [7] | 23 |
| 2.8 | Simple representation of the ECAP-Conform process. Reproduced from [8] | 24 |
| 2.9 | Schematic of the modern day Conform process with modifications for direct powder feed into the groove. Reproduced from [9] | 26 |
| 2.10 | Range of possible extruded profiles in aluminium and copper from a BWE Ltd. Conform machine [10] | 27 |

| | |
|---|----|
| 2.11 Macrograph of the flow within a rod sample Conform extruded from DryFlo Copper [11]. Scale not reported. | 30 |
| 2.12 Representative macrostructure flow pattern within aluminium rod extruded via CRE using pure aluminium powders. Reproduced from [12] | 30 |
| 2.13 Concept drawings of early Conform TM theoretical designs. Redrawn from [13] . . | 32 |
| 2.14 Examples of the curling phenomenon in Conform TM . Reproduced from [14] . . . | 34 |
| 2.15 Examples of surface defect forming in Conform TM . Reproduced from [15] | 34 |
| 2.16 Preliminary FEM results from COMTES FHT [16] showing the state variable fields in the COMTES modified Conform process with 10 mm diameter CP-Ti grade 2 rod. | 36 |
| 2.17 Comparison of Conform FEM results using different friction coefficients with a macrograph of the workpiece remaining in the abutment zone (left $\mu=0.2$, centre $\mu=0.7$). Reproduced from [16] | 37 |
| 2.18 Grip length in the generation of extrusion pressure in a) LINEX (LINear continuous extrusion) [17] and b) Conform [18] | 37 |
| 3.1 Schematic of the modern day Conform process with modifications for direct powder feed into the groove. Reproduced from [9] | 41 |
| 3.2 Schematic representation of the hopper and chute setup for the experimental trials. | 42 |
| 3.3 Vibrating chute with powder flowing across it and into the wheel groove during an experimental trial. | 43 |
| 3.4 Particle size distribution for CP-Ti HDH powder used in this study. | 44 |
| 3.5 Secondary electron micrograph of grade 2 HDH powder. | 45 |
| 3.6 Live monitoring plot of current vs wheel speed for different ‘abutment stress’ values used during experimental trials 2-5. | 46 |
| 3.7 Schematic cut through view of the custom powder hopper used in the fourth set of trials. | 50 |
| 3.8 Measured mass flow rate from the hoppers used in the experimental trials. . . . | 51 |
| 3.9 Conform wheel coated with consolidated titanium following experimental trial 4. Irregular oxidised flash can be seen either side of the groove. | 53 |
| 3.10 Dimensions used in the wheel coating theory for the start up process in the Conform processing of titanium powders. | 55 |

| | | |
|------|--|----|
| 3.11 | Graph of the effective shear ratio between the average wheel surface within the groove and a powder particle in free fall. The dashed blue line shows the critical shear ratio needed to consolidate CP-Ti HDH powder 45-150 μ m within the flash gap and coat the wheel groove. | 56 |
| 3.12 | Close up of the abutment and die port following an interrupted test in Trial 2 with a wheel speed of 2 RPM | 57 |
| 3.13 | The die chamber at the end of Trial 2 showing the fracture surface of the failed abutment with partially consolidated titanium processed over the top. | 57 |
| 3.14 | Raw data tool temperature and abutment stress (torque derived) from trial 1. . . | 59 |
| 3.15 | Abutment stress analysis plot from data obtained during trial 1. | 60 |
| 3.16 | Abutment stress vs wheel speed curves for trial 1 overlaid on the data from every trial conducted in this project. | 62 |
| 3.17 | Raw data tool temperature and abutment stress (torque derived) from trial 2. . . | 64 |
| 3.18 | Abutment stress analysis plot from data obtained during trial 2. | 65 |
| 3.19 | Abutment stress vs wheel speed curves for trial 2 overlaid on the data from every trial conducted in this project. | 66 |
| 3.20 | Raw data tool temperature and abutment stress (torque derived) from trial 3. . . | 67 |
| 3.21 | Abutment stress analysis plot from data obtained during trial 3. | 68 |
| 3.22 | Abutment stress vs wheel speed curves for trial 3 overlaid on the data from every trial conducted in this project. | 69 |
| 3.23 | Raw data tool temperature and abutment stress (torque derived) from trial 4. . . | 70 |
| 3.24 | Abutment stress analysis plot from data obtained during trial 4. | 71 |
| 3.25 | Abutment stress vs wheel speed curves for trial 4 overlaid on the data from every trial conducted in this project. | 72 |
| 3.26 | Raw data tool temperature and abutment stress (torque derived) from trial 5. . . | 73 |
| 3.27 | Abutment stress analysis plot from data obtained during trial 5. | 74 |
| 3.28 | Abutment stress vs wheel speed curves for trial 5 overlaid on the data from every trial conducted in this project. | 75 |
| 3.29 | 5 mm diameter CP-Ti wire emerging from the BWE Conform TM machine before entering a water trough to be quenched. | 76 |
| 3.30 | 5 mm diameter CP-Ti wire emerging from the BWE Conform TM machine before entering a water trough to be quenched. | 77 |

| | | |
|------|--|----|
| 3.31 | Close view of the back of the shoe with 5 mm diameter CP-Ti wire emerging from the BWE Conform TM machine. The wire glows red hot due to the large amount of heat generated during the process. | 78 |
| 3.32 | Close up of the abutment and die port following an interrupted test in Trial 2 with a wheel speed of 2 RPM | 79 |
| 3.33 | The die chamber at the end of Trial 2 showing the fracture surface of the failed abutment with partially consolidated titanium processed over the top. | 79 |
| 3.34 | The die chamber at the end of Trial 3 following a maximum wheel speed of 7 RPM | 79 |
| 3.35 | The die chamber and entry block within the shoe at the end of Trial 4 showing good consolidation. The fractured abutment is hidden by the titanium processed over the top of it. | 79 |
| 3.36 | Macrostructures of the cross section of the extruded 5 mm diameter CP-Ti wire. Images taken under polarised optical light were converted to binary format to highlight the flow profiles. | 80 |
| 3.37 | Macrostructures of the longitudinal section of the extruded 5 mm diameter CP-Ti wire. Images taken under polarised optical light were converted to binary format to highlight the flow profiles. | 80 |
| 3.38 | Cross-polarised light micrographs of a sample extruded at 8 RPM with locations indicated on the cross-section. | 81 |
| 3.39 | Cross-polarised light micrographs of a sample extruded at 8 RPM with locations indicated on the longitudinal section. | 83 |
| 3.40 | Cross-polarised light micrographs of a sample extruded at 10 RPM with locations indicated on the cross-section. | 84 |
| 3.41 | Average grain sizes from micrographs taken at five locations in the cross sections of extruded 5 mm CP-Ti wire. | 85 |
| 3.42 | Composite cross-polarised light micrograph taken from a cross section of 5 mm diameter CP-Ti wire heat treated at 950°C for two hours. | 86 |
| 3.43 | Macro image of the flow within the cross section of extruded product using the rectangular die in the vertical orientation. Taken using polarised light. | 87 |
| 3.44 | Micrograph of the cross section of extruded product using the rectangular die in the vertical orientation. Taken using polarised light. | 87 |
| 3.45 | Two die back end discards from Trial 3.1 (left) and 3.1 (right) | 87 |

| | | |
|------|--|-----|
| 3.46 | Composite polarised light macrograph of a section taken from the die discard using the rectangular die in the vertical orientation. Material dead zones can be seen above and below the die as regions of larger grains. | 88 |
| 4.1 | Simple visual representation of the two regions considered in the analytical model. The upper vertical region represents the generation of the drive force within the wheel groove while the horizontal cylinder is a simplification of the deformation occurring within the die chamber port and die. | 90 |
| 4.2 | Dimensions of the wheel groove used in derivation of the analytical pressure model | 91 |
| 4.3 | Schematic of a 2D Conform extrusion with labelled dimensions relevant to the analytical model. Dead metal zones (DMZ) are shaded and assumed to be the same shape above and below the die entrance for ease of calculations. | 94 |
| 4.4 | Pressure on different faces of the slabs under consideration taken as transverse sections through a direct extrusion a) in the cylindrical billet prior to extrusion b) and c) while extruding through a circular die with entry angle α and diameter D_P | 95 |
| 5.1 | Flow stress data from the DEFORM TM database. | 98 |
| 5.2 | Schematic representation of the 2D FEM simulation setup showing the defined mesh windows with their corresponding absolute element sizes. Wheel contact is defined as a boundary condition on the right hand side of the workpiece. | 100 |
| 5.3 | Schematic representation of the 2D FEM simulation setup. Wheel contact is defined as a boundary condition on the right hand side of the workpiece. Important geometry variables that are varied in the study are labelled on the figure. | 101 |
| 5.4 | Important tool loads and points of interest monitored in the post processing of each 2D simulation. | 102 |
| 5.5 | Representative finite element simulation in 2D with frames taken at ~ 0.2 second intervals showing the evolution of the upset height during the establishment of steady state Conform extrusion of grade 2 titanium. Maximum upset height and abutment load is achieved at $t = 0.6$ s. | 103 |
| 5.6 | Representative data extracted from a single 2D simulation. | 104 |
| 5.7 | Plots of tool loads, principal stresses, temperatures, extrusion velocity and workpiece upset height with increasing port height | 105 |
| 5.8 | Plots of tool loads, principal stresses, temperatures, extrusion velocity and workpiece upset height with increasing port depth | 106 |

| | | |
|------|---|-----|
| 5.9 | Plots of tool loads, principal stresses, temperatures, extrusion velocity and workpiece upset height with increasing die size | 107 |
| 5.10 | Plots of tool loads, principal stresses, temperatures, extrusion velocity and workpiece upset height with increasing die height from the base of the port | 109 |
| 5.11 | Graph showing the correlation between the abutment load and upset height for both the maximum attained values and those during steady state extrusion. | 111 |
| 6.1 | The full 3D tooling setup of the Conform machine experimental trials. Tools that do not contact with the workpiece are not considered in the simulations. | 115 |
| 6.2 | Slice through a side view of the 3D Conform tool geometries showing their relative positioning. | 115 |
| 6.3 | View of the abutment, die chamber, die and entry block tools when looking out from the wheel in the direction of extrusion | 116 |
| 6.4 | Example of the mesh used in the 3D Conform FE simulations on the workpiece surface and internal. Mesh windows were defined to refine the mesh with element sized indicated in the figure. | 117 |
| 6.5 | Theoretical representation of the consolidated powder within the Conform process as it relates to the truncated workpiece FE simulations. The transition between fully consolidated material and unconsolidated powder is shown schematically with a black dashed line. | 118 |
| 6.6 | Die back end discard showing how high above the abutment the CP-Ti HDH powder is fully consolidated. | 119 |
| 6.7 | The placement of the truncated workpieces for FEM analysis of the effective abutment stress, abutment load and grip length relationships. | 119 |
| 6.8 | Point tracking positions used in 3D FEM post processing | 121 |
| 6.9 | Simulation data of the tool loads and point tracked temperatures and stresses. | 122 |
| 6.10 | Evolution of the workpiece during the upset phase of DEFORM TM -3D simulation of Conform with a 5 mm round die | 123 |
| 6.11 | Material dead zones shown in red on a 2D slice through the 3D workpiece. 3D velocity isosurface (blue) delineated by 3 mms ⁻¹ velocity surface contour. Material in this zones is classed as ‘dead’ and tends to remain in the shoe tooling rather than be extruded. | 125 |
| 6.12 | Evolution of an overlaid 3D flow net during steady state Conform extrusion of CP-Ti. Two slices on the labelled planes 1 and 2 were taken either side of the die entry and shown below the side-on view | 126 |

| | | |
|------|---|-----|
| 6.13 | Effective strain profile in the CP-Ti workpiece in both full 3D and on a central slice. | 127 |
| 6.14 | Cross sections of the extruded workpiece once it has exited the die showing the both the full workpiece in the -Z direction and the final effective strain profile. | 128 |
| 6.15 | Line plots of the effective strain in the vertical and horizontal orientations on a cross section of the workpiece as it moves through the die bearing. | 128 |
| 6.16 | Effective strain rate profile in the CP-Ti workpiece in both full 3D and on a central slice. | 129 |
| 6.17 | Line plots of effective strain rate at the top, middle and bottom of the abutment zone showing the two main deformation zone that the workpiece undergoes. Distances are measured from the die face at $d = 0$ horizontally towards the wheel groove. | 130 |
| 6.18 | Effective stress profile in the CP-Ti workpiece in both full 3D and on a central slice. The estimated upset height is shown on the left hand side image. | 131 |
| 6.19 | Nodal velocity profile in the CP-Ti workpiece in both full 3D and on a central slice. | 132 |
| 6.20 | Cross sections of the extruded workpiece once it has exited the die showing the both the full workpiece in the -Z direction and the final velocity profile. | 133 |
| 6.21 | Line plots of the velocity in the vertical and horizontal orientations on a cross section of the workpiece as it moves through the die bearing. | 133 |
| 6.22 | Temperature profile in the CP-Ti workpiece in both full 3D and on a central slice. | 134 |
| 6.23 | Cross sections of the extruded workpiece once it has exited the die showing the both the full workpiece in the -Z direction and the final temperature profile. | 134 |
| 6.24 | Line plots of the temperature in the vertical and horizontal orientations on a cross section of the workpiece as it moves through the die bearing. | 135 |
| 6.25 | Wheel torque data converted to abutment stress values for the truncated sample simulations. | 136 |
| 6.26 | Average abutment stress vs truncated sample height for DEFORM TM CP-Ti grade 2 material data at 20°C | 137 |
| 7.1 | | 141 |
| 8.1 | Theoretical representation of the abutment stress (torque related) vs wheel speed plots and the relationship with measured abutment temperature. | 143 |

List of Tables

| | | |
|-----|--|-----|
| 1.1 | Summary of previously or currently used titanium alloys in commercial automotive applications [19]. | 6 |
| 1.2 | Cost of titanium compared with other common metals in the automotive industry as of 2004 [2] | 7 |
| 2.1 | Property improvement and degradation as a result of certain microstructural features in titanium alloys. | 17 |
| 3.1 | Experimental trial equipment | 40 |
| 3.2 | Experimental trials tooling | 41 |
| 3.3 | Chemical composition of CP-Ti grade 2 powder. All percentages are by weight | 44 |
| 3.4 | Parameters of interest to this work from the possible 53 logged field on the BWE machine control console. | 47 |
| 3.5 | Room temperature mechanical properties of the as-extruded 5 mm diameter CP-Ti extruded at three different wheel speeds. | 85 |
| 5.1 | Parameters and range of values used in the 2D FEM study of Conform with grade 2 titanium | 99 |
| 6.1 | Data for each of the DEFORM TM -3D simulations. | 114 |
| 7.1 | Comparison of results from numerical modelling techniques used in this study with experimental trials with CP-Ti HDH powder on a Conform 315i machine. | 140 |

Acknowledgements

I would like to thank my supervisor Dr. Martin Jackson for developing original idea behind this research during his time at Imperial College, London, for finding extra funding sources and providing me with a great deal of support during my PhD. I would also like to thank Dr. John Dawson (former Technical Director at BWE Ltd.) for his assistance during the experimental trials and useful discussion as I learned about the Conform process. Finally I would like to thank my partner Cath for her unwavering support in my choice to do a PhD, for moving to Sheffield, her tolerance of my ups and downs during the last four years and for not complaining once during the ‘thesis-writing widow’ phase.

It doesn't matter how beautiful your theory is, it doesn't matter how smart you are. If it doesn't agree with experiment, it's wrong.

Richard P. Feynman

Introduction

Titanium has long been regarded as an ideal metal for usage in many aerospace, petrochemical and biomedical applications due to its high specific strength, low Young's modulus, corrosion resistance and bio-compatibility. Titanium is also a highly abundant element making up 0.6% of the Earth's lithosphere and is the fourth most abundant structural metal after iron, aluminium and magnesium. If titanium is such a desirable metal, why does it not experience more widespread usage?

Approximately half of all titanium production is utilised in aerospace [1] and as a result technological developments have been dominated by the industry's requirements. With titanium being used in airframes and aero-engines microstructural defects are not tolerated by manufacturers. Double and triple vacuum arc remelts are common for titanium billets to ensure purity levels and alloy specifications are met. Further downstream processing in air requires multiple forging, reheat and surface oxide removal steps adding to product cost. Final machining stages cause a large yield loss resulting in 'buy to fly' ratios as low as 80-90%. The resulting high cost of titanium products create a market entry barrier for the automotive industry who instead rely on high strength steel and aluminium alloys as their main metallic materials. If the cost of titanium could be reduced in line with these 'commodity' materials it is conceivable that the automotive industry would begin to put it in their cars and lorries. The light weighting benefit of using titanium over steel in certain areas of the automobile would result in lighter vehicles, better fuel economy, reduced emissions and better engine performance.

Industry and academic efforts to reduce the cost of titanium products have been ongoing but has in the past focused on increasing the efficiency of the Kroll Process or optimising machining processes. While cost reductions have been made in the price of titanium it is still not seen as a cost effective metal for industries with large scale outputs like automotive. Until a true step change occurs in the economics of titanium its usage will lag behind steels and aluminium alloys.

Recent attempts by a few companies have focused on producing a viable cost effective re-

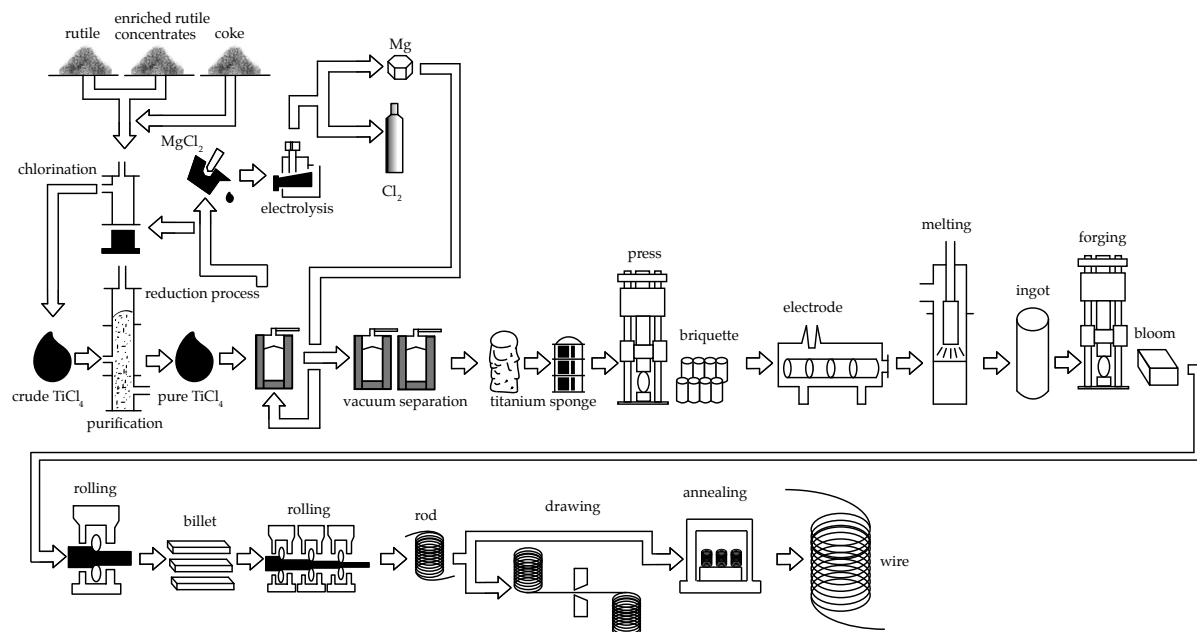


Figure 1.1: Current manufacturing stages required to produce spring wire from rutile via the common Kroll/VAR and rod rolling route.

placement for conventional sponge. In a 2004 report by Kraft [1] those technologies that could produce cost reductions of greater than 30% compared with traditional Kroll titanium were outlined in order to determine the current ‘state of the art’. Those technologies that were classed as ‘Direct Powder’ and produced granules or particles of titanium in the solid state were identified as having the largest cost reduction potential of all the technologies considered.

As shown in figure 1.2 the biggest economic step change will be only be fully realised with the addition of an cost effective downstream thermomechanical processing route. In particular, direct electrochemical powder production coupled with a solid state powder consolidation process could provide the disruptive technology necessary for significant uptake of titanium products into, as yet unexplored industries such as automotive.

1.1 Automotive Weight Reduction and fuel efficiency

The automotive industry is continuously striving for fuel consumption reductions through a combination of engine and aerodynamic efficiencies. Weight reductions in various parts of a vehicle can help companies in this fuel efficiency drive and titanium is ideally suited for this task. A report by the Advanced Propulsion Centre, UK highlights the importance of vehicle lightweighting in generating ‘Future industrial prosperity’ in the UK [20]. The APC Lightweighting

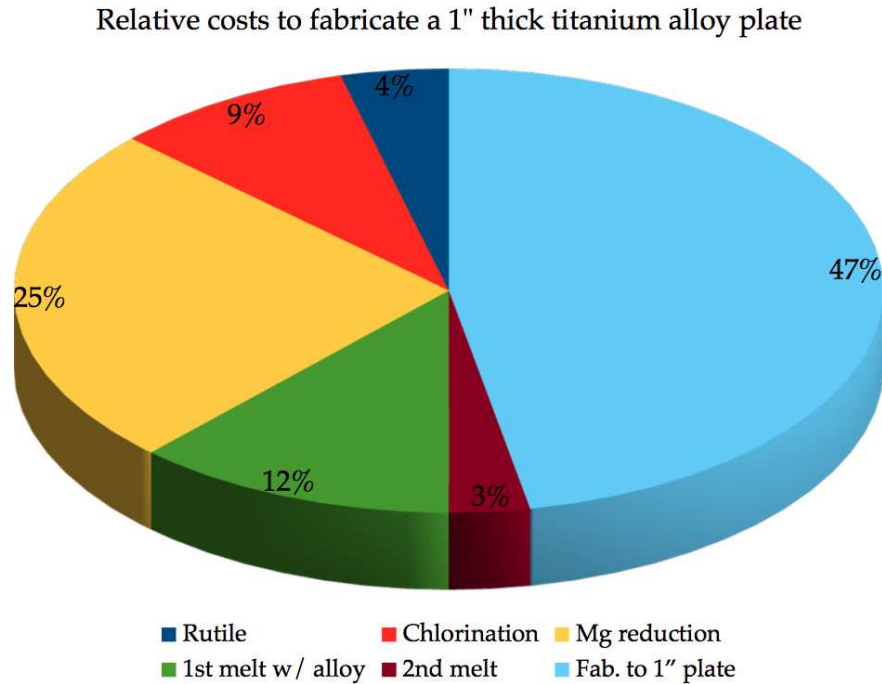


Figure 1.2: Cost break down of the production of 1" titanium alloy plate. Modified from [1]

Working Group found that in order to meet the expected EU CO₂ reduction targets of ~60% by 2050 vehicles such as a family car would have to reduce their mass by around 300 kg. Such weight reductions may come from improvements in ultra-high strength steels, high-strength aluminium alloys, increased uptake of composite materials or magnesium alloys. Titanium was also mentioned as a possible material for mass production light-weighting, but a considerable cost barrier has to be overcome before this could be a viable option.

Despite this identified need to reduce weight, there has been a recent trend in the automobile industry of increasing vehicle mass as a result of consumer requests for increased comfort and safety. Features such as air conditioning, satellite navigation and entertainment systems all add to the curb weight of vehicles. Two distinct parts of the automotive industry have been identified and can be roughly defined as family or passenger cars and heavy duty vehicles. While these definitions may have some technical overlap they are distinct enough to the general observer and need to be separated as they have different industrial reasons for vehicle light-weighting.

1. Emission reductions are a primary target for manufacturers in order to comply with legislation to reduce toxic and greenhouse gases direct from vehicles. However it has been suggested by Blue *et al.* [21] that a reduction in exhaust emissions alone is not a sufficient incentive for the high capital cost of developing significant light-weighting

technologies.

- Lightweighting of a vehicle has a side effect of also helping to reduce exhaust emissions. Reducing the kerb weight of a vehicle means that less engine power is required for a journey, all other things being equal. Without redesigning the engine this would enable less fuel to be used. Consequently the maximum fuel capacity of the car could be reduced in order to further save weight. However there becomes a limiting point at which weight reductions in the chassis, bodywork or engine begin to impact on the safety or performance of the vehicle.

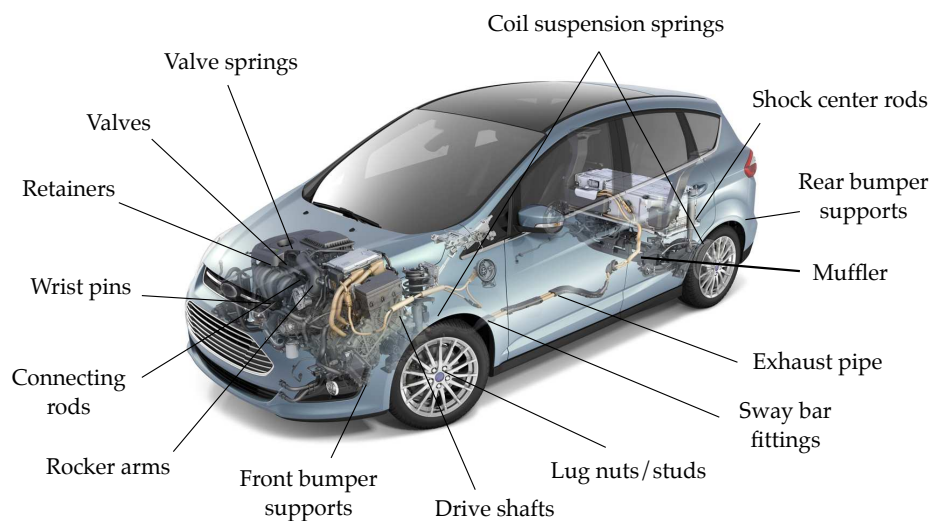


Figure 1.3: Possible applications for titanium in a family car. Identified by [2–4]

Figure 1.3 adapted from the TIMET Automotive Division (2002) shows a number of possible ways in which titanium products might be introduced into a family car. Most applications are static in nature and rely solely on the weight reduction and corrosion resistance of titanium. However, spring applications offer a greater chance for performance improvement due to dynamic weight reduction. Engine valve springs and suspension compression springs are currently made from various chromium-vanadium and silicon-chromium alloys of steel and all require surface coatings to prolong their working life, something that is not normally needed by titanium alloys. In 2000 Volkswagen introduced TimetalTM-LCB (Low Cost Beta) compression springs into the suspension of the Lupo. TimetalTM-LCB was subsequently scrapped from the Lupo's design after the Ferro-molybdenum master alloy become too costly for automotive applications. Other examples of the Toyota Altezza (TiB/BetaC valves), Mitsubishi (valve spring retainers) and Corvette (CP-Ti exhaust) all show a desire for the use of titanium by those companies at the heart of the automotive industry. Many other reports [1,21–24] have detailed the benefits

of developing low cost titanium for the automotive industry and all mention the large potential cost saving of powder metallurgy processing of ‘cost-effective’ titanium powders as shown in section 1.2.1 A current list of known titanium parts in consumer level cars is shown in table 1.1

Table 1.1: Summary of previously or currently used titanium alloys in commercial automotive applications [19].

| Type | Alloy | Component | Manufacturer and Model | Year |
|------------------|------------------------------------|---------------------|---------------------------|------|
| α | CP-Ti ASTM grade 2 | Exhaust system | Porsche GT3 RS 4.0 | 2011 |
| | | | Porsche Cayenne II S V8 | 2011 |
| | | | Audi TTS | 2008 |
| | | | Koenigsegg CCR | 2004 |
| | | | Nissan Fair Lady Z | 2003 |
| | | | GM Corvette Z06 | 2001 |
| α | CP-Ti ASTM grade 1, Al-plated | Exhaust system | Bugatti Veyron 16.4 | 2005 |
| α | TIMETAL®XT (Ti-0.45Si-0.25Fe) | Exhaust system | Porsche GT 2 | 2007 |
| | | | BMW Alpina B6 Biturbo | 2013 |
| | | | Audi RS4 Avant | 2013 |
| $\alpha + \beta$ | Ti-3Al-2.5V-RE | Connecting rods | Honda Acura NSX | 1992 |
| $\alpha + \beta$ | Ti-6Al-4V | Connecting rods | Porsche GT 3 RS 4.0 | 2011 |
| | | | Koenigsegg | 2006 |
| | | | Bugatti Veyron 16.4 | 2005 |
| | | | GM Corvette Z06 | 2002 |
| | | | Porsche GT 3 | 1999 |
| | | | Ferrari (all 12-cyl) | 1994 |
| | | | Daimler-Benz Truck Diesel | 1999 |
| | | | GM Corvette Z06 | 2005 |
| $\alpha + \beta$ | Ti-6Al-4V | Valves | Nissan Infinity Q45 | 2002 |
| | | | Toyota Altezza 6-cyl | 1998 |
| | | | Bugatti Veyron 16.4 | 2005 |
| Near- β | TIMETAL®LCB (Ti-4.5Fe-6.8Mo-1.5Al) | Springs | Ferrari 360 Stradale | 2003 |
| | | | Volkswagen Lupo FSI | 2000 |
| | | | Mitsubishi Lancer | 2000 |
| TiAl | γ TiAl | Turbocharger rotors | | |

1.1.1 Challenges for automotive titanium

The overwhelming trend in the literature surrounding automotive titanium is that the potential improvements from weight reductions could be considerable. However, the cost of parts is always the defining factor in the uptake of titanium into mass production vehicles. Part of this comes from the increased cost of mining and extracting titanium from its ores, rutile and ilmenite when compared with iron and aluminium. Titanium’s high affinity for oxygen and nitrogen makes it an energy intensive metal to extract. Subsequent fabrication of titanium parts is also difficult due to its low Young’s modulus, high yield stress and tendency to re-react with gasses in the atmosphere resulting in a need to vacuum or inert environments. Machining of titanium components is also difficult as its low thermal conductivity tend to increase heat transfer into the machining tool, resulting in both increased tool material diffusivity and tool wear. Each of these issues adds exponentially to the cost of the final titanium product when

compared with other commonly used automotive materials (see table 1.2).

Table 1.2: Cost of titanium compared with other common metals in the automotive industry as of 2004 [2]

| Item | Material (\$ per lb contained) | | | |
|-------|--------------------------------|-----------|-----------|------------|
| | Steel | Aluminium | Magnesium | Titanium |
| Ore | 0.02 | 0.10 | 0.01 | 0.30 |
| Metal | 0.10 | 0.68 | 0.54 | 2.00 |
| Ingot | 0.15 | 0.70 | 0.60 | 4.50 |
| Sheet | 0.30-0.60 | 1.00-5.00 | 4.00-9.00 | 8.00-50.00 |

1.2 Cost effective production of titanium

1.2.1 Extraction processes

1.2.1.1 Cristal Metals: Formally ITP Armstrong process

The Cristal Metals process is a continuous version of the Hunter process, which is a sodium reduction process, as opposed to a magnesium reduction (Kroll). Gaseous TiCl_4 is reduced and cooled then injected into a stream of molten Na. This process is currently producing CP titanium and Ti-6Al-4V alloys by injecting mixed metal chlorides into the molten Na in form of powder and “briquettes” [25]. A drawback currently with this process is that a further powder processing step is required to densify a very porous and fine particulate product and the corrosiveness of some chlorides, such as AlCl_3 [26]. Research on Ti-6Al-4V has showed that a ball milled powder that is cold compacted followed by sintering at 1300°C for 1 hour, produced a final density of 99.6% [27].

1.2.1.2 CSIRO TiRO™

Using the same process chemistry as the Kroll process CSIRO’s TiRO™ process utilises fluidised bed technology, where solid particles are suspended in a gas and their behaviour is comparable to a fluid [28]. In this process the gas used is argon, which avoids potential contamination with oxygen and nitrogen [28] and similar to the Cristal Metals process allows conversion from a batch process to a continuous one. Information on the process is limited and what is available comes from CSIRO themselves [28], but from what is available the advantages claimed over the Kroll process all revolve around the lower cost associated with a continuous process such as; large turndown ratios (fewer stops and starts), reduced labour costs, higher conversion rate [28]. However, much like the Kroll process many of the disadvantages still occur such as; use of chlorine gas (Cl_2) and TiCl_4 , which are hazardous, the requirement for an large inert atmosphere, the high cost of magnesium and the lack of *in situ* alloying possible in other processes.

1.2.1.3 CSIR Process

The CSIR process uses a continuous reduction of TiO_2 using TiCl_4 , following the same chemical reaction pathway as the Kroll process. The owners of the technology (CSIR) believe that a reduction in cost of 50% will be achieved, reducing price for 40 to 20 $\text{\$.kg}^{-1}$ for milled prod-

uct [29]. An additional drawback is that the resultant titanium is molten, compared to solid for the Kroll process, meaning an increased energy demand. However, confirmation of this information is difficult as very little has been published on the development of the process in open literature. The likely result is that the cost of titanium will be reduced but, as with Cristal Metals and TiROTM, this is an incremental improvement on the existing, high cost, Kroll process and downstream processing will remain equally labour and cost intensive.

1.2.1.4 Metalysis Process (formally FFC Cambridge process)

The Metalysis process, formerly the FFC Cambridge process, is the electrochemical reduction of a metal oxide to the base metal, which was first reported in 2000 [30]. The reduction cells consist of a titanium crucible containing molten calcium chloride (CaCl_2) in the temperature range of 800-1100°C. A graphite anode and a metal oxide cathode are submerged in the molten CaCl_2 and a maximum of 3 V is applied. The result is a progression through a series of reduction stages, which all link together as described by Schwandt [31]. Once progression through these reduction steps is complete, the formation of O^{2-} occurs, which reacts with the graphite anode to form carbon monoxide (CO) and carbon dioxide (CO_2). The result is pure titanium, with oxygen in solid solution, at the cathode. The full pathway is described in detail by Bhagat *et al.* [32].

1.2.2 Low cost titanium powder metallurgy

Attempts at reducing the cost of titanium is not only limited to the extraction of titanium, but involves the entire manufacturing chain as costs are relatively high at all stages. The relatively recent developments regarding low cost titanium powder has opened up an entire market focused on maintaining the relatively low-cost factor introduced with the new production methods and extending it to the downstream processing.

Powder metallurgy (PM) processing techniques make up a very mature field of research and their development has been driven by their flexibility to provide near-net shape products for increased material yields. Titanium powder metallurgy (PM) has only been utilised in bespoke applications in the automotive and aerospace sectors and is traditionally not used in mass production. The conventional PM techniques only enable small components to be manufactured and in limited size batches. Powder sources also tend to be lower quality than wrought alloys

(e.g. blended elemental) or too expensive, such as plasma rotating electrode powder (PREP), hydride-dehydride (HDH) and gas atomised (GA) pre-alloyed powder. In addition to the high expense of feedstock powders, PM routes have a high propensity for contamination, inclusions and porosity. Typically, methods such as Cold/Hot Isostatic Pressing (CIP/HIP), Extrusion or Direct Particle Rolling (DPR) are required to consolidate the particulate material into a green billet/sheet with further sintering to reduce residual porosity or forging to improve mechanical properties. Inert atmospheres are usually required to prevent significant oxygen pick up from the large surface area presented by the powder particles.

From the above arguments an ideal theoretical processing route through which to create low cost titanium parts from cost-effective powders can be inferred. From these points the size and shape of such parts can be limited to long, semi-continuous or continuous cross sections.

1. **Minimal Process steps** A suitable downstream process should have as few steps as possible between the input of powder feedstock and a final output product. This would reduce the energy involved in manufacture and hence the final cost of the product. A continuous process that involves negligible downtime for maintenance, changes to product size or shape and changes to feedstock chemistry would be the ideal solution. If powder can be consolidated into a final product in one or two stages, the number of companies involved in the supply chain for the product can also be reduced resulting in both lower costs and time-to-market for the product.
2. **No feedstock preconditioning** Many powder metallurgy processes involve multiple stages of powder preparation before consolidation can take place. Eliminating the need for powder preheating, powder or liquid binders and vacuum canning would further curtail the process' impact on final product cost.
3. **Insensitive to feedstock powder morphology or chemistry** The process should also be capable of consolidating a wide range of particle morphologies while still maintaining tolerable product properties eliminating the need for stringent upstream quality control or extensive powder separation steps. Sensitivity to changes in feedstock chemistry would also eliminate the need for time intensive modifications to tooling or process parameters and result in decreased capital costs for the manufacturing company.
4. **Operational in air** With titanium's strong affinity for oxygen and nitrogen many downstream processes are performed in inert atmospheres of argon, especially if the metal is

heated above its β transus where oxygen diffuses ~ 100 times faster than in the α phase. In order to negate this requirement the process must be ‘low’ temperature, i.e. well below the β transus. The process should also only hold the powder at temperature for a short time, of the order of seconds and may end with a quenching step to further minimise oxygen pickup.

5. **Properties similar to or exceeding Kroll/VAR wrought product** Using new ‘low-cost’ powders comes with a degree of uncertainty as to their initial purity and to the ease at which they will consolidate through different processes. The drive for lowering the cost of titanium should not come at the expense of performance by generating parts with high porosity or high density inclusions.

The ideal ‘low-cost’ downstream consolidation process should seek to reduce the price of titanium close to that of the metal it is trying to replace in the vehicle. While it may still have better physical properties than the current steel or aluminium parts replace, the overwhelming driving force behind its general uptake into the automotive industry is likely to be raw unit or tonnage costs.

1.3 The Conform process

Upon review of the available literature presented in chapter 2 it was concluded that conventional powder metallurgical techniques such as press-sinter (PS), hot isostatic pressing (HIP), direct powder rolling (DPR) and direct powder extrusion (DPE) were inadequate for the requirements outlined above. Both PS and HIP are limited by the end product size and require inert atmospheres or expensive steel cans. DPR and DPE also require inert atmospheres to limit oxygen pick up but also tend to require subsequent post-treatments such as sintering. DPE requires high preheat temperatures of above 1000°C , argon atmospheres and tends to be limited by billet sizes and expensive tooling costs. The process chosen for investigation for the subject of this thesis is the Conform Process; a true continuous process suitable for particulate feeds that requires minimal powder preconditioning. A proposed, ‘ideal’ processing route for automotive springs based on FFC-Conform technologies is shown in figure 1.4. While springs is the ideal, high performance product route to aim for there are many other possibilities for continuously extruded titanium wire/rod as shown in figure 1.5. The Conform process was, until commencement of the project, unproven with titanium feedstocks in all forms. There exists a large gap in the research community into the continuous extrusion (Conform) of high strength feedstocks and in particular, particulate feedstocks.

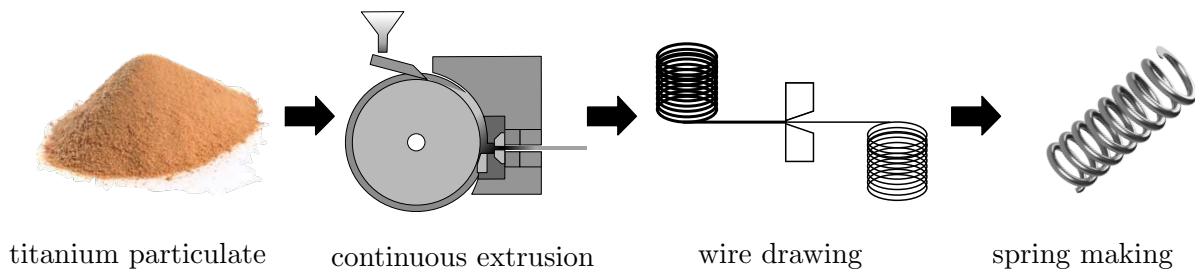


Figure 1.4: Processing route of low cost titanium particulates to generate a true step change in the cost of titanium parts for automotive spring applications

1.4 Thesis overview

The work presented in this thesis begins with a critical review of the current available literature for both severe plastic deformation batch and continuous powder metallurgy processes. The experimental methodology of trials conducted on a Conform machine at BWE ltd, Ashford, United Kingdom are described. A procedure for reading the machine output data is presented and described in such detail that it could be used in not only Conforming other metallic powders but rod feedstock too. The rod output from the machine is then analysed to determine how the powder was consolidated and the material flow in the Conform tooling. Macrographs illustrating the bulk flow of the powder during processing and micrographs showing the grain structure produced are presented.

An analytical model of the Conform process is derived using input from existing direct extrusion and Conform models. Finite element simulations using the commercial code DEFORMTM in both 2D and 3D are presented. Results are discussed in relation to the experimental trials and how they could help predict the process windows for new materials processed through Conform and other continuous extrusion machines. Finally the implications and impact of such a process are presented with the required further work in order for scale-up.

Please note that while in the final thesis results are presented so that FEM informs discussion of the experimental work, both work streams occurred simultaneously over the course of the project. This work is also extremely novel in the academic field and hence relatively little literature was openly available available to the author with most publications being historically restricted by industry.

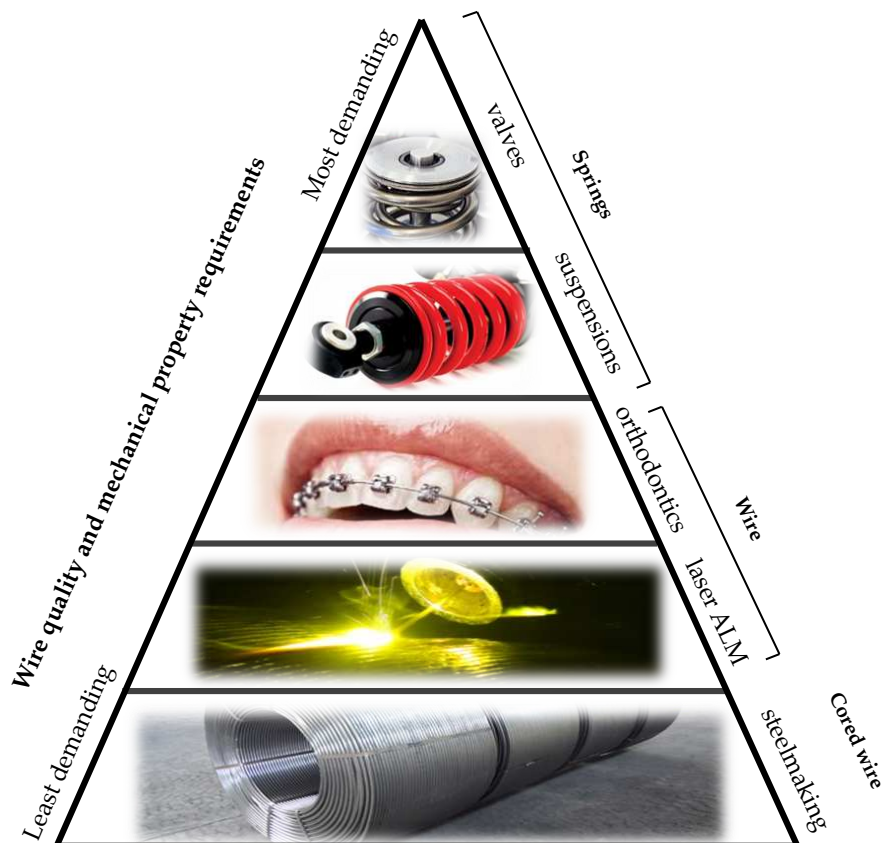


Figure 1.5: Pyramid showing the potential applications of Conform extruded titanium wire. Applications at the top of the pyramid are those that require the best mechanical properties in terms of strength and fatigue and hence are deemed the highest risk, highest reward.

Literature review

2.1 Titanium metallurgy

Titanium is an allotropic material, whose structure can exist in two crystallographic states. The alpha (α) phase has a hexagonal close-packed (HCP) structure while the beta (β) phase is body-centred cubic as shown in figure 2.1. Unalloyed titanium has a stable α crystal structure up to its beta transus temperature of 882.5°C where it transforms to the β phase at temperatures above this until reaching its melting point at 1678°C. Due to α titanium anisotropic nature there is a variation in properties depending on the how HCP phase is aligned to the direction of principle stresses. For example, the application of tensile stress directly along the HCP c-axis will yield an ideal elastic modulus of 145 GPa as opposed to the 100 GPa if the stress is applied at 90° to the c-axis. In reality polycrystalline titanium does not suffer as greatly from this anisotropic behaviour but it can have important implications for processing of high textured titanium product such as sheet and extrusions.

Deformation in α titanium is primarily through twinning as well as the more common dislocation slip. The available slip planes and direction are illustrated on the HCP unit cell in figure 2.2. There are 12 different slip systems consisting of the $\langle 11\bar{2}0 \rangle$ close packed direction and the (0002), three $10\bar{1}0$ and six $10\bar{1}1$ planes. The Von Mises Criterion for the plastic deformation of polycrystalline material requires 5 independent slip systems. The slip modes mentioned previously reduce to four independent systems due to rotational symmetry meaning that a combined $\bar{c} + \bar{a}$ system is also required in $\langle 11\bar{2}3 \rangle$ $11\bar{2}2$.

Completely pure titanium is not generally used in commercial applications and all forms have some degree of alloying additions. Elements are added to stabilise certain phases in titanium and are referred to as either α or β stabilisers. Interstitial elements such as oxygen, nitrogen and carbon tend to concentrate in the α phase and raise the beta transus temperature and hence are called α stabilisers. Beta stabilisers are classified into two groups i) isomorphous, which include other BCC metals such as vanadium, molybdenum and niobium and ii) eutectoid such as copper, manganese, iron and chromium. Both types of β stabilisers lower or suppress the β transus

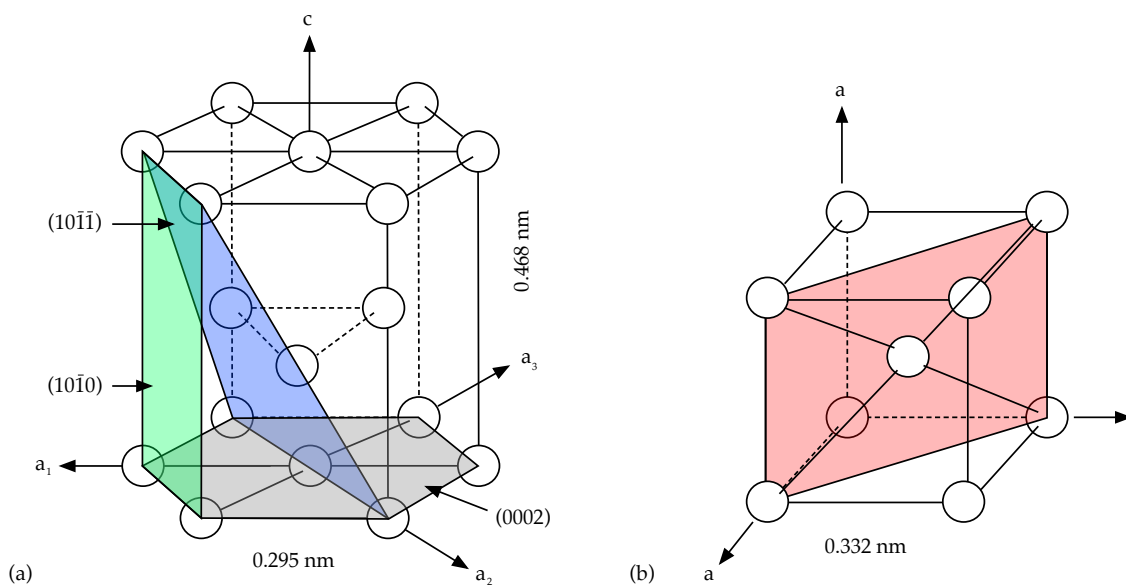


Figure 2.1: Unit cells of a) HCP α and b) BCC β phases in titanium with their respective lattice parameters and main deformation planes indicated. Reproduced from [5].

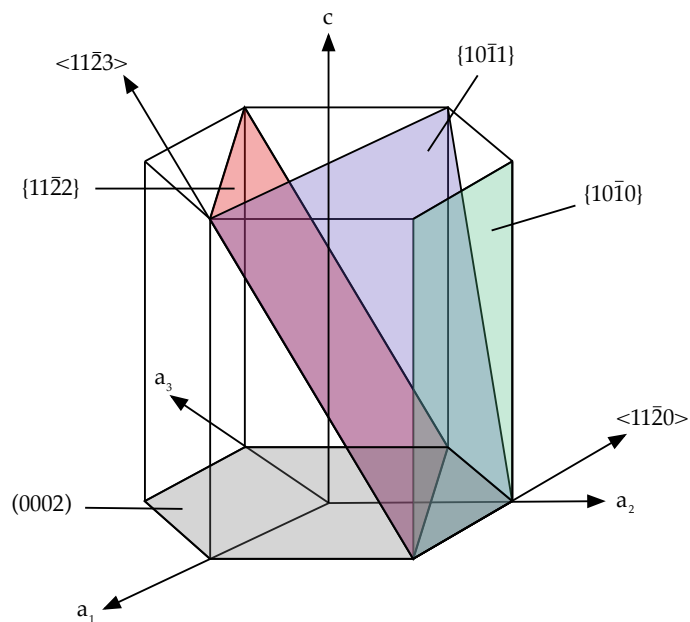


Figure 2.2: Slip planes and directions in the titanium HCP α phase

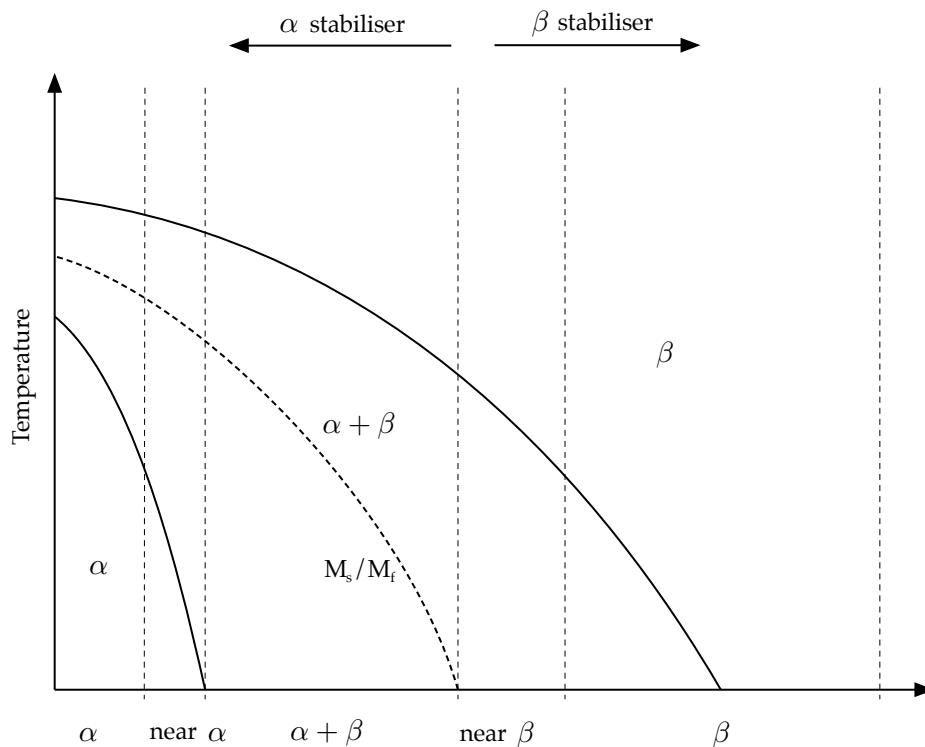


Figure 2.3: Pseudo phase diagram for the addition of alpha and beta stabilising elements in titanium alloys

temperature enabling a larger proportion of this phase to be retained at room temperature. The alloy chemistry is only one way of manipulating the resultant phase percentages in the final titanium product as the equilibrium state is often different to that attained through the addition of thermomechanical treatments. Through the addition of work and heat into the titanium matrix the mechanical properties can be optimised for certain applications. Table 2.1 shows the advantages and disadvantages on the mechanical properties of titanium alloys by generating certain microstructures.

Commercially pure titanium (CP-Ti) has four ASTM grades, numbered 1-4 with each increasing alloy number containing larger percentages of oxygen and iron additions. The interstitial element oxygen is a particularly important alloying addition in titanium alloys. In CP-Ti oxygen is added in a controlled manner to raise the strength of the alloy from 0.18 max wt.% (ASM grade 1) with a yield strength of 170-310 MPa to 0.4 max wt.% (ASM grade 4), which provides a yield strength of 480-550 MPa. As oxygen concentration goes up, ductility drops until the metal matrix is embrittled. It is this strong effect on mechanical properties and α phase stabilisation, coupled with titanium's strong affinity to oxygen that makes it difficult to process. Inert or vacuum atmospheres are frequently employed to limit oxygen, nitrogen and hydrogen pick up, all of which have deleterious effects on surface mechanical properties.

Table 2.1: Property improvement and degradation as a result of certain microstructural features in titanium alloys.

| Feature | Enhances | Degrades |
|-----------------------------|--|--|
| Equiaxed α | Strength Ductility Fatigue initiation resistant | Fracture toughness Fatigue crack growth resistance Notched fatigue resistance |
| Widmanstätten α | Fracture toughness Fatigue crack growth resistance Notched fatigue resistance Creep | Strength Ductility Fatigue initiation resistance Low cycle fatigue resistance |
| Bi-modal α | Strength Ductility Fatigue initiation resistance Low cycle fatigue resistance | Fracture toughness Fatigue crack growth resistance |
| Colony α | Fracture toughness Fatigue crack growth resistance Notched fatigue resistance | Strength Ductility Fatigue initiation resistance Low cycle fatigue resistance |
| Coarse prior β grains | Fracture toughness Creep | Strength Ductility Fatigue initiation resistance Low cycle fatigue resistance |
| Fine prior β grains | Strength Ductility Fatigue initiation resistance | Fracture toughness Notch fatigue resistance |
| Grain boundary α | Fracture toughness Fatigue crack growth resistance Notch fatigue resistance | Ductility Fatigue initiation resistance Low cycle fatigue resistance |

2.2 Severe plastic deformation processing

Severe plastic deformation (SPD) processing is typically defined by the application of very large plastic strains within a metal in order to produce an ultra-fine grained microstructure. The aim of SPD is to artificially increase the strength of the bulk material by taking advantage of the Hall-Petch strengthening effect [33] [34]. Hall-Petch strengthening is governed by equation 2.1 where σ_0 is the friction stress and A is a constant and states that the yield stress of the material increases with the square root of the grain size.

$$\sigma_y = \sigma_0 + Ad^{-1/2} \quad (2.1)$$

While large increases in proof stress and UTS are possible through SPD processing, most processes are limited in their product size. Processes such as equal channel angular pressing (ECAP) [35] and high pressure torsion [36] or geometrical variants thereof are used to produce ultra-fine grained materials for small scale applications such as dental implants [37]. The increase in strength induced by strain hardening in process such as rolling, drawing or extrusion can also reduce the ductility of the final product. During SPD processing it has been found that nano-sized grains increases the ductility of the material [38]. SPD produced products are sought after for their combined high strength and high ductility.

2.2.1 Discontinuous SPD processing

2.2.1.1 Equal Channel Angular Pressing (ECAP)

Although the concept of ECAP was developed by Segal in 1972 most research was initially only published by Russian researchers in their native language, which stalled progress in the rest of the world. Interest grew in the 1990s as research demonstrated the process's ability to generate ultra-fine grained and nano-structured metals. ECAP functions by passing a billet through a die with two intersecting channels of equal cross section positioned at some angle. As the billet is deformed through a simple shear and passed through the channel [35] as demonstrated by the example unit in Figure 2.4. For a single pass the strain experienced in the centre of the billet is typically of the order of 1-1.5 depending on the die angles [35, 39–41]. The billet is usually passed back through the die up to 16 times, sometimes with rotations to the billet in between passes to further work the material and create an ultra-fine microstructure.

Four separate routes have been suggested and reported for the reinsertion of the billet during

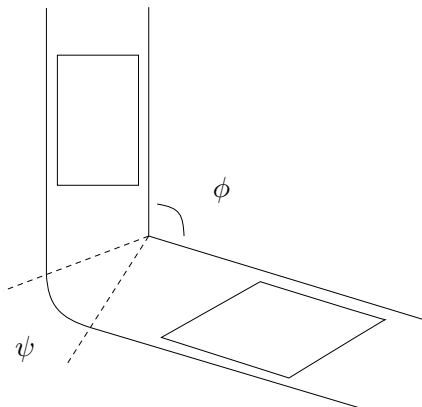


Figure 2.4: Schematic representation of the ECAP Process and deformation of a unit volume.

multiple pass ECAP and each involve rotating the extruded billet by a certain angle around its long axis. Route A involves a 0° rotation and hence the shear developed is compounded on each subsequent pass. Route B requires a $\pm 90^\circ$ rotation so that for each even pass number the billet is returned to its original orientation. Route C is similar to Route B but has a 180° rotation between passes and Route D has a 90° rotation in the same direction so that the original orientation is returned after multiples of four passes (See Figure 2.5). Other routes such as BC and BA, which are composites of the main four routes have also been used to tailor the accumulated strain through the billet for microstructural control [42].

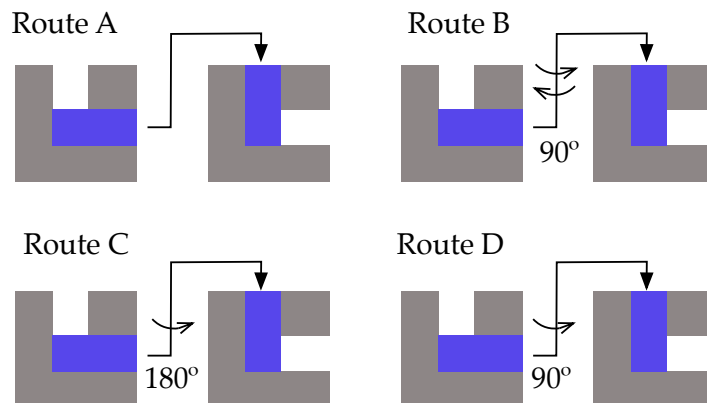


Figure 2.5: Representation of the four main multiple pass ECAP processing routes.

Despite the suitability of ECAP to produce novel nano-structured materials it is ultimately limited by small billet sizes and very high die loads. The feedstock billet also needs to be pre-heated in order increase its ductility, limit product cracking and can only be operated with one billet at a time [35]. Multiple passes through the ECAP die are required to create an ultra-fine grain structure. The inhomogeneity of the deformation field at the front and back of the billet

also reduces the usable length of material. Powder consolidation through ECAP requires more than one pass to ensure adequate particle breakup and oxide dispersal [43]. This is a problem that would limit ECAP commercialisation to high-cost/ low volume applications. Other processes have been suggested to circumvent these issues such as ECAPConform [44,45] where a high friction wheel continuously pulls rod feedstock around its circumference into an angled die. Other continuous techniques have been highlighted such as Rolling-ECAP and LINEX-ECAP [46]. Theoretically an infinite length of material can be processed and the only limits are set by tool wear, storage of the feedstock/product and reinsertion for multiple passes.

Published literature on the subject of ECAP has mainly focused on aluminium alloys due to their relative ease of deformation, however modern research trends point to difficult-to-work metals such as magnesium and titanium alloys. Both pure Ti and commercially pure Ti of various grades have been processed through ECAP under similar conditions [42,47–51]. The research has many similarities; following a processing schedule of 8-12 ECAP passes at warm temperatures ($\sim 400^\circ\text{C}$) created a grain size of 200-300 nm, which appeared to be the limit of grain refinement as further passes did not result in smaller grains [51]. Only small differences in end product grain sizes were observed when the ECAP route was changed. Changes in process temperature only affected the number of passes required to attain the minimum grain size. Lower purity titanium such as grade 4 also created a stronger final product than pure Ti. Ductility was reduced in all cases down to elongations of $8\pm 3\%$.

Subsequent processing of ultra-fine grained titanium from ECAP has also been reported [42,48,52]. Cold extrusion of pure Ti following eight pass warm ECAP increased the material's UTS from 460 MPa to 1050 MPa. Cold rolling of the ECAP billet resulted in a similar increase in strength when the cross section reduction was similar to that performed in the cold extrusion ($\sim 50\%$). It is therefore feasible to assume that if in-line continuous post-processing via rolling is possible from a cost and engineering standpoint that increased mechanical properties may be generated within mill product consolidated from powder feedstocks.

Direct titanium particulate processing via ECAP has been reported in the literature [43,53,54] utilising a back-pressure plunger to constrain the particles. CP-Ti grade 2 machining chips were consolidated via ECAP for two, four and eight passes at temperatures of 450°C and 590°C . It was found that the consolidated billet strength decreased with increasing passes contrary to solid billet ECAP and that the mean grain size for eight passes at 590°C was essentially the

same as the original chips. Micrographs showed significant elongation and alignment of chip boundaries during the first four passes, but experienced significant breakup during the next four passes. From this work it was suggested that the higher temperatures result in significant recovery and recrystallisation, which counteracts the grain refinement at lower temperatures [43].

It is clear that powder processing via the ECAP process is not feasible in generating a semi-continuous or fully continuous cost effective consolidation route. However the research in this area is at a far more mature stage than powder processing via severe plastic deformation of other methods. A lot is known about the mechanics of ECAP and how changes in die geometry and temperatures affect the resultant billet's microstructure and properties. There are geometrical and physical similarities between both ECAP and the processes detailed in the following sections.

2.2.1.2 Friction Extrusion

Friction Extrusion can be split into two types; Friction Stir Extrusion (FSE) and Direct Friction Extrusion (DFE) (see Figure 2.6). Unfortunately there is a lot of confusion in naming conventions in the literature and DFE is often referred to as Friction Stir Extrusion due to its prevalence over true FSE. FSE is extremely similar to friction stir welding and high pressure torsion where a circular tool is plunged into a flat cylindrical sample to induce severe plastic deformation and refine the grain structure. In true FSE the tool has a hole in its centre where processed material is back extruded while the tool rotates and plunges into the work piece [55]. FSE is severely hindered as a commercial process by its small product size due to the small plunge distance and high back pressures. Due to this, the process is limited to lab scale research and high-cost/small-volume applications. The DFE process has much in common with indirect extrusion where the die is moved into a stationary billet and container. In DFE the container and billet rotate rapidly (~ 100 's RPM) while the die is moved. Using DFE with particulates enables rapid heat input without feedstock preheating and a very long strain path to generate the conditions for successful consolidation.

ORNL successfully extruded various lengths up to 16 ft of various Al-6xxx alloys from machining chips as well as co-extruding 6xxx/13xx powders [6]. Various degrees of success was reported in terms of product density, defects and quantity of extrusion. It was noted that the main limitation on extruded product length was the available volume in the extrusion container.

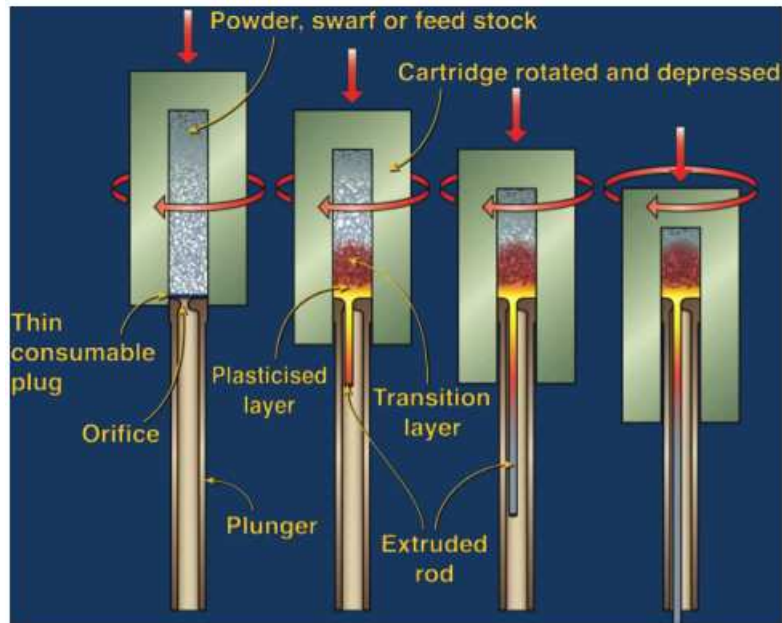


Figure 2.6: Schematic of Direct Friction Extrusion Process. Often referred to as Friction Stir Extrusion in the literature. Reproduced from [6]

Microstructures were shown but no discussion of grain sizes was offered, only that there was a mixture of fine and coarse grains. This was probably a result of the wide range of temperatures that the feedstock was exposed to ($\sim 0.3 T_m$ - $0.8 T_m$). The process development was targeted at the power generation market with no discussion of any structural applications. The inherent batch process could be seen as a major limiting factor in the commercialisation of DFE. Despite this apparent limitation the industry has predicted extremely large energy savings if DFE were to be used to process aluminium machining swarf rather than remelting. Conservative estimates of the size of the global secondary aluminium industry places it at 16.7 million metric tons in 2011. If DFE were to be employed globally then there would be savings of 2.5 TBtu (733 GWh) by 2025. For comparison the whole of the United Kingdom used approximately 302 GWh of electricity in 2014 [56]. The operational costs of DFE were estimated to be $\sim 20\%$ that of secondary aluminium melting and casting but the authors admitted there was no reliable data on the process scale up.

2.2.2 Continuous SPD processing

2.2.2.1 Direct Particle Rolling

Direct Particle Rolling (DPR) has been shown to produce a near fully dense sheet product direct from powder. Processing involves pouring loose powder between two rolls positioned

so that powder will fall under gravity through the gap between them. If the gap is set such that there is significant bridging within the bulk powder a large shear zone forms between the rolls generating the required pressure and heat to partially consolidate the powder. Long strip product has been successfully produced with ‘low-cost’ TiRO™ Ti-6Al-4V and CP-Ti powders by CSIRO [7]. They achieved 580 mm of 130 mm wide strip at $0.75\rho_0$ before hot rolling at 1300°C and annealing at 750°C to obtain almost full density ($0.996\rho_0$). Figure 2.7 details the production route used.

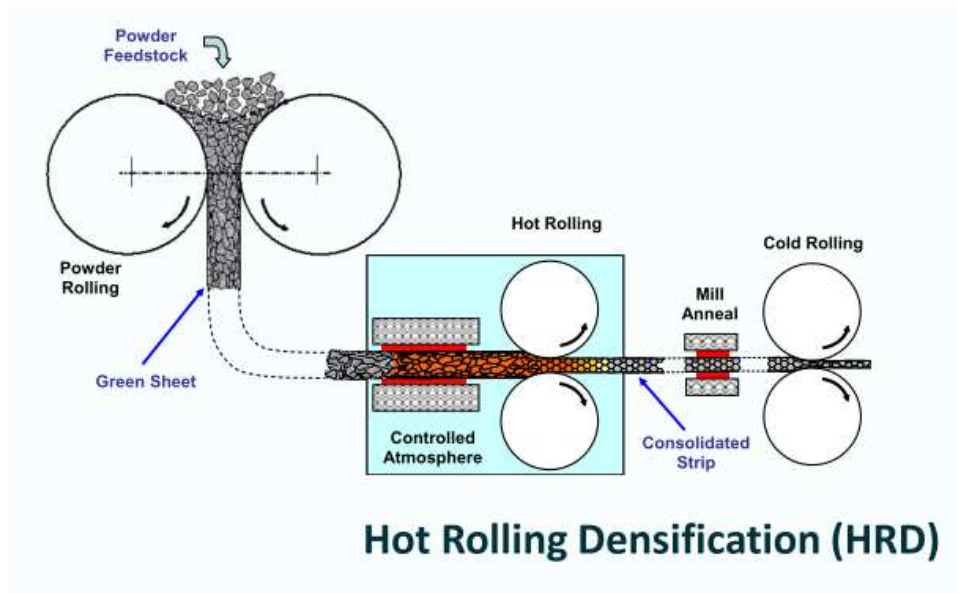


Figure 2.7: Schematic representation of the CSIRO Direct Particle Rolling (DPR) process using TiRO™ powders (Also known as Hot Roll Densification (HRD)) [7]

Of particular interest is a review by Dube *et al.* [57] who detailed the mechanics of the DPR process. The literature shows that there is an optimum gap between the rolls required to consolidate powders of different size fractions for a given roll speed. Furthermore, while full consolidation can be achieved in iron powders at low roll surface speeds of $0\text{--}100\text{ mms}^{-1}$ speeds faster than 250 mms^{-1} resulted in a change in the flow behaviour of the powder. Fast wheel speed resulted in the powder being dragged through the roll gap and fluidising with the effect becoming more pronounced for smaller rolls gaps. Similarities can be drawn between the consolidation behaviour in DPR and that occurring in Conform/CRE within the abutment-groove flash gap (see section 2.3). Particle size and morphology may need to be optimised depending on the flash gap, required product properties and how the CRE process responds to such changes in feedstock.

2.2.2.2 Continuous Equal Channel Angular Pressing - (ECAP-Conform)

ECAP-Conform process has a very similar design to the discontinuous and more common equal channel angular pressing (ECAP or ECAE) in that a solid billet is fed through a channel with a continuous cross section and extruded at some angle, ϕ , from the input channel (see figure 2.4).

In ECAP the extrusion force is provided by a ram, designed to completely fill the channel and push the billet through the die. The extrusion force for ECAP-Conform is provided by a grooved wheel which drags the workpiece rod around its circumference until it is diverted into the die by an abutment member which protrudes into the groove. While increased friction presents problems in ECAP due to the resultant increase in extrusion force, ECAP-Conform relies on a this friction for successful extrusion. Segal [46] detailed the mechanics of ECAP-Conform explaining the importance of friction in the wheel groove to drive the process and suggesting how such a continuous process might develop into a commercially viable process. Al-6061 was processed through Conform-ECAP by Xu *et al.* [45] and the average grain size was reduced from $\sim 350 \mu\text{m}$ to $\sim 150 \text{nm}$ in four passes using the BC route, which is the combination of Routes B and C in figure 2.5. The microstructure differed greatly from standard ECAP in that the grains were elongated rather than equiaxed but no plastic anisotropy was found during mechanical testing.

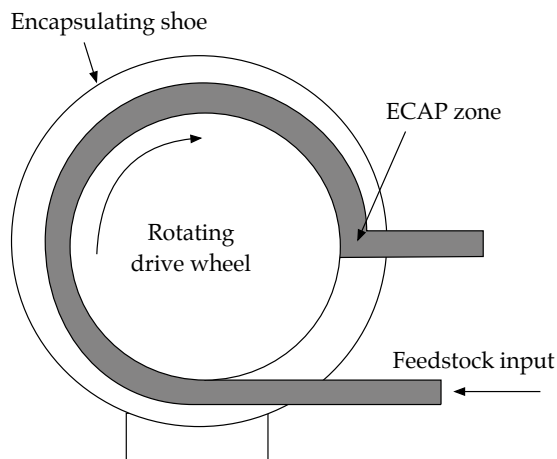


Figure 2.8: Simple representation of the ECAP-Conform process. Reproduced from [8]

A few papers demonstrate the use of ECAP-Conform to produce a nano-scale structure of $\sim 200\text{-}300 \text{nm}$ grained rods of grade 4 CP-Titanium with a final drawing step to produce a round cross section rod [58–60]. Tensile properties were found to far exceed that of conventionally produced grade 4 rod following six passes/subsequent drawing with 0.2% proof stress of 985/1300 MPa and UTS of 1085/1350 MPa. Grade 2 CP-Ti was also processed on the same schedule and

found to have strength properties only 150-200 MPa lower than those of the Grade 4 rod due to the lower quantities of impurities.

While ECAP-Conform has been proven to produce very fine grained microstructures within titanium, research has been limited to relatively short lengths of rod (~ 6 m) and require several passes. Single pass ECAP-Conform results have not been explicitly reported but it is expected that intermediate annealing steps would be required in order to limit cracking within the extruded product. There is no known modification to ECAP-Conform that would allow for powder feed so pre-extrusion of a green powder billet would need to be conducted to produce a suitable feedstock for the process.

2.3 Conform process¹

The Conform process is a continuous severe plastic deformation thermomechanical processing route which derives the extrusion force from the friction between a rotating grooved wheel and the workpiece being extruded. The process was invented by Derek Green at the UK Atomic Energy Authority (UKAEA) and was initially detailed in a patent in 1973 [62]. During processing a shoe member retains the workpiece within the wheel groove and is attached at a pivot point below the wheel so that during operation the forces on the tooling force the shoe onto the wheel. The shoe and tooling are preheated, typically to 300-500°C by induction coils in the shoe before the apparatus is moved into position against the wheel. The machine is designed such that the tools (die chamber, die, abutment and entry plates) are all replaceable as these can suffer from the greatest wear during service. Figure 2.9 shows a schematic representation of a Conform machine in its modern form and modified for powder feeds. Several other similar designs have been developed at Southwire Company [63, 64] and BWE Ltd. [65].

Conform processing of powder feeds involves using a gravity feed hopper positioned on top of the machine so that powder either falls directly into the groove or is guided via a vibrating chute. Once in the groove the powder falls under gravity into the abutment zone where it begins to be consolidated. During the process startup, a small volume of powder is lost through the

¹Please note that the process names Conform and Continuous Rotary Extrusion (CRE) are sometimes used interchangeably as the processes are very similar in their tooling designs and operation. The name CRE was used by companies such as Meltech CRE so as to not infringe upon the Conform trademark owned by BWE Ltd. following lengthily litigation issues over the trademark in the 1990s [61]. CRE differs from Conform in that the tools and surrounding shoe are retained by hydraulic rams positioned to give translational control in the vertical and horizontal directions as opposed to the rotational control in a Conform machine. The topology of the tools also differ but the core points of contact with the workpiece remain almost identical between both Conform and CRE as both processes evolved from the same concept.

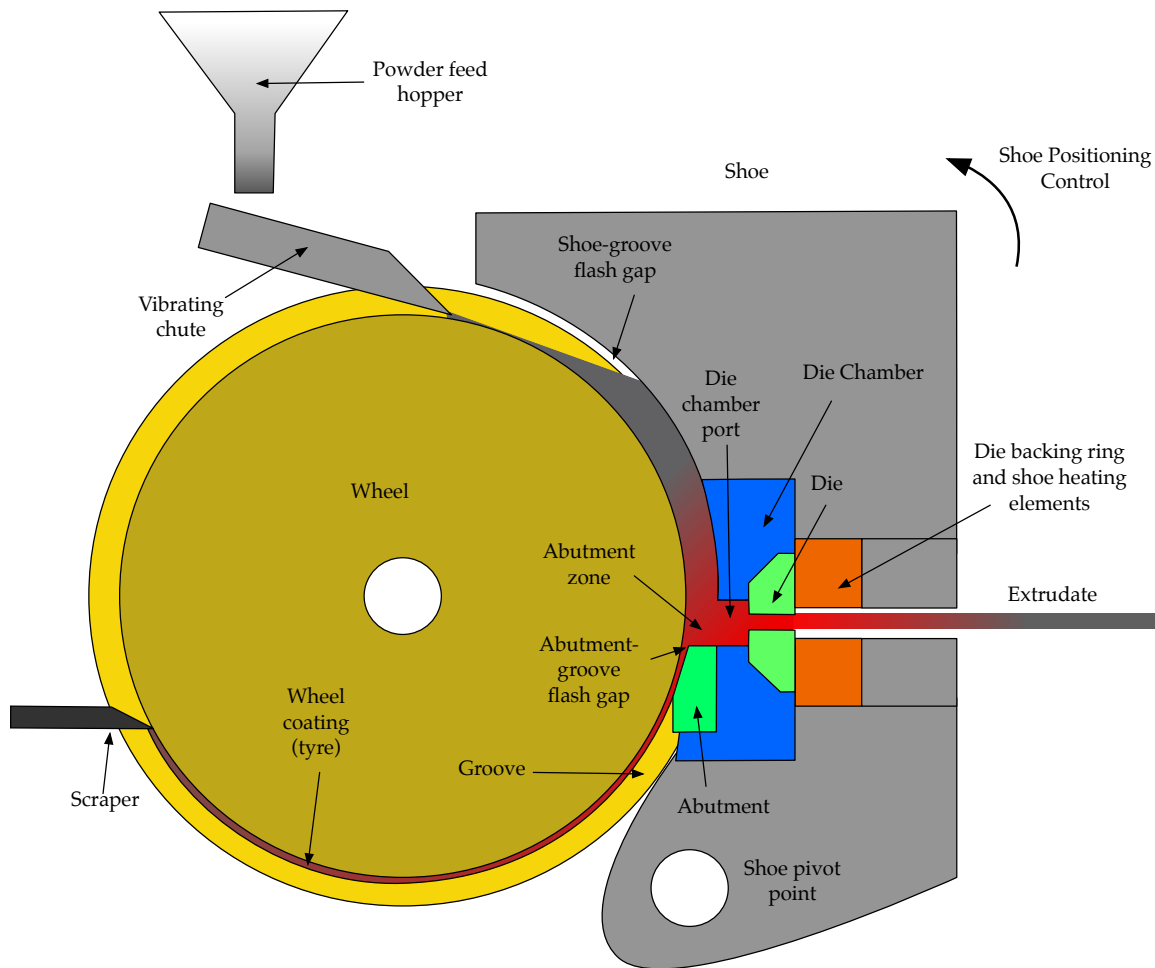


Figure 2.9: Schematic of the modern day Conform process with modifications for direct powder feed into the groove. Reproduced from [9]

flash gaps (within the groove and between the wheel outer surface) but yield loss through this route is significantly reduced once powder consolidation begins. As powder is consolidated in the flash gap the wheel is coated in a ‘tire’ of processed metal. Once the wheel is coated fresh powder fed from above is contained within the groove by the coat and the abutment. The high friction and shear of the wheel against the powder and between individual powder particles imparts significant amounts of heat to the powder bulk. In turn the mechanical deformation of the powder particles causes local particle to particle welding to occur, consolidating the once loose powder. Once the powder is consolidated above the abutment there is sufficient pressure generated by the wheel to begin extrusion. The consolidated powder then flows through the path of least resistance, through the die chamber port into the die. Sufficient pressure is then generated in the port and the metal is extruded through the die to form a fully dense rod. The rod travels a short distance in air before entering a cooling trough where it is quenched before being coiled for storage or transportation. A wide range of product profiles can be produced

from Conform machine typically require no further down stream processing before they are used (see figure 2.10)

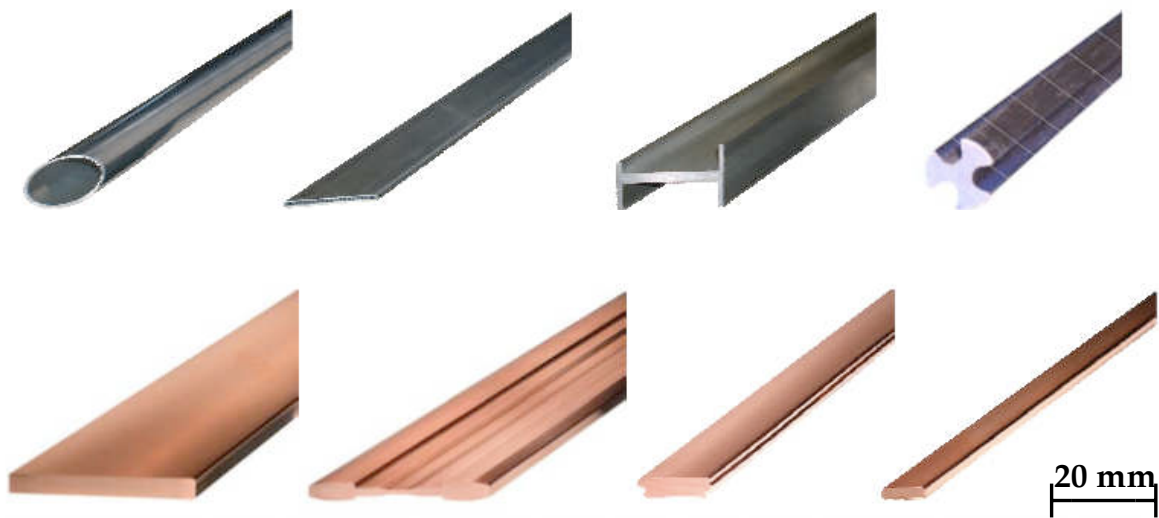


Figure 2.10: Range of possible extruded profiles in aluminium and copper from a BWE Ltd. Conform machine [10]

2.3.1 Conform of particulate feedstock

There are several parts of the Conform process that are of particular interest when a powder feedstock is considered. When the powder is fed into the moving wheel groove there is almost zero work performed on the particles within the channel. These particles will simply fall into the abutment zone through a combination of gravity and minor frictional effects from the wheel. As more powder is pushed into the channel the abutment zone fills up with powder until the packing density equals that of the powder's tap density. Particle porosity, yield strength, size, morphology and hence degree of cohesiveness and interlocking would then influence the exact compaction behaviour. The pressure increases in the abutment due to the addition of more powder within the channel and the force from the high friction wheel interface causes local yielding of the particle to particle contacts. The amount of work generated is sufficient to break oxide layers surrounding the particles and result in welding of the powder into a fully dense bulk structure. The pressure required for this compaction is balanced by the required pressure for the lateral extrusion. The general conclusion from the literature is that the Conform or CRE processes are a combination of DPR, ECAP and Direct Extrusion. Similarities can be drawn between the roll gap/speed in DPR and the flash gap/wheel speed in Conform, likewise the pressure and temperature effects in ECAP and Direct Extrusion of titanium and its alloys will give a strong indication of the likely process parameters and rod properties that would be

observed in the Conform of these feedstock metals.

To date much work on direct consolidation of metallic powders into product have speculated, with logical reasoning, the impact that variation in powder properties (i.e. particle size, distribution, porosity, morphology and yield strength) would have upon individual processes rather than demonstrated experimentally. However, of the available experimental work some trends can be identified. Firstly, studies of powder morphology in direct particle rolling show that completely spherical particles are undesirable for compaction, as they lack the necessary friction and interlocking behaviour observed with angular morphologies [66]. Alternatively use of overtly angular particles can cause increased interlocking and therefore give a significantly reduced and irregular flow, which is also undesirable. This has been demonstrated by Etherington [13] who observed blistering and fold defects and is supported by work published by Chikosha *et al.* [67].

Secondly, post compaction density is seen to increase with increasing particle size, up to a point [67], with particles larger $\sim 300\text{-}400\ \mu\text{m}$ makes consolidation difficult. However, work by Eborall [66] shows the reverse of this trend, the reason for this being that the roll gaps applied during their work were so small ($-0.15\text{ - }0.15\ \text{mm}$) that particles were unable to enter the roll gap parallel to the rolling force, this means generating sufficient force to cause welding of particles to be increasingly difficult.

The first noted report of the material properties resulting from the Conform process was presented by Marsh in 1977 [68]. The Conform of copper was initially of great interest because of its potential low cost application to the continuous production of power cables. Marsh [68] Conformed both 8 mm/9.5 mm copper rods to 2 mm/2.4 mm respectively with a 300 mm diameter at a wheel speed of 12 RPM. Copper powder was also reported to have been Conformed to 2 mm rod in the same study. The initial grain size of $150\ \mu\text{m}$ was reduced to about $10\ \mu\text{m}$ in the high shear region and $30\text{-}40\ \mu\text{m}$ elsewhere in the extrudate. The grains were stated as being equiaxed following recrystallisation during/after the process. The consolidated powder rod had a fine grain structure, which might be assumed to be typically less than the $10\ \mu\text{m}$ of the rod fed product. The fine grains did not experience appreciable growth during annealing at 400°C despite the 17% loss in 0.2% proof stress, presumably solely due to static recovery or remnant dislocations. The lack of grain growth was suggested to be a result of oxide dispersal from the surface of the powder particles during processing [18], which would suggest that dislocation an-

nihilation was the dominant recovery mechanism to explain the reduction in proof stress rather than grain growth resulting in a reduction of Hall-Petch strengthening. Oxide inclusions were also suggested as a strengthening mechanism in the ECAP of CP-Ti swarf [43, 53, 54] but such a process has not been corroborated by others. Metallography of the cross section revealed a small triangle of oxidised material extending $50\ \mu\text{m}$ into the bulk of the rod and was attributed to the collection and slow extrusion of such material from the dead zone above the abutment. The importance of this triangular zone was that it was fully coherent with the bulk material and did not negatively affect the fracture behaviour of the rod during tensile tests. The oxide material was hence tolerated in the final properties of the rod and might backup the idea that the grain structure was strengthened by oxide dispersoids.

From the first development stages of Conform the concept of processing granulated materials was accounted for as a solution to recycling large quantities of chopped aluminium and copper electrical cables. It was first mentioned in the wording of the original patent [62] and worked on by a team at United Kingdom Atomic Energy Authority (UKAEA) in the following decade [11, 13, 18, 69]. Etherington successfully extruded lengths of rod from particulate feedstocks of chopped copper wire, copper alloy powder, aluminium granules and an unspecified aluminium powder. Detailed investigations were not carried out into the mechanics of how powder compaction took place and data on the exact process parameters were not reported. However it was found that the powder used created an irregular feed flow into the 8 mm channel and this resulted in blistering and fold defects. This may have been due to inclusions of flash back into the process but evidence to this effect was not presented. A unique flow profile in the as-extruded rod was found (Figure 2.11) due to oxide stringers. Other such defects were thought to be caused by potential contamination from either insufficient cleaning of lubricant from the particles or leftover wire insulation from the recycled copper. It was found that the wheel groove size had to be made big enough to allow sufficient packing of chopped cathode wire for consolidation and extrusion to take place.

Macrostructures similar to those observed in Etherington's work [11] were observed by Stadelmann [12] as shown in figure 2.12. It is therefore reasonable to assume that these are characteristic macroscale flow structures, unique to powder feedstocks as they are not reported in any work involving rod feeds.

Adkins and Tsakirooulos [70] compared the effects of Conform and standard direct extrusion routes on two similar gas atomised powder Al-Cr-Zr-Mn alloys; one solute lean and one solute rich. Two separate size fractions of powders were used $45\text{-}200\ \mu\text{m}$ and $45\ \mu\text{m}$ both

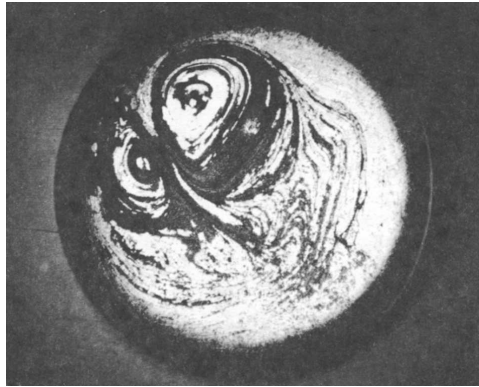


Figure 2.11: Macrograph of the flow within a rod sample Conform extruded from DryFlo Copper [11]. Scale not reported.

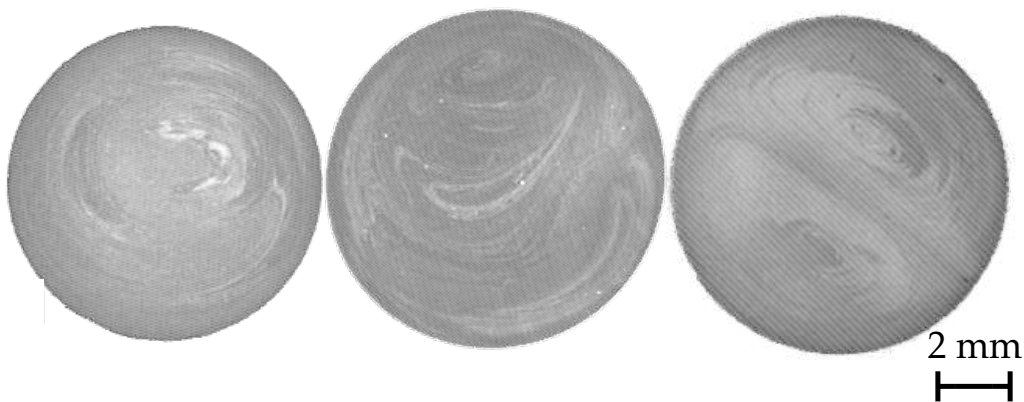


Figure 2.12: Representative macrostructure flow pattern within aluminium rod extruded via CRE using pure aluminium powders. Reproduced from [12]

of which contained particles that were spherical in nature. Some also had satellite particles attached to their periphery, which may have helped to improve the particle interlocking during deformation. The Conformed powders were consolidated but resulted in inconsistent extrusion conditions and samples were only taken from appropriately consolidated sections of the rod. The as-Conformed microstructures were undisclosed except for comments on the precipitation of dispersion strengthening species during aging heat treatments. Very little was concluded about the difference in the two processing routes on the alloys as the research focus was on the development of the two alloys. They did however comment that the canned extruded powder resulted in a “stronger and harder product than the Conformed product” but quantitative data was not reported. Detailed information about the Conform process conditions would be required for adequate comparisons to be drawn between it and canned direct extrusion.

Katsas *et al.* [71] also Conformed aluminium powders and it was found that a novel microstructure was produced with fine and coarse grains of average $1.6 \mu\text{m}$ in size. The cross

section of the extruded rod exhibited a ring-like structure with a denser ‘onion-skin’ like structure nearer the edges of the cross section. The structure can be partly explained by the unusual processing of powdered materials via Conform from the wheel shear to the abutment zone and extrusion die. The exact mechanism of powder flow and material flow through the process is not very well understood, which is a limiting factor in enabling microstructural control in Conform extrusions product. To the author’s knowledge no published literature has attempted to discuss the unusual macro flow within the resultant microstructure. Few papers publish microstructures relating to the processed Conform material, and those that do fail to present the full cross sectional view to show the heterogeneity in the microstructure.

CSIRO, Australia were the first group to publish information relating to the Conform of titanium powders from the in-house TiROTM process [72, 73]. The powders were preheated to temperatures in excess of 1000°C in a hopper before being fed into the machine. Throughout the entire process the powder was shrouded in argon to prevent unwanted oxygen pickup, requiring extensive modification of the machine. While the patent [72] is extensive in its description of certain parameters in the Conform process to extrude TiROTM titanium the broad process window in the claims means there is no certainty as to the exact process window used the reported work presented to the public [73]. The extensive preheating of powders means that even with a protective atmosphere of argon the small amount of oxygen remaining in the machine will be soaked up into the powder, greatly increasing the interstitial oxygen and decreasing the ductility of the extruded rod.

2.4 Modelling the Conform Process

2.4.1 Analytical models

The simplest approximation for how the Conform process works was presented by UKAEA during their development. In direct extrusion where the extrusion pressure is generated by a punch at the rear of the billet, the friction generated between the extrusion container and billet is a significant hindrance to the process. Indirect extrusion on the other hand removes this barrier by keeping the billet and container stationary and pressing the die into the billet. Once sufficient pressure has been generated, the billet deforms into the die and is extruded in the opposite direction to the die’s movement. Etherington [13] explains that if the billet was sufficiently long, the friction contact between the billet and container would be sufficient to resist the force applied by the die and hence the punch or retaining cap could be removed

from the equipment. It was noted that once the die had travelled a certain distance there is a critical billet length below which there would not be sufficient friction generated to continue the extrusion. As the ram could theoretically be removed it was postulated that there was no limit to how long the billet could be. UKAEA therefore developed the continuous extrusion principle that is demonstrated in Figure 2.13 where they assume a rectangular ‘billet’ container, bounded on three sides by moving walls and retained by a stationary fourth wall. A stationary die is included to allow extrusion parallel to the direction of the drive force generated by the moving walls.

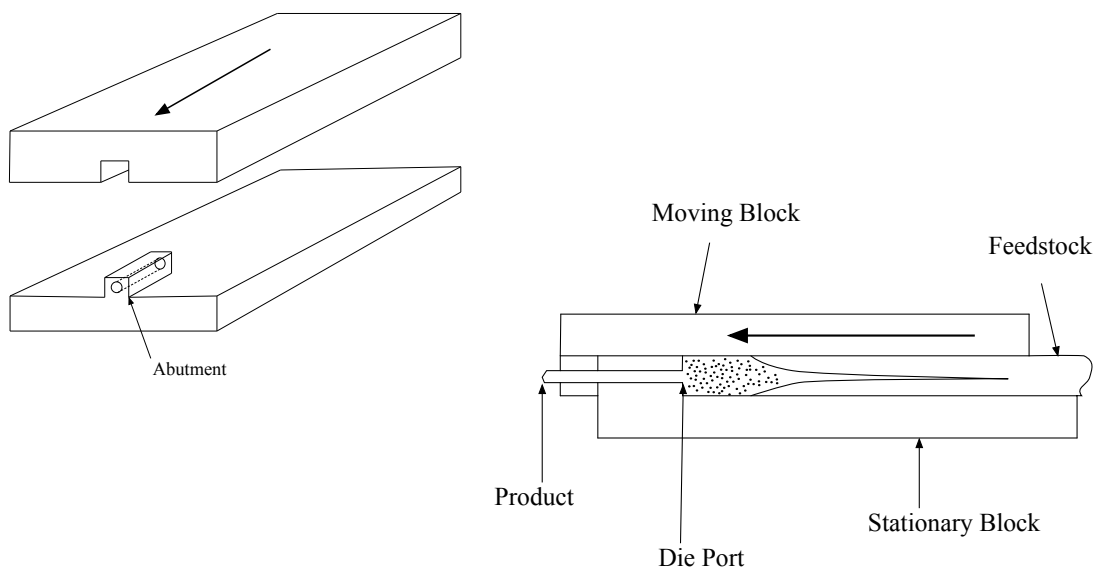


Figure 2.13: Concept drawings of early ConformTM theoretical designs. Redrawn from [13]

While the process concept illustrated in Figure 2.13 is inherently discontinuous, if the moving walls are replaced by a grooved wheel and the stationary block with a curved shoe the modern ConformTM process takes shape. Further modifications to the original concept plans include provision for radial as well and tangential extrusion allowing for easier product take-up and retention of loose powder feeds.

The original UK patent [62] showed basic calculations relating to the mechanics of the process. As the solid rod workpiece is fed around the circumference of the wheel it experiences a small amount of plastic deformation which increases with decreasing wheel radius. When it reaches the abutment it was stated that the resultant force acting on the material results in an applied extrusion pressure. This pressure acts on the abutment face over area A , which is

roughly equal to the cross sectional area of the wheel groove if the flash gap is neglected. They assume a square channel cross section so that $A = w^2$ and that the abutment face surface area is exactly equal to this. Assuming a Tresca yield criterion they produce a simple equation for predicting the extrusion pressure, P , given the material yield strength and the channel width w . l is the contact length along the circumference of the wheel between it and the workpiece and $\sigma_y = 2k$, where k is the shear strength of the material.

$$P = \frac{\sigma_y l}{w} \quad (2.2)$$

This is an extremely crude way of calculating extrusion pressure but it can assist in giving a rough determination of whether a material can be extruded or not based on the abutment and die material yield stresses. Further detailed analysis of the basic process with a tangential extrusion is detailed by Tirosh *et al.* [74]. Tirosh *et al.* were successfully able to predict the optimum shoe coverage and wheel load for a given wheel diameter and extrusion ratio to minimise the required extrusion pressure. Although representative of the theoretical work and visually the same as a standard Conform machine the apparatus used differed significantly in its operating parameters. Most notable of these is the angular velocity of the wheel, which was able to operate between 1400 RPM and 1730 RPM when compared with the 12 RPM maximum steady state velocity reported by Ardor [18]. The report states that the experiments were run at low speeds to limit the dynamic effects of the material slippage but the exact speeds are not quoted if they differed from the original capabilities of the machine. It is possible that such a high-speed wheel created much more heating in the workpiece than other published work at the wheel-workpiece interface due to the large amount of frictional heat evolved.

Other attempts at creating analytical models of the Conform process have come from multiple sources. Wood [75] took the work by Green [62], Etherington [13] and Tirosh *et al.* [74] and added a constitutive equation for the material plasticity generated from compression tests. The theoretical results agreed well with those from the experimental extrusions for solid rod. It was suggested that applying such considerations to powder feedstock would not work due to the unexplained observation of decreased extrusion pressures when using powders. The work conducted by Wood considered only pure aluminium rod feedstock and involved extrusion through an expansion chamber common in the production of large cross sections of aluminium with Conform [18, 76, 77]. From consideration of the literature presented here possible that the reduction in extrusion force for powder feedstocks is due to the lack of an upset length and a reduction in bulk density within the wheel groove compared with rod feeds.

2.4.2 Finite element models

Cho et.al [14, 15] studied the how the abutment height, flash gap and die opening affected the occurrence of defects. Surface separation (Figure 2.14) and curling (Figure 2.15) were identified as potential defect problems if certain process parameters were combined in an unfavourable way. Increasing abutment height, increased friction coefficient at the workpiece-wheel interface and increased flash gap size all contributed individually to a decrease in the surface defect occurrence. It was determined by multiple sources [15, 78, 79] that angular speed of the wheel did not affect the surface separation or folding defect development. This was true in speeds up until there was significant slippage between the wheel groove and the workpiece.

The curling phenomenon as identified by [14] was mitigated by reducing the abutment height and the flash gap size. This was attributed to the decrease in the material dead zone, which limited the velocity difference between material flow on the top and bottom of the extrudate. The curling phenomenon is now prevented by the addition of straightening apparatus before the extruded product is cooled. All of the finite element modelling that has been done on the Conform process has been limited to optimising process parameters for an arbitrary workpiece material. The geometry of the tooling has been modified in each case to investigate certain defects, each of which has yet to be reported in the literature from experimental studies.

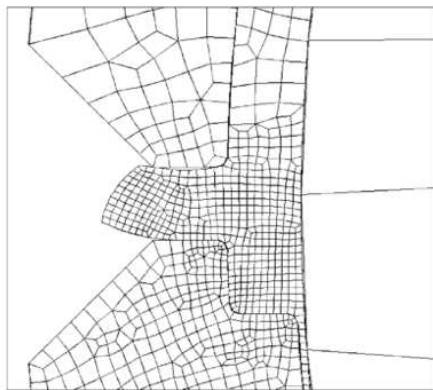


Figure 2.14: Examples of the curling phenomenon in ConformTM. Reproduced from [14]

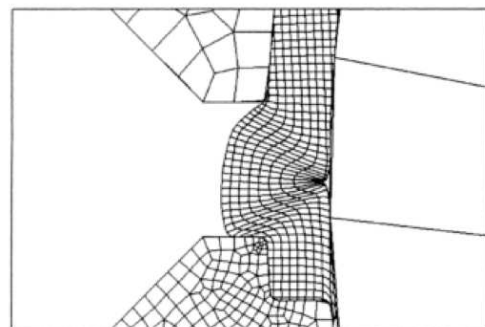


Figure 2.15: Examples of surface defect forming in ConformTM. Reproduced from [15]

COMTES FHT, a materials research company in the Czech Republic published preliminary reports [16, 80–83], which stated the successful processing of grade 2 titanium cylindrical rod

feedstock of 10 mm diameter with an initial equiaxed grain size of 25 μm through a BWE Conform 315i machine. An induction loop preheated the 10 mm feedstock rod to approximately 500°C before they extruded rod through modified tooling to simulate the ECAP-Conform process. The wheel speed used was only 0.95 RPM, much slower than reported in other work on Conform. Although not explicitly stated, the wheel speed, tool geometries and feedstock preheat are thought to have been chosen to mirror the press speeds used in ECAP.

While this extrusion was not true ECAP-Conform, as the rod experienced a change in cross section while moving through the process, the cross sections of the feedstock and product were identical. The extruded rod had a fully annealed microstructure with a grain size of ~ 750 nm following three passes of the rod through the machine. The grain size of the Conformed rod is similar to that attained during multi-pass ECAP studies of CP-Ti, however ECAP results in an extensive retained sub-grain structure.

It is possible that due to the continuous nature of Conform that the adiabatic heating within the abutment zone resulted in the tools reaching higher temperatures than those found in ECAP, aiding further deformation and providing more energy for dynamic recrystallisation. Unfortunately the authors do not mention the degree of oxygen pickup within their product as a result of heating the titanium feedstock rod in air [80]. It might be expected that the existing oxide layer prevented significant oxygen pickup during the first pass but it is unclear as to whether this would become an issue during multi-pass extrusions and if the oxide layer folds into the product bulk creating internal defects as described in [15, 78, 79].

The authors also used DEFORMTM to model the process (see Figure 2.16) and compared this to their experimental results with good agreement. Empirically they found appropriate values for the wheel-workpiece thermal conduction coefficient through the experimental machine temperature output data. They also determined the workpiece-tool friction by comparing the state variables for various friction coefficients in DEFORMTM to macrographs of the material remaining in the abutment zone (see Figure 2.17).

Work at COMTES FHT is the first known attempt at the continuous extrusion of solid titanium rod. However the tooling was intentionally modified to emulate the ECAP-Conform process, which differs from the tool geometry typically used in traditional Conform process. While not true ECAP-Conform as the workpiece changes dimensions in the abutment zone, the initial and final workpiece cross sections are the same as per the definition of ECAP. The process offers a significant improvement over previous SPD processes with titanium alloys, if the process can be scaled up to be fully continuous in a commercial environment. Use of commercially available Kroll-produced feedstock rod that needs to be preheated limits the potential

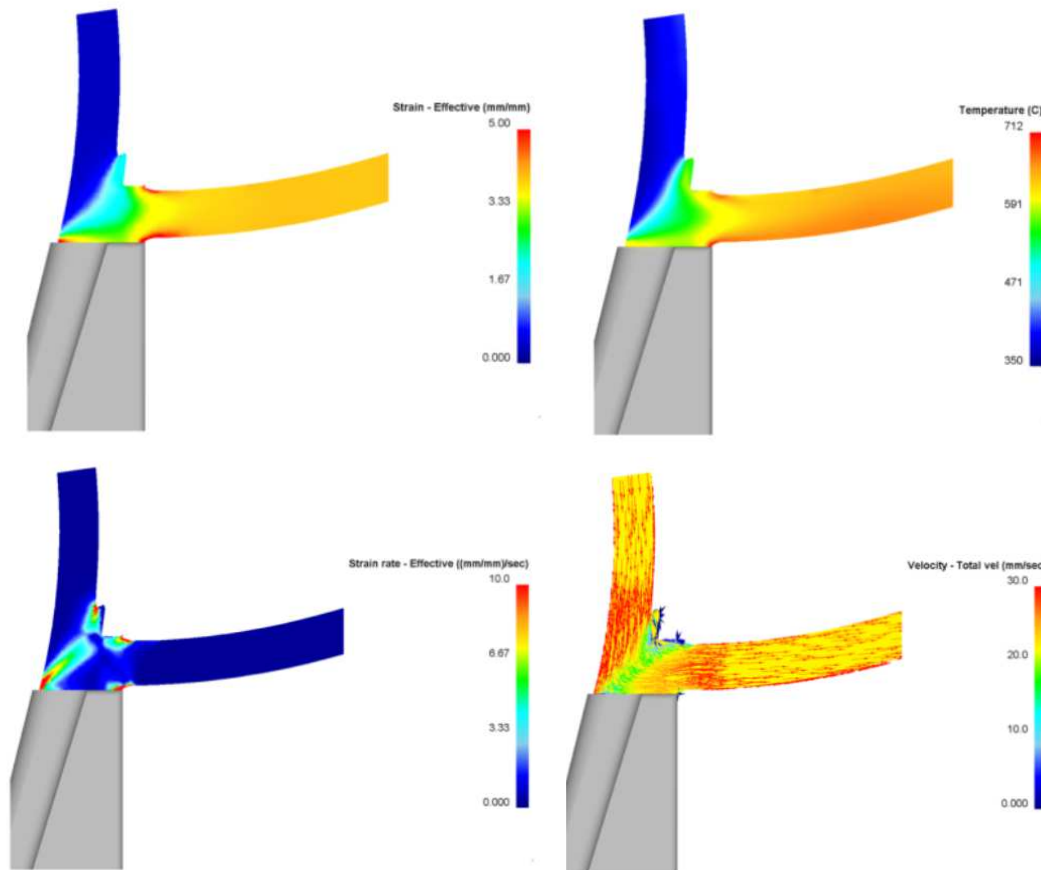


Figure 2.16: Preliminary FEM results from COMTES FHT [16] showing the state variable fields in the COMTES modified Conform process with 10 mm diameter CP-Ti grade 2 rod.

long term cost reductions of the final product.

2.4.3 Grip length in continuous extrusion processing

A recurring but often overlooked factor in Conform is that of grip length in the generation of the extrusion pressure (see figure 2.18). This is mentioned throughout the literature [13,69,75,84,85] as an indicator of the amount of pressure generated within the wheel groove as a result of the extrusion pressure needed to extrude material through the die. The grip length is most often mentioned in relation to solid rod feedstocks where it is easy to see how the rod upsets within the groove when the shoe is retracted post-extrusion [11]. In general it is shown that as the grip length, or upset length increases so does the extrusion pressure. This is presented in the literature as those extrusion conditions that generate the most pressure at the die also present the greatest grip/upset lengths. This has a very important implication when high strength alloys are considered as unnecessarily high grip lengths, hence extrusion pressure could impact greatly on tool life [86]. Conversely, for low strength alloys, increased upset heights within the

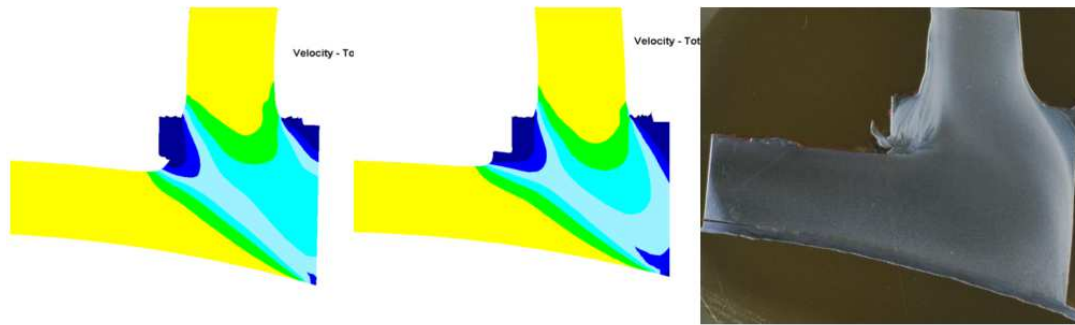


Figure 2.17: Comparison of Conform FEM results using different friction coefficients with a macrograph of the workpiece remaining in the abutment zone (left $\mu=0.2$, centre $\mu=0.7$).

Reproduced from [16]

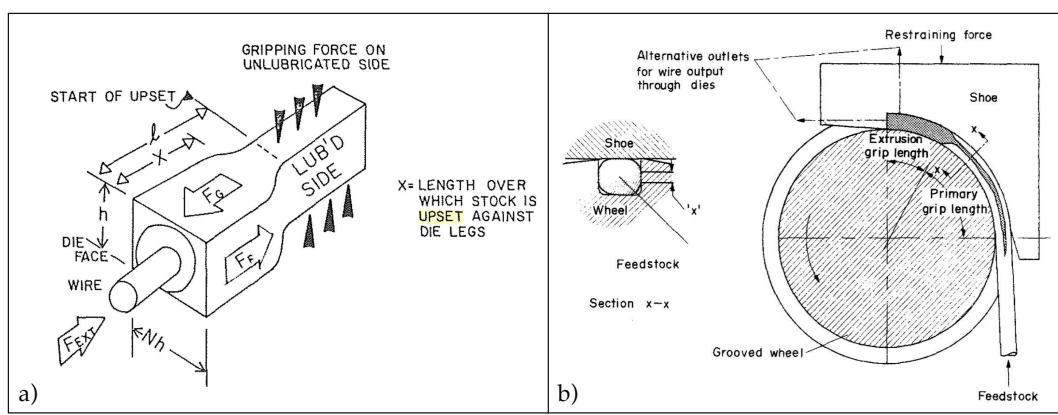


Figure 2.18: Grip length in the generation of extrusion pressure in a) LINEX (LINEar continuous extrusion) [17] and b) Conform [18]

groove may also increase the amount of flash produced due to material being forced out higher up in the groove.

2.4.4 Importance of extrusion ratio in Conform

The extrusion ratio for direct extrusion is normally defined as the ratio of billet cross sectional area to extrudate cross sectional area or A_i/A_f . If this is applied to the Conform process then there are different ways to define the extrusion ratio when related to the different zones within the machine. From the literature [84] and from two independent continuous extrusion machine manufacturers the extrusion ratio of the process is usually defined as the ratio of the feedstock cross section to the extrudate cross section. However as the feedstock changes cross section area after coining, during upset and during transfer through the die chamber port it is proposed that this definition of the Conform extrusion ratio is invalid or at least only considers part of the problem. It is proposed that there are three separate definitions of extrusion ratio as opposed to the commonly considered single ratio. The first is only valid for rod feeds but is defined as

the ratio of feedstock cross section to groove cross section. This will affect the amount of cold work required to coin the feedstock and the force required to upset it fully within the groove. Such a relationship is mentioned in [86] where it is stated that the groove size is chosen to minimise the amount of upset required in the the rod once it hits the abutment. This ratio is normally set within a narrow range as the groove must be selected to closely match the profile of the feedstock to minimise the required degree of coining and hence cold work done on the rod. Second is the ratio between the groove cross section and the port cross section. Here it is important to generate sufficient extrusion force from the wheel groove to the back of the port at the die. The minimum required force is then dictated partly by the third ratio of port cross section to extrudate cross section. The three ratios are defined as A_i/A_g , A_g/A_P , A_P/A_{ex} , where A_g is the cross sectional area of the groove, A_P is the cross sectional area of the port and A_{ex} is the cross sectional area of the extrudate.

Experimental Trials

The experimental trials detailed in the following chapter were conducted prior to and alongside the finite element modelling in chapters 5, 6 and analytical model in chapter 4. As such there was no predefined method to allow for die design iterations in the trials as a result of the modelling. This feedback loop of FEM, die manufacture, experimental verification is the subject of further work and is mentioned briefly in chapter ??

Experimental trials conducted at BWE Ltd., Kent, UK were undertaken at various points between January 2010 and December 2013 in order to determine whether low cost titanium powders could be successfully consolidated in the Conform process. Initial trials were performed with grade 2 hydride-dehydride powder from Reading Alloys, U.S.A. with a view to understanding how the process reacted to high strength metallic powders.

3.1 Equipment

The machine used for this work was a BWE Conform 315i machine used on their site exclusively for development work. While specific tool geometries cannot be reported due to restrictions imposed by collabration agreements certain dimensions are shown in table 3.1. A fully labelled schematic of the machine used in the trials is shown in figure 3.1.

3.2 Trial Methodology

Due to the lack of available literature on the Conform processing of particulates there was no known starting point from which to generate an experimental plan. BWE personnel involved with this Ph.D. project had previous experience of Conforming pure aluminium, AgSnO_2 and oxygen free high conductivity copper (OFHC) particulates but not higher strength metal powders. Extrusion trials 1-3 described in this work were preliminary trials to collect data, which could then be used to improve the extrusion process in later trials Trials 3 and 5 were conducted on the same days as Trials 2 and 4 respectively. Trials 4-5 were focused on determining a processing window for the Conforming of CP-Ti HDH powders. This process window was defined

Table 3.1: Experimental trial equipment

| Item | Geometry | Note |
|--------------|---|--|
| Wheel | 300 mm outer diameter | AISI-H13 steel |
| Wheel groove | Semi-circular bottom with straight sides. 12 mm wide and 13 mm deep. | AISI-H13 steel |
| Die chamber | Port: 10 mm wide and 17mm high with 5 mm radius on the top corners to form an arch | Tool is used to contain both the die and abutment. Material passes from the wheel groove to the abutment and through the port before entering the die. |
| Die | Profiled to sit close to the wheel within the die chamber. | AISI-H13 with WC inserts |
| Abutment | High wear tool, which is profiled to almost completely block off the wheel groove to redirect material into the die chamber port. Profile allows a small (≤ 1 mm flash gap to be maintained around the top edge of the tool and the wheel groove) | Powder metallurgy Stellite TM 21 for this study. |

by tool failures or a lack of extrudate formation. It was thought that the process window would depend on various controllable parameters in the running of Conform machine such as tool preheat temperatures, wheel speed, flash gap size as well as tool geometries and powder feed rate.

The BWE Conform 315i machine was set up according to a ‘standard’ copper extrusion for powder feed into a 5 mm wire. Comparisons of this work with copper powder continuous extrusion were not able to be made due to the commercial sensitivity of individual R&D projects. Table 3.2 describes the differences in certain parameters between each trial. The rectangular dies were used in two orientations defined by their aspect ratio; either horizontal (6.6x2.6 mm) or vertical (2.6x6.6 mm) to determine if die orientation had any effect on the success/quality of the extrusion and resultant macro and microstructure of the extruded strip.

There was an initial wheel-abutment tip gap of 1.2 mm when the tools were cold, which changed as the powder was processed both due to thermal expansion/stresses on the tool faces and abrasive wear from the titanium powders. The cobalt based alloy StelliteTM 21 abutments were formed from a press-sinter process and were and still are used for high wear resistance in standard Conform processing. The StelliteTM abutments were standard tools for aluminium Conform extrusion and were used as a benchmark so that other abutment materials might be

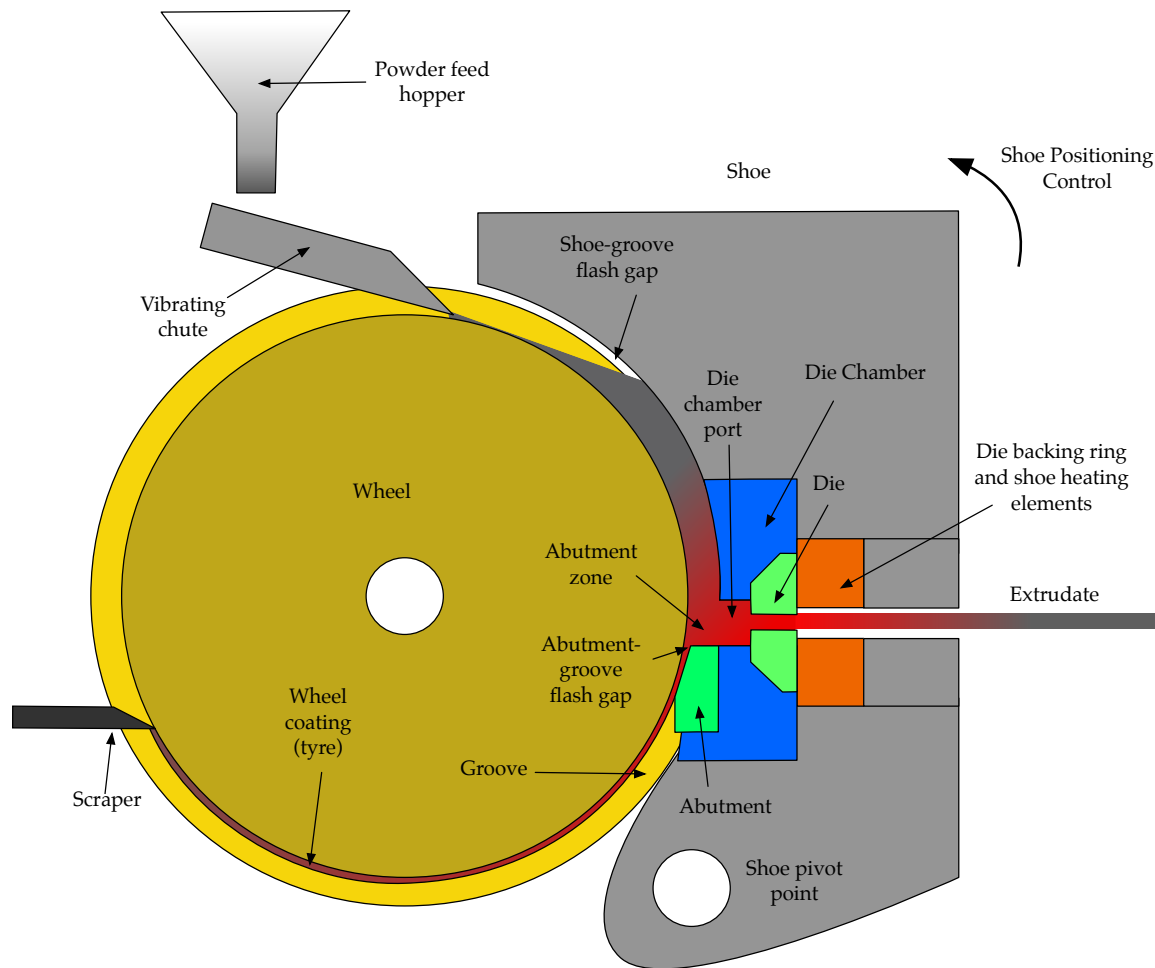


Figure 3.1: Schematic of the modern day Conform process with modifications for direct powder feed into the groove. Reproduced from [9]

used in subsequent trials.

Table 3.2: Experimental trials tooling

| Trial | Die | Abutment |
|-------|---|--------------|
| 1 | 5mm round | Stellite™ 21 |
| 2 | 6.63 x 2.24 mm rectangular (Horizontal orientation) | Stellite™ 21 |
| 3 | 6.63 x 2.24 mm rectangular (Vertical orientation) | Stellite™ 21 |
| 4 | 5mm round | Stellite™ 21 |
| 5 | 5mm round | Stellite™ 21 |

The shoe and tools were preheated with an inbuilt induction heater to a 500°C set point and held for 10 minutes to ensure thermal homogeneity. The shoe was brought up into position by the wheel, which was started at 2 RPM and rotated slowly (jogged) to make sure the tools and wheel were not touching. The wheel jogging also helped to clean the wheel groove of any flash and left over powder from previous trials. Clean CP-Ti HDH powder at room temperature (12-18°C) was fed into the machine in one of two ways while the wheel was moving at 2 RPM.

During trials 1-4 the powder was fed onto a pneumatically actuated vibrating chute using a hand scoop. The vibrations of the chute helped to moderate the amount of powder from the scoops running into the groove. It was impossible to reliably control the rate of powder feeding due to the sporadic nature of the scoop feeding method. In these trials the powder was fed in at a rate that tried to prevent too much powder over spill in to the bottom of the machine. If a significant amount of powder was observed to be flowing around the tools and into the bottom of the machine the feed rate was dropped. Conversely if the motor current began to drop and the extrudate stopped moving the feed rate was increased to try and generate enough pressure to continue extrusion. For trials 5 and 6 a funnel hopper was used to automatically dispense powder onto the vibrating chute. The tip of the chute was positioned just over the apex of the wheel so that loose powder flowed down freely into the abutment zone (see Figure 3.2). The same reasoning behind the feed rate control was also used for the funnel hopper in the later trials.

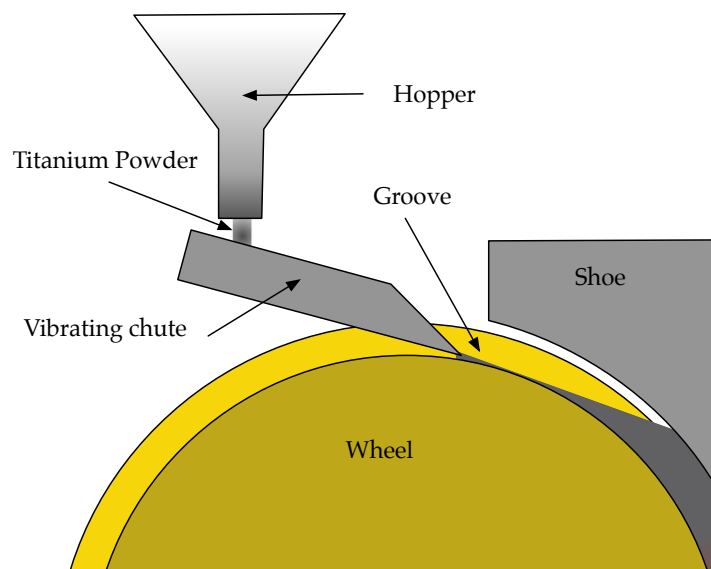


Figure 3.2: Schematic representation of the hopper and chute setup for the experimental trials.

Once powder was being fed into the machine at a steady rate the wheel speed was raised in 1-2 RPM increments until extrusion began and rod was observed to exit the die. With increasing wheel speed the powder feed rate was also increased though the exact rate of increase was not the same for both. For example if the wheel speed increased from 4 to 8 RPM then the powder feed rate should theoretically double to account for the higher mass flux of titanium leaving the machine. In practice it was likely that while the powder feed rate would need to be increased, it was not exactly in line with the wheel speed increase as this would cause unsatisfactory extrusion conditions due to wheel slippage. The wheel speed was varied up to 10 RPM where



Figure 3.3: Vibrating chute with powder flowing across it and into the wheel groove during an experimental trial.

the longest lengths of extruded rod were produced until the feedstock powder ran out. Once extrusion began the extrudate was allowed to feed into a water cooling trough one metre away from the die exit. The water trough was approximately three metres long, allowing adequate time for complete quenching of the extruded wire. Once the rod exited the trough it was allowed to continue moving to the end of the room until it was sectioned and stored. The rod was not coiled to help try and retain its extruded-quenched microstructure without unnecessary plastic deformation occurring.

3.2.1 Feedstock powders

Commercially pure (CP) grade 2 hydride-dehydride (HDH) powder from Reading Alloys was used in all of the trials. The only exception was the addition of grade 5 HDH powder (Ti-6Al-4V) also from Reading Alloys near the end of Trial 1 when the available supply of CP-Ti HDH powder ran out. The CP-Ti HDH powder had a nominal chemical composition as shown below in table 3.3. The powder was sieved to between $45 \mu\text{m}$ and $150 \mu\text{m}$ and had a particle size

distribution determined measured by laser diffraction given in 3.4. The powder particles had an irregular and angular morphology as shown in the secondary scanning electron microscopy image in figure 3.5.

Table 3.3: Chemical composition of CP-Ti grade 2 powder. All percentages are by weight

| Ti | Fe | O | C | H | N |
|-----------|-----------|----------|----------|----------|----------|
| 99.9 % | 0.003 % | 0.18 % | 0.011 % | 0.014 % | 0.007 % |

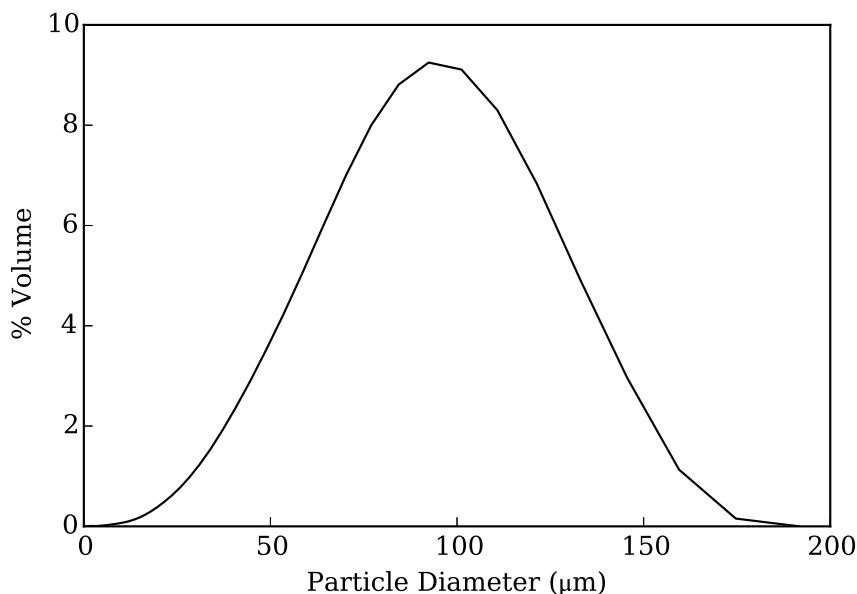


Figure 3.4: Particle size distribution for CP-Ti HDH powder used in this study.

3.2.2 Abutment stress metric

The engineering design of modern Conform machines prevents direct observation of the material processing within the machine. Once the powder flows into the groove and falls beneath the height of the shoe entry plates the material is not seen again until it exits the die and moves out of the shoe. The consequence of this is that it is impossible to observe what is occurring to the feedstock as it is processed. Anecdotally, Conform machine operators will modify wheel speeds and tool preheat temperatures based on wheel-feedstock slippage and visual tension in the rod product as it is wound onto a coil. The only other way to track how the feedstock is being processed is to analyse the data output from the machine sensors, such as motor ammeters and thermocouples inserted into the tools.

Following the first experimental trial it was determined that the torque generated by the wheel could potentially show what was going on inside the machine during powder processing. This theory is something that both machine manufacturers and end users are familiar with but

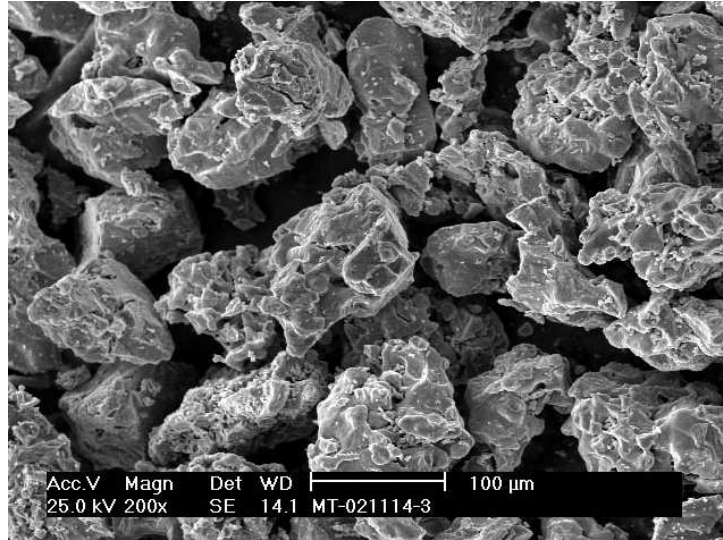


Figure 3.5: Secondary electron micrograph of grade 2 HDH powder.

in most cases any available data on it is subjective. Experienced machine operators may have a ‘feel’ for how the wheel torque changes during the Conform process of their particular alloy and profile but such values tend to remain reasonably constant once extrusion has been started and has reached a steady state. On commercial Conform machines, wheel torque is a parameter directly measured at the motor and logged like any other variable. This was not possible on the test machine used in this study as the relevant parts had not been retrofitted. Instead, the wheel torque was calculated from the available data during the log file post-trial processing.

The wheel torque is related to the ratio of the motor current and rotational speed through equation 3.1

$$\tau = \frac{2\pi VI\gamma}{60\omega} \quad (3.1)$$

where V is the supply voltage of the DC motor driving the wheel (415 V for this work), I is the operating current of the motor, γ is the motors electrical to mechanical efficiency, assumed to be 0.8 [87] and ω is the angular velocity of the wheel in rad s^{-1} .

If this torque τ is considered to be a force working at a distance equal to the radius of the center of the wheel groove R it is possible to determine an average stress acting on the abutment face with area A_{abut} within the groove through equation 3.2.

$$\sigma_{abut} = \frac{2\pi VI\gamma}{60\omega RA_{abut}} \quad (3.2)$$

This is a very simplified consideration of the process and fails to account for varying grip lengths, changes in frictional coefficients and the extra torque generated by the scraper at the

back of the wheel. The torque generated at the top and bottom of the groove will also be different resulting in a graduated stress distribution across the abutment face. Despite these limitations it still provides a useful metric from which trends can be inferred and then used to determine safe operating parameters for the conforming of titanium powder.

The abutment stress calculated for certain phases of the process from the trials 1-3 were used in subsequent trials to probe the consolidation and extrusion phases. It was not possible to plot the actual abutment stress σ_{abut} live during the trials without significant rewriting of the machine's control software. Instead, the abutment stress was back calculated in order to generate an observable motor current value at each wheel speed. The plot used to monitor the live trials is shown in figure 3.6. Analysis of trials 1-3 provided a general processing window from which the motor current for each wheel speed was then inferred. During processing of the CP-Ti HDH powder the machine and powder feed could be changed in-situ to manipulate the current draw from the wheel and hence alter the processing characteristics. Further detail on this is provided in the results and discussion sections.

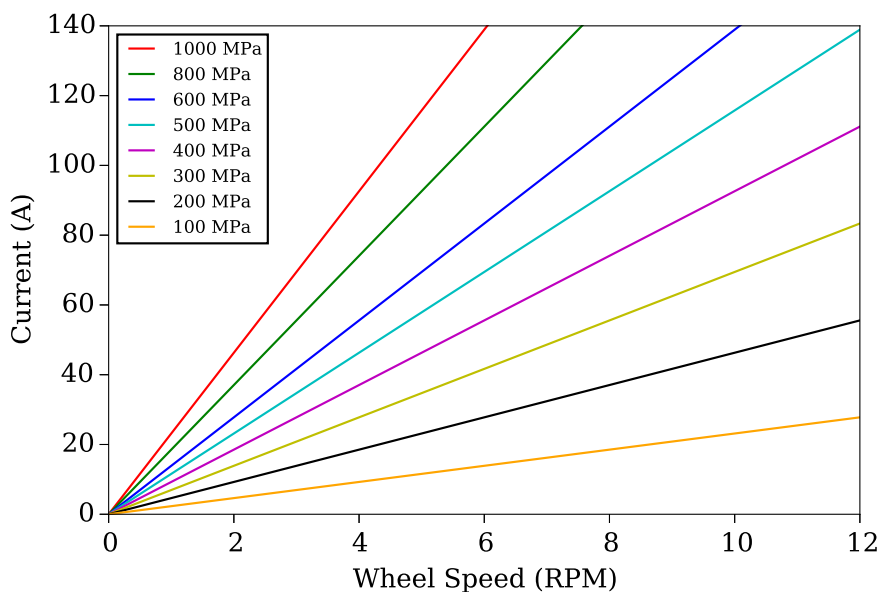


Figure 3.6: Live monitoring plot of current vs wheel speed for different 'abutment stress' values used during experimental trials 2-5.

3.2.3 Process Control

A Conform machine has numerous feedback loops and thermocouples to measure a range of variables relating to the active process. Thermocouples of particular interest are fed into the machine through small holes located behind the abutment, die chamber and inside the wheel

to measure the temperature response to both the tool induction preheating and heating during processing of the feedstock material. The locations of the thermocouple tips are at an undisclosed distance from their point of interest, which makes it difficult to determine what the actual temperature is on the tool faces. It is generally accepted [87] that while a quantitative measurement of temperature is useful during post process analysis, the rate of change of temperature is far more critical for active monitoring of the Conform process. The rate of change of temperature is indicative of changes in powder consolidation brought on by changes in wheel speed or powder feed rate and especially true within the abutment zone.

The parameters in table 3.4 show some of the data that is currently available to the Conform machine operator in a post process analysis. Any combination of these are able to be plotted live on a connected PC running Windows XP. The parameters that were commonly used during the processing of titanium powders in this work are indicated within the table.

Each of the parameters are logged once per second into a comma separated variable (.csv) file, which can be imported into a spreadsheet program or read directly by a user programmed application for analysis. The data from each of the trials was extracted from the .csv files, analysed and plotted using Python 2.7.5, NumPy and Matplotlib.

Table 3.4: Parameters of interest to this work from the possible 53 logged field on the BWE machine control console.

| Parameter | Notes |
|-------------------------|--|
| Date/Time | Excel Format |
| Abutment Temperature | Measured abutment temperature measured on its back face ($^{\circ}\text{C}$). |
| Motor Current | Current drawn by the wheel motor operating at constant number of revolutions per minute. |
| Wheel Speed | User set wheel speed (RPM) |
| Wheel Temperature | Wheel Temperature measurement ($^{\circ}\text{C}$) |
| Die Chamber Temperature | Temperature measured at the back of the die chamber away from the processed powder ($^{\circ}\text{C}$) |
| Product Speed | Extrudate exit speed measured by a tachometer six metres away from the extrusion die (mm^{-1}). |

3.2.4 Rod analysis methodology

Once titanium rod had exited the die and travelled through the quench trough it was cool to the touch. Continuous lengths of the rod were cut at the back of the die and coiled loosely for transport. The die was removed with the back-end defect intact for further analysis. If the trial resulted in a machine shutdown due to an abutment failure the die was removed with a pneumatic press resulting in damage to the back-end defect. In these cases it was not possible to obtain any useful metallographic data from these damaged defects due to extensive cracking and plastic deformation.

Several metallographic samples of extruded CP-Ti rod were taken at random locations from the longest lengths produced at three different wheel speeds 6, 8 and 10 RPM. Each sample was hot mounted in conductive bakelite to present both the cross and longitudinal sections to the observer. The samples were then ground using 120 grit SiC papers to remove 2.5 mm of material so that the longitudinal section was cut in half. A standard metallographic preparation was then followed with a finishing mechanical-chemical polish using a 0.06 μm Silica and 20% by volume H_2O_2 solution on a StruersTM MD-Chem pad. The final polishing step was alternated twice with a tap water polish for a five minute mechanical-chemical polish, 5 minute water polish schedule.

Optical micrographs were taken with a range of magnifications to show the macro and microstructure in both the cross and longitudinal sections. Polarising filters were used for all the optical images to aid in differentiation between the alpha grains in CP-Ti. Specific areas of interest were identified from the low magnification macrostructures and micrographs were taken at the points in both X and Y directions, when Z is considered as the extrusion axis.

3.2.5 Powder flow in to the Conform machine

It has been suggested that powder flow into the Conform machine would be a critical parameter in enabling the successful extrusion of high strength metal powders [75,86]. It was commonly accepted in the early stages of Conform development that filling the groove entirely with powder to the point of overflowing would provide an adequate reservoir of material to prevent extruded defects [86] by allowing a long residence time to deaerate the powder. This was determined not to be the case and adequate extrusion could be obtained by metering the powder feed while reducing the tooling pressures and temperatures. To this end a hopper was designed in order to provide a measured titanium powder feed into the Conform machine. Based on the geometry and wheel speed of the machine used in this work powder flow rates are also calculated based on true continuous extrusion with a high yield.

3.2.6 Powder flow from a hopper

Equation 3.3 is the empirical Beverloo equation, commonly used for the flow rate of granular solids through a circular orifice [88]. The work was performed primarily using the seeds of various vegetables and crops with some results using sand. Using sand as the granular solid produced significantly different coefficients for the empirical relationship (Equation 3.4). The sand used was similar in morphology and size to the largest particles within CP-Ti HDH powder, which allows the use of the Beverloo equation coefficients for sand to predict a theoretical mass flow rate from the hopper.

$$W = 35\rho_B\sqrt{g}(D_0 - 1.4d)^{2.5} (\text{g min}^{-1}) \quad (3.3)$$

$$W = 38.8\rho_B\sqrt{g}(D_0 - 2.9d)^{2.5} (\text{g min}^{-1}) \quad (3.4)$$

where

W = Powder flow rate (g min^{-1})

ρ_B = Bulk density of the powder (g cm^{-3})

g = Constant of gravitational acceleration (cm s^{-2})

D_0 = Diameter of orifice (cm)

d = Average particle diameter (cm)

3.2.7 Hopper design and mass flow rates within the Conform machine

Using equation 3.4 it is possible to calculate what size of orifice is required for a certain rod extrusion speed if certain assumptions are made about the progression of the extrusion process. The first assumption is that the consolidated powder will only flow through the extrusion die and not flow out as flash either at the abutment face or between the wheel and the tooling. Secondly that the loose powder flowing into the wheel groove is of sufficient quantity to balance the mass of material that has been extruded and is assumed not flow out of the machine until it is consolidated. In this way there is conservation of mass from the point that powder leaves the hopper to when the rod is extruded. During the experimental trials detailed in chapter 3 it was found that the extrusion speed varied between 0.3 and 1.5 m min^{-1} . This would result in a mass flux out of the die of 26.5 and 132.5 g min^{-1} for the 5 mm diameter CP-Ti rod. Figure 3.8 shows the predicted mass flow rates for different hopper orifice diameters and the corresponding estimated extrusion speed for the 5 mm CP-Ti rod from powder particles with an average 100 μm diameter.

These assumptions will not be valid during the process startup when a considerable amount of powder is lost through the flash gaps prior to the wheel coat forming and extrusion beginning. However, experience from the experimental trials suggest that once the coating is fully formed fresh powder only flows into the groove and is prevented from escaping by the flash at the edges of the groove. A small fraction of powder may be lost as the tools wear and the gaps between the shoe and wheel open up but this is likely to only be a very small percentage of the overall wire yield.

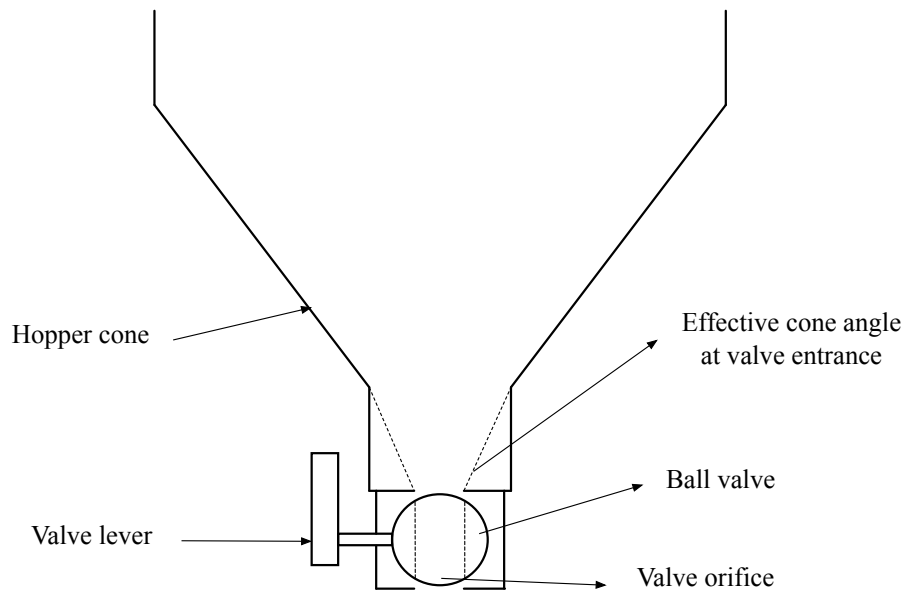


Figure 3.7: Schematic cut through view of the custom powder hopper used in the fourth set of trials.

The powder hopper used for the fourth and fifth set of trials was created from a plastic car oil funnel with a 150 mm entry diameter. It was modified to include a simple plumbing ball valve with a small handle on the side to allow a change in the exit orifice size. The valve had a nominal orifice diameter of 7 mm. When the valve lever was moved through 90° from its open position the effective exit orifice sized was reduced to zero cutting off the flow of powder to the machine completely. The powder exiting the hopper was designed to flow onto a pneumatic vibrating chute attached to the Conform machine before being fed into the wheel groove. The hopper was designed solely for the purpose of regulating the powder flow, not to directly feed powder into the wheel groove.

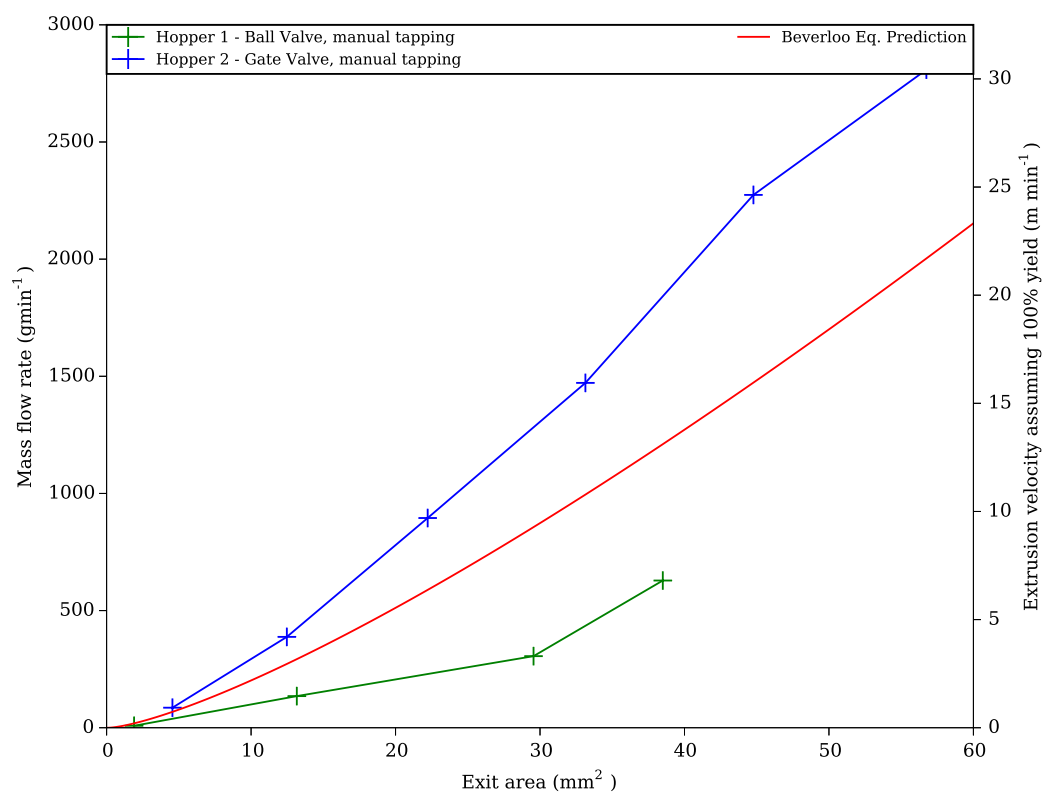


Figure 3.8: Measured mass flow rate from the hoppers used in the experimental trials.

3.2.8 Wheel coating process

The start up phase of the Conform process with particulate feedstocks can be difficult as the unconsolidated powder tends to spill out from the flash gaps. If inadequate space is left between the wheel and tools in the shoe contact can occur resulting in premature tool failures. CP-Ti HDH powder with a 45 - 150 μm size fraction has a strong tendency to spill out from the wheel due to its small size in relation to the flash gap. When powder is initially put into a clean Conform machine there is a nominal flash gap between the wheel groove and the abutment. In the case of this work the gap was 1.2 mm when the machine was cold but decreased once extrusion began and temperatures rose. The effect of gravity and size of the powder particles is such that the powder is most likely to fall through this gap until the wheel is coated and the flash gap is filled in. Once this is done, fresh powder fed in behind the initial charge can be consolidated in the abutment zone and extruded as product rather than solely flash. Of course depending on how the grip length varies throughout the process there will also be flash generated between the shoe plates and the wheel's outer surface. As well as blocking off the gap between the abutment and wheel groove the coating process also has the effect of heating up the wheel, which can then transfer heat to the fresh, cold, unconsolidated powder. Figure 3.9 demonstrates the flash that is generated at the shoe-wheel interface to contain the fresh powder as it is consolidated.

Previous experience from the manufacturers of the test machine was that powders of aluminium and copper alloys could be consolidated at low wheel speeds of 2-4 RPM (John Dawson, BWE Ltd. private communication, December 2012). During the trials with CP-Ti HDH powder it was determined that there is a minimum wheel speed below which the powder will not begin consolidation and will be unable to coat the wheel. Instead, the powder will flow out from the flash gaps into the bottom of the machine. The small amount of inter particle contact will heat up the individual particles and in some cases create sparks so as to ignite the waste powder and cause a fire. In the case of Trial 2 the powder began to consolidate above the abutment but remained relatively cold compared with those trials that produced an extrudate. This cold consolidation transferred a large amount of pressure onto the abutment resulting in it fracturing.

As powder is fed into the Conform machine from the hopper it flows around the circumference of the wheel groove and into the abutment zone. With an open flash gap this means the powder's bulk density will be less than that of its tap density. Particles can flow almost freely through the wheel-groove and abutment flash gap and out of the machine. The flow is

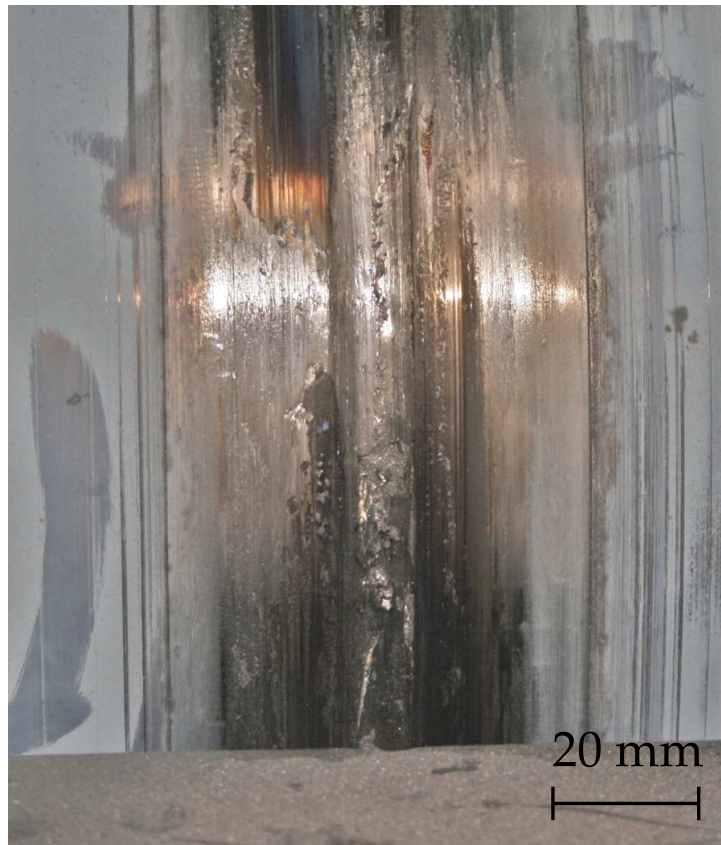


Figure 3.9: Conform wheel coated with consolidated titanium following experimental trial 4. Irregular oxidised flash can be seen either side of the groove.

not completely unrestricted and there is a degree of shear induced in the powder as it moves through the flash gap. The magnitude of this shear is dictated by, particle morphology, powder size fraction, packing density, wheel speed, friction coefficients. While packing density is intimately linked to morphology, size fraction and friction coefficients are likely to be fairly consistent between powder/machines therefore the main parameter that the machine operator has control over during processing is wheel speed.

This shear is generated by the difference in surface velocity between the wheel and the abutment and shoe plates. If the conditions are correct then there will be sufficient particle interlocking to transfer forces from the wheel to the abutment, using the powder as a medium. This will cause individual particles to deform, heat and break down their oxide layers. This fresh metal-on-metal contact allows particle-to-particle diffusion bonding and rapid powder consolidation without feedstock conditioning such as preheating in inert atmospheres. If there is no interaction between the powder and the abutment or groove there will be no shear generated in the powder bulk in the flash gap. In reality this is an impossible condition and there will always be some degree of shear in the powder, whether it is induced by the wheel movement or

just from the loose powder flow.

Consider a single powder particle positioned in the middle of the flash gap at the height of the abutment top face. If it is released from this stationary point, it will accelerate downwards under the action of gravity until stopped or deflected by another object. Consider the powder just above the abutment and close to the wheel groove surface, a volume of which will be in contact with both the abutment and the wheel. If the wheel is stationary then the powder will flow through the flash gap only affected by its flow characteristics, which is dictated by the particle size distribution, particle morphology and friction with the tools. The flash gap is not constant with vertical distance from the abutment face and creates a diverging gap. After the powder flows past the initial gap at the abutment tip it will experience an ever decreasing interaction with neighbouring particles until it is in complete free fall. The height at which this occurs below the abutment face is not yet known and could be the subject of future work. If the surface velocity of the wheel is less than the velocity the powder could attain under free-fall, then the friction between the powder and the groove will prevent this uninhibited motion. If the wheel's surface velocity exceeds this minimum requirement then there will be an induced shear within the powder. This shear is what helps to generate the required heat and pressure within the cold powder to consolidate a layer of powder closest to the wheel. This consolidated powder forms the coat or 'tire' within the groove, blocking off the flash gap and allowing sufficient pressure to be built up within the abutment zone to begin extrusion of material through the die.

Consider now that the wheel is moving with an angular velocity ω . At the radius of the bottom of the wheel groove $R = 147.5$ mm the surface velocity is given by $v_t = \omega R$. The powder's instantaneous velocity is given by the equation $v = \sqrt{2gh}$, where the acceleration due to gravity is $g = 9.81 \text{ ms}^{-2}$ and h is the drop in height below the abutment face. As we assume that the powder is in unobstructed vertical free fall the vertical component of the wheel's tangential velocity is given by $v_y = v_t \cos(\theta)$ where $\theta = \tan^{-1}((h_0 + h)/R)$ and h_0 is the distance from the port centre to the abutment face. This adjustment is necessary in this particular case as the shoe was setup to allow for a true radial extrusion. While these assumptions are not completely accurate they represent an upper-bound on the possible vertical velocity of the powder and hence lower limit on what the shear ratio will be at any point down the abutment. A schematic of these dimensions are shown in figure 3.10. At each point in height from the abutment face it is possible to calculate the effective shear ratio between the wheel and powder near the abutment (see figure 3.11). The shear within the powder will actually depend on many

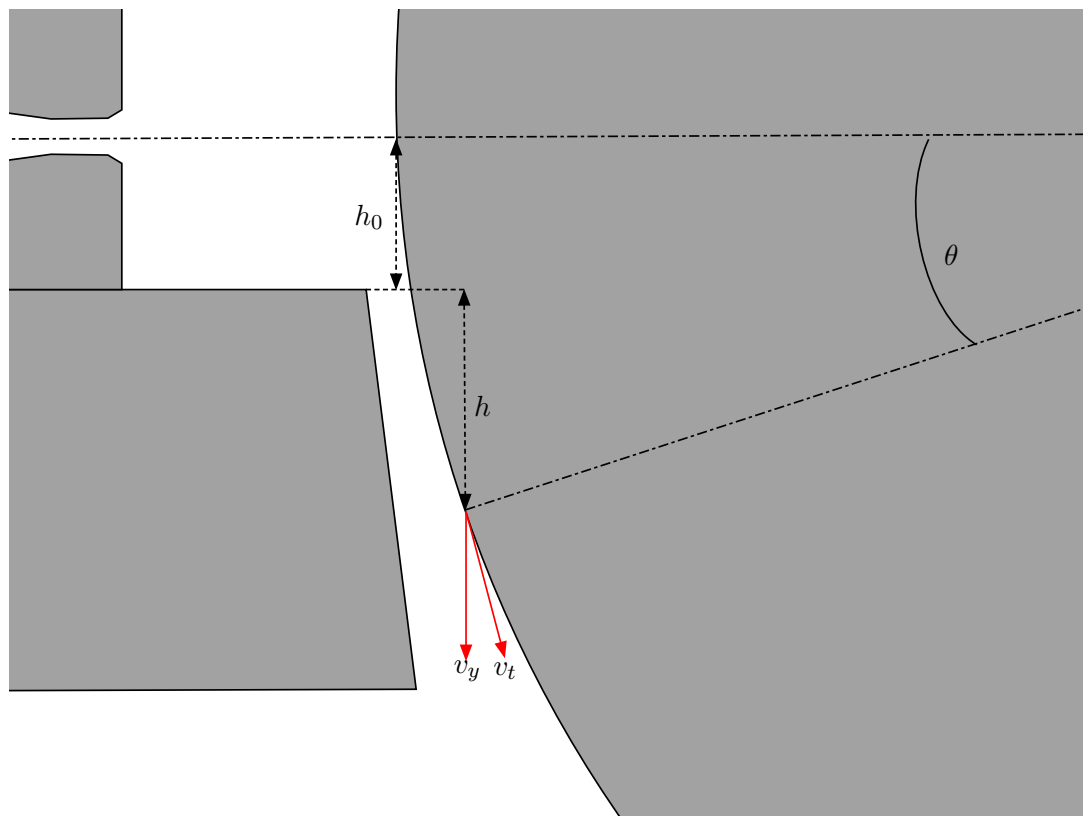


Figure 3.10: Dimensions used in the wheel coating theory for the start up process in the Conform processing of titanium powders.

other factors. Particle size and morphology will affect the flow behaviour and hence the speed of flow. It also dictates the likelihood of particles bridging across the flash gap. If this happens, the bridge will undergo a mixed shear and compression forcing powder consolidation higher up the wheel groove. It is this that initiates a transfer in process stage from wheel coating to abutment zone consolidation.

With each wheel speed there is a maximum distance from the abutment face below which the shear ratio drops below a critical value. Below this distance the shear ratio is favorable for powder consolidation to occur within the flash gap. It is obvious that with increasing shear ratio there is an increase in stress within the powder bulk. Particles are more likely to yield, deform, heat adiabatically resulting in particle to particle bonding. This shear will be greatest at the edge of the wheel by 8.6% when compared with the bottom of the groove.

The resulting plot of shear ratio at certain points below the abutment face in figure 3.11 shows two important regions. First is the intersection between the shear ratio of 0.1 and 2 RPM where the first 5 mm of drop has the potential to cause significant shear within the powder almost independent of wheel speed. When we compare this to figure 3.12 it is clear that while abrasion of the abutment by the powder has occurred down to approximately 5 mm powder consolidation has not yet begun. A lack of oxidation of the tools or remnant powder

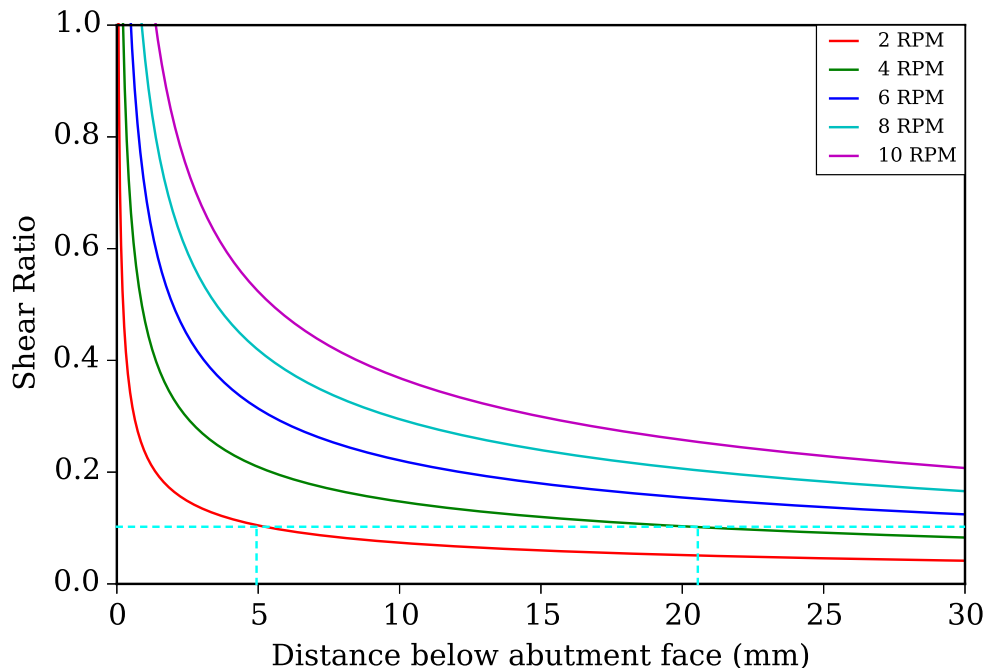


Figure 3.11: Graph of the effective shear ratio between the average wheel surface within the groove and a powder particle in free fall. The dashed blue line shows the critical shear ratio needed to consolidate CP-Ti HDH powder 45-150 μ m within the flash gap and coat the wheel groove.

also suggest that significant frictional heat was not generated. The second important region is the intersection of shear ratio 0.1 and 4 RPM at 19 mm when also compared with figure 3.13, which shows that when a wheel speed of 4 RPM is used consolidation can begin. The height of consolidated material down the die chamber face in this example is consistent with this intersection of a shear ratio of 0.1 and 4 RPM. Data is only plotted up to a distance of about 30 mm from the abutment face as there is a relief facet in the abutment. Further consolidation of powder is impossible past this point due to an inability to feed in fresh powder to account for the rapid increase in flash gap size.

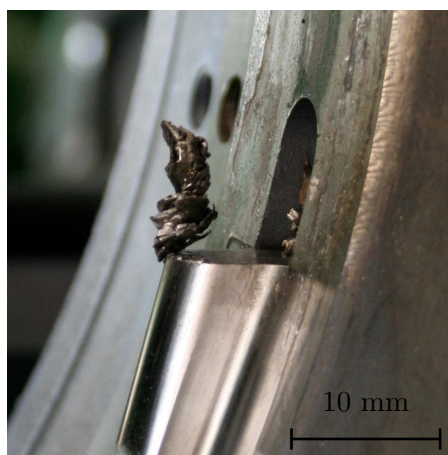


Figure 3.12: Close up of the abutment and die port following an interrupted test in Trial 2 with a wheel speed of 2 RPM



Figure 3.13: The die chamber at the end of Trial 2 showing the fracture surface of the failed abutment with partially consolidated titanium processed over the top.

3.3 Machine data from trials

Conform machines have a wide array of instrumentation in order to safely control tool temperatures, coolant flow rates and monitor the load on the wheel motor. The data read by the appropriate thermocouples, flow meters, ammeters are all fed back to a central control panel, which displays the data on screen and also logs it to a text file. At least 53 different types of data can be plotted in real-time during experimental trials but not all are relevant for powder feed due to the lack of ancillary equipment when compared with rod feeds. By downloading the data file from the control panel the raw machine data can be selectively plotted in a spreadsheet program such as Microsoft Excel. Data is recorded by the machine at a rate of 1 Hz and the quantity of data over the course of a one hour trial is sufficient to crash spreadsheet programs when manipulating the whole data set. As such it is preferential to use a scripting program such as Python or Matlab, which enables the researcher to specify a post-processing template to read in, manipulate, plot, compare and fit functions to large quantities of data. The analysis can also be standardised to ensure that the same level of analysis is provided for each trial in the project.

The graphs presented in this section have been manipulated to display only the relevant section of data for the trial and do not include machine warm-up or cool down periods. Abutment stress, as described in section 3.2.2 is provided as a method of estimating the amount of work being performed in the abutment zone. It can also be used to monitor the degree of consolidated material within the groove. More discussion on this matter is included at the end of this section. Each trial has three graphs of data associated with it. The first is a simple chronological representation of key temperatures, wheel speed and the measured abutment stress during the trial. The second is an analysis of the abutment stress values by calculating a running mean and standard deviation within a 30 second (30 data points) window. The third is a plot of the range of abutment stress at each wheel speed used during the trial.

3.3.1 Trial 1

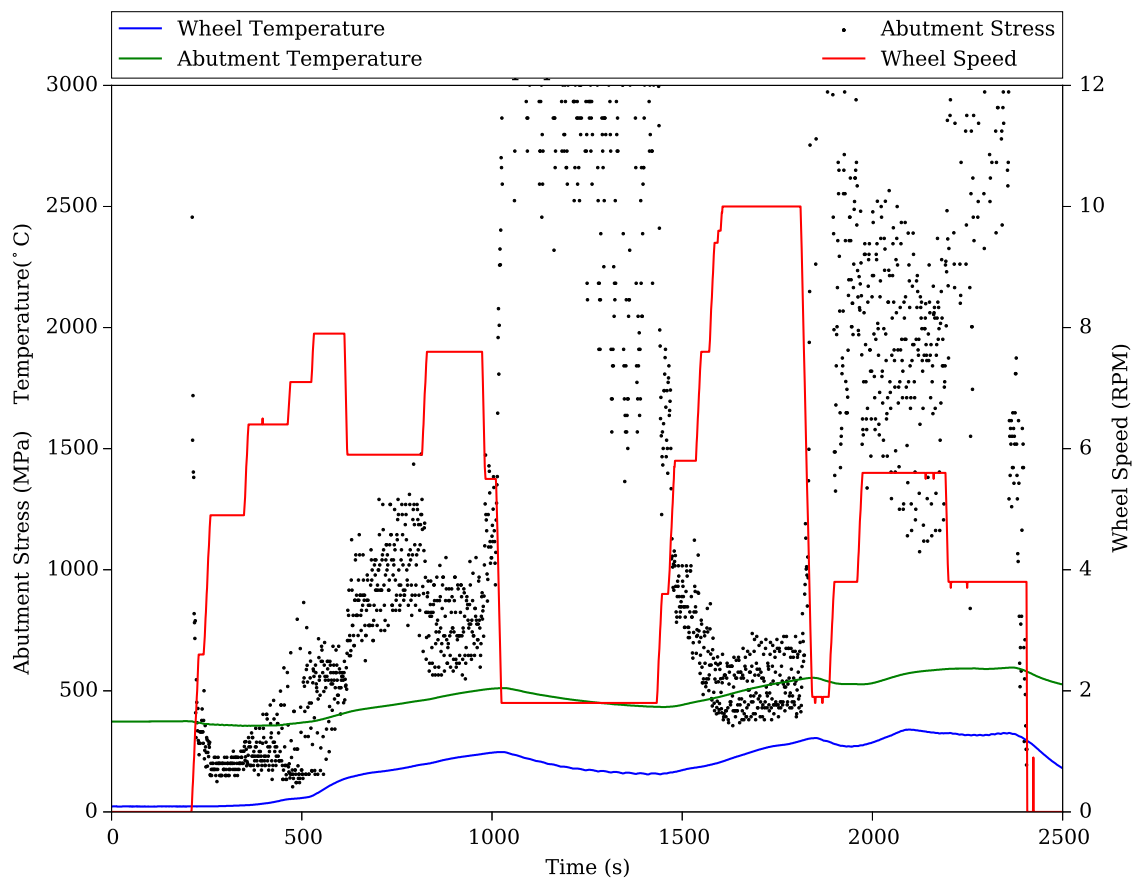


Figure 3.14: Raw data tool temperature and abutment stress (torque derived) from trial 1.

Trial 1 was conducted following early phase scoping trials on both Holton-Conform and BWE Conform machines. For this trial powder was fed in manually without a hopper system as one was not available at the time of the trial. The shoe temperature was set at 500°C , which was measured by the die chamber thermocouple (not shown for clarity) to be consistent upon commencement of the powder feed. While the die chamber reached 500°C at the position of the thermocouple in its back face near the centre of the shoe, the abutment was cooler. This was due to its exposure to the air and the fact that while the heat source from the shoe was at the abutment's back face the thermocouple was touching the bottom face. The wheel was not preheated during this trial and hence was at ambient temperature when the trial started.

The wheel was started at 3 RPM at $t = 150$ s and the CP-Ti HDH powder was fed in immediately. The abutment temperature showed an immediate drop of about 40°C as the room temperature powder acts as a heat sink against the hot tools. The abutment stress registered at this wheel speed indicating that the motor was doing a lot of work on the powder in the groove. The wheel speed was quickly increased to 5 RPM where the abutment stress immediately

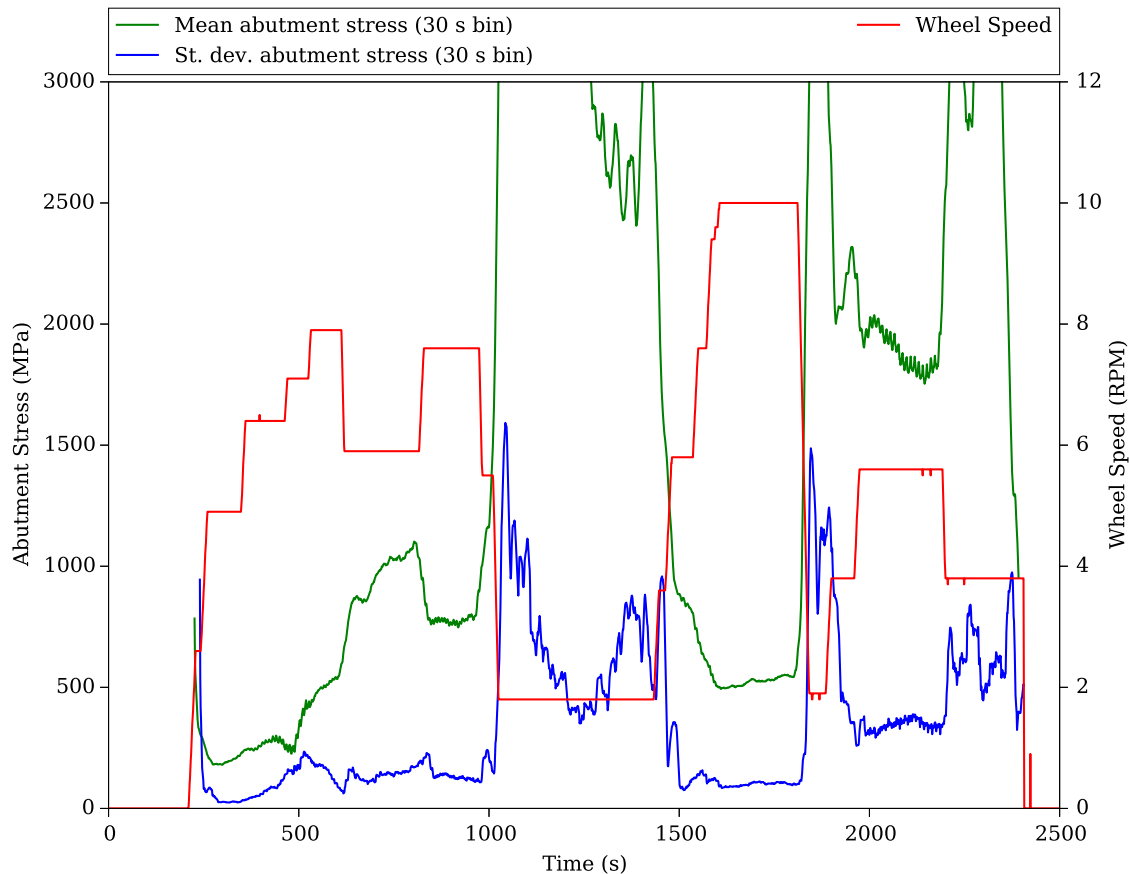


Figure 3.15: Abutment stress analysis plot from data obtained during trial 1.

dropped to 220 MPa. The low abutment stress observed at this point was indicative of loose unconsolidated powder in the groove and abutment zone. The wheel remained at 5 RPM for a few minutes before it was gradually increased to 8 RPM. At this point it can be seen the average abutment stress increased but also became more erratic with a larger spread. The top and bottom data points in this spread of abutment stress was due to a slight ovality in the Conform wheel. The powder began to be consolidated in the abutment zone and as the long axis of the wheel approached this zone the pressure on this consolidated material increased and the measured abutment stress reached its high value. When the short axis came into alignment with the abutment zone, pressure on the consolidated titanium eased off and the abutment stress value dropped back to its minimum in that particular cycle. The powder consolidation is thought to be indicated by a steady increase in both the average abutment stress and fluctuation.

The indication of the stability of the consolidation and extrusion process is given by the running standard deviation value. As the spread of the abutment stress gets wider due to an unstable grip between the wheel and workpiece so the standard deviation value increases. An example of this change of the overall process from stable to unstable occurs at $t = 400 - 500$ s

in figure 3.15. Here both the average abutment stress and standard deviation increase steadily as material is consolidated in the abutment zone. Both the abutment and wheel temperatures increase steadily during this consolidation period as the increased density of material in the abutment zone creates a larger resistance to deformation.

At $t = 500$ s the wheel temperature and average abutment stress increase rapidly when compared with the machine behaviour earlier in the test. From $t = 700$ s the tooling began to emit a screeching sound, which was determined by the BWE machine operator to be due to touching tools and the wheel speed was dropped back from 8 RPM to 6 RPM. This had the effect of increasing the abutment stress while retarding the rate of increase of both wheel and abutment temperatures. The 6 RPM samples were collected from the wire extruded during this phase. The wheel speed was increased from 6 RPM to 8 RPM at $t = 850$ s, which had the effect of reducing the abutment stress and also improved the stability of the extrusion. This is shown in the post-processed data in figure 3.15 but it was also observable as a decrease in the stick and slip of the wire within the die. It was during this period of 8 RPM wheel speed that the 8 RPM wire samples were extruded.

Loose powder that was not consolidated was able to fall sideways from the wheel groove as it was pushed through the wheel and die chamber flash gap above the area of consolidated material. Powder that exited the wheel groove in this way tended to be extremely hot and created sparks. The powder was left to collect in the bottom of the machine without being removed from the powder stream and at $t = 1000$ s the loose powder pile was ignited by sparks. Powder feed and hence the extrusion was stopped at this point and put into a slow run at 2 RPM to prevent the wheel welding to the titanium and tools. During this slow run the abutment stress immediately increased before slowly declining with time as the wheel and abutment cooled. It is suggested that the resultant low measured abutment stress observed during the process prior to the fire and wheel slow run was because of sliding motion between the titanium and the wheel. Therefore the rapid increase of abutment stress with the reduction in wheel speed from 8 to 2 RPM may be due to a reinitiation of static friction between the wheel and workpiece.

After the titanium fire was extinguished at $t = 1450$ s the wheel speed was ramped up to 10 RPM and further powder was added to the wheel groove. The abutment stress quickly reduced to around 500 MPa as the wheel speed was increased. During this phase of 10 RPM wheel speed the wire extruded very steadily at around 40 mms^{-1} and there were no significant areas of stick and slip lines observable on the surface of the wire.

Figure 3.16 is a composite plot of the recorded data points from Trial 1 showing the wheel speed and abutment stress at each point. The points are also coloured according to what

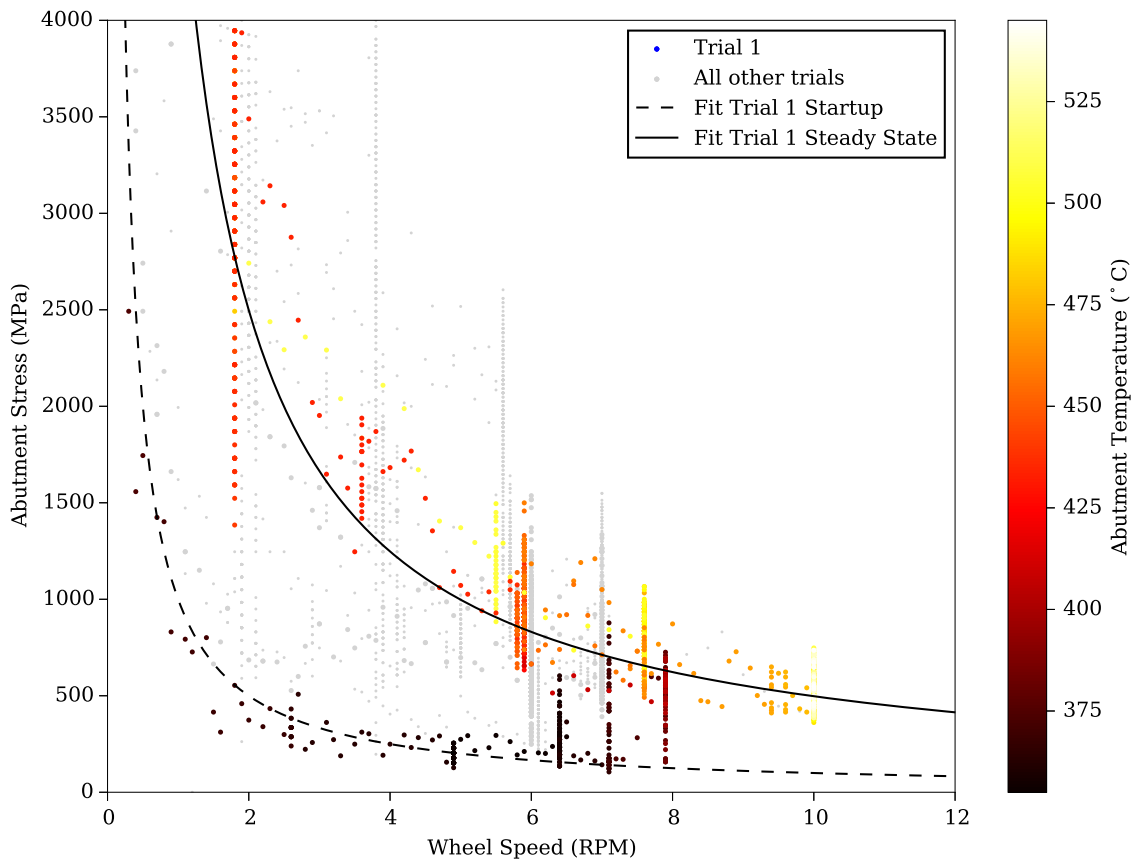


Figure 3.16: Abutment stress vs wheel speed curves for trial 1 overlaid on the data from every trial conducted in this project.

temperature the abutment thermocouple was measuring at the time the data was logged. While there is no temporal dimension to the graph it is clear that the trial data can be split into two distinct populations. The dark, cooler data points follow the lower dot-dashed line of best fit at low values of abutment stress. These data points were collected at the beginning of the trial when the tools were clean and the powder was still cold and loose. As the wheel speed is maintained at 6-8 RPM during the consolidation and early extrusion phases the abutment stress value increases shifting the data points up to the second dashed line of best fit. This transition is seen as the dark red vertical line of points in figure 3.16 above the 8 RPM x axis tick mark.

During the titanium fire in the middle of the test the wheel speed is reduced before being increased up to 10 RPM. This results in the data points following the curved dashed upper line. Both line of best fits follow a $y = \frac{Ae^{-Bx}}{x}$ form and were fitted to the two distinct populations of data. For Trial 1 the startup curve fit parameters for the loose, preconsolidated powder are $A = 1000$ and $B = 0.0005$, while the ‘steady’ extrusion phase with fully consolidated powder follows $A = 0.0005$ and $B = 0.0005$. The region on the graph represents a processing window

suitable for the Conform processing of grade 2 CP-Ti HDH powder. These lines of best fit have been over-plotted on each of the wheel speed vs abutment stress graphs for trials 2-6. This illustrates the proposed processing window and how it was explored in subsequent trials.

3.3.2 Trial 2

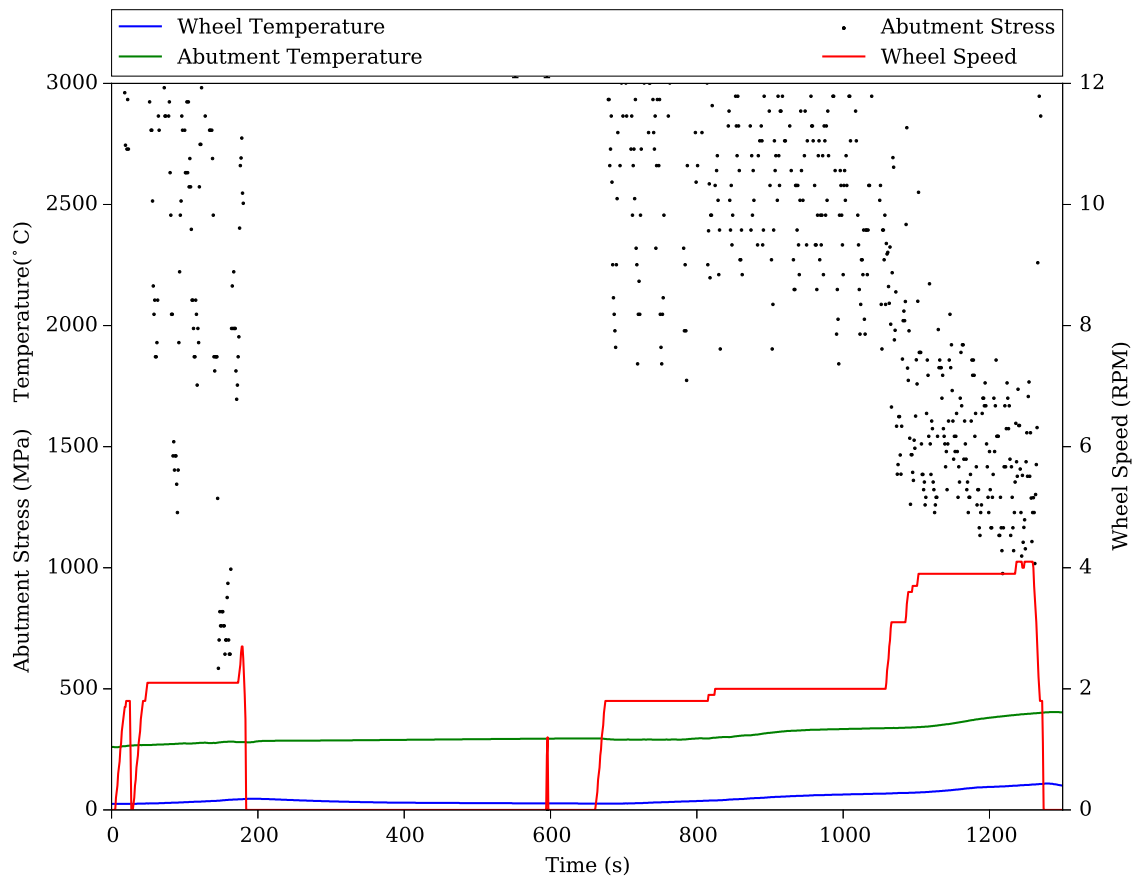


Figure 3.17: Raw data tool temperature and abutment stress (torque derived) from trial 2.

Trial 2 was conducted to determine the effects of a rectangular die as opposed to the 5 mm round die used in trial 1. Here the die was orientated so that its longest side was parallel to the floor or in the horizontal direction. The cross sectional area of the die land was about 12% smaller than that of the 5 mm round die making it slightly harder to extrude.

The trial (shown in figure 3.17) started with a 2 RPM wheel speed, a moderate powder feed and a relatively low abutment temperature of 250°C. As soon as powder was fed into the machine the abutment stress response was extremely high, especially when compared to the startup process of trial 1. Powder feed rates were not available to be logged during these trials, so it is not clear what effect this may have had. However, with a low wheel speed of 2 RPM, as with trial 1 it may show the increased proportion of grip between the groove and wheel. With this the powder would be simply cold compacted in the abutment zone resulting a large abutment stress reading. Indeed the stability of the process shown in figure 3.18 at this point is considerably higher than that observed during the periods of extrusion in trials 1. Waste titanium powder in the bottom of the machine was ignited at $t = 180$ s and the shoe was

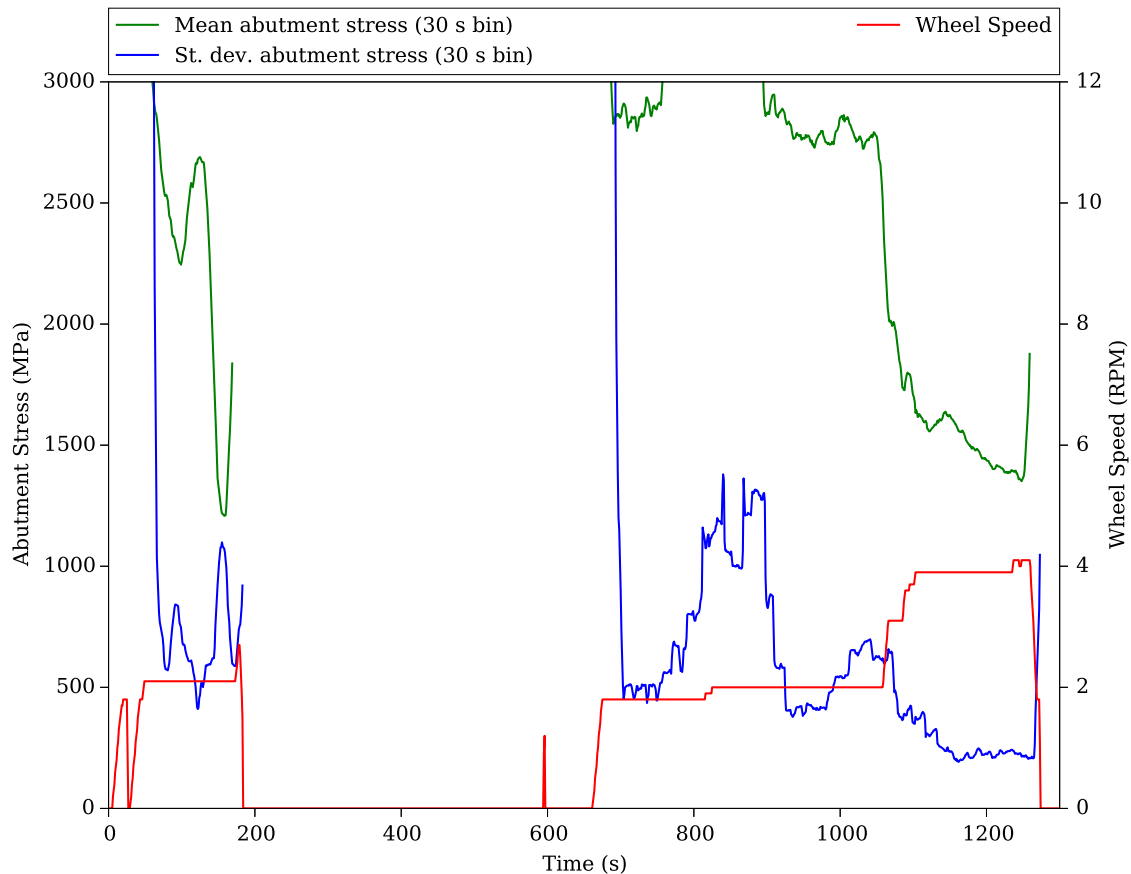


Figure 3.18: Abutment stress analysis plot from data obtained during trial 2.

retracted to clean out any partially consolidated powder.

The trial recommenced with a wheel speed of 2 RPM, before being increased to 4 RPM. This increase caused a large drop in both the average abutment stress and standard deviation. During this phase a short amount of titanium strip was extruded through the die before the abutment failed at $t = 1350$ s. It is clear from this trial that 2 RPM is too slow a wheel speed to extrude titanium powders at. The increased proportion of grip coupled with cold powder causes it to be cold compressed against the tools, preventing significant tool, powder shear and hence heat generation between particles. The short extrusion that occurred at 4 RPM indicates that while this may also still be too slow, it helps to relieve some pressure on the tooling while also generating more heat in the powder assisting in its consolidation.

Examination of the abutment stress vs wheel speed graph in figure 3.19 for trial 2 also shows the large number of data points and hence time at high (> 1000 MPa) stress that the process generated. With a relatively small quantity of powder in the machine a large proportion of this stress will have been directed onto the abutment face creating the premature failure that halted the trial. There are no data points on the lower ‘startup’ approach line where it was shown in

the previous section 3.3.1 this was necessary in order to successfully consolidate the titanium powder without yielding the abutment.

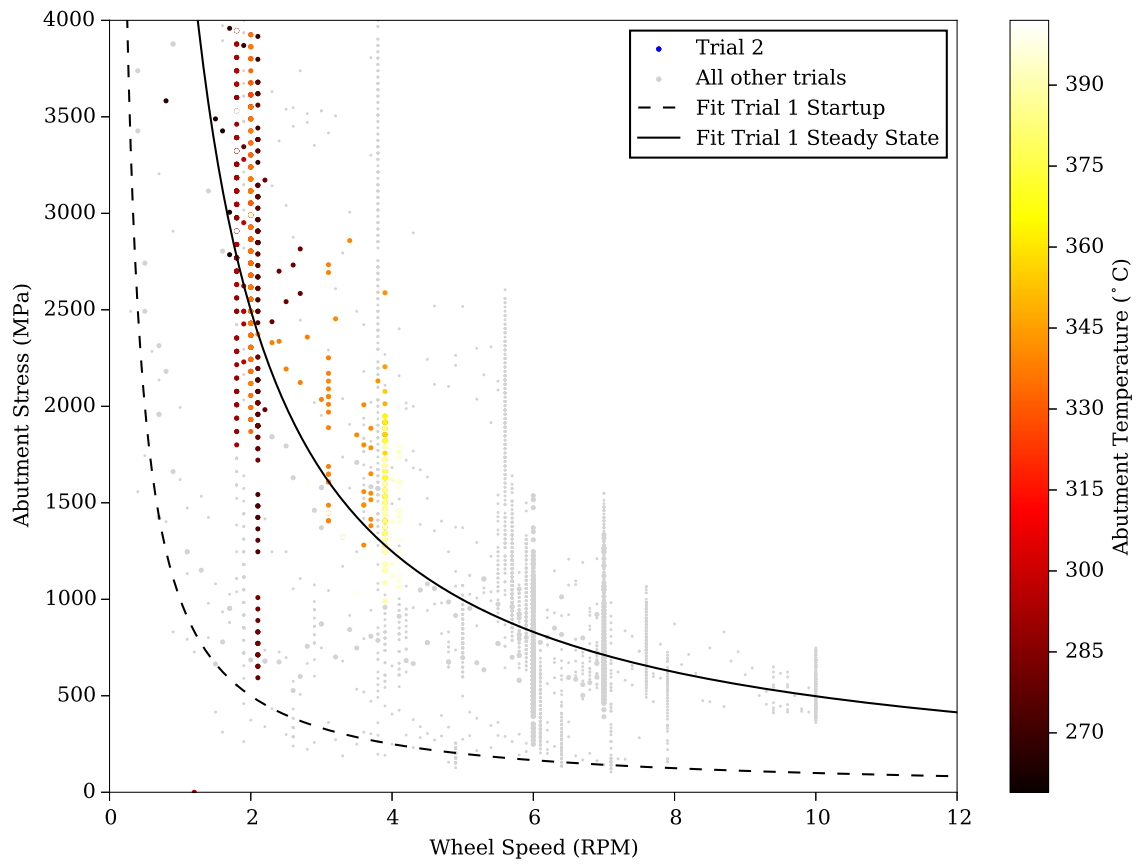


Figure 3.19: Abutment stress vs wheel speed curves for trial 2 overlaid on the data from every trial conducted in this project.

3.3.3 Trial 3

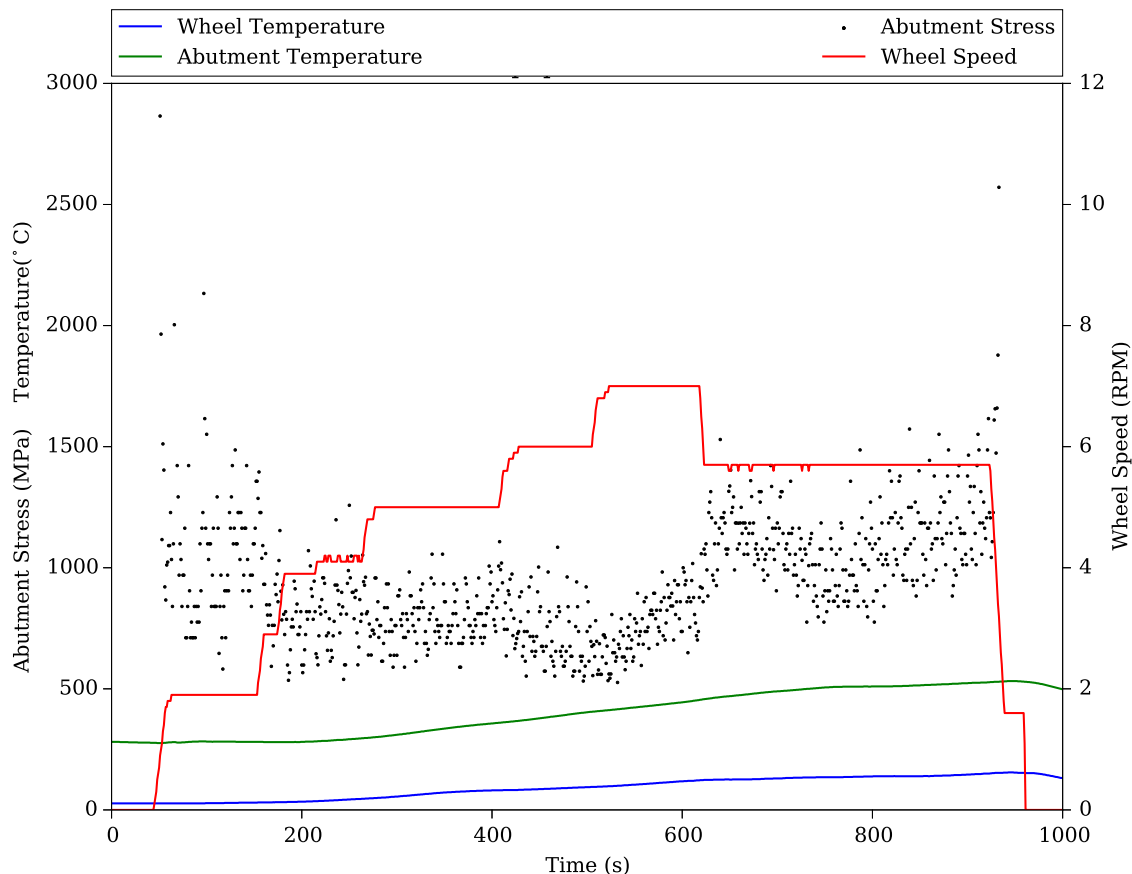


Figure 3.20: Raw data tool temperature and abutment stress (torque derived) from trial 3.

Trial 3 was conducted on the same day with exactly the same machine setup as trial 2 but with a rectangular die setup at 90° to the previous trial. Powder feed was reduced compared with trial 2 but kept constant throughout the trial. Wheel speed was increased to 4 then 5 RPM to prevent cold compaction of the powder. Significant heat was generated once the wheel was at 5 RPM, but not at lower wheel speeds as shown in the abutment and wheel temperatures in figure 3.20. The rate of increase of temperature was not as great as during the startup of trial 1, indicating that faster wheel speeds are better at generating more heat within the powder, which is then observed in the temperature traces of the abutment and wheel.

During the trial phase at 7 RPM wheel speed the stability of the process can be seen to improve slightly but with a marked increase in the abutment stress between $t = 500$ s and $t = 660$ s. It was at this point that a significant amount of consolidation occurred and began to extrude solid titanium strip. The abutment failed suddenly at $t = 920$ s, which suggested

Trials 2 and 3 were conducted on the same day and as such the groove on the wheel used for trial 3 contained powder coated during trial 2.

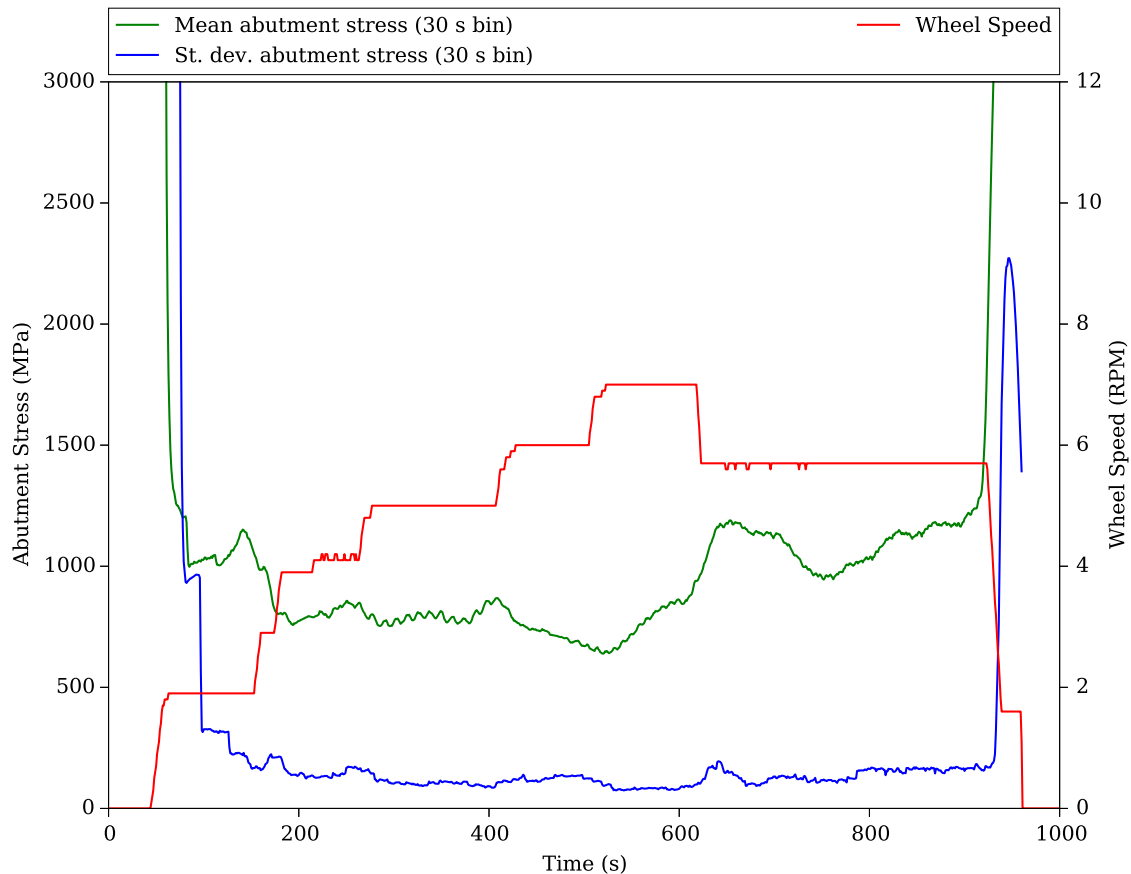


Figure 3.21: Abutment stress analysis plot from data obtained during trial 3.

that while there was sufficient pressure to extrude the titanium, the temperature as measured at the abutment was too low to reduce the flow stress of material in the abutment zone enough to prevent the abutment failure.

The abutment stress vs wheel speed plot in figure 3.22 shows the difference in the startup of the process when compared with the trial 1 data. While the approach curve of lower abutment temperature data points is lower than that in trial 2 it is above the ‘ideal’ line from trial 1. The shape of the curve is also different, with a high abutment stress ‘tail’ at 8 RPM. It is these data points that resulted in the abutment failure at the end of trial 3.

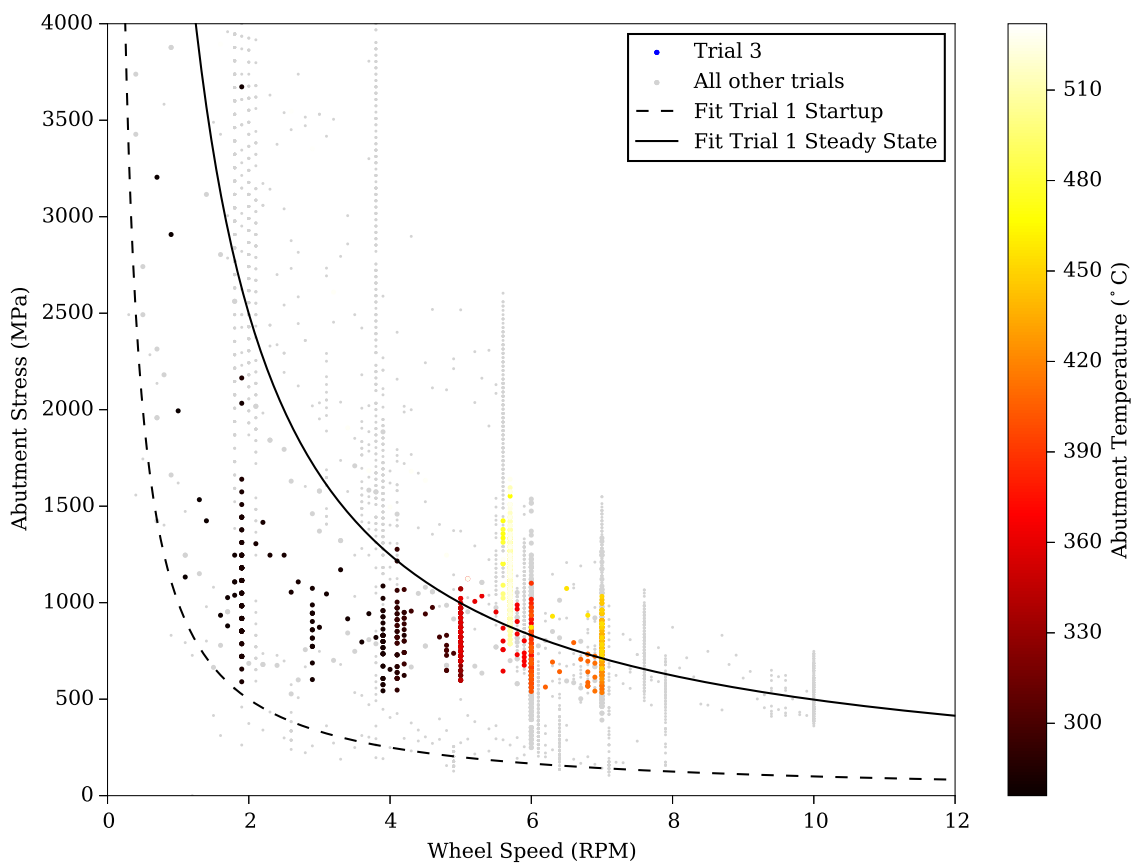


Figure 3.22: Abutment stress vs wheel speed curves for trial 3 overlaid on the data from every trial conducted in this project.

3.3.4 Trial 4

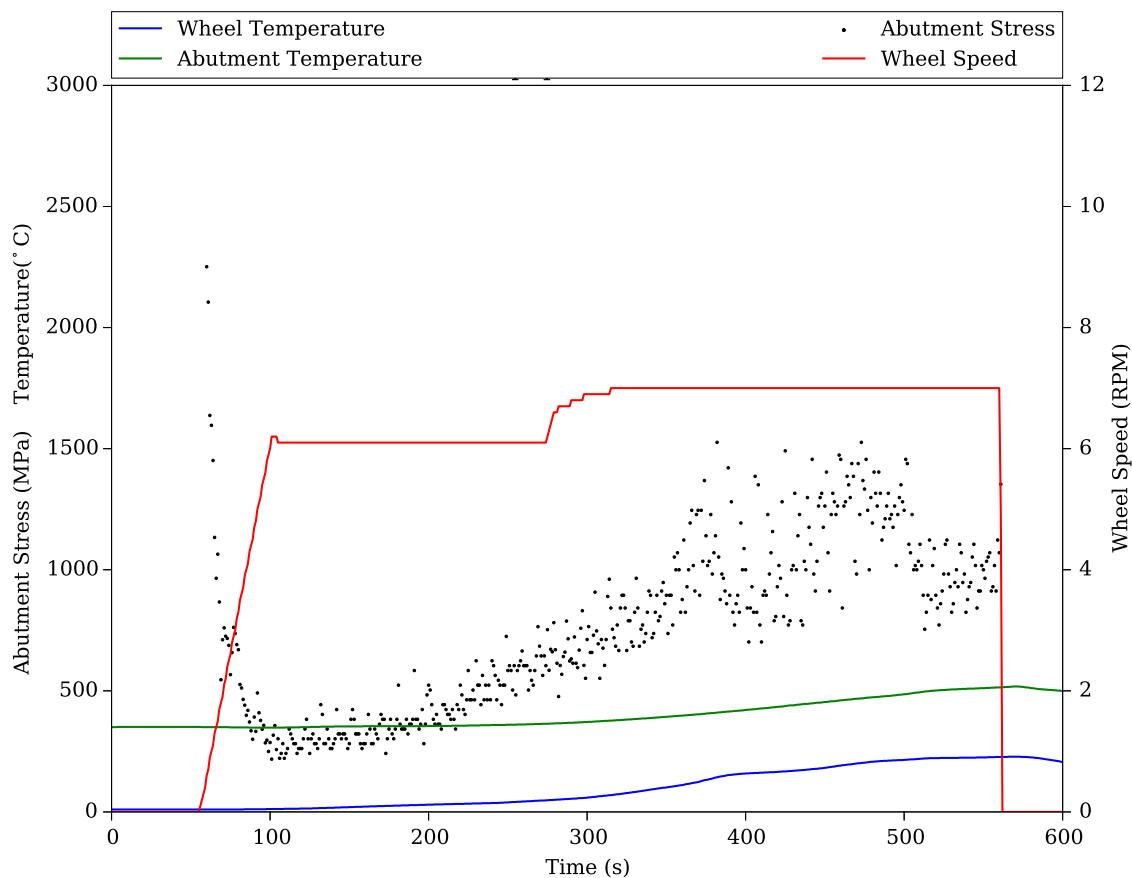


Figure 3.23: Raw data tool temperature and abutment stress (torque derived) from trial 4.

Trial 4 used a funnel hopper as described in figure 3.7 so that the powder flow rate could be repeated with subsequent trials but also kept constant for long periods of time. It was determined from the previous trials that a wheel speed of 2-4 RPM was too slow for successful extrusion without failure of the abutment. Therefore trial 4 started at a wheel speed of 6 RPM. Powder feed was kept at a steady 200 gmin^{-1} during the trial with the hopper valve set by the BWE operator and held over the vibrating chute above the groove. There was no build up of powder on the chute, which meant that the powder feed rate into the machine was equal to that from the funnel.

It can be seen in figure 3.23 that the abutment stress starts out very low at a similar 300 MPa value to trial 1 and also slowly increases over the next 200 s. During this phase the stability of the process remains at a low value as observed in figure 3.24 and starts to increase at $t = 300$ s when the wheel heating rate also increases. This is indicative of the beginning of extrusion and material enters the die and experience the maximum amount of contact with all the tools. During this trial a 300 mm length of wire was extruded. At $t = 500$ s the abutment broke and

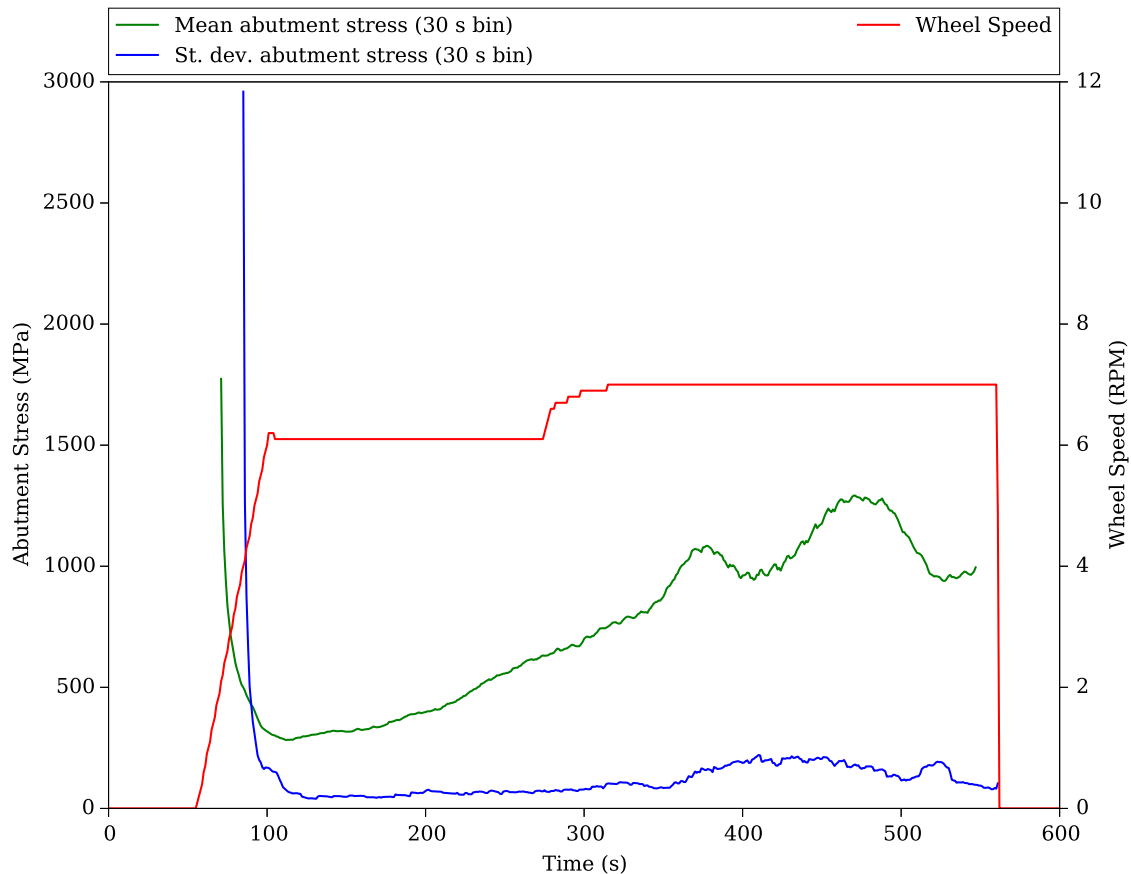


Figure 3.24: Abutment stress analysis plot from data obtained during trial 4.

the trial was stopped. The abutment failure can be seen in figure 3.24 as a drop in the average abutment stress and a small peak in the standard deviation value at $t = 500 - 530$ s.

Examination of figure 3.25 shows that the process startup approach curve from trial 1 was followed very closely. The consolidation occurring between $t = 100$ s and $t = 280$ s can be seen as a dark brown vertical line above 6 RPM. When the wheel speed was increased to 7 RPM the abutment stress remained on the steady state line. At this point powder continued to be consolidated in the wheel at ever increasing grip lengths resulting in high abutment loads and eventually failure of the tool. It is possible that by increasing the wheel speed to 8 RPM after the abutment stress reached 900 MPa that the resultant drop in stress would not have yielded the abutment. The increased shear in the powder caused by this faster wheel speed would also have generated more heat in the powder assisting its deformation and further reducing the effective load on the abutment.

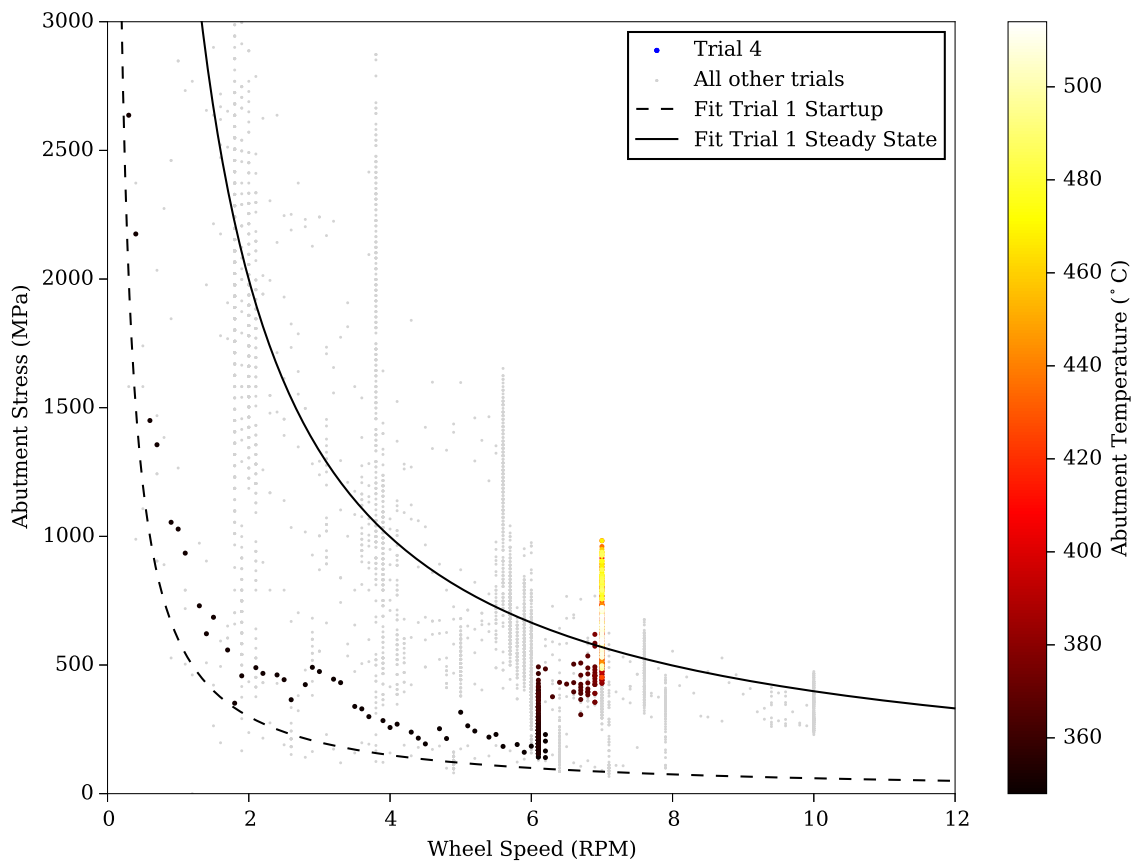


Figure 3.25: Abutment stress vs wheel speed curves for trial 4 overlaid on the data from every trial conducted in this project.

3.3.5 Trial 5

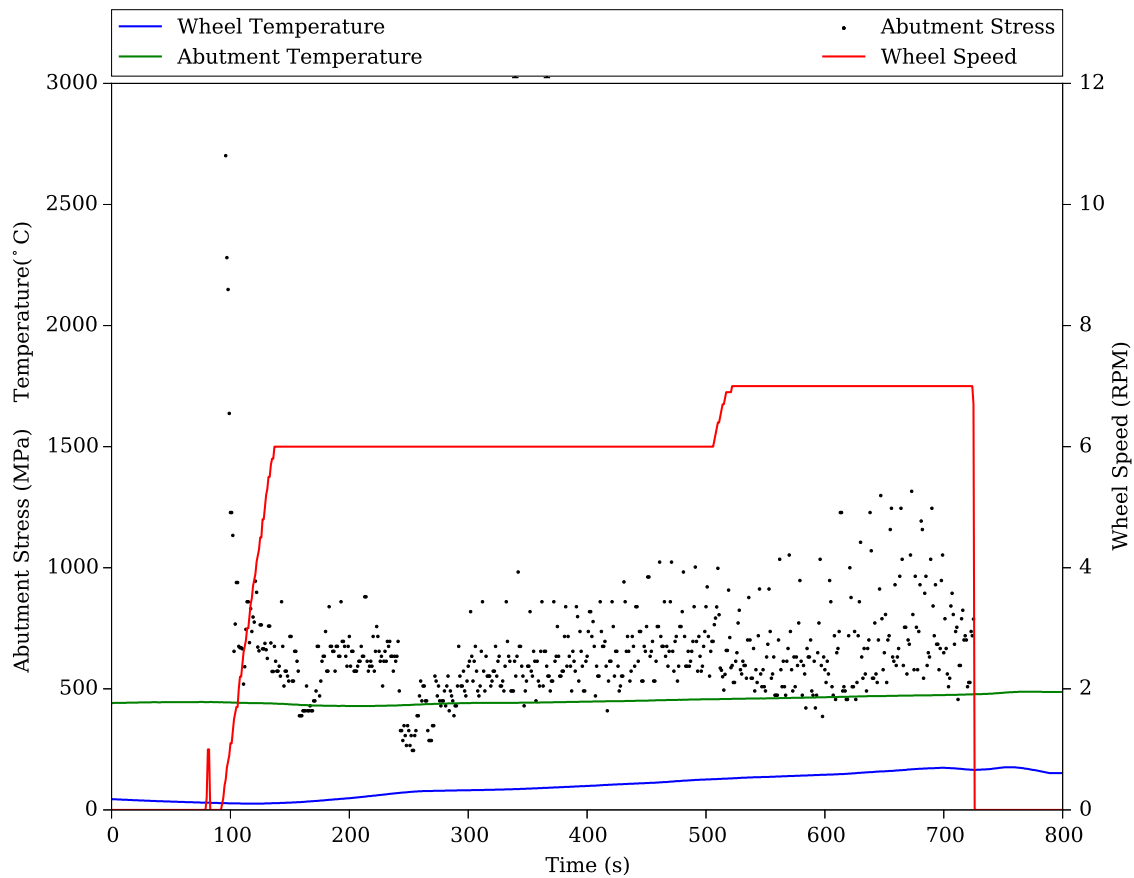


Figure 3.26: Raw data tool temperature and abutment stress (torque derived) from trial 5.

For trial 5 the powder hopper was used with an initial 200 gmin^{-1} mass flow rate onto the vibrating chute as per trial 4. The wheel was run at 6 RPM as the powder was fed into the groove. The powder feed rate was varied according to the motor current observed from the machine display as per figure 3.6. As the wheel was pre-coated from the previous trial and waste powder from the vibrating chute was in the abutment zone the wheel was rotated several times without powder feed from the hopper in order to clear the groove. Powder was fed into the machine at $t = 150 \text{ s}$ where the nominal abutment stress created by the pre-filled tooling began to drop from 600 MPa to 480 MPa. The powder feed was adjusted according to the observed motor current but it was discovered during post processing that the pre-coated wheel and consolidated waste powder produced a nominal loading on the machine, which masked the motor current reading changes from variations caused by changes in the powder feed.

The initial approach curve of the darkest points seen in figure 3.28 closely matches that of

Trials 4 and 5 were conducted on the same day, which meant that the groove on the wheel used for trial 5 contained powder coated during trial 4.

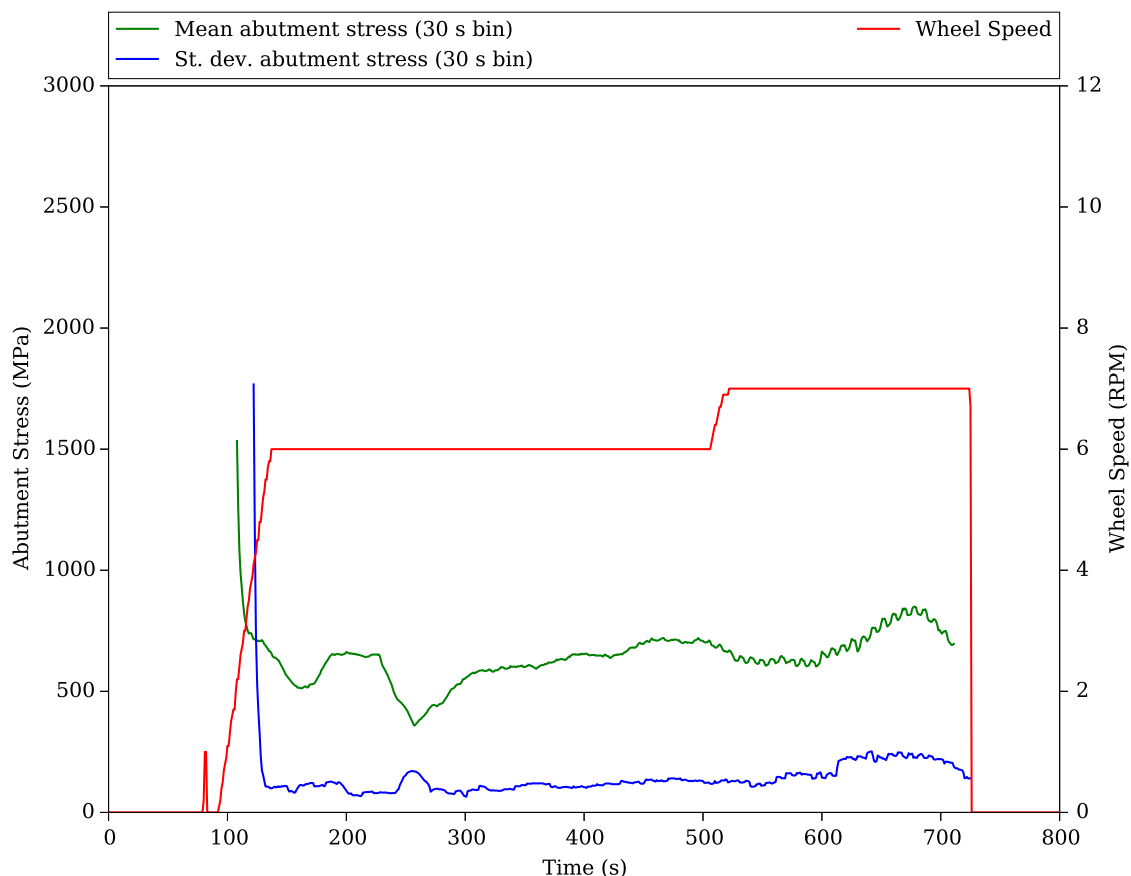


Figure 3.27: Abutment stress analysis plot from data obtained during trial 5.

the steady state curve in trial 1 producing a large load on the wheel and abutment. The second attempt at startup of the extrusion is shown as orange data points and matches the trial 1 startup approach line closer than the initial attempt. Speeding up the wheel to 7 RPM slightly dropped the abutment stress but with the extra material around the groove the powder feed rate was not able to be successfully managed to keep the stress level down.

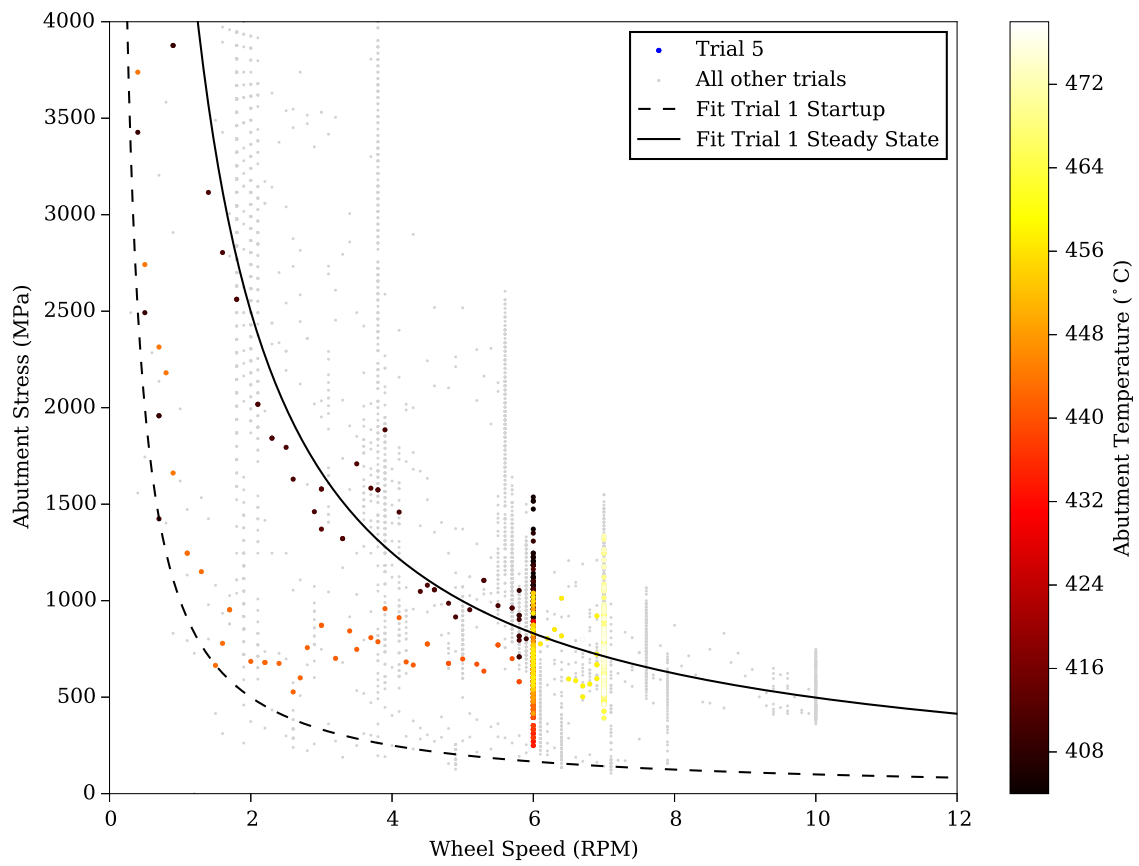


Figure 3.28: Abutment stress vs wheel speed curves for trial 5 overlaid on the data from every trial conducted in this project.

3.4 Analysis of extruded titanium wire and strip

Analysis of extruded products from each of the trials was conducted to determine what effect the Conform process had on the feedstock powder. It is not clear from the available literature what flow path stress state metal powder particles experience through the Conform process. A lack of standardisation in how Conform machines are configured and run further prevents direct comparisons of results. Figures 3.29, 3.30 and 3.31 show 5 mm diameter CP-Ti wire emerging from the back of the shoe after extrusion. The wire emerged yellow-red hot from the die and travels a distance of one metre in air before entering a water trough to be further cooled. For fast (over 100 mms^{-1} extrusion speed) extrusions with large cross sectional areas the water trough will act as a quench tank to control the degree of recrystallisation and grain growth in the product. For this work, the small cross sectional area and relatively slow extrusion speed meant that an appreciable amount of cooling had already occurred before the wire entered the water trough.



Figure 3.29: 5 mm diameter CP-Ti wire emerging from the BWE ConformTM machine before entering a water trough to be quenched.

Figure 3.32 shows the tooling following the unintentional interrupted test during the first phase of trial 2. A number of titanium chips can be seen on the tip of the abutment indicating that consolidation had possibly begun. It is also possible that the chips came from the abutment shaving off a section of the wheel coating, as there are no significant markings from consolidated



Figure 3.30: 5 mm diameter CP-Ti wire emerging from the BWE ConformTM machine before entering a water trough to be quenched.

powder on the die chamber or abutment sides as expected from the other trials. Abrasion of the abutment can be seen on its side down to a depth of ~ 4 mm from its top face. From the powder shear wheel coating theory in section 3.2.8 this suggests that at a wheel speed of 2 RPM the critical shear ratio between the wheel and powder is ~ 0.1 .

At the end of trial 2 the shoe was retracted revealing the fractured abutment and titanium coating (see figure 3.33). The powder had consolidated at the back of the abutment zone and completely filled the die chamber port. There was a domed surface on the discard nearest the die indicating a transition between consolidated material and loose powder. Consolidated titanium is also coated on the sides of the die chamber tool where it leaked from between the wheel surface and shoe. The visible interaction between the powder and tools to a depth of ~ 24 mm from the abutment face, at a maximum wheel speed of 4 RPM shows from figure 3.11 in section 3.2.8 that the critical shear ratio is also 0.1. This agrees with the abutment abrasion seen earlier in trial 2 from the interrupted test. The titanium had oxidised as shown by the change in colour but only to gold-yellow indicating that the temperatures reached on the tool surfaces were relatively low at $\sim 500^\circ\text{C}$. In other trials that showed measured abutment temperatures of $100\text{-}200^\circ\text{C}$ higher blue and purple oxide colours were observed in the consolidated titanium remaining on the tools post-trial. White TiO_2 can also be seen coating the lower parts of the tools following the titanium fire that occurred mid-trial.

Figure 3.34 shows the die chamber following trial 3 where the StelliteTM 21 abutment failed. The oxide colours observed indicate that the temperatures reached at the tool, wheel interface were far higher than during trial 2. Consolidation in the powder can be seen to reach approximately 45 mm above the abutment face before the discard becomes more friable and can be

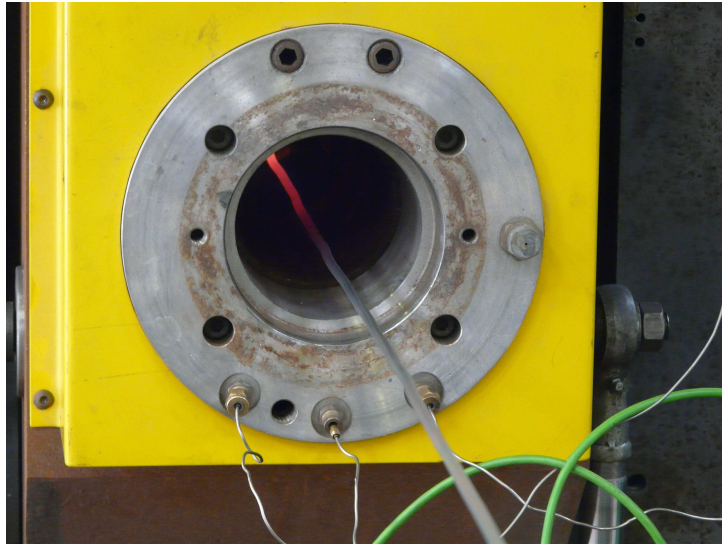


Figure 3.31: Close view of the back of the shoe with 5 mm diameter CP-Ti wire emerging from the BWE ConformTM machine. The wire glows red hot due to the large amount of heat generated during the process.

seen to bend away from the die chamber. Similarly the powder consolidation height is also similar following the completion of trial 4 as seen in figure 3.35. The powder at the top of the die chamber was only lightly compacted and could be broken apart by hand. Oxide colours again indicate that the gold-yellow-purple-blue progression from top to the bottom of the die chamber indicate surface temperatures of 500-800°C . Friable powder below the surface at the top of the die chamber did not have a visible oxide colour, which suggests that it did not undergo appreciable heating in the centre of the wheel groove. Therefore it is possible to conclude that the powder is shearing and heating up most at the surface of the groove rather than undergoing a bulk shear throughout the entire groove cross section. The majority of heat imparted to the powder would therefore be from contact with the die chamber and the frictional heat generated between the groove (wheel coating) and the powder layer nearest the groove surface.

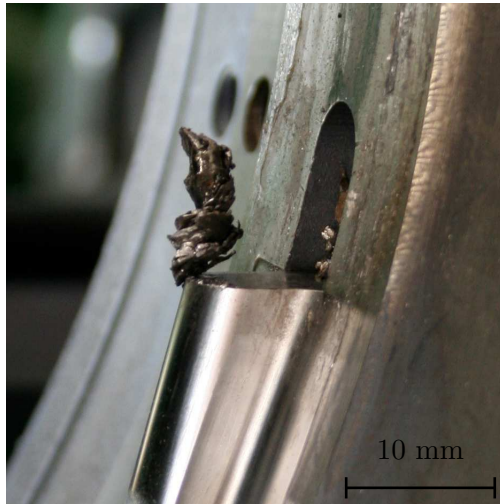


Figure 3.32: Close up of the abutment and die port following an interrupted test in Trial 2 with a wheel speed of 2 RPM

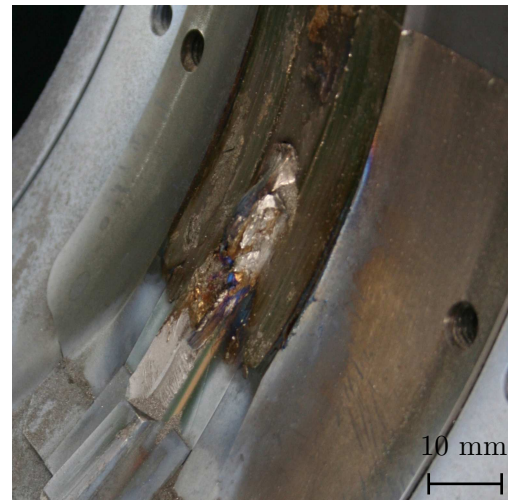


Figure 3.33: The die chamber at the end of Trial 2 showing the fracture surface of the failed abutment with partially consolidated titanium processed over the top.

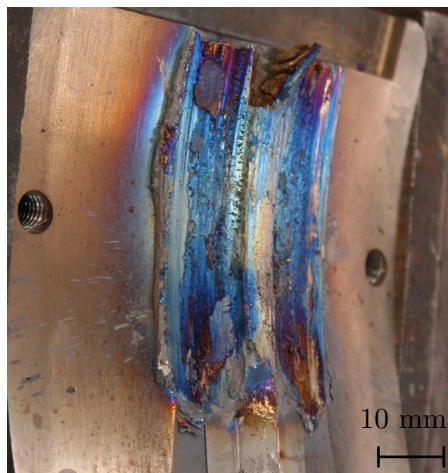


Figure 3.34: The die chamber at the end of Trial 3 following a maximum wheel speed of 7 RPM

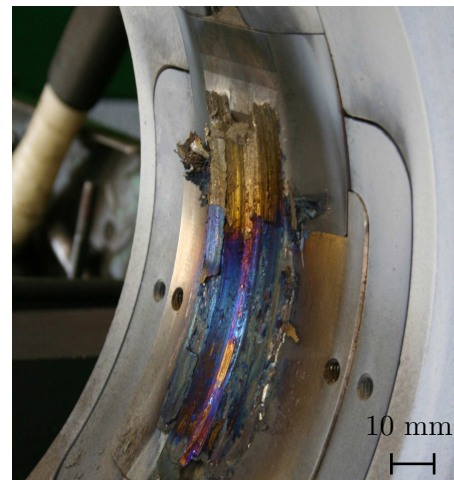


Figure 3.35: The die chamber and entry block within the shoe at the end of Trial 4 showing good consolidation. The fractured abutment is hidden by the titanium processed over the top of it.

3.4.1 Round 5mm Die

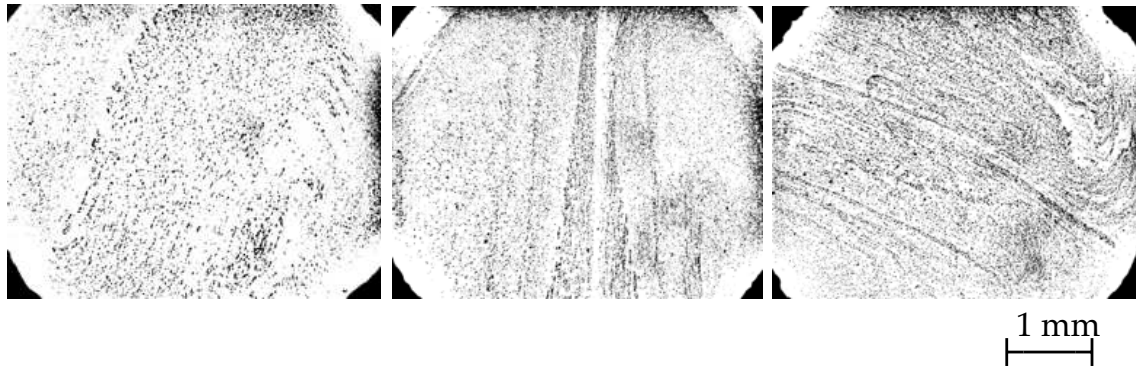


Figure 3.36: Macrostructures of the cross section of the extruded 5 mm diameter CP-Ti wire. Images taken under polarised optical light were converted to binary format to highlight the flow profiles.



Figure 3.37: Macrostructures of the longitudinal section of the extruded 5 mm diameter CP-Ti wire. Images taken under polarised optical light were converted to binary format to highlight the flow profiles.

The majority of wire was extruded from trial 1 with trials 2/3 used to explore the extrusion or strip through rectangular dies and 4/5 used aid in defining the processing window. Round wire of diameter 5 mm was extruded at three distinct wheel speeds. Rod was also extruded during periods of transition between wheel speeds but were not included in the analysis due to the transient nature of the pressure and temperature distributions. Macrostructures of the rod cross sections are shown in figure 3.36 for each of the 6, 8 and 10 RPM wheel speeds. The macrostructures are representative of a general powder Conform extruded wire/rod with distinctive flow profiles, which are also observed in aluminium [12] and copper [11]. Each flow profile is different from the next and are also different between samples taken from the same wheel speed. The strength the swirls within the macrostructure appear to be related to the yield strength of the parent material. Aluminium powders extruded through a CRE machine by Stadelmann [12] producing flow patterns with fully circular or ‘swiss roll’ type structures as

shown in figure 2.12. By comparison the titanium powder feed cross sections exhibit far weaker flow patterns.

There are several structural similarities between the macrostructures of the metallographic samples despite the apparent visual differences. Around the outside of the wire is a visible onion-skin of larger 20-50 μm grains that form within a depth of 200-400 μm from the surface of the wire. The central vertical flow contains the smallest grains of 1-4 μm , while either side (region 2) the larger grains of 10-20 μm are found. No prior grain boundaries or porosity was observed and grain sizes were significantly smaller than that in the feedstock powder indicating that the powder particles microstructure had been completely reworked during extrusion.

Macrostructures of the wire samples also exhibit a wide range of flow profiles as shown in figure 3.37. In two of the samples shown there is a central chevron pattern surrounded by laminar regions. The spacing between the flow lines that define these laminar regions decreases as they get closer to the wire surface at the top and bottom of the images.

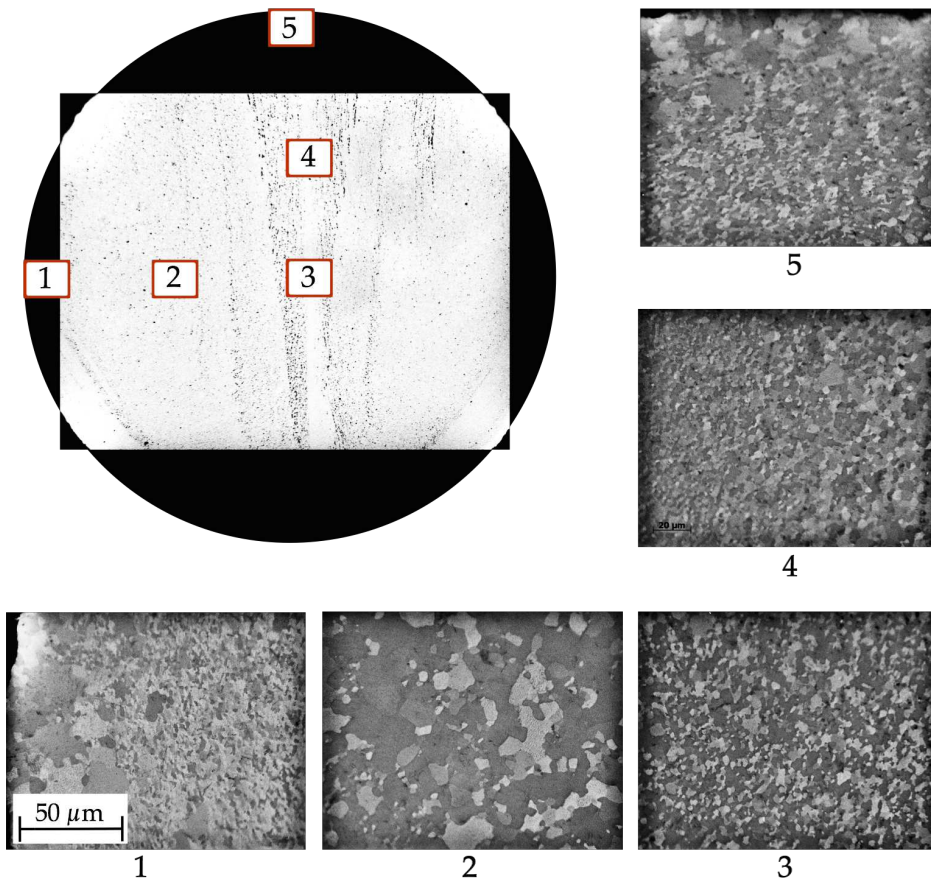


Figure 3.38: Cross-polarised light micrographs of a sample extruded at 8 RPM with locations indicated on the cross-section.

Microstructures from a sample of wire extruded at 8 RPM are shown in figure 3.38 along

with their locations on the sample's cross section. The grain sizes varies considerably at different points in the wire cross section and appears to be linked to the macrostructure. Each of the microstructures show fully equiaxed grains with no twinning or visible remaining deformation. The abutment temperature was approximately 500°C when this sample was extruded and was continuing to rise suggesting that the temperature the wire was much higher. There is no evidence of a β to α phase transformation at the wire cooled indicating that the temperature of grade 2 titanium did not exceed its beta transus of 882°C. Larger grains can be seen at the surface of the rod on the left hand side of micrograph 1 in figure 3.38, which may indicate that there was a large degree of frictional interaction between this region and the die surface. The dies had no special coating treatment and only underwent a final hand polish before use. Abrasion from the titanium prior to this sample being extruded may have significantly increased the coefficient of friction in the die bearing. This region of larger 20-40 μm grains extends all around the wire surface and forms the outside of the 'onion skin' layer that is visible in the macrostructure image of figure 3.38.

The main bulk of the 'onion-skin' layer consists of a small region of fine equiaxed grains 2-4 μm in diameter. There are some larger 10-15 μm grain randomly positioned within the matrix of fine grains with no apparent pattern to their location. Inside this layer is a region of much larger 20-50 μm grains that extend into the central vertical flow. This vertical spine of fine grain extends from the top to the bottom of the cross section and contains fine grains of 2-5 μm in size (see images 3 and 4 in figure 3.38). There is no change in morphology or size of these grains along the entire length of this central spine.

Micrographs were taken of samples on a section in the longitudinal plane of the rod. The orientation of the rod was lost following removal from the machine, transport and sample preparation so it is not know what angle the observed planes were to the central plane of the Conform wheel. It is clear from the cross section images in figures 3.38 and 3.40 that orientation information needs to be retained to allow accurate analysis of micrographs taken from longitudinal sections. It can be seen from figure 3.39 that all the grains are equiaxed with very little evidence of elongation due to extrusion through the Conform die.

Microstructures from a sample of wire extruded at 10 RPM are shown in figure 3.40 along with their locations on the sample's cross section. The macrostructure share only a few similarities as that from samples extruded at 8 RPM (figure 3.38). Micrographs from the cross section show that there is a far more homogeneous microstructure in the rod extruded at 10 RPM than 8 RPM.

This is also shown in figure 3.41, which shows the average grain sizes in each of the five

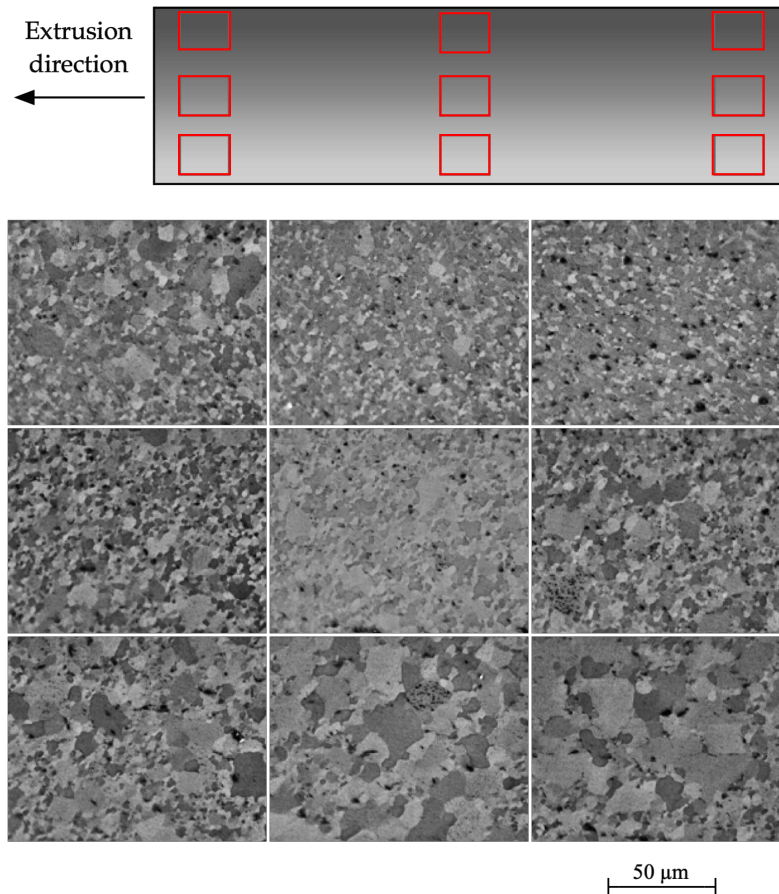


Figure 3.39: Cross-polarised light micrographs of a sample extruded at 8 RPM with locations indicated on the longitudinal section.

inspected regions from the cross sections of the three wheel speeds 6, 8 and 10 RPM. In general smaller grain sizes are observed in wire samples extruded at higher wheel speeds. There is also a trend towards a more homogeneous microstructure at higher wheel speeds as shown both by the error bars and spread amongst the five regions in figure 3.41.

It should be noted that no prior particle boundaries or oxide layers were visible throughout all of the microstructures observed demonstrating that the particles have been severely deformed prior to extrusion. There appears to be full diffusion bonding between all the particles with no visible voids.

3.4.2 Grain growth for diffusion bonding

Figure 3.42 shows a composite macrograph of a cross section of heat treated CP-Ti wire extruded at 10 RPM. The image is made from stitching together 121 individual optical light micrographs to give a full view of how different areas of the macro flow react to a super-transus heat treatment. It was thought that by taking the sample above the beta transus that grains that were fully diffusion bonded following extrusion would exhibit significant grain growth in

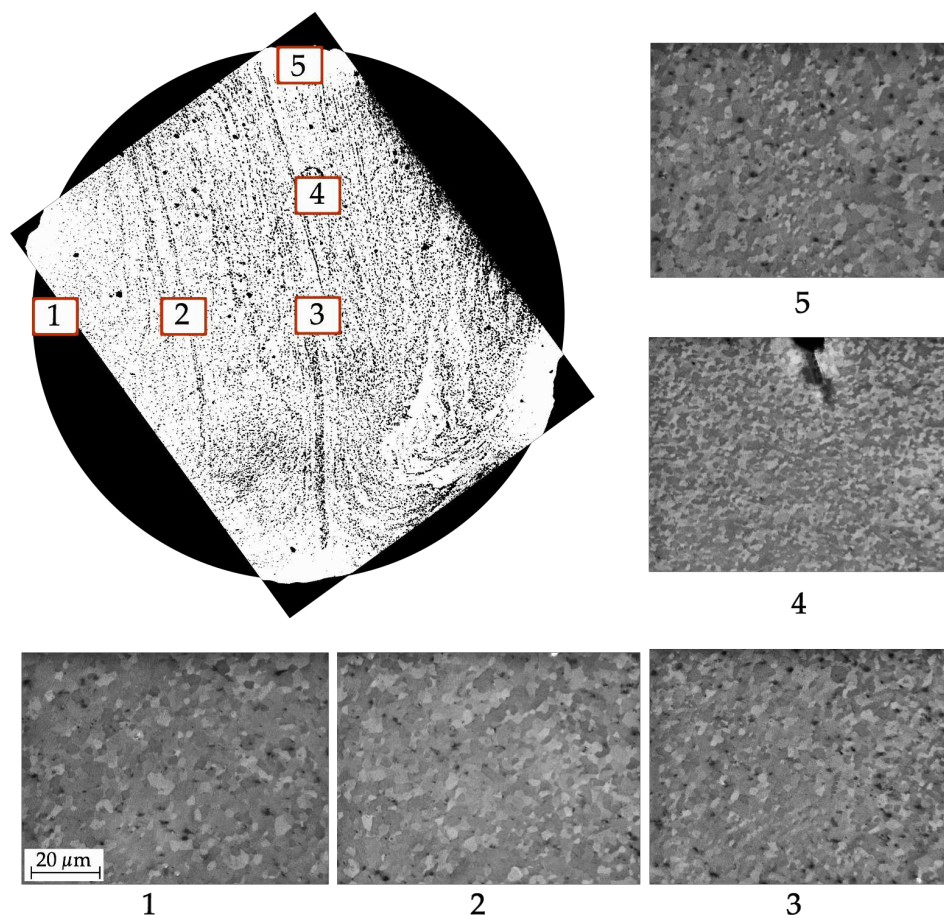


Figure 3.40: Cross-polarised light micrographs of a sample extruded at 10 RPM with locations indicated on the cross-section.

the beta phase. The observable transformed alpha laths would indicate the regions that had large prior beta grains during the heat treatment.

It can be seen in figure 3.42 that the regions in the ‘onion skin’ and those inside this such as region 2 from figure 3.38 contain large transformed alpha laths that come from beta grains $\sim 300 \mu\text{m}$ in size. These area appear to be fully diffusion bonded and have allowed significant grain growth during heat treatment. By comparison there are some small but well defined areas of relatively small equiaxed alpha grains. These small alpha grain regions follow the central spine and arc regions visible in the macrostructures of the extruded wire. The small size of these grains in relation to the surrounding matrix and their equiaxed form suggest that they are not fully bonded to the surrounding regions and hence have not been able to exhibit the grain growth seen in the rest of the rod.

Tensile samples from the 5 mm diameter wire were tested to failure according to the ASTM E8 2015 standard [89] and the results presented in table 3.5. The spread of results for the elongation and reduction of area all suggest that there is a wide range of properties along the

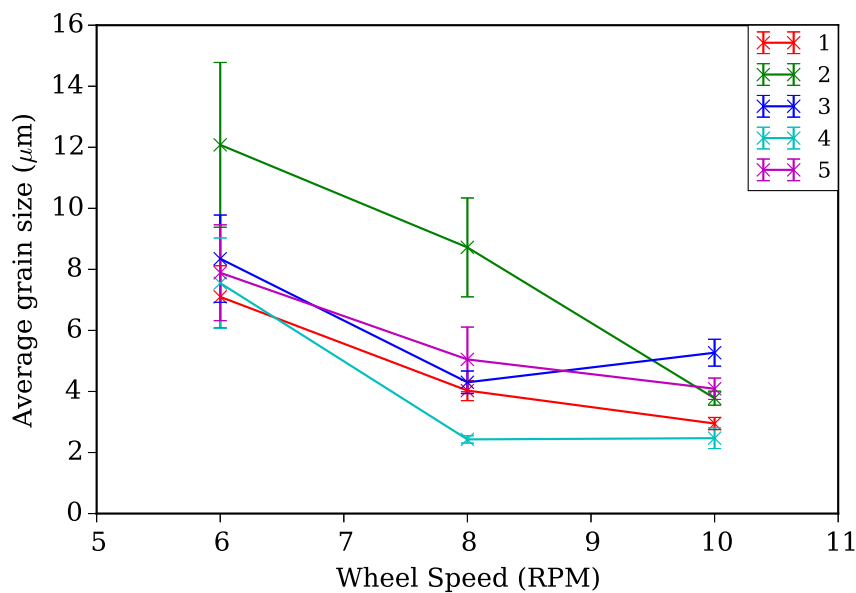


Figure 3.41: Average grain sizes from micrographs taken at five locations in the cross sections of extruded 5 mm CP-Ti wire.

Table 3.5: Room temperature mechanical properties of the as-extruded 5 mm diameter CP-Ti extruded at three different wheel speeds.

| Wheel speed | E (GPa) | $\sigma_{0.2\%}$ (MPa) | UTS (MPa) | RA (%) | Elong. % |
|-------------|--------------|------------------------|--------------|-------------|------------|
| 8 | 109 ± 14 | 492 ± 13 | 608 ± 7 | 37 ± 14 | 12 ± 4 |
| 10 | 124 ± 15 | 557 ± 28 | 627 ± 12 | 22 ± 12 | 6 ± 2 |

lengths of the extruded rod. The lack of consistency in mechanical properties also correlates with other research on the Conform of powder where the uneven feedstock flow resulted in poor extrusion conditions [68]. Both yield strengths and ultimate tensile strengths exceed those specified for grade 4 wrought titanium [90]. They are also similar to those presented by Wilson *et al.* [73] from the Conform of preheated TiROTM titanium powders.

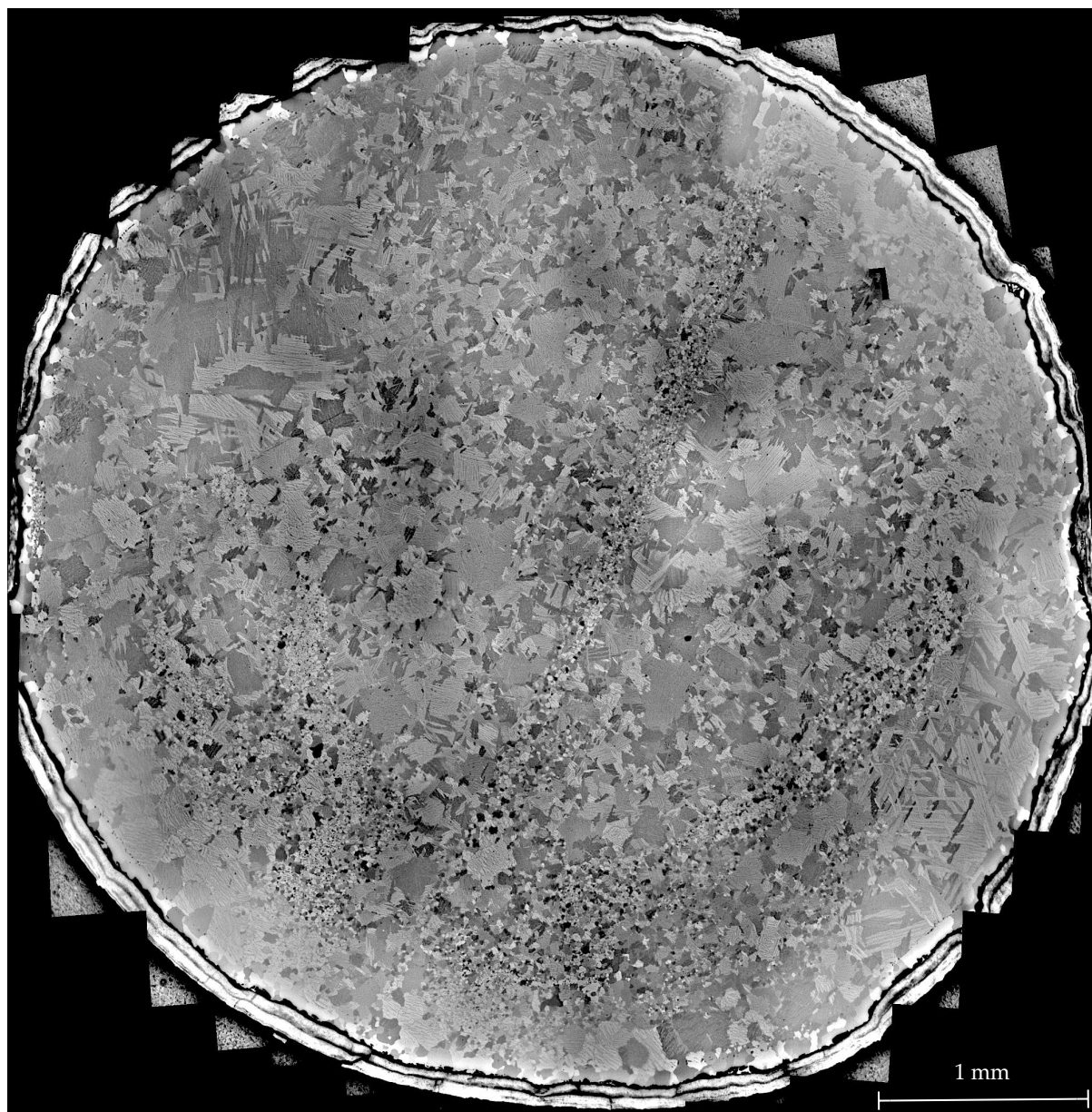


Figure 3.42: Composite cross-polarised light micrograph taken from a cross section of 5 mm diameter CP-Ti wire heat treated at 950°C for two hours.

3.4.3 Rectangular Die

Rectangular dies were used during trials 2 and 3 but only short lengths of wire were extruded during the startup phase of the process. The resultant microstructures shown in figures 3.43 and 3.44 are therefore taken from a transient extrusion without a stable pressure and temperature profile. Despite this the die discards obtained from the die chamber port and abutment zones do provide some information as to the how the Conform process progresses.

The macro flow observed in the strip extruded from trial 3 figure 3.43 shows a strong circular flow of titanium in the cross section. This flow is much more curved than the previous examples from the 5 mm diameter round wire and is similar in profile to that observed in aluminium in figure 2.12 from [12]. Figure 3.44 shows the fine 3-5 μm grains in the strip cross section. While the grains themselves are nearly fully equiaxed they show a small amount of elongation that links the flow on the micro scale and the macro flow seen in figure 3.43.

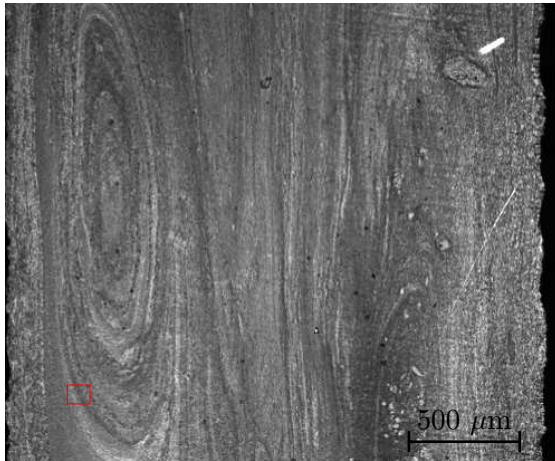


Figure 3.43: Macro image of the flow within the cross section of extruded product using the rectangular die in the vertical orientation. Taken using polarised light.

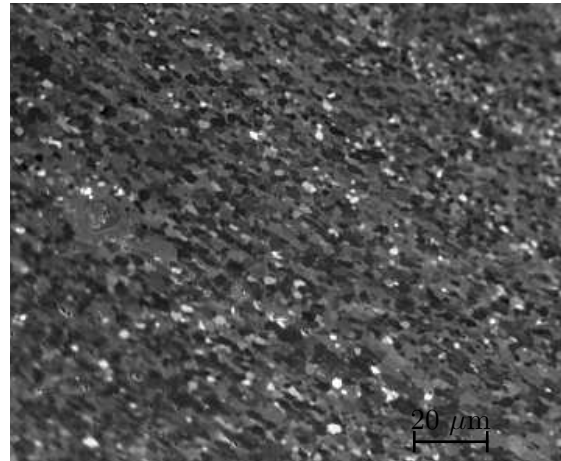


Figure 3.44: Micrograph of the cross section of extruded product using the rectangular die in the vertical orientation. Taken using polarised light.



Figure 3.45: Two die back end discards from Trial 3.1 (left) and 3.1 (right)

A half section taken through the die discard from trial 3 is shown in figure 3.46. The image, a composite of many polarized light micrographs shows the material flow within the die chamber during extrusion. Material dead zones are seen at the top and bottom right of the figure as regions of larger grains. The main bulk of the material consists of strongly defined layers of titanium that flow towards the die entrance. The layering of the titanium hints at the process of consolidation within the Conform process. Layers are shown to be formed as far back as the entrance to the port. Difficulty at removing the sample from the tools prevented observations of material any closer to the wheel groove.

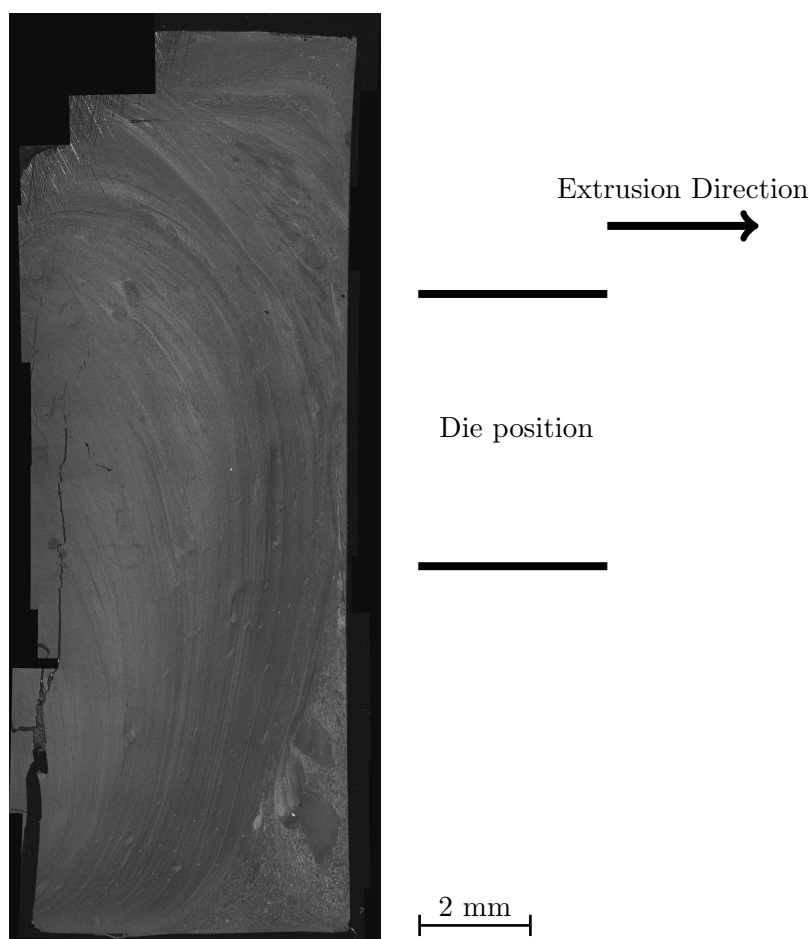


Figure 3.46: Composite polarised light macrograph of a section taken from the die discard using the rectangular die in the vertical orientation. Material dead zones can be seen above and below the die as regions of larger grains.

Analytical model of the Conform process

4.1 Analytical model for extrusion pressure and fill height

The pressure and forces at different points within the direct/indirect extrusion processes are relatively easy to calculate analytically through a range of different theories including the slab method [91] the same cannot be said for the Conform process. While there have been attempts to do this analytically, the community seems to have determined that the best methods for analysing the Conform process are numerically intensive finite element models [14, 15, 78]

Computational methods such as finite element modelling have made up the bulk of publicly available research into the Conform process and publications have increased in frequency with increasing computational affordability. FEM has previously been used for static or elastic bodies of small displacements or deflections but as hardware and software for personal computers have seen an exponential increase in calculation speed and efficiency they have brought about the possibility of running large three dimensional simulations. Improvements in automatic remeshing methods have also provided the ability to model large plastic deformations without significant user intervention during runtime. Today's multi-core processors coupled with solid state drives and large RAM modules allow for desktop PCs to perform simulations that 10 years ago would have required a research grade supercomputer cluster.

The majority of the work within this thesis is concerned with numerical modelling through FEM of the Conform process in both 2D and 3D. Time scales involved in running different sizes of simulations can vary greatly depending on user skill, simulation time to obtain steady state extrusion, processor clock speed, hard drive write speed and the scale of any parametric studies required. For a manufacturer a simple 2D FEM simulation can take between 30 minutes and 5 hours, quick enough to turn around a customer request to solve a production problem. However in the case of new products there are often many unknowns within the process setup and only some can be solved by referring back to similar existing products. In this case FEM can be employed in order to reduce the number of required trials with different die chamber and die designs, the cost of which can take up a significant amount or any profit on a machine

sale. Often though a customer may simply want a quick answer from the machine manufacturer over the phone as to whether continuous extrusion is a feasible forming route for their product. In this case, running a whole parametric FEM study is neither fast enough nor cost effective. Instead an analytical tool is required in order to give such a customer a quick answer and to prove that further FEM studies and experimental trials can be run to validate such a tool.

Presented below is the derivation of an analytical tool suitable to give a first approximation in designing tool geometries for Conform extrusion when certain basic information about the thermomechanical processing of the feedstock material is known. Derivations have been adapted from analysis of other models by Wood [75] and Valey [84] and combined with a slab analysis of direct extrusion [91].

It has been assumed that after a certain distance from the wheel to the die that the material flow and forces can be thought of as being the same as direct extrusion with an axisymmetric flow profile for a round extrudate [75]. The efficacy for such an assumption increases with larger distances between the die and wheel due to a decoupling of the two major deformation zones at the abutment face and die entrance.

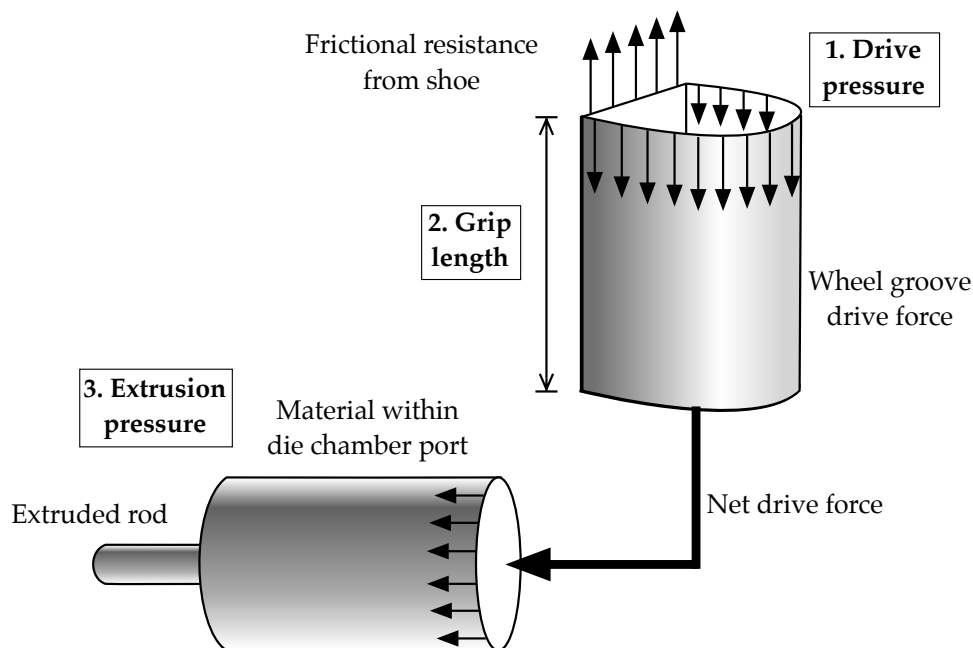


Figure 4.1: Simple visual representation of the two regions considered in the analytical model. The upper vertical region represents the generation of the drive force within the wheel groove while the horizontal cylinder is a simplification of the deformation occurring within the die chamber port and die.

4.1.1 Drive Pressure

The following derivation is presented based on a discontinuity between the drive force generated by certain grip length between a workpiece within the wheel groove and the extrusion force required at the extrusion die as illustrated in figure 4.1. Here the measureable dimensions of the wheel groove in figure 4.2 are converted to a contact areas and lengths before being related to an equivalent cylinder in a simplification of the drive pressure generation.

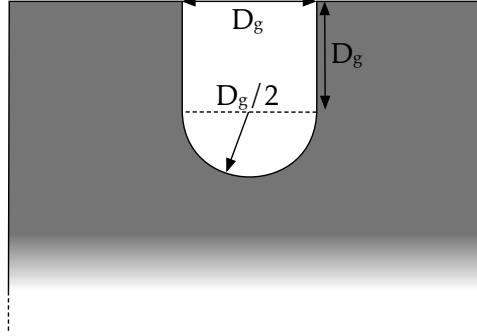


Figure 4.2: Dimensions of the wheel groove used in derivation of the analytical pressure model

Consider two parts to the driving force generated by the contact between the wheel groove surface and the workpiece, which can either be solid rod or loose powder. In the case of solid rod there are two distinct pressure zones within the wheel groove. Once the rod has been coined into the groove there is a initial contact length l_i and contact circumference C_i between rod and groove.

The drive created by the wheel is opposed by the friction of the workpiece and the shoe as it moves towards the abutment. The net driving force is given by:-

$$F_{net} = F_{groove} - F_{friction} \quad (4.1)$$

Assuming contact between wheel groove and workpiece is the circumference of the groove and contact between workpiece and shoe is the width of the groove, D_g .

$$F_{net} = F_i = \mu\sigma_y l_i C_i - \mu\sigma_y l_i D_g \quad (4.2)$$

Where σ_y is the compressive yield strength of the feedstock, μ is the friction between the tools and the feedstock and l_i is the initial grip length. Substituting for the contact circumference the net drive force can be written as:

$$F_i = \mu\sigma_y l_i D_g \left(1 + \frac{\pi}{2}\right) \quad (4.3)$$

This drive force is opposed by the presence of the abutment within the groove and acts to cause the feedstock to be upset within the abutment zone and wheel groove. In order for this to occur the feedstock must yield under compression. Therefore the following must be true:

$$F_i = \sigma_y A_g \quad (4.4)$$

$$F_i = \sigma_y D_g^2 \left(1 + \frac{\pi}{8}\right) \quad (4.5)$$

Substituting for F_{net}

$$\sigma_y D_g^2 \left(1 + \frac{\pi}{8}\right) = \mu \sigma_y l_i D_g \left(1 + \frac{\pi}{2}\right) \quad (4.6)$$

where A_g is the area of the groove bounded by the shoe and is equal to D_g . Rearranging to solve for the initial grip length, l_i gives

$$l_i = \frac{D_g}{\mu} \left(\frac{1 + \frac{\pi}{8}}{1 + \frac{\pi}{2}}\right) \quad (4.7)$$

4.1.2 Upset Length

Once the feedstock has been upset there is complete filling of the wheel groove. The feedstock also starts to yield in shear at the tool interfaces. In the same way as the initial grip length was derived above the upset length can also be determined.

$$F_{upset} = \mu \tau_{ys} l_u D_g \left(1 + \frac{\pi}{2}\right) \quad (4.8)$$

where τ_{ys} is the yield of the feedstock in shear and l_u is the upset grip length.

For extrusion to occur the drive pressure $P_{drive} = \frac{F_{upset}}{A_g} + \frac{F_i}{A_g} = P_{upset} + P_i$ must be equal to or greater than the required extrusion pressure P_{ex} at the die, which is derived below. While it is assumed that if $P_u + P_i = P_{ex}$ then no flash will be produced, if $P_u + P_i \geq P_{ex}$ it is possible for extra flash to be pushed out between the wheel's outer surface and the shoe. Given these conditions it can be said that for a successful extrusion to occur

$$\mu \tau_{ys} l_u D_g \left(1 + \frac{\pi}{2}\right) \geq P_{ex} D_g^2 \left(1 + \frac{\pi}{8}\right) \quad (4.9)$$

where P_{ex} is the minimum required extrusion pressure at the die and the Tresca Yield Criterion is given by $\sigma_y = 2\tau_{ys}$. Rearranging and solving for l_u gives:-

$$l_u \geq \frac{2P_{ex}D_g}{\sigma_y} \left(\frac{1 + \frac{\pi}{8}}{1 + \frac{\pi}{2}} \right) \quad (4.10)$$

Putting the equations for l_i and l_u together gives us the required total grip length for successful extrusion to occur in the Conform process.

$$l_i + l_u \geq \left(\frac{2P_{ex}D_g}{\sigma_y} + \frac{D_g}{\mu} \right) \left(\frac{1 + \frac{\pi}{8}}{1 + \frac{\pi}{2}} \right) \quad (4.11)$$

4.1.3 Extrusion Pressure

Derivation in this section has been adapted from [91] to suit the geometry of the Conform process.

In direct extrusion there are three distinct zones through which the material must pass before it exits the die. The cylindrical billet of diameter D is pressed with a ram towards a die with circular orifice of diameter D_E . The pressure required to extrude a billet with an average material flow stress σ three parts of the process need to be considered. The billet deforms to go through the die, it interacts through friction with the container walls and it shears internally at the boundary with the dead metal zone. Consideration of these three things gives the total required extrusion pressure.

$$P_{ex} = P_D + P_F + P_R \quad (4.12)$$

For this analysis it is assumed that the Conform die chamber port is cylindrical with diameter D_P and has a uniform force profile on its back end. This later assumption can only be truly correct for large flow lengths where the die is sufficiently far away from the $\approx 45^\circ$ shear zone above the abutment so that the metal flow is uniform around the axis of the die. The die has a circular orifice of diameter D_E and the flow within the material forms a dead metal zone of semi-angle α . Consider a section of material of finite thickness dz within the metal flow bounded by the dead metal zone and with forces acting on each side as shown in figure 4.4. In an equilibrium state the forces acting on the element are balanced.

$$P_z \frac{\pi D_P^2}{4} + P_r \pi D_P ds \sin \alpha + \tau_f \pi D_P ds \cos \alpha = (P_z + dP_z) \frac{\pi (D_P + dD_P)^2}{4} \quad (4.13)$$

where P_z is the pressure in the direction of extrusion and P_r is the radial pressure within the port.

Rearrange, substitute in for the geometrical simplifications $ds \sin \alpha = \frac{dD_P}{2}$ and $ds \cos \alpha =$

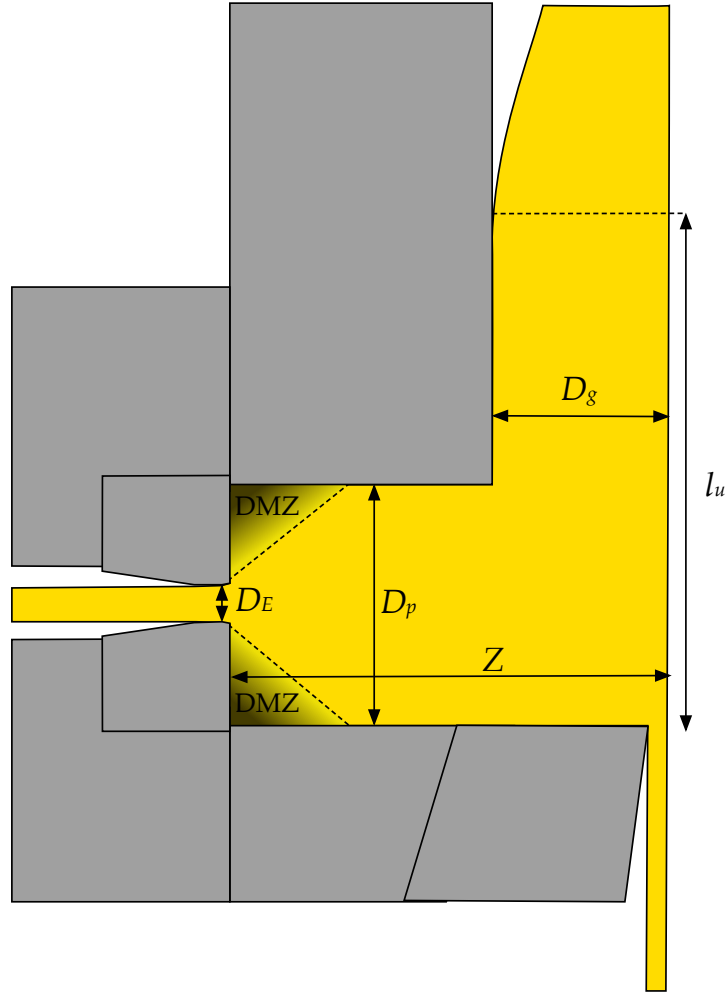


Figure 4.3: Schematic of a 2D Conform extrusion with labelled dimensions relevant to the analytical model. Dead metal zones (DMZ) are shaded and assumed to be the same shape above and below the die entrance for ease of calculations.

$\frac{dD_P}{2 \tan \alpha}$ given in figure 4.4. Using the yield criteria $P_r = P_z + \bar{\sigma}$ and $\tau_f = \frac{\bar{\sigma}}{\sqrt{3}}$ and removing those terms that are negligible due to their small contribution to the overall pressure gives us:

$$\frac{dP_z}{\bar{\sigma} \left(1 + \frac{\cot \alpha}{\sqrt{3}}\right)} = \frac{2dD_P}{D_P} \quad (4.14)$$

If we perform the indefinite integral we obtain:

$$\frac{P_z}{\bar{\sigma} \left(1 + \frac{\cot \alpha}{\sqrt{3}}\right)} = \ln D_P^2 C \quad (4.15)$$

Where C is the constant of integration. Using the boundary condition $D_P = D_E$ when $P_z = 0$ gives $C = \frac{1}{D_E^2}$ and allows the calculation of the required extrusion pressure at the back of the die chamber port as:

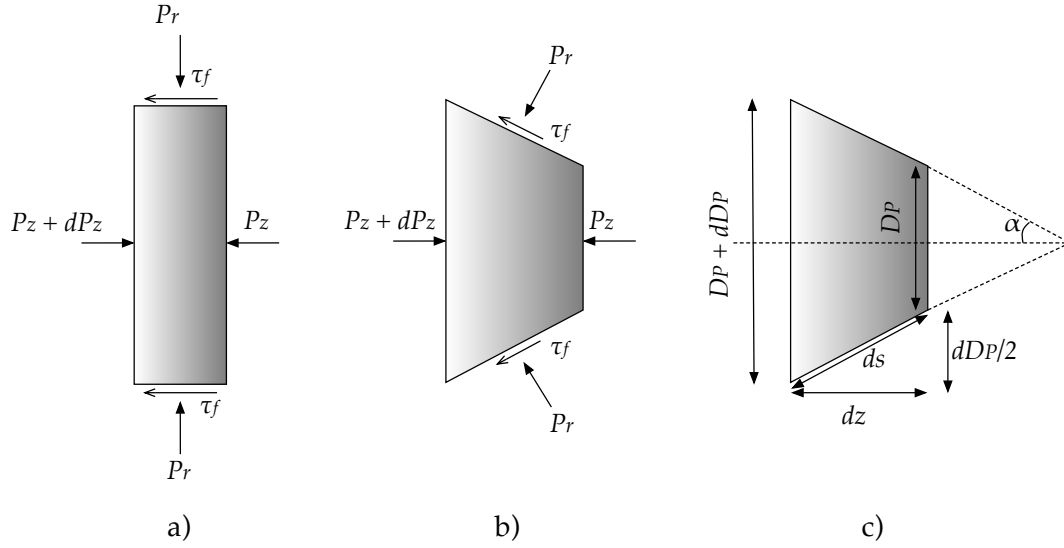


Figure 4.4: Pressure on different faces of the slabs under consideration taken as transverse sections through a direct extrusion a) in the cylindrical billet prior to extrusion b) and c) while extruding through a circular die with entry angle α and diameter D_P .

$$P_{ave,z=0} = \bar{\sigma} \left(1 + \frac{\cot \alpha}{\sqrt{3}} \right) \ln \frac{D_P^2}{D_E^2} \quad (4.16)$$

If a similar analysis is performed on the frictional forces acting on the slab under equilibrium it can be shown that:

$$(P_z + dP_z) \left(\frac{\pi D_P^2}{4} \right) - P_z \frac{\pi D_P^2}{4} = \tau_f \pi D_P dz \quad (4.17)$$

$$dP_z = \frac{\bar{\sigma} 4}{D_P \sqrt{3}} dz \quad (4.18)$$

Integrate and use the boundary condition $Z = 0$ when $P_{ave,z=0}$ give the constant of integration $C = 0$.

$$P_Z = \frac{4\bar{\sigma}Z}{D_P\sqrt{3}} + P_{ave,z=0} \quad (4.19)$$

The final extrusion pressure is defined below:

$$P_{ex} = 2\bar{\sigma} \left(1 + \frac{\cot \alpha}{\sqrt{3}} \right) \ln \left(\frac{D_P}{D_E} \right) + \frac{4\bar{\sigma}Z}{D_P\sqrt{3}} \quad (4.20)$$

As stated above the criteria for success extrusion is $P_{drive} \geq P_{ex}$ the following relationship can be drawn

$$\frac{\sigma_y}{2D_g} \left(\frac{l_i + l_u}{b} - \frac{D_g}{\mu} \right) \geq 2\bar{\sigma} \left(1 + \frac{\cot \alpha}{\sqrt{3}} \right) \ln \left(\frac{D_P}{D_E} \right) + \frac{4\bar{\sigma}Z}{D_P\sqrt{3}} \quad (4.21)$$

where

$$b = \frac{1 + \frac{\pi}{8}}{1 + \frac{\pi}{2}} \approx 0.54 \quad (4.22)$$

As initial grip length serves to upset the feedstock in the groove, as such it doesn't provide a significant contribution to the extrusion force. The derivation above considers solid rod feed but is also applicable to powder feed Conform. The upset length can be compared with the height of fully consolidated powder within the groove. The pressure generated within the groove in partially consolidated powder will seek only to increase the local powder density and will not contribute significantly to the overall drive pressure. Instead, as with l_i and l_u for rod feed the consolidated height of powder will generate the drive pressure. There will be a minimum height of fully consolidated material required to generate sufficient pressure to extrude material at the die. The term l_i will therefore be neglected from the pressure considerations and it will be replaced with a new term $l_{grip} = l_i + l_u$.

Finite element modelling - 2D

5.1 Methods

Analytical models of the continuous extrusion process can be helpful to illustrate the differences between process changes such as feedstock flow stress, die size and flow length. Unfortunately such models tend to rely on inaccurate assumptions, and those assumptions that are accurate can have large errors associated with them. These models should therefore be used in conjunction with more accurate modelling techniques such as finite element modelling.

Finite element modelling has been used extensively in both industrial and research environments to model metal working process since computers were able to run punch card programs. Companies such as Battelle led the way in early development of FEM techniques in order to simulate simple metal forging processes. Simulations of two dimensional models with 10-20 elements would take weeks or months to run on early industrial computers in the 1950s-1960s, whereas in the year 2015 it is possible to run 1 million 3D element simulations in a few days using a desktop PC. There is still a limitation in effectiveness of the FEM process, especially when used in industry. Accuracy and time for the simulations to run are often traded off against one another so that product development is not slowed by potentially long simulation runtimes. Because of this and in order to compare to previous FEM work into Conform/CRE, 2D simulations are presented in this chapter to compare with both the analytical model presented in chapter 4 and 3D FE models in chapter 6.

5.1.1 Simulation setup in DEFORMTM-2D

The material data used for all FEM in this work was based on data obtained from the DEFORMTM Material Data Library, which is built into the program and is presented in figure 5.1. The same flow stress data is used in the 3D FEM study presented in chapter 6. DEFORMTM uses a logarithmic interpolation method to determine the applicable flow stress and strain rate from the available nodal velocities and forces. The workpiece was modelled as a rigid-viscoplastic material, with no elastic properties and no thermal expansion. User generated material data

can produce more accurate results but it was deemed unnecessary for this work as comparative results were far more important than accuracy.

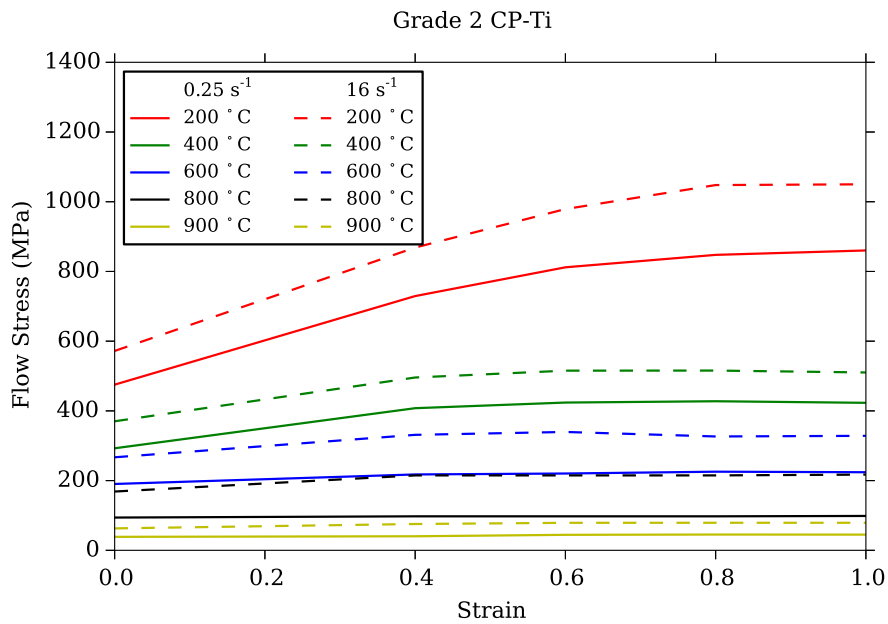


Figure 5.1: Flow stress data from the DEFORMTM database.

In two dimensions the workpiece is only influenced by one edge of the wheel at the bottom of the groove and there is no interaction into or out of the plane of view. This can be correct when taking a central slice from the 3D process but fails to include the extra drive effect of the sides of the wheel groove. Attempts were made to use a 2D round wheel in order to drive the workpiece into the abutment but wheel-workpiece contact was easily lost following automatic remeshing steps. Such a loss in contact resulted in a loss of extrusion drive pressure and hence prevented the workpiece from extruding through the die. Instead the wheel was removed and modelled as a velocity boundary condition of $v_y = -91.2 \text{ mms}^{-1}$, $v_x = 0 \text{ mms}^{-1}$ on the right hand side of the workpiece (see figure 5.2). The workpiece was initialised as a vertical rod, rather than a preformed curved rod, fitted to a wheel groove of radius 145.0 mm. This lack of curvature in the initial rod was deemed to not be a significant factor in generating the drive pressure, the resultant workpiece stresses and forces on the tooling geometries. Mesh windows were used to refine the element sizes around positions of interest in the abutment zone and die as well as allowing sufficient spatial resolution around sharp die edges. All other nominal tooling geometries were taken as from a central slice through the 3D tool geometries used to manufacture tools for the experimental trials.

Figure 5.3 shows the important geometry parameters that were studied in DEFORMTM-2D. Each of these parameters are shown in chapter 4 to be influential in the pressure evolved at different places within the Conform machine; from the groove to the die chamber port to the die. Table 5.1 shows the range of values used for each of the geometry dimensions that were changed. The nominal geometry dimensions are in the middle of each of the ranges. The effective groove size, workpiece thickness and die entry angle was kept constant for all simulations.

Table 5.1: Parameters and range of values used in the 2D FEM study of Conform with grade 2 titanium

| Parameter | Value |
|--------------------------|---------------|
| Port height | 15 - 25 mm |
| Die chamber depth (port) | 10 - 20 mm |
| Die size | 2 - 8 mm |
| Die height | 7.5 - 13.5 mm |

The workpiece for each simulation began with it's bottom face in contact with the abutment and allowed to go through the upset and port filling stages before any results were monitored. Each simulation ran until the upset height, effective stress and temperature profiles had stabilised. This typically equated to roughly 1.5 seconds of simulation time or 12-18 hours of run time depending on the number of automatic remeshing steps required by DEFORMTM. Databases for the 2D simulations were loaded in to the built in DEFORM-2D post processor.

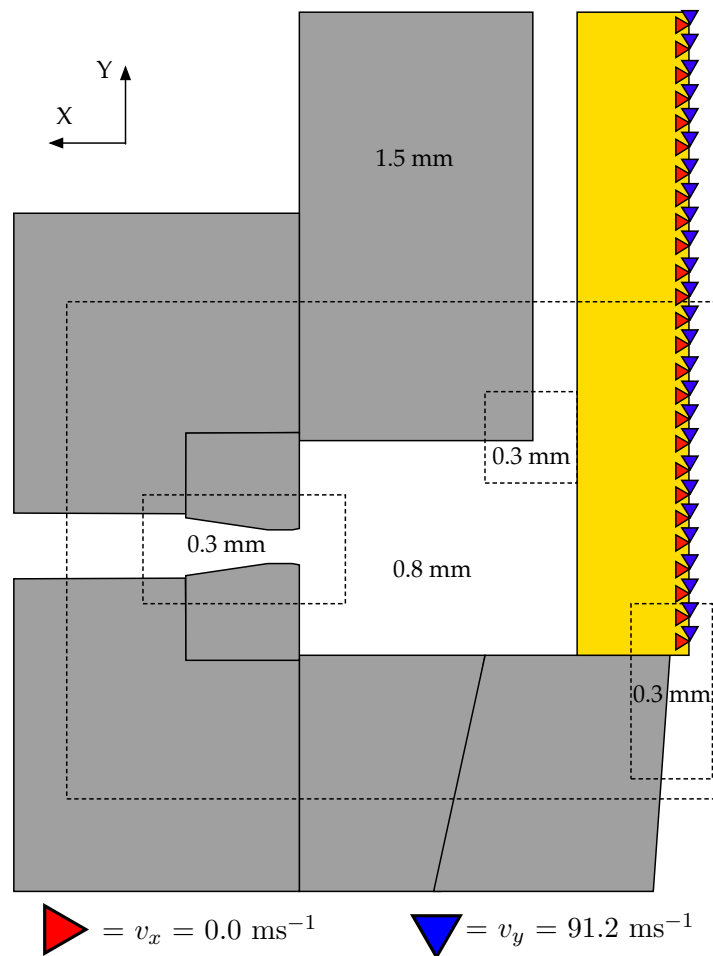


Figure 5.2: Schematic representation of the 2D FEM simulation setup showing the defined mesh windows with their corresponding absolute element sizes. Wheel contact is defined as a boundary condition on the right hand side of the workpiece.

Data was extracted by tracking the workpiece moving through three separate stationary points in the workpiece; 1) in the groove 2) in the port and 3) in the die bearing (see figure 5.4). The following data was automatically extracted for every step in the simulation databases: tool loads in X and Y directions, maximum principal stress at points 1 and 2, temperature at all three points and the upset heights throughout the simulation. Due to the orientation of the tools to the process not all loads were plotted for each tool. For instance the primary loading on the abutment in the 2D simulations is in the Y direction so the X load was left out of the data plots. The maximum principal stress at point 1 (in the groove) and point 2 (in the port) represent the extrusion pressure at these points. As such there is no stress on the extruded rod at point 3 so data at this point is neglected. The temperature and velocity at all three points were also extracted and both the maximum values and steady state values were calculated. Upset height of the workpiece was measured manually by monitoring the contact between the workpiece and the die chamber in the wheel groove. Upset height is thought to be directly related to both the

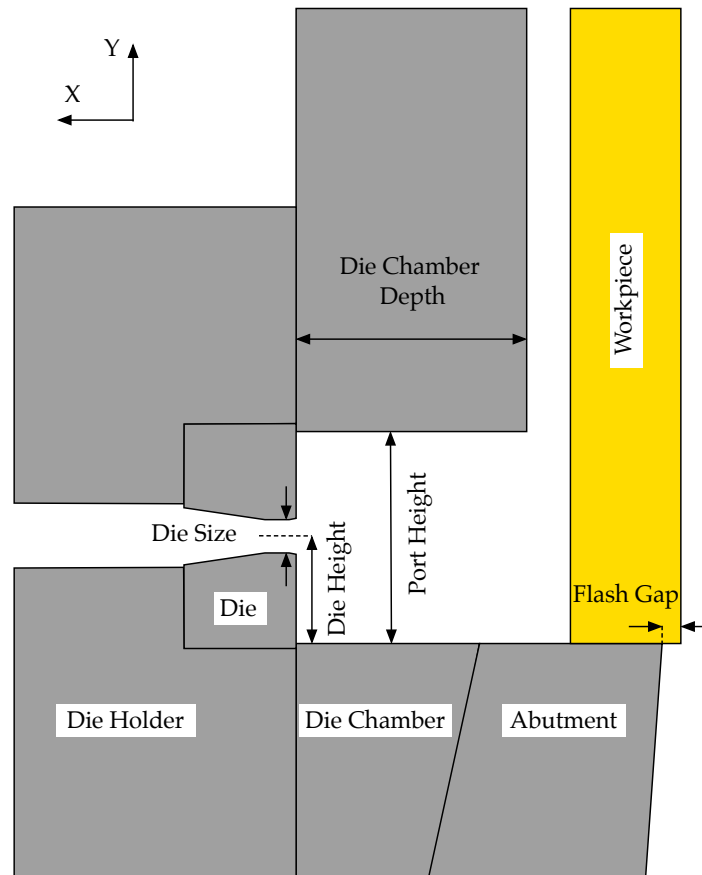


Figure 5.3: Schematic representation of the 2D FEM simulation setup. Wheel contact is defined as a boundary condition on the right hand side of the workpiece. Important geometry variables that are varied in the study are labelled on the figure.

load and pressure on the abutment as well as the pressure required for extrusion.

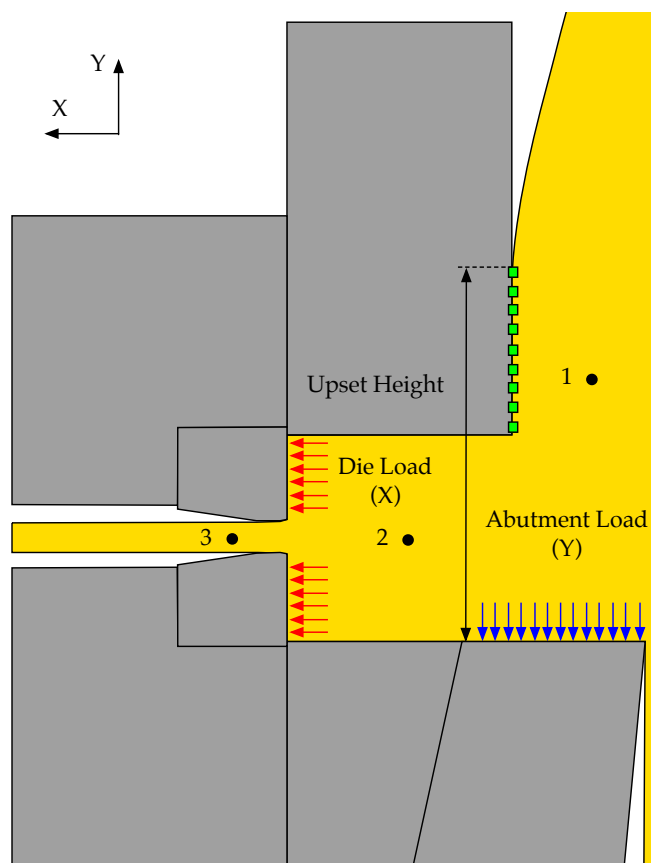


Figure 5.4: Important tool loads and points of interest monitored in the post processing of each 2D simulation.

5.2 Results



Figure 5.5: Representative finite element simulation in 2D with frames taken at ~ 0.2 second intervals showing the evolution of the upset height during the establishment of steady state Conform extrusion of grade 2 titanium. Maximum upset height and abutment load is achieved at $t = 0.6$ s.

Figure 5.6 shows the raw extracted data from one of the simulations. The tool loads plot in the top left of the figure demonstrates the need to run simulations of the Conform process through to a steady state. As the workpiece is upset against the abutment first this is the first piece of geometry to register a reactive load. The workpiece then enters the die chamber and the back pressure generated causes the workpiece to preferentially fill the port rather than generate any extrudate in the die. A nominally small load is registered on the top and bottom faces of the die while the workpiece continues to upset and fill the die chamber. Finally the upset height of the workpiece within the groove increases to a maximum, which coincides with the maximum pressure measured within both the groove and port. As the workpiece is extruded, temperatures at each of the three points increase until a steady thermal and mechanical state is reached. This state is characterised by a flattening of the tool load curves and continuation of the simulation will yield the same results at any time during this steady state phase. Errors

It should be noted that DEFORMTM models 2D plane strain simulations with a predetermined depth in the z axis of 1 mm. As such all measured loads can be converted (roughly) into 3D loads by multiplying by 10; the width of the abutment in 3D.

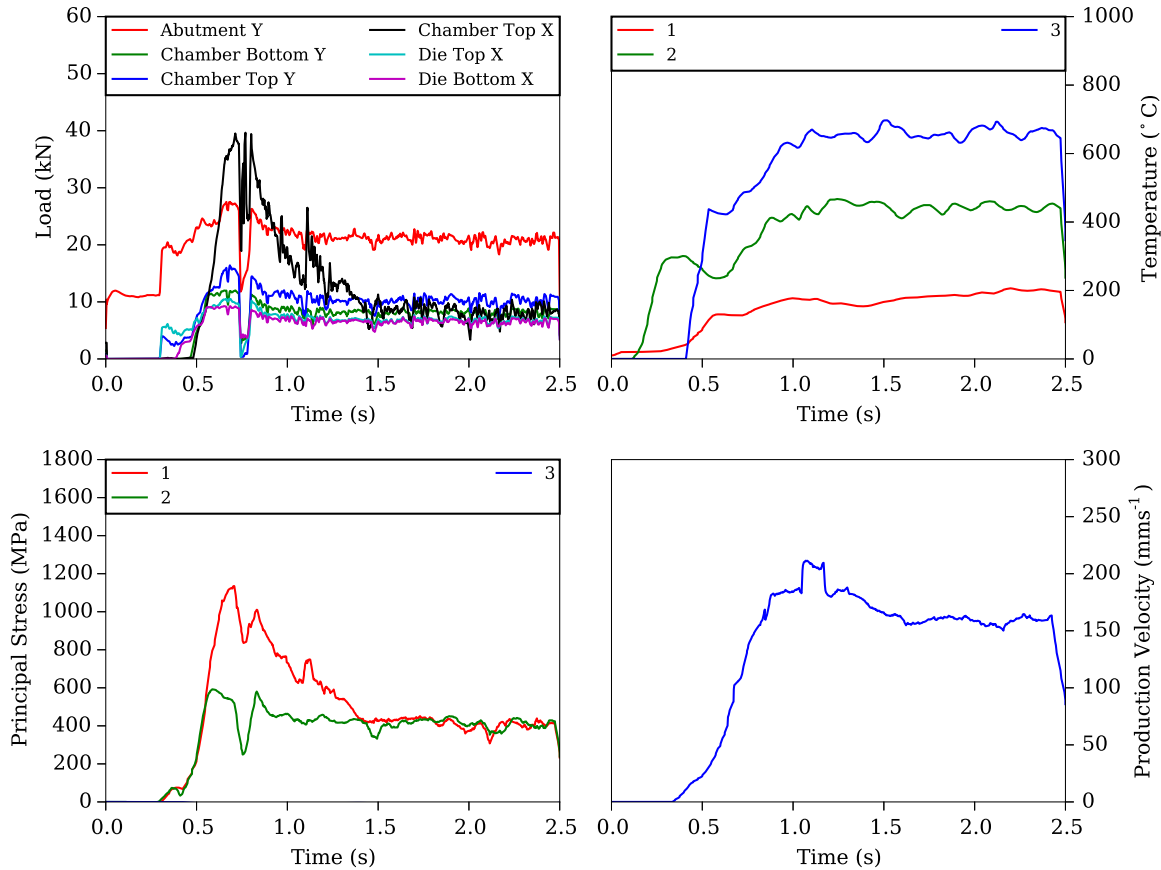


Figure 5.6: Representative data extracted from a single 2D simulation.

are generated within the tool loads due small changes to the workpiece geometry caused by the DEFORMTM automatic remeshing routine. Following a remesh step the geometry may partially lose contact with tool geometry and hence require a few steps to re-equalise the stress profile. Such errors occur frequently in simulations that have large bulk deformations and tend not to cause problems for the forging and rolling processes that DEFORMTM was originally designed for. Results extracted from the simulation raw data were time-averaged in order to negate the effects of these remeshing errors.

It is important to note that the results presented here illustrate the need to run finite element simulations of the Conform process for a sufficiently long time in order to attain a steady state extrusion. Transient results from simulations taken at a time where tool loads and workpiece upset height are at a maximum cannot be said to be fully representative of a process that is inherently meant to be run continuously for a long time and in a steady state (see section 5.2.5 for expansion on this point).

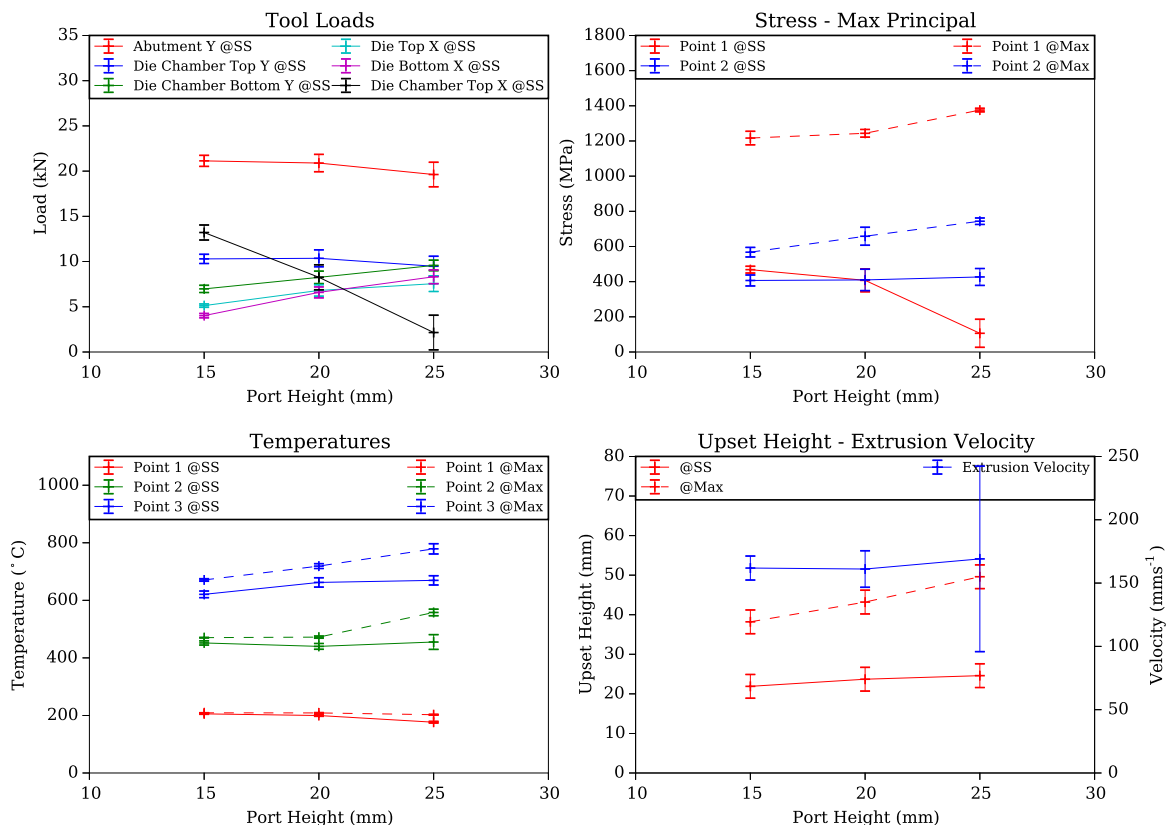


Figure 5.7: Plots of tool loads, principal stresses, temperatures, extrusion velocity and workpiece upset height with increasing port height

5.2.1 Effect of changing port height

Figure 5.7 shows the results from simulations where only the port height was altered. The effective extrusion ratio can be defined by the ratio of the area of the port to the area of the die if each was revolved around the extrusion axis. In essence, converting 2D geometry to 3D cylinders to compare cross sectional areas. The extrusion ratios A_p/A_{ex} were 9:1, 16:1 and 25:1 for each of the 15, 20 and 25 mm port heights respectively.

Tool loads at most points tend to increase with increasing port height. It should be noted that with constant pressure the effective contact length on the top and bottom die will respond linearly with increasing port height. Therefore any increase in load measured at the die should be normalised for the increase in contact length. Conversely the drop in Die Chamber X load can be partly attributed to the decrease in contact length due to the upset height remaining constant. Abutment load Y, point 2 stress at steady state and upset height all stay relatively constant with increasing port height. There is very little change in the steady state temperatures in the groove (point 1) and port (point 2) but a small increase in extrudate temperature measured at the die. This leads to the assumption that any change in port height has a minimal effect on

extrusion pressure and temperature despite the effective increase in extrusion ratio A_p/A_{ex} .

5.2.2 Effect of changing port depth

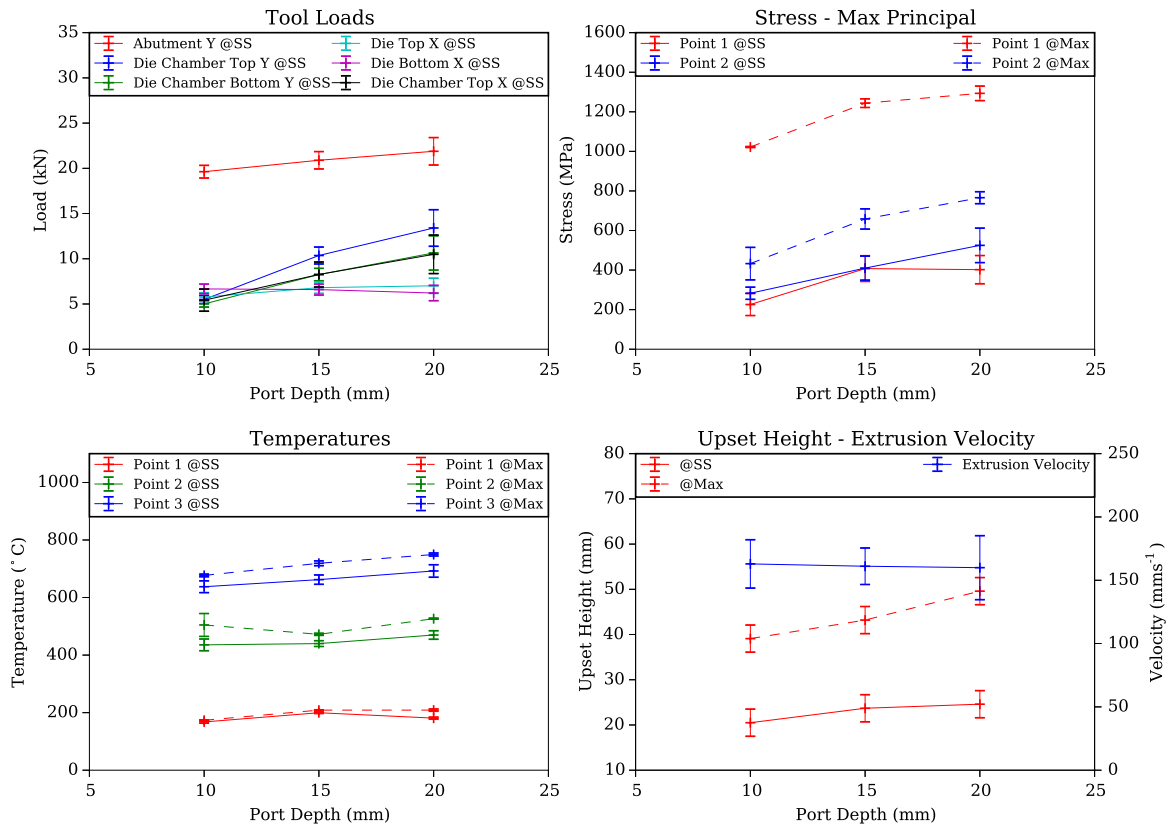


Figure 5.8: Plots of tool loads, principal stresses, temperatures, extrusion velocity and workpiece upset height with increasing port depth

Figure 5.8 shows the results from simulations where only the port depth was altered. All of the tool loads increase when the port is lengthened except for the die top and bottom. This implies that the required extrusion pressure at the die face remains constant yet the pressure further back in the workpiece, in the port and groove gets higher. This is most likely due to added extrusion force required to overcome the wall friction with the die chamber. Making the die chamber thicker and lengthening the port means that the workpiece, die chamber friction has a greater effect on the extrusion pressure generated by the wheel drive. The pressure at both points 1 (groove) and 2 (port) and upset height increases rapidly with port depth. It is clear that the back pressure in the process rises with increasing port depth and requires a larger driving force for steady state extrusion. Extrusion temperatures were affected to a greater degree by the changes to port depth than port height on a mm by mm basis.

While the port depth or die chamber thickness is the dimension of tool geometry changed in this section, the real change occurring is a geometrical factor called ‘Flow Length’. This

is a term used to describe the distance between the main ‘ECAP-like’ shear zone and the entrance to the die. It is generally accepted by those whose work in the Conform or Continuous Rotary Extrusion industry that longer flow lengths create higher extrusion pressures within the port [87]. This can be seen from the analytical consideration of the Conform process in section 4.1 where an increase in Z (flow length) results in a rapid linear increase in extrusion pressure. In this analytical model, the equations involving Z were originally taken from the slab method of estimating extrusion pressure in direct extrusion, where Z describes the billet length. There is therefore an important analogue between the billet length in direct extrusion and the flow length, or port depth in Conform.

5.2.3 Effect of changing die size

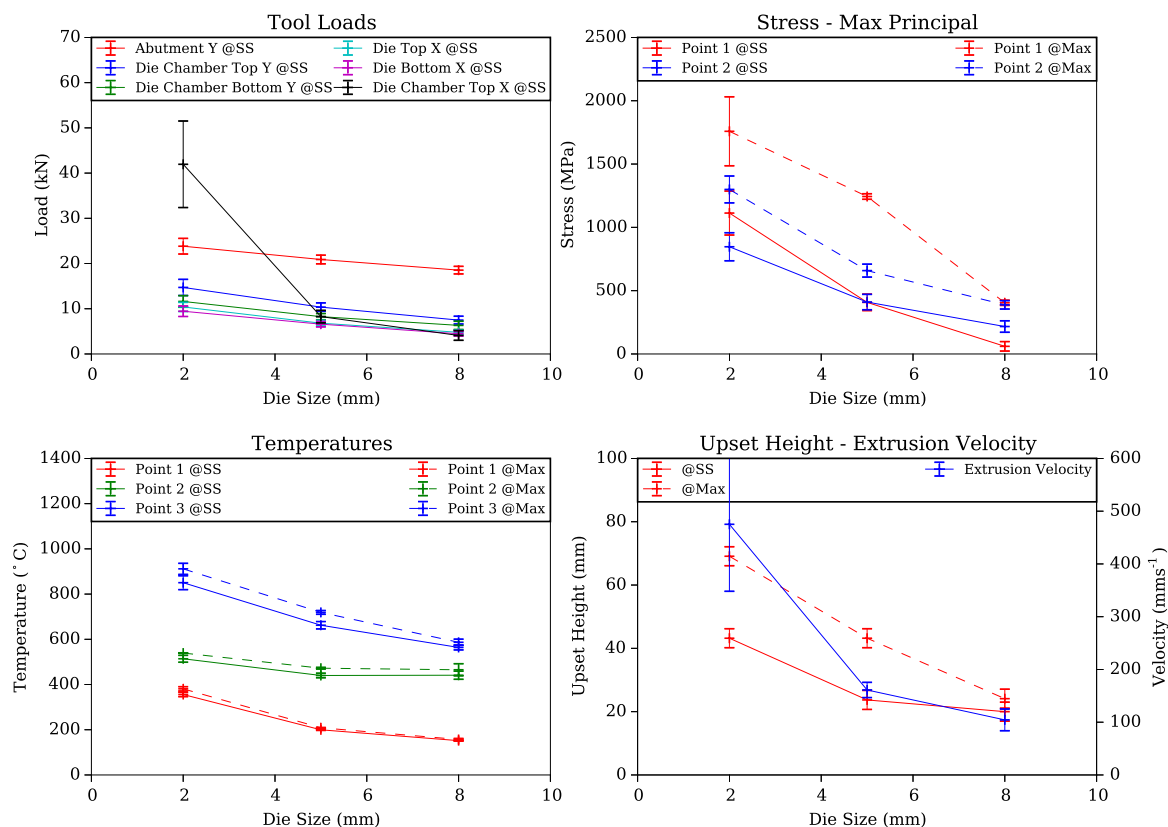


Figure 5.9: Plots of tool loads, principal stresses, temperatures, extrusion velocity and workpiece upset height with increasing die size

Figure 5.9 shows the results from simulations where only the die size was varied. The variation in the observed properties is perhaps the easiest to predict due to the ease of relating the change in dies size to the mechanics of direct extrusion. It can be seen that with increasing die size there is a uniform drop in all tool loads. As with the previous results in sections 5.2.1 and 5.2.2, the change in die load is masked by the reduction in workpiece-tool contact length

with increasing die size. However the reduction in tool loads is also mirrored in the reduction in stresses measured at both points 1 and 2. As expected from direct extrusion, the reduction in extrusion ratio A_p/A_{ex} from 100:1 to 16:1 to 6:1 for each of the 2, 5 and 8 mm dies, respectively, is the dominant cause of the change in tool loads and stresses. These reductions in loads and stresses are also seen in the temperatures at each of the three measurement points. As the die size decreases for a set input speed the strain rates in the main deformation zones above the abutment and in the die entrance increase.

The largest reduction in tool load is observed in the Die Chamber Top X measurement, which peaks at 42 kN for the 2 mm die before dropping to 9 and 4.5 kN for the 5 and 8 mm dies respectively. If this is compared with the change in upset height and the fact that the port height for these simulations is 20 mm the tool load can be explained. The increase in extrusion pressure for the 2 mm die over the larger dies results in a larger upset height in order for the Conform process to generate sufficient extrusion pressure and maintain the expulsion of extrudate for the given input mass flux. Conversely the reduced extrusion pressure for the 5 mm die results in an upset height of 22.5 mm only just over that of the port height of 20.0 mm but still enough to completely fill the port. In the same way, while the extrusion pressure required for the 8 mm die is significantly less than that for the 5 mm die the measurable upset height can only be a minimum of the port height. The process may only require an upset height of lower than the port height to produce an extrudate but this would not be observable within the FE model. The stress profile shows that the point 1 stress at steady state is actually less than 100 MPa and would normally not be sufficient to upset the rod, if it were not for the initial increase in temperature caused by the initial upset that generated the maximum stress point. From these results, it can be shown that there is a self-regulating minimum extrusion pressure required by the machine, as dictated by the upsetting of the workpiece and deformation in the abutment zone. If the extrusion pressure and forces required to conduct this part of the process is higher than that to extrude the workpiece through the die then this is will show up as the plateau in upset height and tool loads as seen in figure 5.9.

5.2.4 Effect of changing die height

Figure 5.10 shows the results from simulations where only the die height was altered. The choice to vary this was made following analysis of experimental results into rectangular dies, where it was thought early on that the orientation of the die had an effect on the extrusion pressure. This is something that is known in the industry to have an effect on the process, usually related to extrusion temperatures and rate of defect occurrence. However, such knowledge is usually

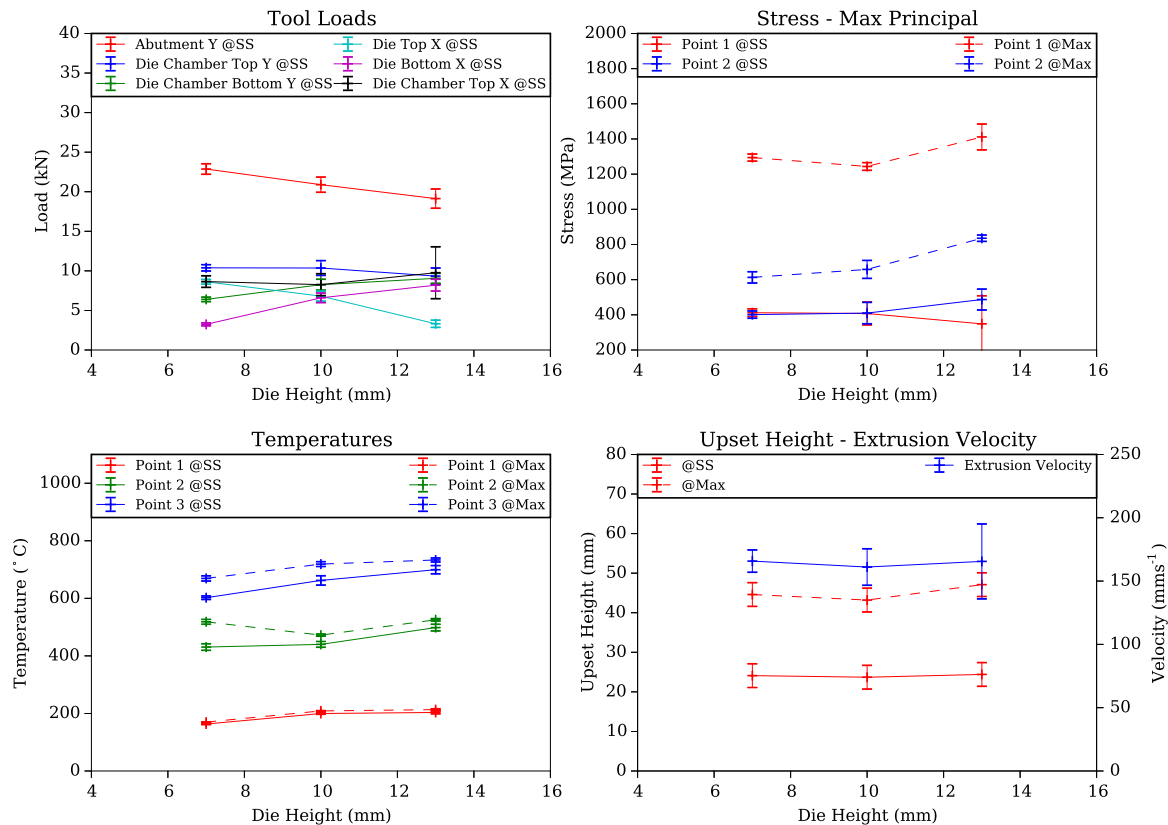


Figure 5.10: Plots of tool loads, principal stresses, temperatures, extrusion velocity and workpiece upset height with increasing die height from the base of the port

developed on a machine user-by-user or supplier basis as there is no known published work that states the effect of die orientation on the Conform process. While both orientations of a rectangular die have the same effective extrusion ratio the strain path for the deforming workpiece is different. Taking this argument further, by observing the material flow within the Conform tooling it might be possible to improve the process efficiency and reduce skin-fold extrusion defects by centering the die in the material flow rather than in the centre of the port as the two points are not necessarily at the same height above the abutment.

There is very little effect in changing the die height on the measured tool loads except for the abutment. Both the Die Top and Die Bottom loads vary significantly and alternate as the effective workpiece-die contact length changes with die height. The increase in abutment load with decreasing die height is not corroborated in the point 2 stress value, which tends to decrease. The point 2 stress value suggests that the pressure required to extrude material is less when the die height is dropped beneath the centre of the port. However, the difference in stress between a die height of 7 - 10 mm is significantly less than that between 10 and 13 mm. Therefore the abutment load result might be explained by a large change in flow profile caused by the change in die height. Moving the die closer to the bottom of the port, shifts the

primary material flow closer to the abutment. Conversely, raising the die height results in the dead zone of material, close to the abutment, increasing in size. This results in a tendency for the workpiece to shear internally, increasing the workpiece temperature rather than moving it against the tooling.

The steady state upset height does not change significantly with die height, despite the pressure at point 2 being highest for the 13 mm high die. The point 2 stress and extrudate temperature increase, cancel each other out, resulting in a consistent upset height or grip length requirement for extrusion to proceed. This indicates that the dominant factor in the extrusion pressure considerations is the die and port extrusion ratio rather than the die position within the port.

5.2.5 Conclusions - 2D FEM

It has been shown in this section that there is a complex relationship between all of the tool geometries and the measure output variables. While it is simple to change a single dimension and observe the changes it creates within the output of an FE simulation, it is harder to segregate the exact cause and effect relationship. For instance, when changing the die size, something that would be routine for product development in the Conform industry, the input speed should also be altered to compensate for the change in extrusion speed. If the input speed is not changed, then it is difficult to determine whether the differences in the process that are observed come from decreased deformation rates (strain rates in the abutment zone), thermal transfer speeds or changes to strain path. When changing the die size, both the port size, die chamber thickness (relates to flow length) and groove size need to be altered to compensate for the change in each extrusion ratio. If this is not done there is the potential for insufficient extrusion pressure, excessive flash production or too much load on the abutment resulting in premature tooling failure.

Overall there was a general trend for the abutment load to increase as the upset height increased. In fact these two parameters are very closely linked as shown in figure 5.11. Although the relationship can be fitted by a straight line with equation $\sigma = 0.36h + 11$, where σ is the abutment stress and h is the upset height, this does not make sense when the physical system of the Conform machine is considered. If the upset height is reduced below the nominal 20 mm height, then the load on the abutment is solely due to work required to upset the workpiece and extrude it through the die. As the upset height increases above the height of the port there is an ever increasing amount of the work used to overcome the frictional resistance from contact with the shoe.

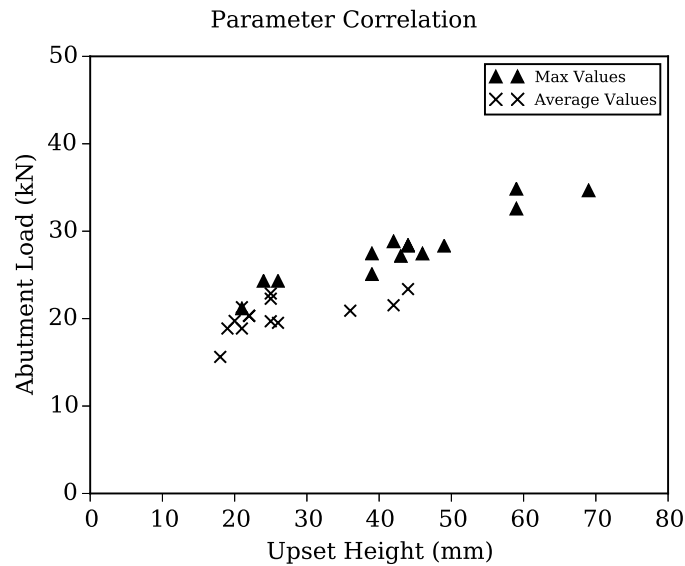


Figure 5.11: Graph showing the correlation between the abutment load and upset height for both the maximum attained values and those during steady state extrusion.

It was suggested by Valey [84] that the upset height in Conform FEM would steadily increase to a maximum where it could be assumed to be at a steady state. Evidence presented here shows that this may not be the case and in fact the upset height begins to reduce after reaching a maximum value. The upset height builds up to a maximum before reducing down as the workpiece is extruded, heats up and hence reduces its resistance to further extrusion. The process self regulates the pressures in the groove/port and corresponding temperatures based on the input speed and tool geometries. If the extrusion ratio is large (i.e. above $\sim 20:1$) then there is an inherently large initial resistance to extrusion, hence the upset height will reach a correspondingly large maximum early in the simulation to 'break through' the die. Once break through has occurred, the large extrusion ratio means that significant adiabatic heat is generated in changing the profile of the workpiece. The subsequent softening of the extrudate lessens the initial resistance to extrusion and hence reduces the extrusion force required after the maximum observed at break through. This maximum extrusion force and post break through reduction in force is also something that is commonly observed in direct extrusion of metals [91]. If the extrusion ratio is small (i.e. below $\sim 10:1$) the adiabatic heating is much less than for larger extrusion ratios. This means that the flow stress of the workpiece at the die is higher, hence, the difference between the break through and steady state force/upset height is less than that for the larger extrusion ratios.

Finite element modelling - 3D

6.1 Methods

6.1.1 Simulation Setup in DEFORMTM-3D

A review of the available literature showed that a large amount of research conducted in the previous 20 years into the Conform has involved finite element modelling. Previous work has aimed to simplify the process into 2D sections, produce known defects or run parametric simulations with no experimental verification. As computing power has increased exponentially over time it is now possible to run full 3D simulations of the Conform process relatively quickly (~2 days). Finite element modelling was conducted as part of this research in order to try and model the Conform process and inform decisions made in performing experimental trials. Determining comparative relationships between process parameters and die geometries were the prime concern rather than absolute accuracy. CAD models were supplied by BWE Ltd. for the machine and tooling used in the experimental trials. These tool geometries were taken as nominal machine setup with any changes for comparisons centering on this setup. Tools positions were measured as per drawings of the full shoe setup at room temperature. It should be noted that despite running the simulations on a high-end workstation it was not possible to include thermal expansion and die stress calculations in the models. Initial attempts to include these aspects resulted in simulations taking weeks to complete, which greatly hindered attempts at a parametric 3D FEM investigation.

The material data used for all FEM in this work was based on data obtained from the DEFORMTM Material Data Library, which is built into the program and is presented in figure 5.1 in section 5.1. DEFORMTM uses a logarithmic interpolation method to determine the applicable flow stress and strain rate from the available nodal velocities and forces. The work-piece was modelled as a rigid-viscoplastic material, with no elastic properties and no thermal expansion. User generated material data can produce more accurate results, but it was deemed unnecessary for this work as comparative results between the simulations were far more impor-

tant than accuracy. Far larger errors were likely to come from modelling a powder material as a solid and using assumptions as detailed further on in this chapter.

DEFORMTM offers a built-in porous material model which models metal forming processes in a similar way to visco-plastic objects but the density is calculated and updated during the simulation. A porous material's compressibility is factored into the flow stress calculations and is solely as a function of the current elemental density, flow stress (defined as $\bar{\sigma} = f(\epsilon \dot{\epsilon} T)$) and limiting strain rate. This material model is adequate for partially sintered, green pressed or foamed metals that have a certain level of bonding between individual particles for green strength. However it fails to accommodate the particle rearrangement and local yielding that occurs in true loose powder materials like the HDH powder used in this work. Trial simulations using a porous material model resulted in extremely large strain and excessive remeshing steps producing unacceptable flow stress and geometry generation errors. These limitations meant that the porous model was not used in either the full or truncated workpiece simulations and instead the workpiece was modelled as a fully dense material.

Table 6.1 shows the general simulation and workpiece parameters using in each of the 3D FE simulations. Tool geometries stated in table 6.1 are only for the nominal simulation setup, which was modelled on the experimental tooling and positions. The workpiece was modelled as a 13 mm diameter rod, preformed to the wheel groove so that there was no pre-upset strain accumulation caused by coining the workpiece into the groove. Although titanium powder in the experimental trials would completely fill the groove rather than be limited to a 13 mm cylinder it was thought that incomplete fill of the groove would allow for observation of the evolving upset height. Contact between the workpiece and wheel groove was generated along the entire length of the workpiece rather than selecting a predetermined grip length. This enabled easier comparisons between all simulations and effective grip length was calculated from the upset height generated in the workpiece. The FEM mesh was refined at areas close to tool corners and also within the abutment zone and die region as shown in figure 6.4. This allowed sufficient elements to keep geometrical accuracy while not unnecessarily extending the simulation runtime with a large total quantity of elements.

CAD files of the BWE Conform machine tools were provided for finite element modelling and are represented in figures 6.1 and 6.2. The tools were redrawn in order to simplify their 3D geometry and provide suitable file formats to ease future tool modifications. In particular the wheel had to be recreated from scratch as the provided CAD file created large facets within the groove resulting in an opening-closing abutment flash gap when the simulation was running. Core tool geometries were not modified and all original faces in contact with the workpiece were

Table 6.1: Data for each of the DEFORMTM-3D simulations.

| Parameter | Value |
|---|--|
| Workpiece material | Grade 2 Titanium |
| Wheel speed | 6 -10 RPM/ 0.628 - 1.047 rad s ⁻¹ |
| Friction μ | 0.98 wheel 0.4 all other tools |
| Time step | 0.005 s ⁻¹ |
| Convergence Δv | 0.001 |
| ΔF | 0.01 |
| <i>Initial Temperatures</i> | |
| Workpiece | 20°C |
| Wheel | 120°C |
| All other tools | 500°C |
| Environment | 20°C |
| <i>Geometries</i> | |
| Wheel radius | 150.0 mm |
| Groove radius | 6.5 mm |
| Circular die radius | 2.5 mm |
| Flash gap | 1.2 mm |
| Workpiece radius | 13.0 mm |
| <i>Material Data</i> | |
| Heat Capacity (N/ mm ² °C) | 3.0 |
| Conductivity (N/ s °C) | 12.0 |
| Convection coefficient (N/ s mm °C) | 0.02 |
| Thermal Transfer coefficient (N / s mm °C) | 5.0 |

retained.

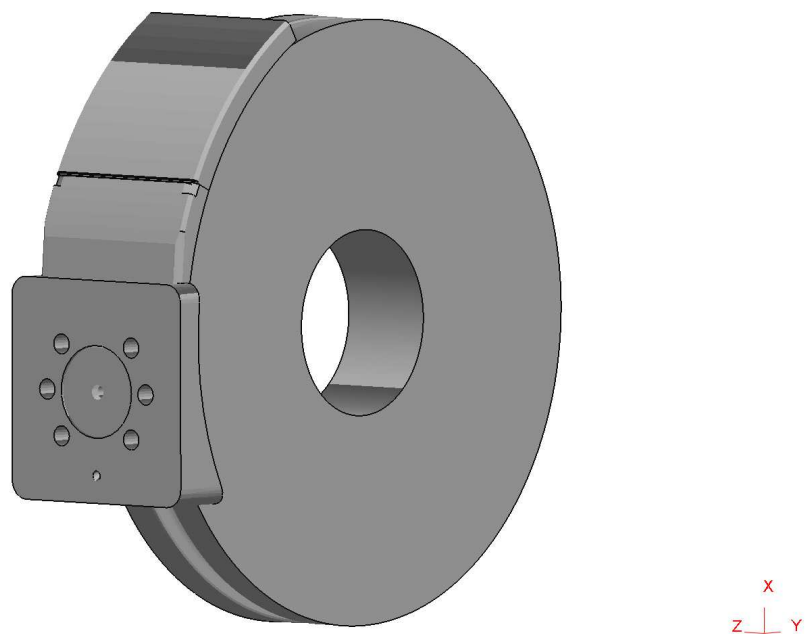


Figure 6.1: The full 3D tooling setup of the Conform machine experimental trials. Tools that do not contact with the workpiece are not considered in the simulations.

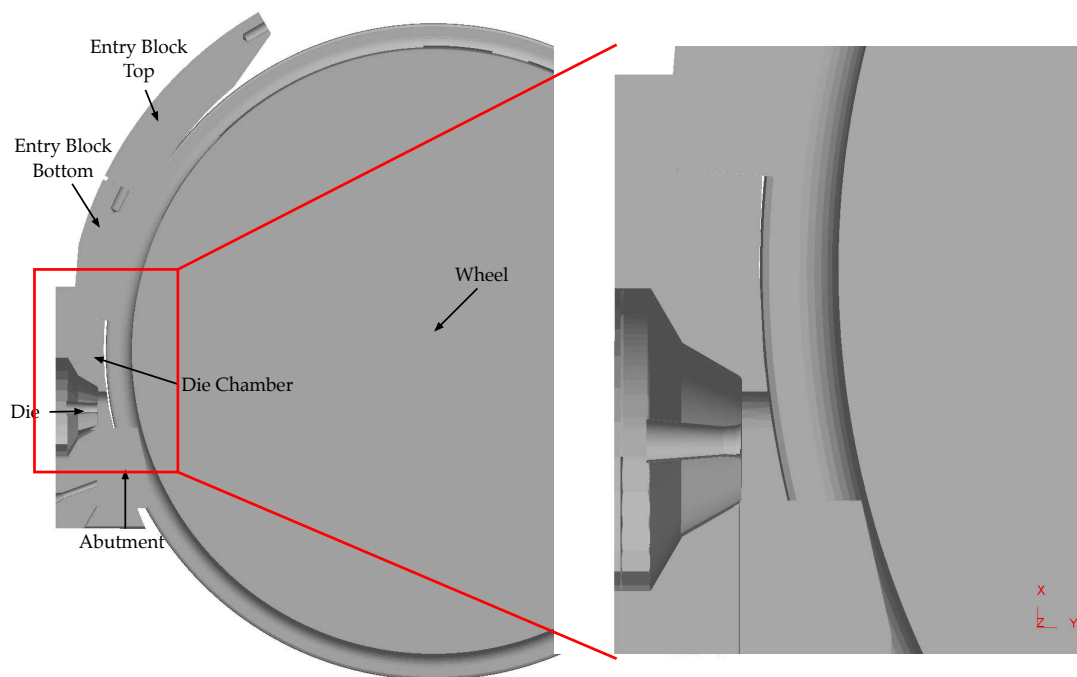


Figure 6.2: Slice through a side view of the 3D Conform tool geometries showing their relative positioning.

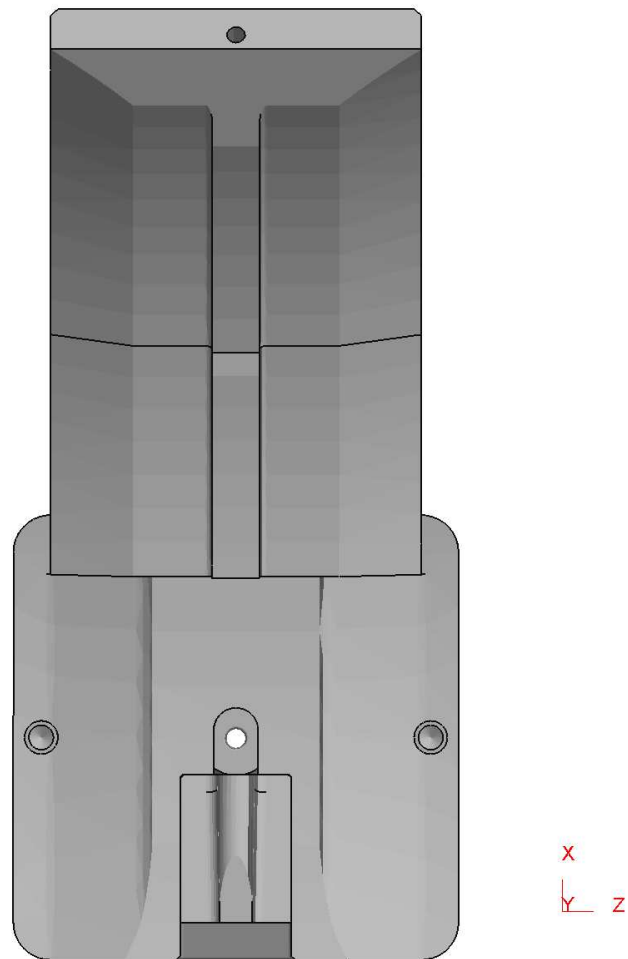


Figure 6.3: View of the abutment, die chamber, die and entry block tools when looking out from the wheel in the direction of extrusion

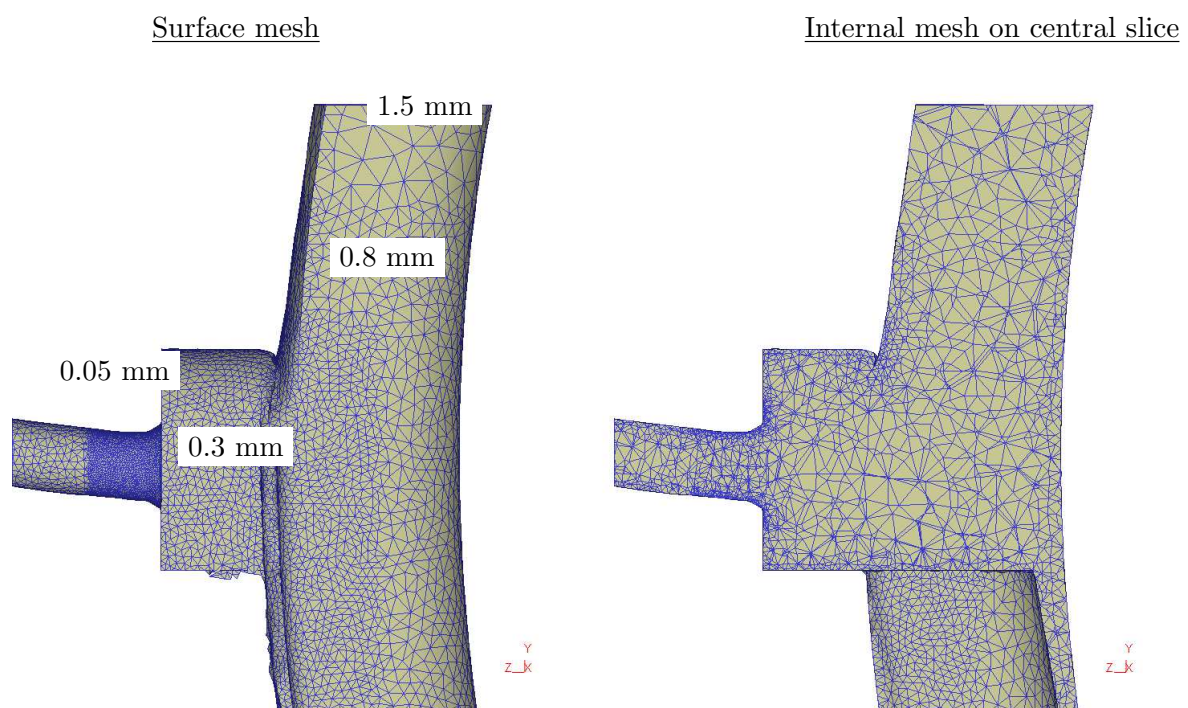


Figure 6.4: Example of the mesh used in the 3D Conform FE simulations on the workpiece surface and internal. Mesh windows were defined to refine the mesh with element sized indicated in the figure.

6.1.2 Truncated Workpiece Simulations

FEM software is inherently a poor choice in modelling loose powders in bulk deformation processes due to the inter-connectivity between nodes and elements. However, there is currently no published work or software suitable for modelling a process such as Conform with loose powder (see chapter ?? for further discussion). It was theorised that there was a certain point in the Conform process beyond which the powder could be assumed to be 100% dense (see figure 6.5). Die back-end defects taken from the tooling following experimental trials gave a rough idea of the height of fully consolidated material formed during steady state extrusion (see figure 6.6). This fully dense metal completely fills the wheel groove and contributes significantly to the driving force from the wheel. For the purpose of this section it was assumed that if the powder in the groove is not fully dense then it does not contribute to the driving force as particle rearrangement and local yielding will be the dominant deformation mechanism in this region. This assumption is similar to that made in the analytical model derived in section 4.1 where only the driving force created by contact between the fully dense workpiece and the wheel is considered.

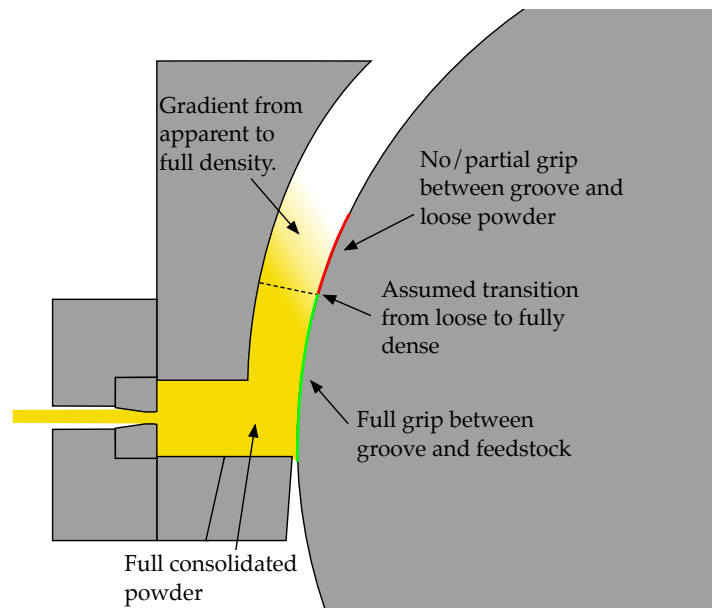


Figure 6.5: Theoretical representation of the consolidated powder within the Conform process as it relates to the truncated workpiece FE simulations. The transition between fully consolidated material and unconsolidated powder is shown schematically with a black dashed line.

If only the fully dense metal contributes significantly to the grip length and hence driving force for continuous extrusion then the process can be modelled using workpieces truncated at a certain height above the abutment. The truncated workpieces were set up so that all of the available workpiece height above the abutment was in full contact with the wheel groove. This height and resultant grip length would require a certain wheel torque to deform. The abutment

would resist the deformation with a certain load, which would be proportional to the truncated height or grip length. Hence by running simulations with a range of different grip lengths and observing how the wheel torque and tool loads respond it should be possible to compare the simulations to the experimental trial data. From the comparison the required grip length of powder for successful extrusion can be inferred. This method can also help determine the upper bounds of the processing window and show why the abutments failed in each of the trials.

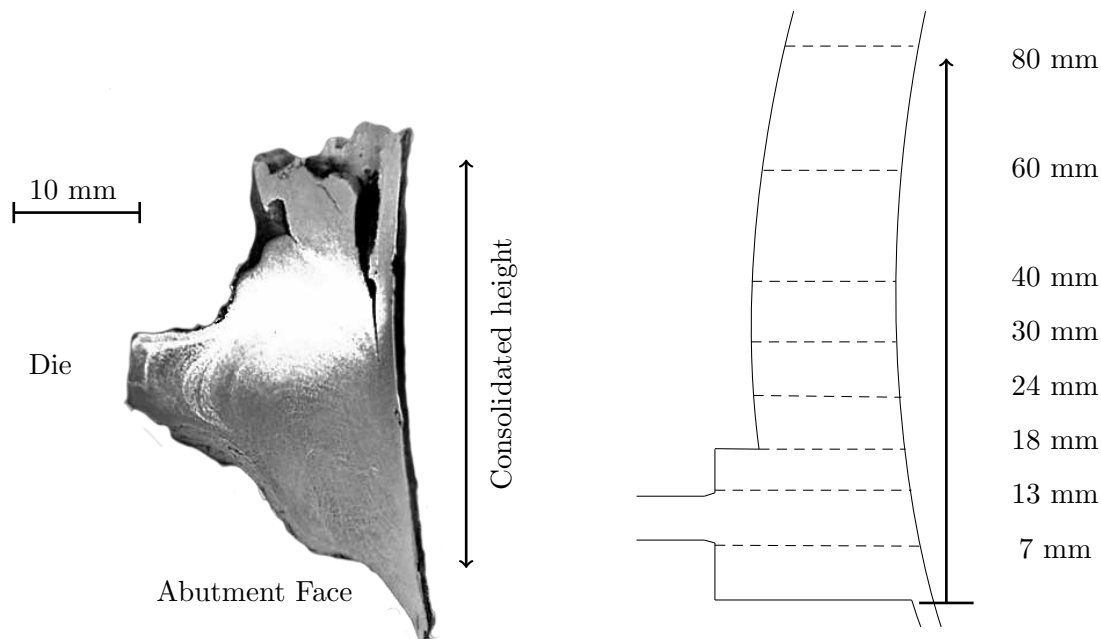


Figure 6.6: Die back end discard showing how high above the abutment the CP-Ti HDH powder is fully consolidated.

Figure 6.7: The placement of the truncated workpieces for FEM analysis of the effective abutment stress, abutment load and grip length relationships.

FEM software is inherently unable to model loose powder flow due to the interconnections of nodes and elements. A more accurate solution would be to use discrete/distinct element modelling (DEM) with defined particle interactions for angular powders. DEM would help in the understanding of the initial powder flow in the wheel groove and particle rearrangement up to the point of particle-particle yielding. The ideal method of modelling powder flow in Conform would be a combined FEM-DEM code where the particles will flow and rearrange according to a rigid particle model then yield and deform when the localised stresses are large enough. The resultant particle deformation would close up intergranular voids and result in a bulk increase in density up until full consolidation. Constitutive or empirical equations could define the particle to particle bonding and give a defined transition from discrete elements to finite elements for the bulk deformation process in the die chamber port. Unfortunately current consumer level computing power is not sufficient to allow such simulations to be conducted in a time efficient manner.

Each truncated workpiece was preformed to the tooling by performing a geometry boolean subtraction to ensure maximum available contact between workpiece and wheel groove. The parent workpiece was truncated at a predetermined height as shown in figure 6.7 by a horizontal plane. Heights were chosen to cover the range in which the consolidated material was expected to transition to loose powder as shown by the die discard in figure 6.6. Workpieces truncated at heights of 7, 13 and 18 mm were chosen to coincide with the die entry and top of the die chamber port. All other parameters were kept the same as the full 3D simulations as shown in table 6.1.

6.2 3D FEM Results

6.2.1 Full 3D simulation results

All 3D simulations were run through to a steady state as the 2D simulations in the previous chapter. The same factors, such as the stabilisation of tool loads and temperature profiles were used to determine when the simulation had reached a steady state. Tool load data was extracted for each simulation and plotted against simulation time. Points of interest in the wheel groove, port and die bearing were also used to track state variables throughout the simulation post processing. The positions of these tracked points were set on the central plane defined by $x=0$ as shown in figure 6.8.

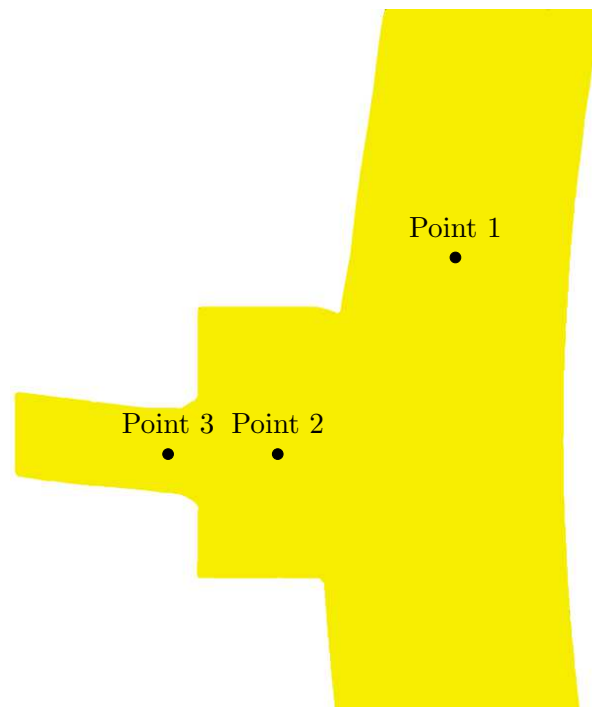


Figure 6.8: Point tracking positions used in 3D FEM post processing

Load data for each of the tools in the Y and Z axis were extracted and selectively post-processing with a script written in Python 2.7.9 and graphs were created using the plotting library Matplotlib. Load data in the X axis was not considered as part of the post processing routine as loads were essentially zero in this axis due to mirror symmetry. Local variations in the X loads for some tools were created by the automatic remeshing routine slightly altering the workpiece geometry but were very small in magnitude and tended to zero when averaged over the entire simulation. The post processed load data was temporally averaged to smooth out local load spikes caused by the frequent remeshes. Both raw and smoothed data were compared to ensure that the data was not altered by the smooth process.

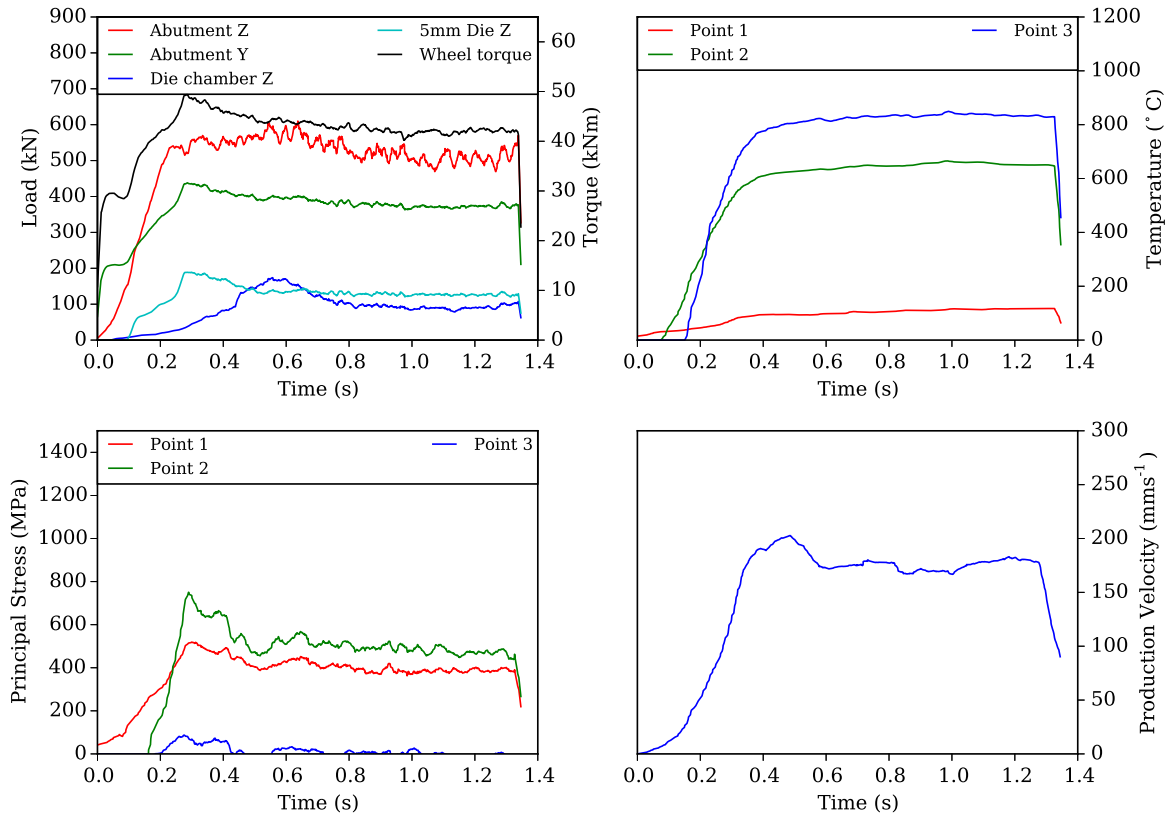


Figure 6.9: Simulation data of the tool loads and point tracked temperatures and stresses.

A plot of the important load data can be seen in the top left of figure 6.9. The abutment (Y axis), die chamber (Z axis) and die (Z axis) data streams are plotted as these are the axes under which these tools experience their primary loads. Due to the mirror symmetry of the process, loads in the X direction are not considered in this work.

The workpiece starts the simulation just touching the abutment’s top face and in full contact with the wheel groove. When the wheel begins to rotate the workpiece is upset into the abutment zone and moves towards the path of least resistance, which is into the port. Flash is also generated between the abutment lip and the wheel groove due to a small ~ 1 mm flash gap remaining.

The workpiece primary upset phase takes place from time $t = 0.00$ s to $t = 0.09$ s when the tip of the upset abutment reaches the die face as shown in figure 6.10. The abutment is the only tool to register a load on it during this first phase. During upset the workpiece remains largely at the initial $T = 20^\circ\text{C}$ that it was initialised at, with the main form of heat generated from adiabatic heating in the $\sim 45^\circ$ primary shear zone.

When the upset workpiece reaches the die at $t = 0.09$ s the load on the die steadily increases, as does the generation of flash between the wheel and die chamber. The evolution of contact between the die and workpiece can be seen in the die loads, which has two visible steps at $t =$

0.14 s and $t = 0.30$ s corresponding to the beginning of material entering the die and the filling of the port.

The increasing contact between the workpiece and the die generates a back pressure causing the upset height to increase at $t = 0.09$ s until it completely fills the port at $t = 0.30$ s. After the workpiece fills the port the extrudate is fully formed and the extrusion velocity increases steadily until it reaches the theoretical maximum velocity dictated by the input cross section and wheel speed. Prior to this the heating of the material in the port is mainly from the conduction of heat from the tools to the workpiece. Once sufficient pressure is built up within the port the extrudate can be pushed through the die and the extra deformation created in the region of the die entry causes the extrudate to heat up further. In turn this extra heat reduces the material flow stress within the die reducing the resistance to extrusion.

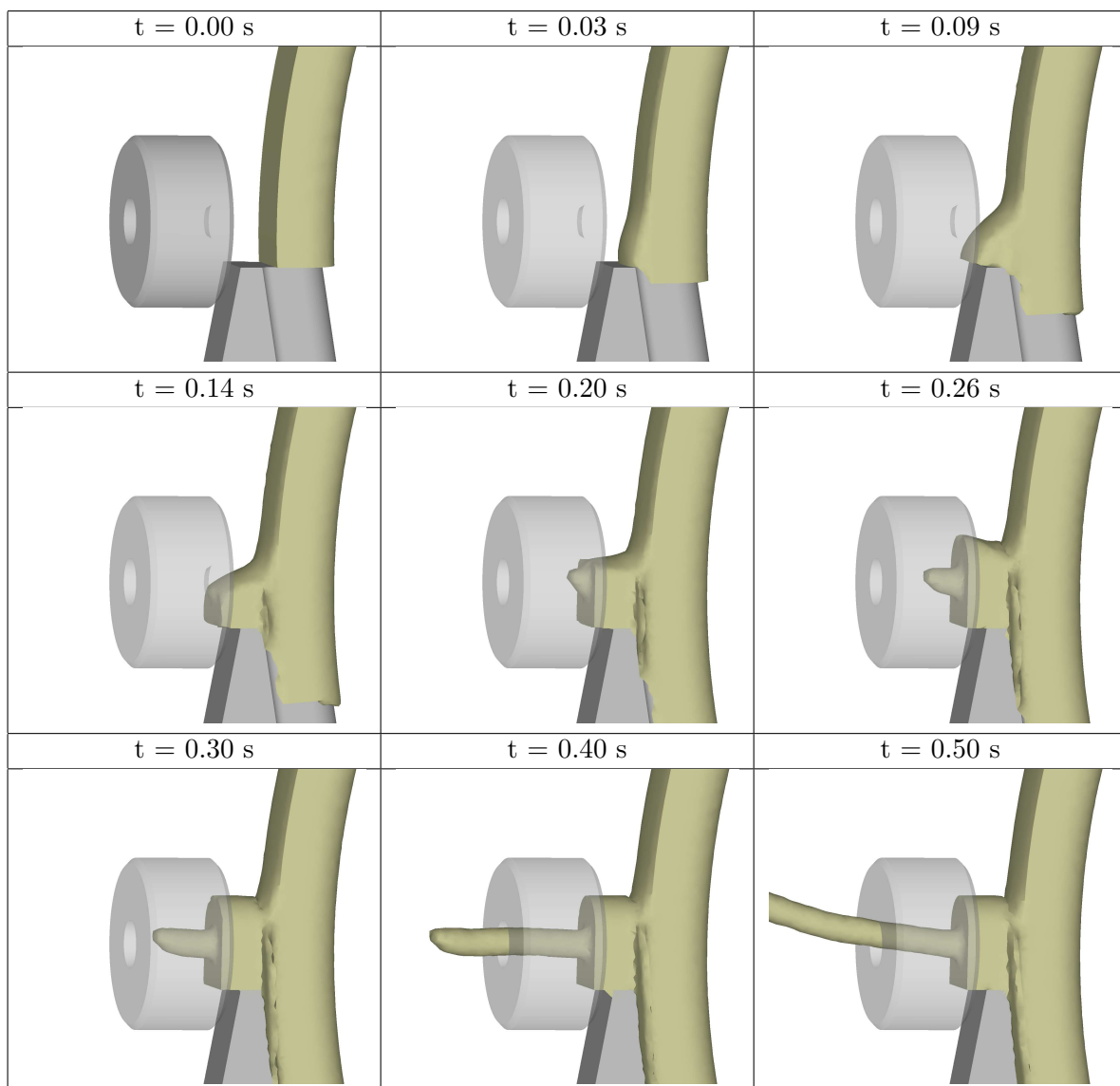


Figure 6.10: Evolution of the workpiece during the upset phase of DEFORMTM-3D simulation of Conform with a 5 mm round die

Maximum die load occurs when the port is completely filled, which also coincides with the maximum abutment load and peak stress within the port at point 2. Following this maximum load the workpiece continues to heat up from the material deformation and heat transfer from the tool bodies, helping to reduce the workpiece flow stress. This effect is then observed in the reduction of tool loads and the processes tends to a steady thermal and mechanical state. The peak temperature of each of the tracked points 1, 2 and 3 all reach a maximum when the tool loads have reduced to their steady state values. The die chamber load can be seen to slowly increase, when compared with the other tool loads and reach its maximum far later in the process at $t = 0.58$ s when the flash rate is at it's maximum. This suggests that while a steady mechanical state is reached quickly within 0.3 s of the simulation beginning, it takes twice as long for the thermal profile to steady and the process to reach a true steady state extrusion. This result has a profound effect on further modelling work of the Conform or CRE processes in that each simulation needs to be run through to a steady state before accurate results can be extracted. If this is not done there is a risk of evaluating the simulation at a time after peak tool loads are observed but before a steady state is reached. In this situation, tool loads and extrusion pressures are likely to be over-estimated while temperatures in the port and die are correspondingly likely to be under-estimated.

6.2.2 Material flow in the Conform process

In finite element modelling of metal forming processes the elements that make up the deforming workpiece are constantly changing in order to account for the bulk change in geometry. For processes, such as forging that may result in relatively small global deformations, the original FE mesh may be used for the entire simulation runtime without creating errors in the calculations of the nodal velocities and forces. However for those processes that create large bulk deformations such as extrusion, specifically Conform or CRE require frequent remeshing steps to help eliminate these errors. DEFORMTM offers an automatic remeshing routine that is activated with a number of user based input parameters such as element stretch length, element interference depth and elemental strain or temperature changes. During post processing of the simulations, these remeshing steps have the unwanted side effect of masking the material flow within the modelled process. Instead it is possible to overlay a deformable but unremeshable cubic array in order to visualise the material flow over a number of simulation steps. This was done for the Conform simulations in this work and the results are shown in figure 6.12.

Figure 6.12 shows a side view of the DEFORMTM workpiece in the abutment zone when it is extruding in a steady state. Slices at points 1 and 2 as indicated in the figure are shown below

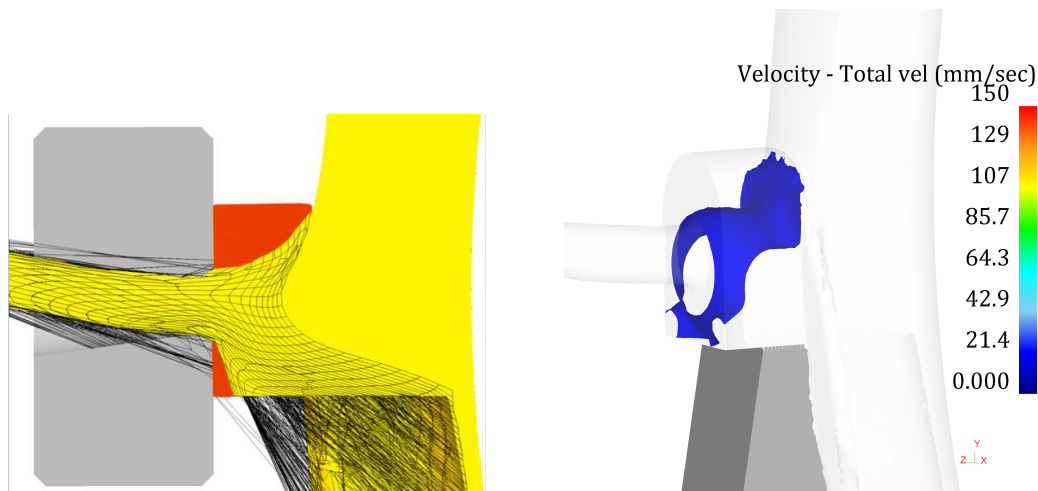


Figure 6.11: Material dead zones shown in red on a 2D slice through the 3D workpiece. 3D velocity isosurface (blue) delineated by 3 mms^{-1} velocity surface contour. Material in this zones is classed as ‘dead’ and tends to remain in the shoe tooling rather than be extruded.

the side view. The flow net begins undeformed and the vertices that link the cubic elements are intimately locked to their initial points of contact with the workpiece. As the extrusion continues the flow net deforms with the workpiece demonstrating both the material flow and dead zones within the modelled process. When this is combined with the dead zone isosurface of 3 mms^{-1} , as shown in figure 6.11, the areas of stationary material are easy to identify. Such material dead zones can have two major effects on extrusion processes. Firstly for the direct extrusion of billets, the dead metal zone tends to trap surface oxides resulting in improved product quality. Secondly, as Conform is touted as a continuous process, the dead metal zones can also act as reservoirs for oxidised material and can produce an unpredictable stream of oxide stringers into the extruded product. This is an ongoing problem in certain Conform extrusions of copper strip profiles [92]. As yet it is unknown what effect this dead zone will have on the extrusion of powder feeds, as surface oxides on the powder particles are broken down within the process to allow particle-particle welding to occur prior to extrusion.

The flow lines shown in the extrudate cross section mirror the macro material flow observed in the 5 mm diameter wire extruded during trial 1 (see figures 3.36 and 3.38). Both the wire macrostructure and flow net show the same central linear ‘spine’ and curved regions on either side. The ‘onion skin’ region is also visible as a highly deformed region around the edges of the extrudate. The flow net indicates how the bulk material flow of the consolidated titanium may have formed during extrusion. The strain, velocity and temperature profiles shown in the next section further demonstrate the macro and microstructure evolution through the Conform process.

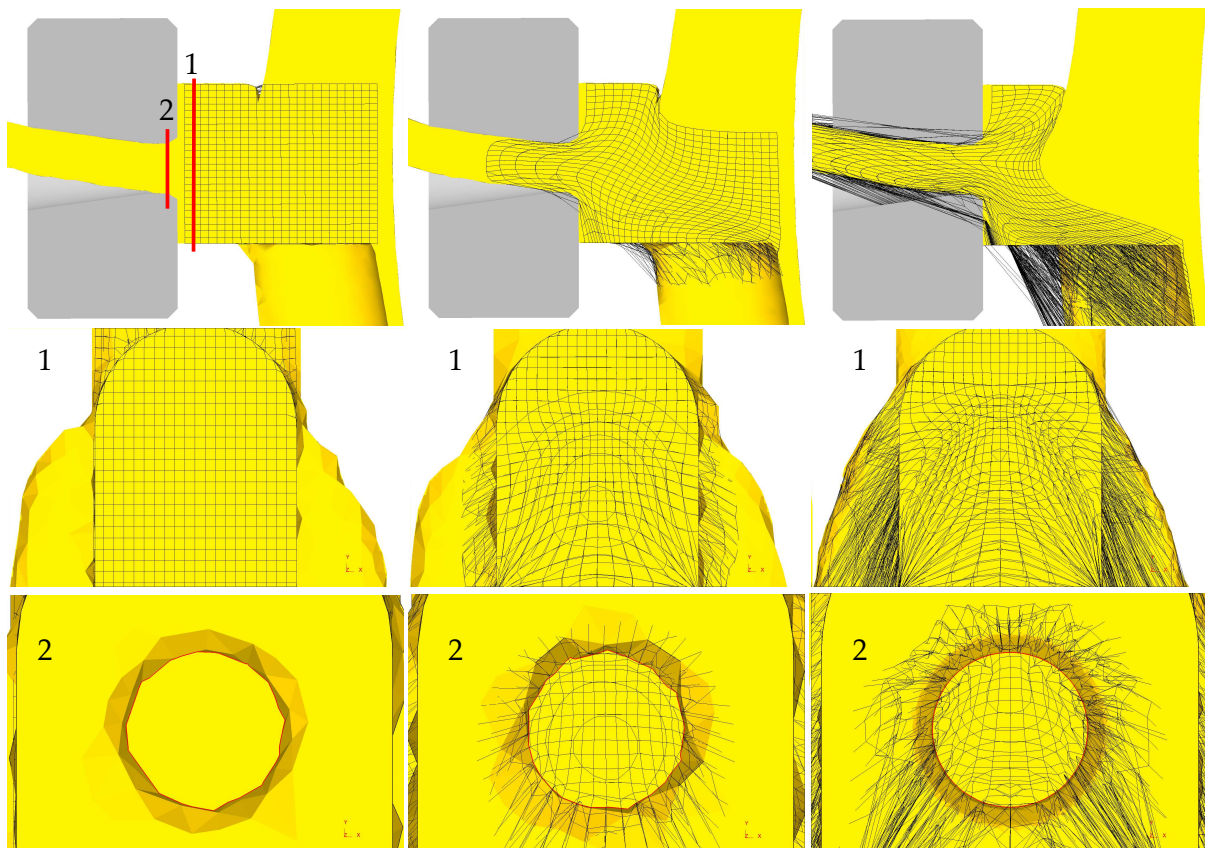


Figure 6.12: Evolution of an overlaid 3D flow net during steady state Conform extrusion of CP-Ti. Two slices on the labelled planes 1 and 2 were taken either side of the die entry and shown below the side-on view

6.2.3 State variables in the workpiece

6.2.3.1 Effective Strain

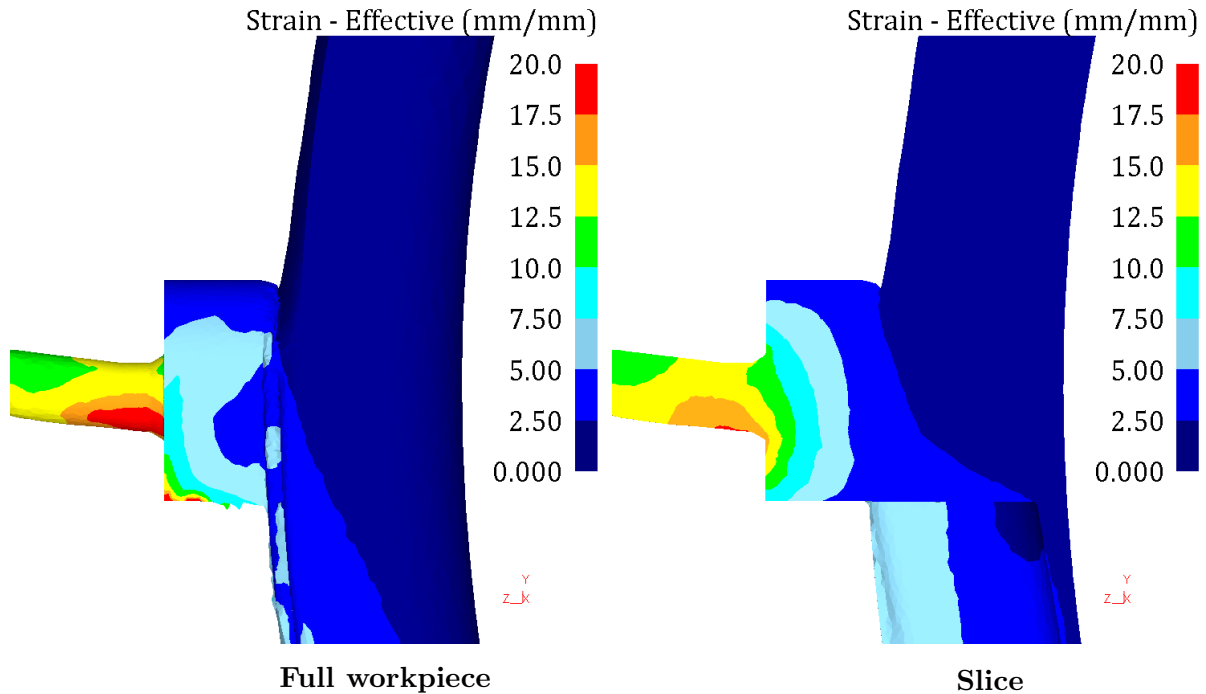


Figure 6.13: Effective strain profile in the CP-Ti workpiece in both full 3D and on a central slice.

The total effective strain within DEFORMTM is usually defined by a combination of the elastic strain, plastic strain, dilational thermal strain, dilational transformation strain and transformation plasticity. For this work with a rigid-visco-plastic workpiece the effective strain reduces to that defined by the plastic strain, which is a function only of flow stress law used any effects of creep are neglected due to the high strain rates involved in ConformTM extrusion. The strain profile shown in figure 6.13 shows how the effective strain varies across the workpiece in on both the outer surface and an inside central slice. A lot of the workpiece remains undeformed during most of the process accumulating only a small proportion of the final strain. There is almost no interaction with the die chamber surface as the workpiece is moved by the groove towards the abutment. Once the material goes through the upset zone and shears at about 45°, 30-50% of the final strain is imparted to it. This shear zone is most visible in the strain rate profile in figure 6.16 as a curved region between the abutment tip and the top of the die chamber - groove interface

Figure 6.14 show slices through the extrudate as it emerges from the die bearing. Line plots of the effective strain were taken in the vertical and horizontal directions as shown on the right

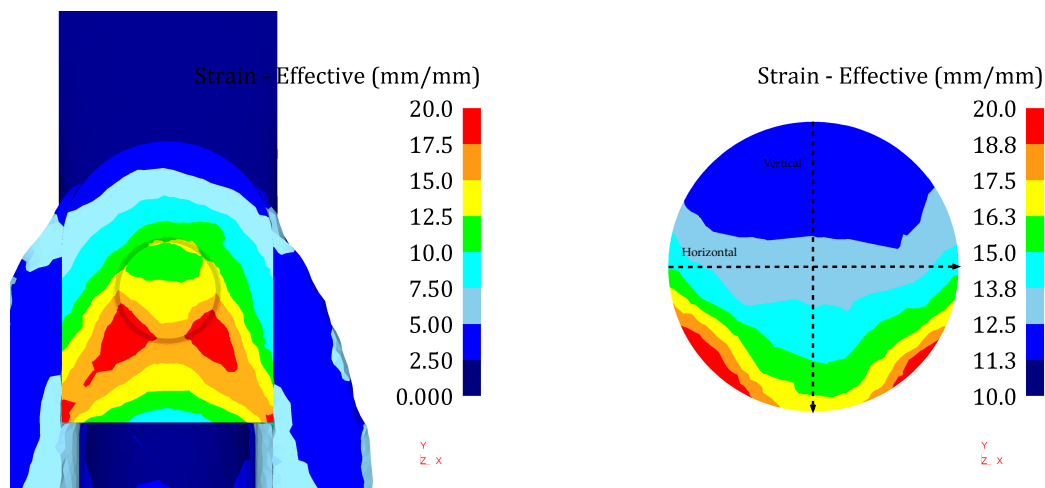


Figure 6.14: Cross sections of the extruded workpiece once it has exited the die showing the both the full workpiece in the $-Z$ direction and the final effective strain profile.

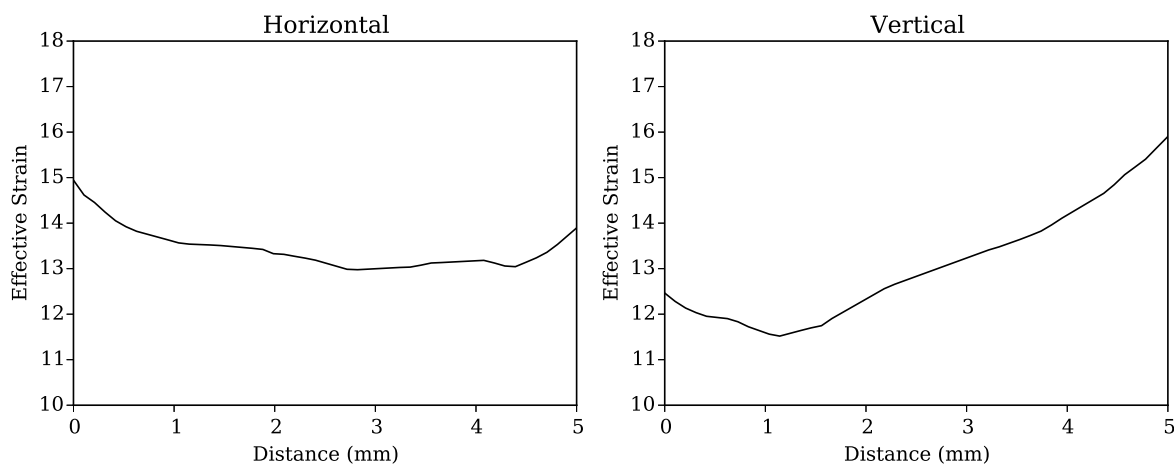


Figure 6.15: Line plots of the effective strain in the vertical and horizontal orientations on a cross section of the workpiece as it moves through the die bearing.

had side of the figure. Distance = 0 in figure 6.15 was taken from the far left and the top of the extrudate cross section in figure 6.14. There is a strongly heterogeneous strain profile across the wire cross section with two regions of high strain accumulation at the bottom right and left of the wire. The strain gradually decreases to half of the maximum value at the top of the cross section. The line plots in figure 6.15 show a slight peak in strain at the edges of the wire as the frictional interaction between the workpiece and the die creates a shear region at the surface of the wire. This shear helps to create the ‘onion skin’ structure observed in the microstructure of the rod.

6.2.3.2 Effective strain rate

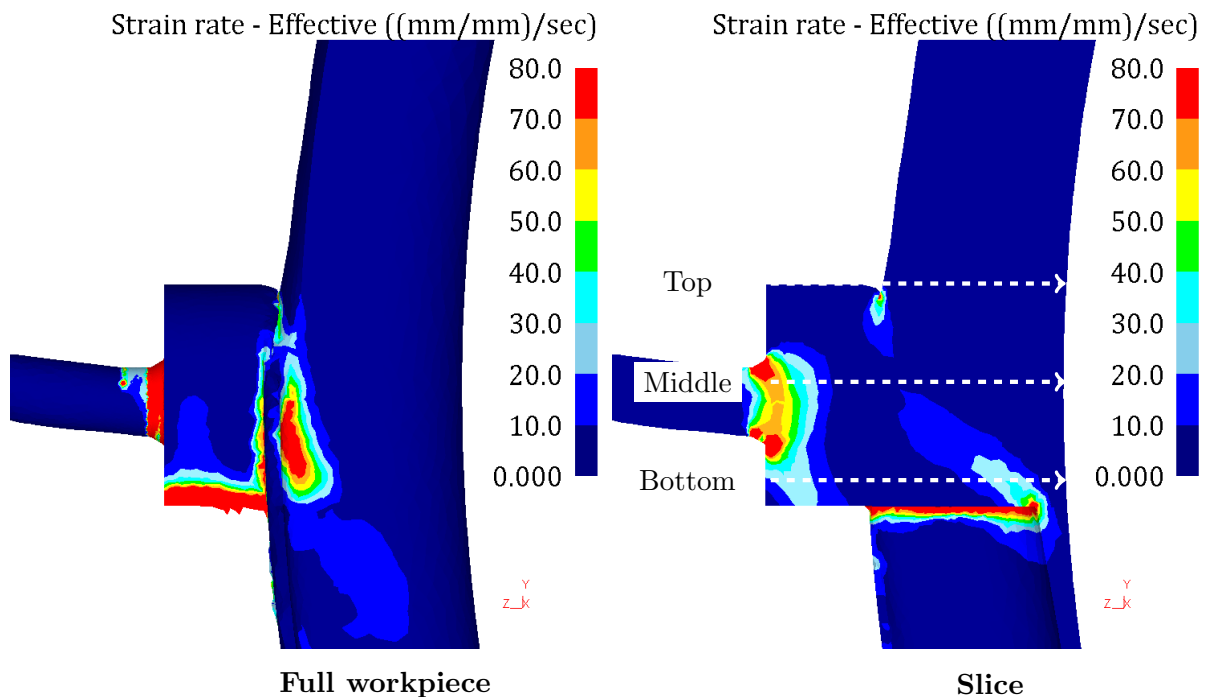


Figure 6.16: Effective strain rate profile in the CP-Ti workpiece in both full 3D and on a central slice.

The strain rate profile at the surface and central slice of the workpiece in figure 6.16 shows the main regions of deformation in the workpiece. The primary shear zone as identified in the effective strain rate profile can be seen to extend from the tip of the abutment at the bottom of the wheel groove to the top edge of the port as material begins to enter the die chamber. This region has a rough 45° angle but is shifted downwards slightly under the force of the cold workpiece above it. The average strain rate in this primary shear region for a wheel speed of 6 RPM is between 10 and 20 s^{-1} . This is also shown by the smaller hump in the line plots in figure 6.17. The strain rate line plots show both their primary shear zones as material is deformed between the groove and die chamber port and a much higher strain rate region by the die entrance. The material entering the die undergoes a strain rate of 20 - 140 s^{-1} depending where in the die entrance it is.

Figure 6.17 also shows a third high strain rate region around the edge of the abutment in the flash gap between it and the wheel groove. This area is where the wheel coating is formed during the experimental trials and the titanium experiences the most heat and pressures. The deformation region around the abutment edge is very small at about 2 mm in depth below the abutment face. This means that loose powder only travels through a small area in which it can be consolidated to form the wheel coating during the process startup. If it is not consolidated in

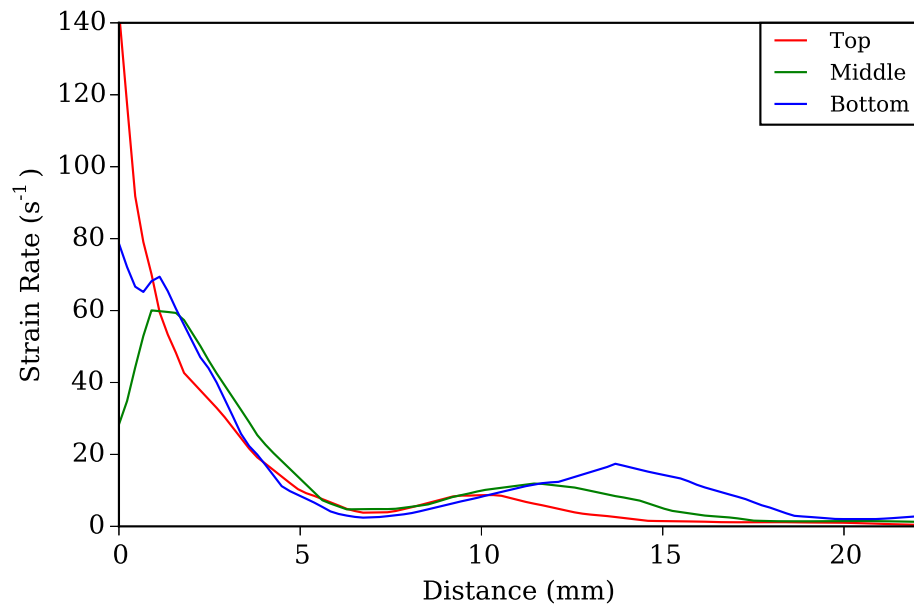


Figure 6.17: Line plots of effective strain rate at the top, middle and bottom of the abutment zone showing the two main deformation zone that the workpiece undergoes. Distances are measured from the die face at $d = 0$ horizontally towards the wheel groove.

this region it is likely that it will simply fall from the bottom of the tooling in to the tray beneath the machine. Accurate control of the temperature and flash gaps in this area is important to allow consolidation of the titanium powder.

6.2.3.3 Effective stress

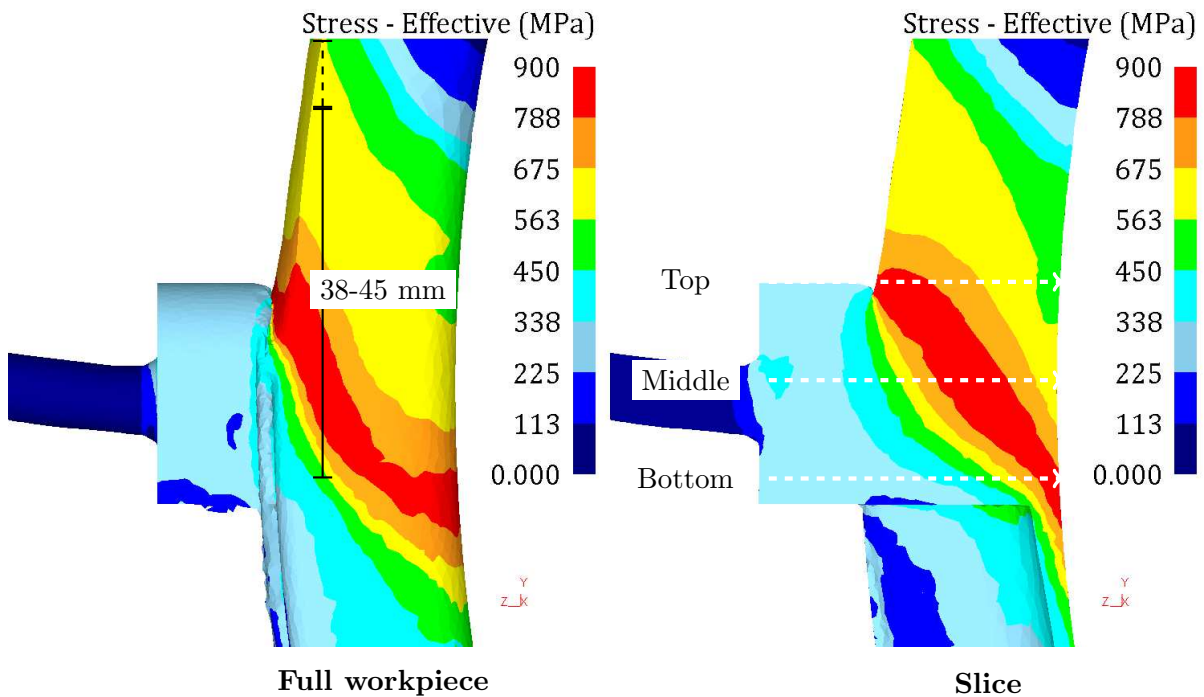


Figure 6.18: Effective stress profile in the CP-Ti workpiece in both full 3D and on a central slice. The estimated upset height is shown on the left hand side image.

The effective stress profile is calculated by DEFORMTM as a function of the elemental strain, strain rate and temperature from the material database. It is an indication of the flow stress that the elements require in order to deform. The effective stress distribution within the workpiece is shown in figure 6.18. The upset height generated within the workpiece as a result of shearing the workpiece at the abutment zone and extruding material through the die can be seen extending towards the top of the figure. The upset height is estimated to be $\sim 38-45$ mm and extends from the abutment face to the point where CP-Ti grade 2 would be expected to yield at approximately 350 MPa (at 20-100°C) within the wheel groove.

The greatest stress is seen in the main shear zone indicated in the red contour as the workpiece is redirected into the die chamber port. It is here that a considerable amount of compaction of fresh powder is likely to occur as it undergoes a mixed shear and compression. The domed morphology of this region on the groove side between the red and orange contours mirror the consolidated powder observed in the die discard taken from trial 2 as seen in figure 3.45. This further suggests that the main mode of consolidation within the Conform process for titanium powders is a compaction of layers that begin to bond in the region prior to extrusion. Loose powder processed behind this acts to generate the compaction force to both consolidate the powder and produce the driving force for extrusion through the port and die.

6.2.3.4 Nodal velocity

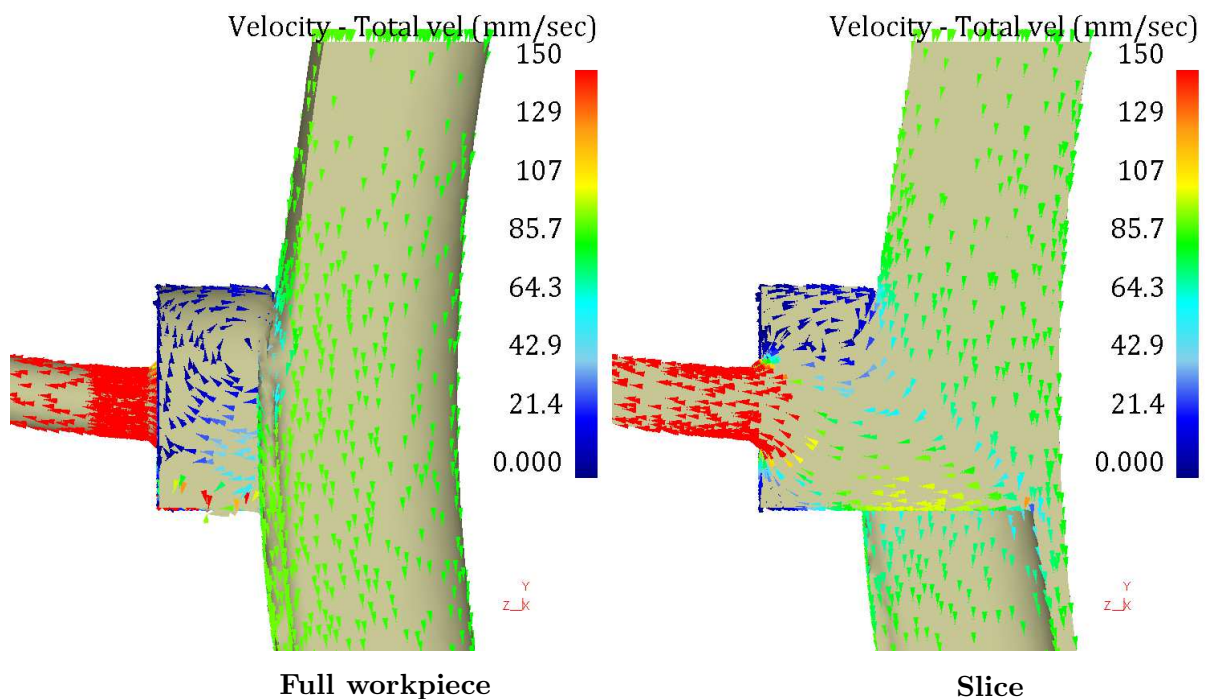


Figure 6.19: Nodal velocity profile in the CP-Ti workpiece in both full 3D and on a central slice.

Velocity profiles of the 3D workpiece are shown in figure 6.19 and are visualised as vector arrows from nodes. For clarity a sampling ratio of 50% was used so that only half of the nodes display a vector arrow. The arrows are coloured according to the magnitude of the vector that they represent. Velocities shown at the bottom corner of the port on the full 3D image suffer from transient spikes in their magnitude due to the tight corner on the tool geometry. Nodes close to this corner tend to have peak velocity orders of magnitudes higher than the surrounding area and hence can be the source of errors during the simulations. This can also be seen in the bottom right and left corners of the port in figure 6.20. The magnitudes of the velocities shown in this area in the full workpiece in figure 6.19 are far larger than they should be despite their direction vectors being correct.

The velocity profile across the workpiece in the groove shows no obvious effective shear at either the groove or shoe side. As the workpiece was slightly undersized to the groove this shows that there is not effective upset of sufficient magnitude to completely fill the groove and hence result in contact with the shoe plates. The main shear zone is visible in the sharp change of direction between the groove and port where material slows slightly before moving towards the die.

Dead zones are shown as areas of slow moving material at the top and bottom of the port.

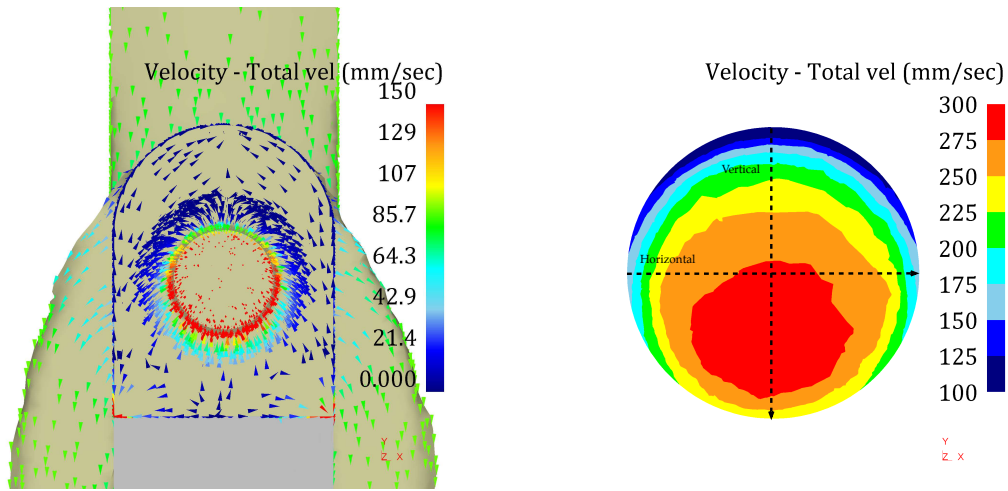


Figure 6.20: Cross sections of the extruded workpiece once it has exited the die showing the both the full workpiece in the -Z direction and the final velocity profile.

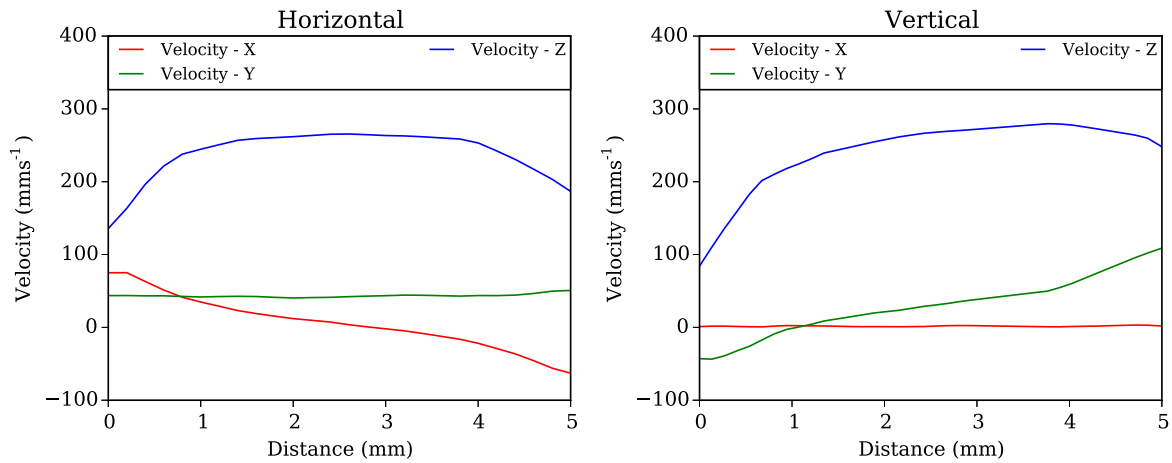


Figure 6.21: Line plots of the velocity in the vertical and horizontal orientations on a cross section of the workpiece as it moves through the die bearing.

The dead zone at the top of the port is significantly larger than that at the bottom and it acts as a barrier to prevent material at the top of the port entering the die directly. Instead the bulk of the metal is pushed towards the bottom of the abutment zone before rising slightly and being extruded through the die. There is a slow turbulent flow induced in the upper dead zone, which could potentially become a source of oxidised material that would be interspersed in the top of the extruded wire. While this was not observed in any of the wire extruded during this work, it may be that oxide stringers would only be observed later on in a fully continuous extrusion.

Cross sections of the extrudate show a large variation in velocity across their profiles as shown in figure 6.21. There is a central region of quick flowing material offset towards the bottom of the die. This is also shown in line plots of the vertical Z-velocity in figure 6.21. The workpiece slows further as it contacts the die bearing and undergoes the shear that produces

the increased strain shown in figure 6.14.

6.2.3.5 Temperature

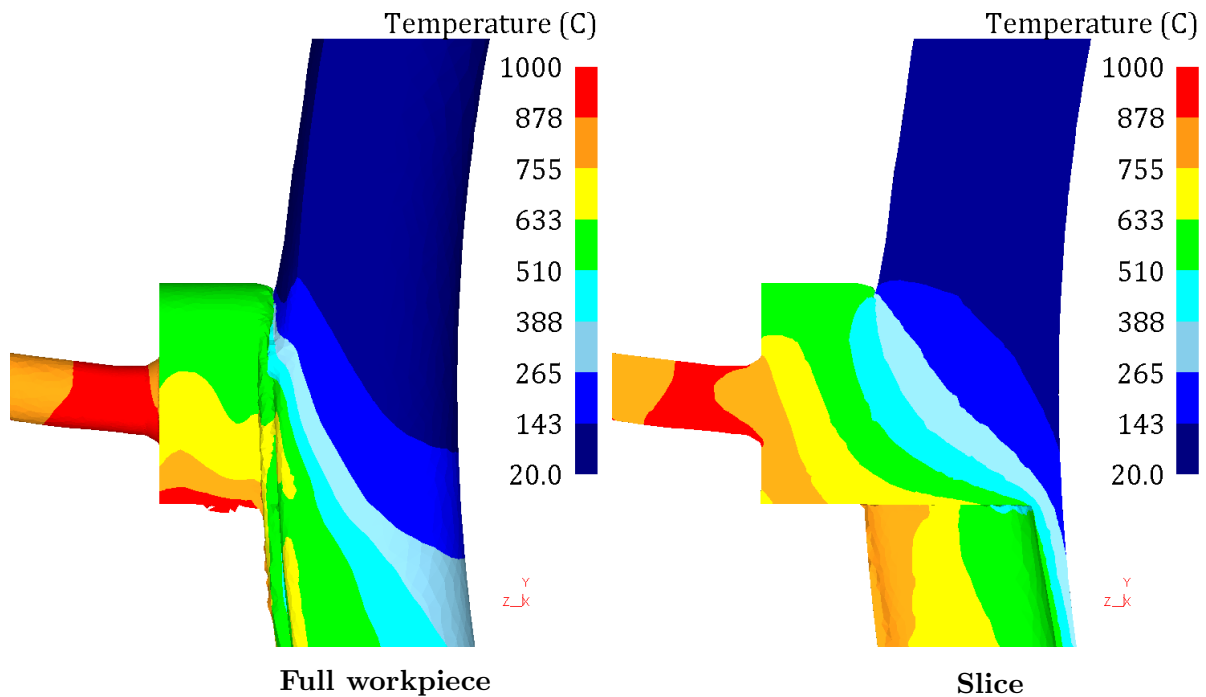


Figure 6.22: Temperature profile in the CP-Ti workpiece in both full 3D and on a central slice.

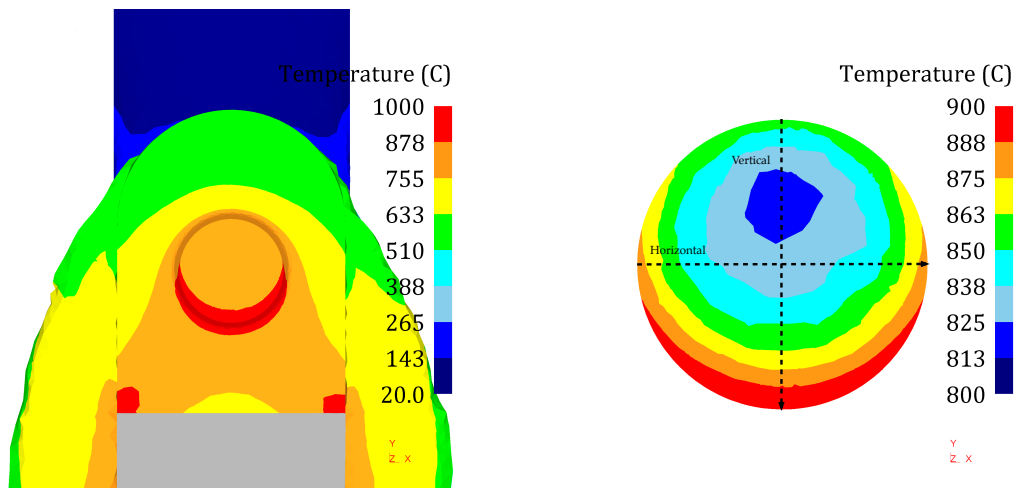


Figure 6.23: Cross sections of the extruded workpiece once it has exited the die showing the both the full workpiece in the $-Z$ direction and the final temperature profile.

The temperature profile in figure 6.22 show that the workpiece enters the abutment zone with very little extra heat imparted to it compared with it's initial state. After three seconds of simulation time the interface of the workpiece with the groove is about 100°C . When it reaches the primary shear zone above the abutment the shear and high compressive stress observed in

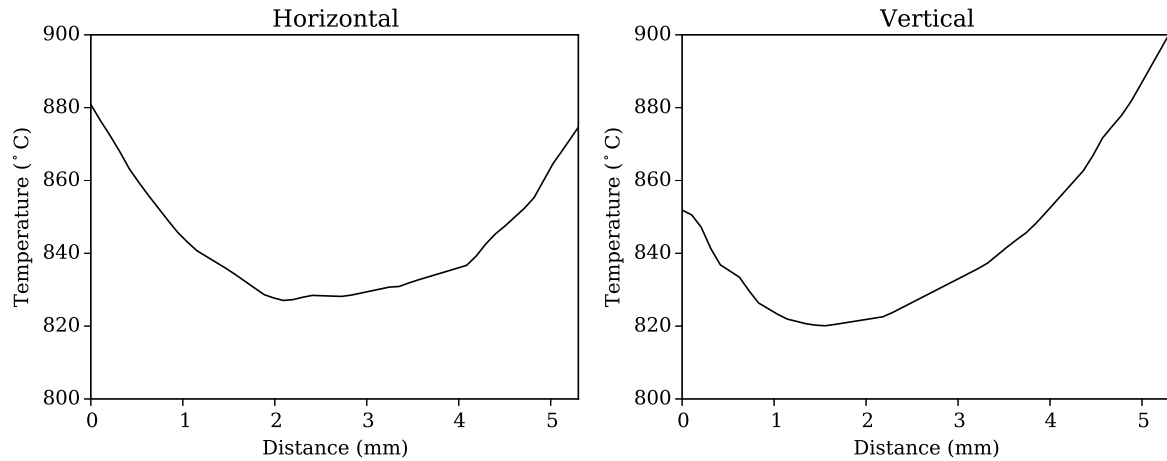


Figure 6.24: Line plots of the temperature in the vertical and horizontal orientations on a cross section of the workpiece as it moves through the die bearing.

the effective stress and strain rate profiles produce a large amount of heat within the workpiece. This has the combined effect of increasing the temperature at a rate of the order of $\sim 1000^{\circ}\text{C s}^{-1}$.

The workpiece exiting the die has a temperature profile as shown in figure 6.23. There is approximately a 100°C temperature difference across the extrudate cross section as it emerges from the die with the hottest parts at the surface of the die. The temperature is also lower at the top of the workpiece where it has undergone far less strain (see figure 6.14) and is moving slower (see figure 6.20).

6.2.4 Truncated workpiece simulations

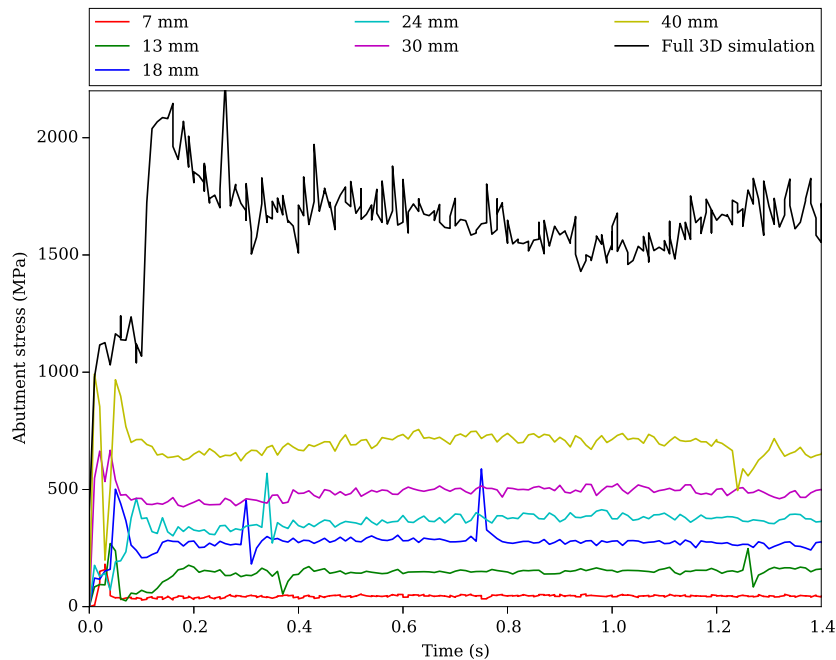


Figure 6.25: Wheel torque data converted to abutment stress values for the truncated sample simulations.

Results from the truncated workpiece simulations demonstrate how the fully consolidated grip length can effect the wheel torque and hence load on the abutment. The wheel torque data was converted into an abutment stress as described in section 3.2.2 and plotted against the simulation time to give figure 6.25. The torque derived abutment stress is also plotted for the full 3D simulation for comparison. It can be seen that the wheel torque varies significantly over the course of the simulation as grip is lost and regained between the wheel and workpiece resulting in slippage and loss of drive force. Remesh steps also result in over/undercompensation of the wheel torque as the workpiece contact nodes oscillate between contact and non-contact. This is evident in the peaks and troughs of the abutment stress plots in figure 6.25. The average abutment stress over the final half of the simulation was taken and plotted against the workpiece height or fill depth as shown in figure 6.26.

The variation of effective abutment stress with fill depth/grip length in figure 6.26 exhibits a near linear relationship. As the grip length increases up to a maximum of 150 mm due to the tooling geometry the abutment stress increases steadily. For each of these simulations the stress level was fairly constant, only changing significantly around remeshing steps. Measurement of the grip length within the full simulation also allowed comparison of the effective abutment stress with the truncated samples as represented by the far right hand point on figure 6.26. It

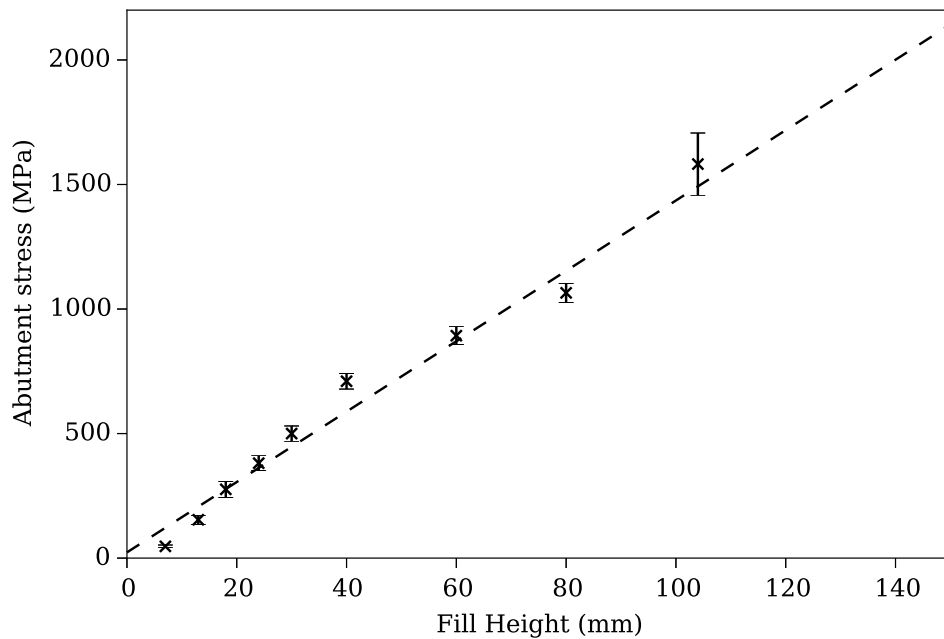


Figure 6.26: Average abutment stress vs truncated sample height for DEFORM™ CP-Ti grade 2 material data at 20°C .

is found that the abutment stress can be estimated to be $\sigma_{abut} = 14.1h$ where h is the height of fully consolidated material above the abutment and in full contact with the wheel. In practice this is likely to be a lower limit to this height as there will be an extra contribution to the wheel torque from partially consolidated powder above the layer that is fully dense. There will also be a contribution to the wheel torque from flash production between the wheel surface and the shoe tools as well as from the scraper at the rear of the machine removing excess flash.

If the abutment stress values from the truncated workpiece simulations are related to the abutment stresses observed in the experimental trials a rudimentary assessment of the abutment failure can be made. From the successful extrusion observed in trial 1 it can be shown that the measured abutment stress is almost always below 1000 MPa. For those trials where the abutment failed such as trial 4 (see section 3.3.4) the abutment stress was raised above 1200 MPa for an extended time with measured abutment temperatures of over 500°C . Relating this back to the truncated workpiece simulation results this shows that if the fill height of fully consolidated titanium within the groove producing the extrusion force exceeds ~ 75 -80 mm while the abutment is at extended temperature of over 500°C there is a good chance that the abutment will fail. In reality this fill height is an upper bound value as the truncated workpieces were treated as room temperature compacts with no prior strain history. This would increase their effective flow stress over 100-200°C loose powder and hence their effective contribution

per mm of grip length to the wheel torque and abutment stress value.

Comparison of Conform modelling techniques

7.1 Comparison with experimental results

The purpose of modelling the Conform process is to provide greater insight into the ‘black-box’ of the Conform machine without the need for costly experimental trials. Modelling techniques may help to visualise the flow path of material within the tools or determine the origin of microstructural defects. It may also be possible to help predict how to conduct initial experimental trials with new metal alloy feedstock. Through the analytical model derived in chapter 4 it can be shown that minimum required extrusion pressures, abutment stresses and hence grip lengths can be estimated. In this section results from the analytical model with parameters suitable for a CP-Ti HDH powder feedstock are compared with the 3D finite element model (chapter 6) and experimental trials on the Conform machine (chapter 3).

Table 7.1 show the parameters used in all the models from this thesis for comparison. The port and groove dimensions were consistent between all the models and experimental work and were converted to effective diameters from calculations of their cross sectional area for input into the analytical model. The flash gap was measured from the experimental setup and was replicated in the FEM simulation. In the analytical model the flash gap only affects the extrusion pressure due to its contribution to the flow length. The yield stress is taken as the compressive yield strength of grade 2 commercially pure titanium at room temperature, 380 MPa [93]. Alpha is taken as an average of the angle of the dead metal zone observed in both the experimental die backend optical micrographs (Section 3.4.3 figure 3.46) and the 3D FEM.

The two greatest unknown quantities in the analytical model are the flow stress at the die and the tool friction coefficients. Figure 7.1 shows how the wheel torque, grip length, abutment load and pressure are affected by changes in the flow stress and tool friction variables. The die temperature can be estimated from the experimental thermocouple readings and the temperature profile from the finite element model. For the purpose of providing a single flow stress figure for the analytical model the temperature used was 700°C. In reality this can change drastically from about 500°C to 800°C and results from figure 7.1 demonstrate how much of an

Table 7.1: Comparison of results from numerical modelling techniques used in this study with experimental trials with CP-Ti HDH powder on a Conform 315i machine.

| Values used in the Conform models | | | |
|--|-----------------------|---------------|---------------------|
| Wheel Radius | 147.5 mm | | |
| Area of port | 176.5 mm ² | | |
| Effective diameter of port | 11.3 mm | | |
| Area of groove | 168.2 mm ² | | |
| Effective diameter of groove | 11.0 mm | | |
| Diameter of extrusion product | 5.0 mm | | |
| Flash Gap | 1.0 mm | | |
| Flow Length | 14.2 mm | | |
| Alpha | 70° | | |
| Yield Stress (at 20°C in the wheel groove) | 380 MPa | | |
| Flow Stress (at 700°C in the port) | 120 MPa | 100-160 MPa | |
| Shoe Friction | 0.80 | 0.98 | Unknown |
| Measured parameter | Analytical | 3D FEM | Experimental |
| Wheel torque (kNm) | 23.2 | 41 ± 2 | 20 ± 5 |
| Abutment load (kN) | 157.2 | 370 ± 20 | Unknown |
| Abutment stress (MPa) | 934.6 | 1600 ± 100 | 750 ± 250 |
| Pressure required at die for extrusion (MPa) | 584.3 | 580 ± 20 | Unknown |
| Grip length (mm) | 23.2 (minimum) | 37 ± 3 | Unknown |

affect the resultant change in flow stress in the die can have on the overall extrusion pressure. For example, if the temperature of the material at the die is decreased from 700°C to 500°C, the flow stress value would rise to from 110 MPa to roughly 160 MPa [93]. This change in temperature would therefore cause an increase in abutment load and pressure of 45% and could mean the difference between causing the abutment to fail mid-trial or successfully extruding 10+ of metres of wire. Therefore it is clear that not only knowledge of the Conform process is required to calculate how to extrude metals through a machine but also knowledge of the feedstock metal or alloy system and how its deformation behaviour changes with temperature.

The contour plots in figure 7.1 are generated from the analytical model in section 4 by varying the tool friction coefficient (μ) and the flow stress of material at the die ($\bar{\sigma}$). Over plotted are the calculated or measured values from the experimental trials, 3D finite element model and the best fit values from the analytical model. The curved, dotted lines represent the encompassed range of values, where as the straight vertical or horizontal lines link the curves to a known value of tool friction or flow stress on the corresponding axis. The area encompassed by these lines can be thought of as showing the possible ranges of wheel torque, abutment load

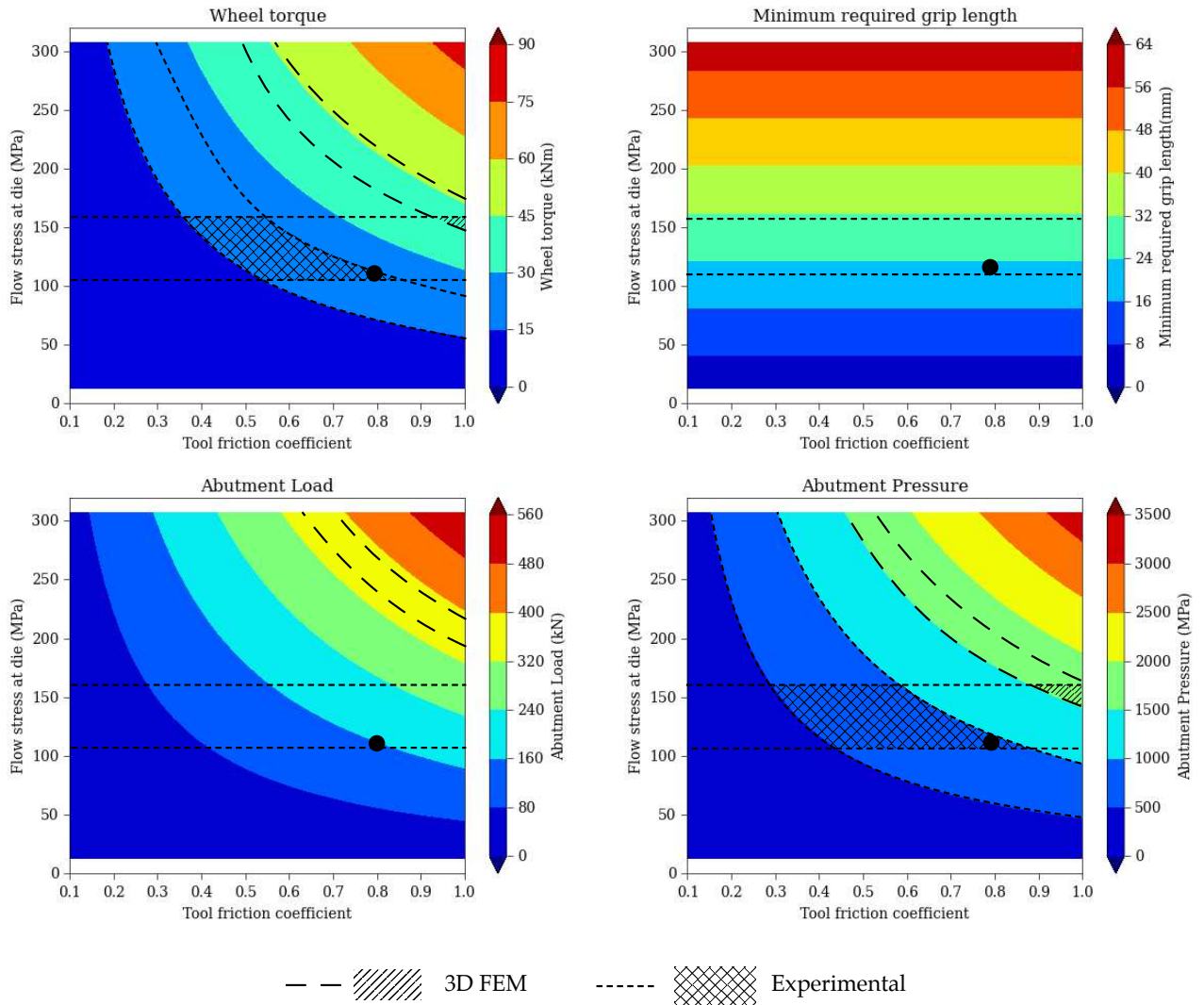


Figure 7.1

or abutment stress on their respective plots.

From first inspection of both table 7.1 and figure 7.1 it is apparent that both the 3D FEM and experimental results are not in agreement with each other. Firstly the wheel torque is significantly high for the 3D FEM simulation than the experimental work, or what is predicted by the analytical model. There is a small area of agreement at a high friction value of 0.95-1.0, which agrees with the value of 0.98 used in the FEM simulations. This is a purposely high value for the finite element modelling of Conform as it was necessary to ensure the workpiece was stuck to the wheel groove to provide the extrusion force. A more realistic value of friction for contact between a hot metal at $\sim 700^{\circ}\text{C}$) and metal that has a highly abraded surface is 0.7-0.8. This is also likely to be higher than the friction value suitable for modelling powder against the wheel groove where the interface layer is likely to shear rather than generating a compressive stress in a bulk material as per rod feed Conform. The wheel torque calculated

from the Conform machine current draw during Trial 1 covers this hatched region from tool friction values of 0.4 to 0.8.

For comparison of grip length predictions it is not possible to include measured results from the experimental trials as the incorporation of flash and partially consolidated powder masked the area of full consolidation. Grip length in the finite element model varied greatly between the total contact length of 370-450 mm and the upset length of 37 ± 3 mm. Once the extrusion had reached a steady state the FEM upset length was consistently around 37 mm and only varied during and immediately after remeshing steps. The analytical model predicts a minimum grip length of 23.2 mm, which is independent of tool friction if we assume that the wheel-workpiece and tool-workpiece friction is equal. The analytical model does not take the generation of flash into consideration, something that will increase the drive requirements from the wheel when considering the FEM simulations. Therefore, it can be stated that the upset length measured in 3D FEM is always greater than that calculated analytically due to the influence of the flash being generated.

As with the grip length it was not possible to measure the abutment load experimentally. Figure 7.1 shows that there is no agreement at all between the analytical and finite element models. The FEM abutment load is approximately double that predicted by the analytical model. Again the generation of flash can partly explain this discrepancy, but unlike the formation of the upset/grip length the flash that is pushed out of the wheel groove does not affect the abutment load. Instead the flash that forms the groove coating also acts to create a downward force on the abutment. In the finite element simulations both the material being deformed on top of the abutment and that pushed down its sides at the groove surface contribute to the measured abutment load. In contrast the analytical model only takes the deforming material above the abutment into account when predicting the load on this tool.

The abutment stress value, as a calculated value is directly proportional to the wheel torque, therefore the comparison of results match that for the wheel torque. While it may seem unnecessary to present both of these results for this particular work, wheel torque measurements are specific to a certain machine but the abutment stress metric can be used to compare results across all types of Conform and Continuous Rotary Extrusion (CRE, also see Holton Conform) machines. The experimental results cover a region of relatively low friction coefficients (0.3-0.5) as well as up to values of 0.85, a common value for unlubricated hot metal working. There is some agreement between all the modelling techniques in terms of calculated or measured abutment stresses. The analytical model assumes that zero flash is produced, which means that for a given flow stress and friction coefficient it offers a lower bound result for abutment stress.

Discussion

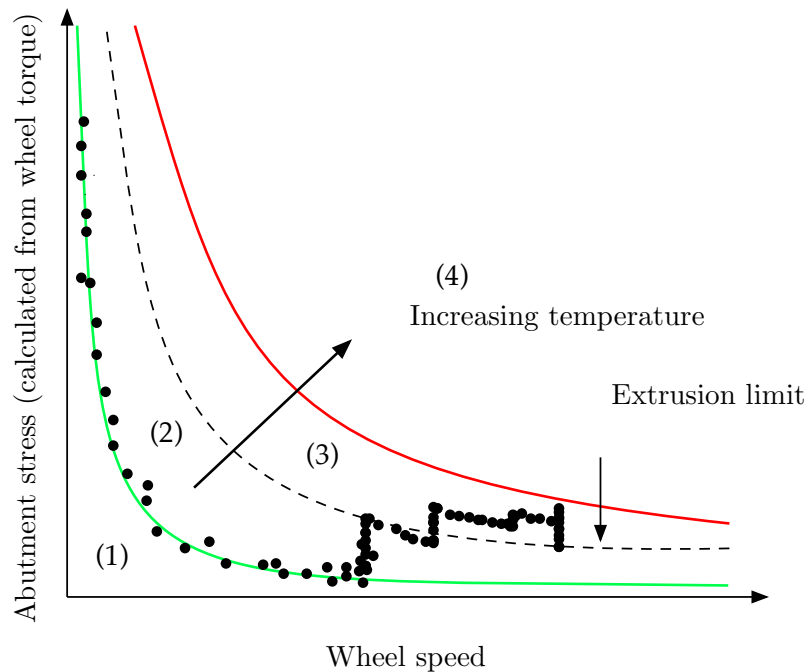


Figure 8.1: Theoretical representation of the abutment stress (torque related) vs wheel speed plots and the relationship with measured abutment temperature.

Figure 8.1 demonstrates a theory of the Conform processing of titanium powders. The figure contains three important lines separating five important regions, (1), (2), (2+3) and (4). Region 1 is the non-consolidation zone where if there is not enough powder going into the machine then any frictional heat generated between the particles is lost as they fall out of the machine. The heat is however imparted to the abutment face as it is this tool, along with the wheel that conducts the most work on the powder particles. With insufficient powder feed, local consolidation may occur but a full grip length cannot form to generate the extrusion pressure.

During the addition of sufficient fresh cold powder the process enters region 2 and there is a number of things that occur within the groove. The new cold powder flows freely according to its initial morphology and has a nominal contact area with the wheel and the entry blocks. This initial contact area results in certain level of resistance to extrusion. As the powder heats up

through contact with the tooling, particle-particle contact and particle deformation the friction conditions within the groove change. The net effect is to considerably increase the overall bulk powder temperature and its contact area with the tooling. During this phase the primary shear occurs higher up the groove in a larger section of loose powder. At first this will consolidate powder close to the abutment and begin to build the pressure required for extrusion through the die. As the powder densifies firstly during particle rearrangement and then particle deformation there is an increase in effective pressure normal to the surfaces of the wheel and shoe. This causes an increase in interface friction in line with Coulombs Law. The process begins to move from the region 1 - 2 interface to the 2 - 3 interface and the extrusion limit. The height above the abutment which is fully consolidated increases as the process continues resulting in an increase in grip length between the powder and wheel. This is observed in the experimental data as a vertical line at a wheel speed where there is no change to the powder feed rate. This increase in consolidated height continues until enough of a grip length causes the extrusion pressure to be reached.

For a given grip length between the wheel groove and the powder there is an increase in extrusion pressure as this contact area increases. With powders of copper and aluminium the tooling is reasonably tolerant of the process startup conditions. Evidence from process data files of low strength alloys ($\sigma_y < 200\text{MPa}$) (John Dawson, BWE Ltd., private communication, December 2013) indicate that the initial wheel speed is not important in obtaining a successful extrusion product. However when processing high strength alloys such as commercially pure titanium the processing window is far smaller. The tooling materials, in particular the abutment have a tendency to yield or fracture early in the process when using titanium powder feedstock. This occurs frequently when using a relatively slow wheel speed of 2-4 RPM but not when the wheel speed is driven above 6 RPM. Analysis of the process data files indicate that the stress normal to the face of the abutment can be an order of magnitude greater at 2 RPM than 6 RPM. For a wheel speed of 2 RPM powder particles would be deformed at a much lower strain rate and have a greater chance to lose more heat evolved from mechanical work. Friction conditions would also be more stable due to the relative lack of particle rearrangement when compared with higher wheel speeds.

The grip between the wheel and the powder at lower wheel speeds needs be strong enough to resist slippage. If this is the case then lower wheel speeds would result in longer effective grip lengths between the wheel and the powder. As the wheel speed increases for a given powder bulk

formation there is a maximum wheel speed to enable a successful grip between the wheel and feedstock. Below this speed, the maximum grip length is determined by the powder feed rate and the tooling geometry. If the wheel groove is only enclosed up to a certain height, powder fed on top of this would spill out of the sides of the groove and the grip length would not increase. If the wheel speed increases above this maximum then appreciable slippage will occur between wheel and feedstock reducing the effective torque required by the wheel to maintain a constant angular velocity. This explains the observations of increasing wheel speed causing a reduction in torque and hence calculated abutment stress. In figure 8.1 this results in a movement of the process along the curved lines.

With rod feedstock wheel slippage is detrimental to extrusion performance as high friction is required to develop the main extrusion pressure. Rod feedstocks in particular can be extruded with little difficulty at low wheel speeds. High wheel speeds are usually only required to meet customers capacity requirements. If slippage occurs with powder feedstock there is an immediate shear at the powder-wheel interface resulting in a high degree of particle rearrangement, frictional heating, deformation and adiabatic heating. This can heat up the powder while maintaining a minimal normal stress on the abutment face. As this slippage continues the powder will heat up within the process and the particle's flow stress will drop considerably. The particles will then preferentially deform rather than rearrange resulting in the aforementioned increase in groove-feedstock contact area and an increase in grip length. This balance of contact area, grip length, wheel speed and feedstock material flow stress all works together to minimise the effective stress on the abutment when extrusion radial to the wheel occurs.

The result from the truncated FEM simulations can be applied to the data gained from the experimental trials to determine what the expected powder fill depth is within the groove. This is something that is impossible to determine experimentally due to the enclosing shoe obscuring the view of the abutment zone. This data allows the estimation of the required powder feed rate for a certain wheel speed. This is an important finding as it is critical with wheel speed sensitive powders such as titanium that the wheel groove is not allowed to fill up to its maximum to prevent failure of the abutment. It is also equally important to ensure enough powder is fed in at a rate appropriate for the current wheel speed so that the extrusion pressure is maintained and that material lost in the flash and extrudate is compensated for. If the powder feed rate is too slow the abutment zone will lose more material than is being added until extrusion stops. This would be detrimental to the rod properties as it sits in the heated die and forms stick/slip lines along its surface. Such lines were visible on the rod from Trial 2, which indicated that the

powder feed was too low for a consistent extrusion but not high enough to yield the abutment.

Two stages of bulk powder deformation can be seen to occur within the process graph shown in figure 3.16 where the slip curve is at the bottom of the graph. Here the wheel grip with the powder is inadequate to produce a significant amount of pressure. As the wheel speed increases there is a slight drop in the effective abutment stress but it remains fairly independent of wheel speed at 200-300 MPa, which is consistent with a velocity independent friction model. The upper curve in figure 3.16 represents the stress levels during active extrusion. If we use the results determined from the truncated FE simulations it can be shown that the change of effective abutment stress with constant wheel speed on this upper curve implies a change in powder feed rate. When we apply this theory to Trial 3.1 in figure 3.19 it can be seen that the powder feed rate during the start up of this trial was much higher than in Trial 2 resulting in an increase in effective grip length and hence abutment stress of an order of magnitude. This correlates with the failure of the abutment early within this trial when running the wheel at 2-4 RPM. The failure of the abutment during Trial 3.2 only occurred after a short length of rod was extruded. Figure 3.22 shows much lower effective abutment stress values at all wheel speeds possibly indicating that the powder feed rate was slower during this trial. The drop in abutment stress with increasing wheel speed could also be attributed to the effect of having a constant powder feed rate. With a steady feed rate the powder would fill the groove much higher with lower wheel speeds resulting in a greater stress on the abutment.

It was originally thought from observations of the process graphs that there was a minimum wheel speed required for successful extrusion of CP-Ti HDH powder within the Conform process. It was assumed that a faster wheel speed would induce greater heat generation within the powder, lowering the flow stresses and improve particle-particle bonding. Instead results from this work indicate that for the successful Conform of CP-Ti HDH and possibly other high strength powders it is critical to not exceed the maximum fill depth within the wheel groove. It is possible to maintain the fill below this critical value by tailoring the powder feed rate depending on the wheel speed. The critical fill depth was found to be approximately 70-80 mm for CP-Ti grade 2 HDH powder based on evidence from the trials data where the abutments failed and the truncated FE simulations. This is very close to the minimum required grip length observed in the simulations where samples of 30 mm and below would fail to deform significantly and those below 50 mm would not extrude. The analytical model in chapter 4 also predicts a minimum required grip length of 23.2 mm for the experimental setup in this work. This

critical fill depth is not unique to Conforming of CP-Ti HDH it only appears that the critical height to cause abutment failure for alloys of aluminium and copper are significantly higher than that allowed by the geometry or the machine. Hence powders of aluminium and copper will tend to overspill from the machine rather than generate sufficient pressure to yield the abutment.

If true this theory makes it possible to successfully Conform CP-Ti HDH at lower wheel speeds than was previously thought by using a lower powder feed rate to ensure the critical fill depth is not exceeded. Processing at lower speeds may have the added benefit of lower processing temperatures and die wear hence allowing for longer tool lifetimes. There will be a lower limit to this as the required extrusion pressure would increase with decreasing powder temperature at lower wheel speeds. Modifications to the current tooling geometry may also make it possible to Conform CP-Ti HDH powder without the need for a metered powder feed. A relief facet added to the die chamber at the height of the critical fill depth would ensure that this value was never exceeded as excess powder would be ejected from the sides of the groove.

It is noted that the data used to predict the grip length with CP-Ti HDH powder is based on simulations using a single wheel speed and does not allow for changes in material flow stress. The workpieces within the truncated simulations did not heat up or deform appreciably resulting in a fairly constant resistance to deformation throughout the entire simulation. In reality the powder heats up rapidly and its flow stress will drop equally as quickly. Further simulations to determine what effect the change in flow stress has to the abutment stress - fill depth relationship are required to enable successful extrusion after the initial start up phase of the Conform process. Simulations using workpiece materials with different flow stresses will also help to predict whether there is an upper limit in terms of the strength of the powder that is possible to be processed using the current Conform 315i machine. The upper limit will be reached when the minimum grip length required to generate enough extrusion pressure exceeds the maximum fill depth before the stress on the abutment causes its failure. With a critical height of 70-80 mm for CP-Ti HDH, there is a reasonably large surplus of available grip length before the powder falls below the theoretical minimum level of 23.2 mm to generate sufficient extrusion pressure. This process window can be extended by running the wheel at faster speeds to generate more heat and lower the flow stress within the powder. The only requirement would be a lower powder feed during the startup phase when the powder and tools are still relatively cold. However, faster wheel speeds would also result in faster abrasive wear of the tool faces.

The issue of correctly manipulating grip length in particulate feed Conform can be done through wheel speed, powder feed rate, powder chemistry, morphology and size fraction. It has also been shown through the 2D FEM that through optimisation of tool geometries it is possible to manipulate the minimum grip length required by the process to extrude the consolidated powder. Therefore with further work and data production for a range of metal powder alloys a generic model could be produced in order to predict the required extrusion pressure for a set die setup, the minimum grip length to generate the pressure and hence the required fill height as a result of the powder rheology characteristics.

The analytical model manages to predict the results from both the experimental work and finite element modelling with reasonable accuracy. The analytical model assumes that no flash is produced and hence there is zero contribution from the flash to the wheel torque. This is not the case for the finite element models and to an even greater extent the experimental work. Therefore it can be concluded that the flash has little effect on the wheel torque, abutment load/stress and grip length when compared with the material being extruded. The dominant contribution to the wheel driving force for the Conform process is the material in the groove, upset above the abutment and being extruded. Proper selection or determination of the material properties for both room temperature and at temperatures expected at the die is imperative for success of the analytical model. The correct friction coefficient is also critical, but far harder to determine for powder feedstocks. The experimental results matched with the analytical model at lower friction values of 0.3-0.5 when compared with the finite element models at 0.98.

It is suggested that the lower friction between feedstock and wheel/tool is due to the effect of the unconsolidated powder in the experimental work; something that cannot be incorporated into the other modelling techniques at this point. In the experimental Conform machine the movement between the wheel and powder may not have resulted in a constant grip and slip at the interface may have dominated. This would mean that while the wheel surface may be moving faster than the powder there is still sufficient force to generate the required extrusion pressure. Indeed it was observed in Trial 1 where the abutment stress increased dramatically when the wheel speed was dropped from 8 to 2 RPM. While the wheel was moving at 8 RPM, the wheel was slipping against the powder but material was being extruded so the extrusion force was still sufficiently high. At 2 RPM, the slower wheel speed prevented slippage at the powder/wheel interface and the abutment stress increases rapidly due to this increase in the effective friction coefficient. To compound this effect the slower wheel speed and lack of slip

would also have caused a drop in temperature, or increase in flow stress, further increasing the expected abutment stress. This effect also explains the drop in abutment stress with increasing wheel speed. It may be expected that higher wheel speeds would result in more cold powder being pulled into the abutment zone, increasing the effective flow stress and therefore the required extrusion pressure. Instead the opposite effect is observed due to the increased amount of slip between the wheel and the powder and the resultant increase in heat imparted from this slippage.

Conclusions

Success of Conforming CP-Ti HDH powder to 5 mm diameter wire with microstructures and properties exceeding that of conventionally produced wrought titanium

This thesis presents the successful extrusion of commercially pure hydride-dehydride titanium powder into 5 mm diameter wire. The rod is fully dense with no observable porosity and has a fine grain size due to the severe plastic deformation, fast extrusion speed and rapid cooling. The wheel speed at which the wire was extruded dictates the final average grain size, with faster wheel speeds resulting in a smaller grain size. The microstructure demonstrates significant recrystallisation with no observable elongation of the grains along the extrusion axis. This is due to the very high temperatures (700-850°C) seen in the process just behind the die, low thermal conductivity of titanium and the long travel time of the wire from the die to the cooling trough. The microstructure shows a distinctive macro-flow pattern, which is unique to the Conform processing of powder feeds. This has only been observed in powder fed Conform and is not unique to this work. The tensile strength of samples extruded at all wheel speeds exceed that of conventionally produced wrought product, which is due in part to the fine grain size.

Abutment stress metric allows for comparisons between all continuous extrusion machines, simulations and numerical models

The abutment stress metric is a calculated quantity derived in this work and is directly proportional to the wheel torque on any single Conform or CRE machine. It is also a value that is suitable for comparison between different tool sets and machines, unlike motor torque, which has been conventionally used to determine how the process is progressing. The abutment stress can also be calculated from the analytical model and from finite element simulations offering a single value for direct comparison between iterative die designs in all virtual spaces without the need for extensive experimental trials.

A model and methodology for determining process windows for the Conform process

The analytical model derived in chapter 4 and analysed in chapter 7 shows good agreement with the results from the experimental trials. It is clear that careful selection of the material properties (yield stress at room temperature and flow stress at the temperature of the die) and friction is important to ensuring the accuracy of the model. This model is not just suitable for powder feedstocks but also rod fed Conform. Indeed it is inherently more accurate for rod feeds due to the lack of consideration for a feedstock with varying density. The model can take multiple inputs for tool geometries and it is possible to use the result to find a near optimal tool design to maximise success when moving to experimental trials. It is possible to get optimised results from this model in a matter of minutes compared with days for FEM and week/months for experimental trials.

Finite element modelling is sufficient for comparative results and rapid iterations of tool designs but should not be used for predictions of experimental trials with powder feedstocks

The finite element method is a common modelling technique used for a range of metal forming processes. Processes such as forging, conventional extrusion and machining all rely on the workpiece being a fully coherent or solid material. When modelling powder metallurgy process with finite elements, only low strains can be reliably simulated. In contrast, Conform of powders provides the finite element method with an insurmountable problem from its very high strains and shears.

2D FEM is not suitable for modelling the Conform process if it is to be used to inform experimental trials. The upset height, leading to predicted flash production, abutment loads are all incorrect when compared with 3D simulations. This can be put down to the fact that there is only one contact length against the wheel to providing the driving force with another length against the shoe retarding this motion. In contrast the full 3D process has a ratio of wheel drive to shoe resistance of approximately 0.67. This increases the effective drive force and hence lowers the upset height that is formed. Instead, 2D FEM should be used for more rapid iterations of process conditions and tool geometries, when compared with 3D FEM. It is suitable to compare FEM results in 2D with 2D but not 2D with 3D.

Future work

Further suggestions to continue the research presented in this thesis are presented below. Limitations to both the experimental and finite element simulation methodologies have been discussed and the points below are put forward to overcome these.

Conform extrusion of titanium alloys - Ti-6Al-4V, near alpha and metastable β Ti alloys, blended elemental powders, low-cost novel alloy powders

This work has presented developmental research into the Conform process and its application not only to the extrusion of commercially pure titanium powder but also to metal powders in general. It is feasible that using the methodology put forward in this thesis that higher strength titanium alloys could be extruded by moderation of the powder feed. It is also possible that due to the high degree of shear and high temperatures that in-situ alloying may be possible by employing a blended elemental feedstock powder.

New tooling materials

Tooling material development across Conform and CRE machine manufacturers anecdotally appears to be very static. However, materials such as StelliteTM chosen for their high wear resistance for abutments indicate that further work needs to be done into high temperature, high strength alloys for these tools. Current suggestions include W-25%w-Re (with or without additions of Hafnium Carbide), which has been used to good effect in the friction stir welding of titanium alloys. A W-25%w-Re abutment was used in a single trial related to this work but it was not possible to collect sufficient data to determine its efficacy for future use in Conform. Other possibilities may include Molybdenum-Hafnium-Carbide (MHC) and Titanium-zirconium-molybdenum (TZM), which are both in direct extrusion dies inserts and forging dies. Abutment and die coatings are also areas for investigation in order to both improve the die integrity for high strength powder extrusion and service life of current copper alloy Conform extrusions in industry. An abutment base material may be chosen to have a high toughness and high yield strength at extended temperatures. It might then be subjected

to a hard coating technique with a coating that has a low propensity to leech elements into the workpiece resulting in contamination of the product.

Investigation into the effect of particle size, size distribution and morphology

Only one size fraction and morphology of CP-Ti powder was investigated in this work. With the proliferation of Additive manufacturing processes such as selective laser melting, electron beam melting and laser sintering the powder manufacturing industry tends to provide vast quantities of spherical powder morphologies from gas and plasma atomisation. These powders are highly spherical and flow far better than HDH powders, but the GA process produces a wide range of size fractions from which the desired particle sizes must be sieved out. The resultant yield loss, which includes relatively large particles of $>200 \mu\text{m}$ are remelted, further increasing the energy input into the products life cycle. Investigations need to be done to determine whether these larger particles, or indeed a large particle size distribution that includes both the small $<45 \mu\text{m}$ and large $>200 \mu\text{m}$ could be successfully extruded through continuous extrusion. This would further increase the economic benefit to using the Conform process as a method for reusing GA waste.

Titanium machining processes in the aerospace industry also create a significant amount of titanium wastage with up to 90% of the original billets being machined away to form the final product. The waste chips/swarf are cleaned and graded before being sent on to other lower quality products, remelted or used in steel making additives. If cleaned machined swarf could be continuously consolidated the economic benefits could potentially revolutionise the titanium industry.

Fully controlled and monitored powder feed

An attempt at controlling the powder feed during this research was made in order to decrease the tools stresses and temperatures within the Conform machine and prolong the abutment life. Due to the crude nature of the hopper designed it was difficult to monitor the exact powder feed rate during the trials meaning powder feed rates had to be measured offline post-trial. It would be useful to conduct further research in this area, not only in titanium but also the more commonly Conformed powders/particulates of aluminium and copper to use a fully controlled powder hopper. Such a hopper should have a large capacity and be able to log the live mass flow rate into the wheel groove and supply the control console this data along with the temper-

atures already monitored. The exact relationship between powder feed rate and consolidation behaviour could then be accurately investigated.

Additional instrumentation on the Conform machine

The current method of live monitoring of the powder consolidation progression is through the motor torque from the machine. This provides one dimensional data and provides a description of the average forces over the whole tooling set. Monitoring of individual tools loads could be conducted through the introduction of high temperature load cells similar to those described and used previously [75]. Load cells underneath the abutment and behind the die would provide the most useful data in separating the drive and extrusion pressures within the process.

Continuous rotary extrusion machines do not have the same shoe movement control limitation as Conform machines. CRE machines have translational control of the shoe in both the X and Y directions (Z being the wheel rotation axis) through hydraulic rams. Pressure meters that logged the hydraulic fluid pressure could also provide whole-shoe force vector measurement to aid in extrusion post-processing.

Discrete element modelling of particulates metal in the Conform process

Finite element modelling has been shown to be partially useful for modelling the Conform of powder feedstocks. However its accuracy is limited when the loose powder flow in the early stages of the process is considered. Instead it would be beneficial to use a different modelling process/software such as the discrete element method (DEM). In DEM the powder is modelled as individual particles that can contact, slide and rebound from each other. Several factors would need to be considered in order to correctly simulate metal powders in the Conform process. Firstly friction conditions both between particles and particles-tools would need to be experimentally determined from Hall Flow Meter and angle of repose tests. Secondly a suitable contact model would need to be developed to allow the compaction behaviour of the powder with a strain and temperature dependence to the contact forces. Finally in order to model the consolidation accurately the contact model needs to incorporate sintering to allow for particle-particle bonding and densification.

References

- [1] E. H. Kraft, Summary of Emerging Titanium Cost Reduction Technologies, Tech. rep., EHKTechnologies (2004).
- [2] F. H. Froes, H. Friedrich, J. Kiese, D. Bergoint, Ti in the family automobile: the cost challenge, *Journal of Materials* 56 (2) (2004) 40–44.
- [3] H. Friedrich, J. Kiese, H. G. Haldenwanger, A. Stich, (eds.) G. Lutjering, J. Albrecht, Titanium in automotive applications - nightmare, vision or reality, in: *Ti-2003 10th World Conference on Titanium*, Wiley-VCH, 2004, pp. 3393–3402.
- [4] L. Wagner, O. Schauerte, Status of titanium and titanium alloys in automotive applications, in: *Ti-2007 Science and Technology*, Vol. 2, The Japan Institute of Metals, 2007, pp. 1371–1378.
- [5] M. Jackson, *Encyclopedia of Automotive Engineering*, John Wiley & Sons Ltd., 2014, Ch. 2. Materials and Manufacturing. doi:10.1002/9781118354179.auto156.
- [6] K. Manchiraju, Direct Solid-State Conversion of Recyclable Metals and Alloys, Tech. Rep. DE-EE003458, Southwire Company, GA, USA (2012).
- [7] C. Doblin, D. Cantin, S. Gulizia, Processing TiROTM powder for strip production and other powder metallurgy applications, Presentation given at TiDA International Titanium Powder Processing Conference (2-4 December 2014) (2014).
- [8] Y. T. Zhu, T. C. Lowe, R. Z. Valiev, G. J. Raab, Continuous equal channel angular pressing (2006).
- [9] J. East, I. Maxwell, Continuous extrusion of metals (1985).
- [10] BWE Ltd., CONFORM and CONKLAD, Printed brochure at BWE Ltd. Ashford, United Kingdom. (2008).

- [11] C. Etherington, Conform and the Recycling of Non-Ferrous Scrap Metals, Conservation and Recycling 2 (1978) 19–29.
- [12] C. Stadelmann, Extrusion von Metallpulven durch kontinuierliches Pulverstrangpressen, Ph.d. thesis, Der Technischen Fakultät der Universität Erlangen - Nürnberg (2009).
- [13] C. Etherington, Conform-A New Concept for the Continuous Extrusion Forming of Metals, Journal of Engineering for Industry (1974) 893–900.
- [14] J. R. Cho, H. S. Jeong, Parametric investigation on the curling phenomenon in CONFORM process by three-dimensional finite element analysis, Journal of Materials Processing Technology 110 (1) (2001) 53–60.
- [15] J. R. Cho, H. S. Jeong, Parametric investigation on the surface defect occurrence in CONFORM process by the finite element method, Journal of Materials Processing Technology 104 (3) (2000) 236–243.
- [16] J. Hodek, M. Zemko, FEM Model of Continuous Extrusion of Titanium in Deform Software, in: COMAT 2012- Recent trends in structural materials, 2012, pp. 1–7.
- [17] J. T. Black, W. G. Voorhes, Theory of Linear Continuous Extrusion - Linex, Journal of Engineering for Industry 100 (1978) 37–42.
- [18] J. A. Pardoe, 'Conform' continuous extrusion of metal powders into products for electrical industry: development experience, Powder Metallurgy 1 (1979) 1–7.
- [19] M. Wollmann, J. Kiese, L. Wagner, (eds.) L. Zhou, H. Chag, Y. Lu, D. Xu, Properties and Applications of Titanium Alloys in Transport in Proc. Ti-2011 12th World Conference on Titanium, Science Press Beijing, 2012, pp. 837–844.
- [20] Advanced Propulsion Centre UK, Lightweight vehicles and powertrain structures: UK opportunities, <http://www.apcuk.co.uk/wp-content/uploads/2015/04/Lightweight-Vehicles-and-Powertrain-Structures-Report-September-2013.pdf> (September 2013).
- [21] C. A. Blue, W. H. Peter, Alloy Design and Thermomechanical Processing of a Beta Titanium Alloy for a Heavy Vehicle Application, Technical report, Oak Ridge National Laboratory (2010).
- [22] E. H. Kraft, Opportunities for Low Cost Titanium in Reduced Fuel Consumption, Improved Emissions, and Enhanced Durability Heavy-duty Vehicles, Tech. rep., EHKTechnologies (2002).

- [23] C. Lavender, FY 2004 Progress Report for Lightweighting Materials - 4. Automotive Metals - Titanium, Tech. rep., Pacific Northwest National Laboratory (2004).
- [24] T. E. Norgate, G. Wellwood, The Potential Applications for Titanium Metal Powder and Their Life Cycle Impacts, *Journal of Materials* September (2006) 58–63.
- [25] Cristal Metals, Cristal metals titanium powder, http://cristalmetals.com/docs/Ti_Metal_Powder_EU_EN.pdf (December 2014).
- [26] M. Jackson, K. Dring, Materials perspective - a review of advances in processing and metallurgy of titanium alloys, *Mater. Sci. Tech.* 22 (2006) 881–887.
- [27] W. Chen, Y. Yamamoto, W. H. Peter, M. B. Clark, S. D. Nunn, J. O. Kiggans, T. R. Muth, C. A. Blue, J. C. Williams, K. Aktar, The investigation of die-pressing and sintering behavior of ITP CP-Ti and Ti-6Al-4V powders, *J. Alloy Compd.* 541 (2012) 440–447.
- [28] CSIRO, Explanation of the Kroll and TiRO™ processes, <http://www.csiro.au/Organisation-Structure/Flagships/Future-Manufacturing-Flagship/Ti-Technologies/TiRO.aspx> (November 2013).
- [29] D. van Vuuren, Piloting a titanium metal production process, http://www.csir.co.za/msm/metals_and_metals_processes/docs/Piloting_titanium_metal_production_process.pdf (2012).
- [30] G. Z. Chen, D. J. Fray, T. W. Farthing, Direct electrochemical reduction of titanium dioxide to titanium in molten calcium chloride, *Nature* 407 (2000) 361–364.
- [31] C. Schwandt, D. J. Fray, Determination of the kinetic pathway in the electrochemical reduction of titanium dioxide in molten calcium chloride, *Acta Electrochimica* 51 (2005) 66–76.
- [32] R. Bhagat, D. Dye, S. L. Raghunathan, R. J. Talling, D. Inman, B. K. Jackson, K. K. Rao, R. J. Dashwood, In-situ synchrotron diffraction of the electrochemical reduction pathway of TiO_2 , *Acta Mater.* 58 (2010) 5057–5062.
- [33] R. Z. Valiev, A. V. Korznikov, R. R. Mulyukov, Structure and properties of ultrafine-grained materials produced by severe plastic deformation, *Materials Science and Engineering: A* 168 (2) (1993) 141 – 148.
- [34] H. Hahn, Unique Features and Properties of Nanostructured Materials, in: *Nanomaterials by Severe Plastic Deformation*, Wiley-VCH Verlag GmbH & Co. KGaA, 2004, pp. 2–17. doi:10.1002/3527602461.ch1a.

- [35] V. M. Segal, Materials processing by simple shear, *Materials Science and Engineering A - Structural Materials Properties Microstructure and Processing* 197 (2) (1995) 157–164.
- [36] R. K. Islamgaliev, V. U. Kazyhanov, L. O. Shestakova, A. V. Sharafutdinov, R. Z. Valiev, Microstructure and mechanical properties of titanium (Grade 4) processed by high-pressure torsion, *Materials Science & Engineering A* 493 (1-2) (2008) 190–194.
- [37] M. Greger, M. Cerny, L. Kander, J. Kliber, Structure and properties of titanium for dental implants, *Metallurgia* 48 (4) (2009) 249–52.
- [38] R. Z. Valiev, I. A. Alexandrov, Y. T. Zhu, T. C. Lowe, Paradox of strength and ductility in metals processed by severe plastic deformation, *Journal of Materials Research* 17 (1) (2002) 5–8.
- [39] V. M. Segal, Equal channel angular extrusion: from macromechanics to structure formation, *Materials Science & Engineering A* 271 (1) (1999) 322–333.
- [40] R. Z. Valiev, T. G. Langdon, Developments in the use of ECAP processing for grain refinement, *Revised Advanced Material Science* (2006) 1–12.
- [41] M. Furukawa, Z. Horita, M. Nemoto, T. G. Langdon, The use of severe plastic deformation for microstructural control, *Materials Science & Engineering A* 324 (2002) 82–89.
- [42] V. V. Stolyarov, Y. T. Zhu, I. V. Alexandrov, T. C. Lowe, R. Z. Valiev, Influence of ECAP routes on the microstructure and properties of pure Ti, *Materials Science and Engineering A - Structural Materials Properties Microstructure and Processing* 299 (1-2) (2001) 59–67.
- [43] P. Luo, D. T. McDonald, S. Palanisamy, M. S. Dargusch, K. Xia, Ultrafine-grained pure Ti recycled by equal channel angular pressing with high strength and good ductility, *Journal of Materials Processing Technology* 213 (3) (2013) 469–476.
- [44] G. J. Raab, R. Z. Valiev, T. C. Lowe, Y. T. Zhu, Continuous processing of ultrafine grained Al by ECAP–Conform, *Materials Science & Engineering A* 382 (1-2) (2004) 30–34.
- [45] C. Xu, S. Schroeder, P. B. Berbon, T. G. Langdon, Principles of ECAP–Conform as a continuous process for achieving grain refinement: Application to an aluminum alloy, *Acta Materialia* 58 (4) (2010) 1379–1386.
- [46] V. M. Segal, Mechanics of continuous equal-channel angular extrusion, *Journal of Materials Processing Technology* 210 (3) (2010) 542–549.

- [47] V. V. Stolyarov, Y. T. Zhu, T. C. Lowe, R. K. Islamgaliev, R. Z. Valiev, A Two Step SPD Processing of Ultrafine-Grained Titanium, *Nanostructured Materials* 11 (7) (1999) 947–954.
- [48] V. V. Stolyarov, Y. T. Zhu, I. V. Alexandrov, T. C. Lowe, R. Z. Valiev, Grain refinement and properties of pure Ti processed by warm ECAP and cold rolling, *Materials Science & Engineering A* 343 (2002) 43–50.
- [49] M. Greger, V. Masek, V. Snasel, Mechanical Properties of Commercially Pure Titanium Grade 2 after Severe Plastic Deformation, in: *Metal 2011*, Brno, Czech Republic, 2011, pp. 1–5.
- [50] G. Purcek, O. Saray, O. Kul, I. Karaman, G. G. Yapici, M. Haouaoui, H. J. Maier, Mechanical and wear properties of ultrafine-grained pure Ti produced by multi-pass equal-channel angular extrusion, *Materials Science & Engineering A* 517 (1-2) (2009) 97–104.
- [51] Y. J. Chen, Y. J. Li, J. C. Walmsley, S. Dumoulin, S. S. Gireesh, S. Armada, P. C. Skaret, H. J. Roven, Quantitative analysis of grain refinement in titanium during equal channel angular pressing, *Scripta Materialia* 64 (9) (2011) 904–907.
- [52] D. Kang, T. Kim, Mechanical behavior and microstructural evolution of commercially pure titanium in enhanced multi-pass equal channel angular pressing and cold extrusion, *Materials and Design* 31 (S1) (2010) S54–S60.
- [53] P. Luo, D. T. McDonald, W. Xu, S. Palanisamy, M. S. Dargusch, K. Xia, A modified hall petch relationship in ultrafine-grained titanium recycled from chips by equal channel angular pressing, *Scripta Materialia* 66 (10) (2012) 785–788.
- [54] P. Luo, D. T. McDonald, S. M. Zhu, S. Palanisamy, M. S. Dargusch, K. Xia, Analysis of microstructure and strengthening in pure titanium recycled from machining chips by equal channel angular pressing using electron backscatter diffraction, *Materials Science & Engineering A* 538 (2012) 252–258.
- [55] G. Grant, J. Darsell, Low Cost Fabrication of ODS Alloys, Presentation given at DOE FE ARM Annual Review, Pittsburgh, Pennsylvania, U.S.A. (9 April 2012) (2012).
- [56] D. of Energy, C. Change, Energy consumption in the uk, Tech. rep., National Statistics (2014).
- [57] R. K. Dube, Metal strip via roll compaction and related powder metallurgy routes, *International Materials Reviews* 35 (5) (1990) 253–291.

- [58] G. I. Raab, A. V. Polyakov, D. V. Gunderov, R. Z. Valiev, Formation of a nanostructure and properties of titanium rods during equal-channel angular pressing CONFORM followed by drawing, *Russian Metallurgy (Metally)* 2009 (5) (2009) 416–420.
- [59] A. V. Polyakov, I. P. Semenova, G. I. Raab, V. D. Sitdikov, R. Z. Valiev, Peculiarities of ultrafine-grained structure formation in Ti grade-4 using ECAP-Conform, *Revisions of Advanced Materials Science* 31 (2012) 78–84.
- [60] D. V. Gunderov, A. V. Polyakov, I. P. Semenova, G. I. Raab, A. A. Churakova, E. I. Gimaltdinova, I. Sabirov, J. Segurado, V. D. Sitdikov, I. V. Alexandrov, N. A. Enikeev, R. Z. Valiev, Evolution of microstructure, macrotexture and mechanical properties of commercially pure Ti during ECAP-conform processing and drawing, *Materials Science and Engineering: A - Structural Materials Properties Microstructure and Processing* 562 (C) (2013) 128–136.
- [61] M. Reynolds, In the matter of application no. 1509530 by Holton Machinery Limited to register the mark Holton Conform in Class 7 and in the matter of opposition thereto under no. 44717 by BWE Limited (1999).
- [62] D. Green, *Extrusion* (1973).
- [63] U. K. Sinha, E. H. Chia, *Conform product thermomechanical treatment* (1989).
- [64] U. K. Sinha, R. D. Adams, *Apparatus for conform extrusion of powder feed* (1994).
- [65] J. Dawson, *Conform technology for cost effective manufacture of copper strip*, <http://www.rautomead.co.uk/resources/media/1311264714BWE2.pdf> (March 2012).
- [66] R. Eborall, D. G. Hunt, The rolling of copper strip from hydrogen-reduced and other powders, *Powder Metall.* 5 (1960) 1–23.
- [67] S. Chikosha, T. C. Shabalala, H. K. Chikwanda, Effect of particle morphology and size on roll compaction of Ti-based powders, *Powder Tech.* 264 (2014) 310–319.
- [68] D. J. Marsh, *Extrusion of Copper by the Conform Continuous Extrusion Process*, TRG Report (1977) 77–83.
- [69] J. A. Pardoe, *Conform Continuous Extrusion Process - Its Contribution to Energy-Conservation*, *Metals Technology* 11 (AUG) (1984) 358–365.

- [70] N. J. E. Adkins, P. Tsakirooulos, Design of powder metallurgy aluminium alloys for applications at elevated temperatures Part 2 Tensile properties of extruded and Conformed gas atomised powders, *Materials Science and Technology* 7 (5) (1991) 419–426.
- [71] S. Katsas, R. J. Dashwood, G. Todd, M. Jackson, R. Grimes, Characterisation of ConformTM and conventionally extruded Al–4Mg–1Zr. Effect of extrusion route on superplasticity, *Journal of Materials Science* 45 (15) (2010) 4188–4195.
- [72] R. Wilson, *Extrusion of high temperature formable non-ferrous metals* (2012).
- [73] R. Wilson, Continuous Extrusion of Titanium Wire from Powder Feeds, Presentation, International Titanium Powder Processing, Consolidation and Metallurgy Conference, TiDA, New Zealand. <http://www.tida.co.nz/upload/files/13—Robert-Wilson—CSIRO,-Australia.pdf> (March 2015).
- [74] J. Tirosh, G. Grossman, G. Gordon, Theoretical and Experimental Study of the Conform Metal Forming Process, *Transactions of the ASME* 101 (1979) 116–120.
- [75] P. K. C. Wood, The Mechanics of the Conform Continuous Extrusion Process, Ph.d. thesis, The University of Aston in Birmingham (1990).
- [76] T. Manninen, T. Katajarinne, P. Ramsay, Analysis of flash formation in continuous rotary extrusion of copper, *Journal of Materials Processing Technology* 177 (1-3) (2006) 600–603.
- [77] F.-r. Cao, J.-l. Wen, H. Ding, Z.-d. Wang, Y.-l. Li, R.-g. Guan, H. Hou, Force analysis and experimental study of pure aluminium and Al-5%Ti-1%B alloy continuous expansion extrusion forming process, *Transactions of Nonferrous Metals Society of China* (23) (2012) 201–207.
- [78] Y. H. Kim, J. R. Cho, K. S. Kim, H. S. Jeong, S. S. Yoon, A Study of the Application of Upper Bound Method to the CONFORM Process, *Journal of Materials Processing Technology* 97 (1) (2000) 153–157.
- [79] J. R. Cho, H. S. Jeong, CONFORM process: surface separation, curling and process characteristics to the wheel diameter, *Journal of Materials Processing Technology* 136 (1-3) (2003) 217–226.
- [80] T. Kubina, J. Dlouhy, M. Kövér, J. Hodek, Preparation and Thermal Stability of Ultra Fine Grained Commercially Pure Titanium Wire, in: *COMAT 2012- Recent trends in structural materials*, Plzeň, Czech Republic, 2012.

- [81] M. Duchek, T. Kubina, J. Hodek, J. Dlouhy, Development of the production of ultrafine-grained titanium with the conform equipment, *Materials and technology* 47 (4) (2013) 515–518.
- [82] J. Hodek, T. Kubina, J. Dlouhy, FEM model and experimental production of titanium rods using Conform machine, in: *Metal 2013*, Brno, Czech Republic, 2013, pp. 1–6.
- [83] M. Zemko, J. Hodek, FEM Modelling of Continuous Extrusion of High-Strength Metals Using Commercial, Unpublished (2013) 1–7.
- [84] X. Valey, Analysis of the Conform process: a specific form of aluminium extrusion, Ph.D. thesis, Bournemouth University (2004).
- [85] D. Kumar Sinha, S. Kumar, A. Kumar, Virtual Design And Fabrication Of A Continuous Extrusion Setup With Process Analysis, *International Journal of Engineering Research and Technology* 1 (8) (2012) 1–7.
- [86] O. P. Childs, J. B. McKenna, Continuous friction-actuated extrusion, patent (1981).
- [87] J. Dawson, Private Communication, e-mail.
- [88] W. A. Beverloo, H. A. Leniger, J. Van de Velde, The flow of granular solids through orifices, *Chemical Engineering Science* 15 (1961) 260–269.
- [89] ASTM International, ASTM E8 / E8M-15a, Standard Test Methods for Tension Testing of Metallic Materials (2015). doi:10.1520/E0008\E0008M-15A.
- [90] ASTM International, Standard Specification for Titanium and Titanium Alloy Bars and Billets, ASTM Standards (2013).
- [91] P. K. Saha, *Aluminium Extrusion Technology*, 2nd Edition, no. 0-87170-644-X, ASM International, 2000.
- [92] J. Dawson, New process generation redefines manget wire industry, *Wire and Cable Technology International* <http://www.bluetoad.com/publication/index.php?i=166056&m=&l=&p=5&pre=> (2013).
- [93] G. Welsch, R. Boyer, E. Collings, *Materials Properties Handbook: Titanium Alloys*, Materials properties handbook, ASM International, 1993.
URL <https://books.google.co.uk/books?id=x3rToHW0cD8C>